TAMPEREEN TEKNILLINEN YLIOPISTO
TAMPERE UNIVERSITY OF TECHNOLOGY

Kirsi Penttinen

Induced Pluripotent Stem Cell-Derived Disease Model for Catecholaminergic Polymorphic Ventricular Tachycardia

Julkaisu 1379 • Publication 1379

Tampere 2016

Tampereen teknillinen yliopisto. Julkaisu 1379
Tampere University of Technology. Publication 1379

Kirsi Penttinen

Induced Pluripotent Stem Cell-Derived Disease Model for Catecholaminergic Polymorphic Ventricular Tachycardia

Thesis for the degree of Doctor of Science in Technology to be presented with due permission for public examination and criticism in Tietotalo Building, Auditorium TB109, at Tampere University of Technology, on the 29th of April 2016, at 12 noon.

Tampereen teknillinen yliopisto - Tampere University of Technology
Tampere 2016

ACADEMIC DISSERTATION
University of Tampere and Tampere University of Technology, BioMediTech
University of Tampere, School of Medicine
Tampere University Hospital, Heart Hospital
Finland

Supervisor of studies
Professor, D.Tech Jari Hyttinen
Department of Electronics and Communications Engineering
Tampere University of Technology
Tampere
Finland

Supervisors
Professor, MD, PhD Katriina Aalto-Setälä
BioMediTech and School of Medicine
University of Tampere
Tampere
Finland

PhD Mari Pekkanen-Mattila
BioMediTech
University of Tampere
Tampere
Finland

Reviewers
Professor, MD, PhD Timo Mäkikallio
Department of Internal Medicine
Oulu University Hospital
Oulu
Finland

Adjunct Assistant Professor, PhD Winston Shim Se Ngie
National Heart Centre Singapore
Cardiovascular & Metabolic Disorders Program
Singapore

Opponent
Professor, MD, PhD Anu Suomalainen Wartiovaara
Research Programs Unit
Molecular Neurology
University of Helsinki
Helsinki
Finland

ISBN 978-952-15-3722-6 (printed)
ISBN 978-952-15-3726-4 (PDF)
ISSN 1459-2045

Abstract

Human induced pluripotent stem cells (hiPSCs) offer significant opportunities for cardiac research. With this technology, it is possible to create patient-specific stem cell lines and differentiate them into cardiomyocytes for cardiac research. hiPSC technology has created many expectations for new therapeutic possibilities, and it holds promise for use in drug-testing platforms and in patient-specific drug therapy optimization, as well as later in regenerative medicine.

Catecholaminergic polymorphic ventricular tachycardia (CPVT) is an inherited, highly lethal arrhythmogenic cardiac disorder. It is primarily caused by cardiac ryanodine receptor gene (*RyR2*) mutations that result in abnormal calcium release from the sarcoplasmic reticulum to the cytosol, leading to the generation of afterdepolarizations and triggered activity. The estimated clinical prevalence of CPVT is 1:10000. Intracellular calcium ions are crucial to the function of the heart muscle, and disturbances in this process can have fatal consequences, as observed in CPVT. Understanding the mechanisms of arrhythmia and the role of intracellular calcium in CPVT pathophysiology is important for improving disease prevention, diagnosis, and treatment.

The main objective of this work was to develop and characterize models of cardiac cells and to develop and improve techniques for studying electrical field stimulation and calcium cycling of cardiomyocytes. Utilizing electrical field stimulation, the orientation and maturation of neonatal rat cardiomyocytes and the increase in the beating rate of an *in vitro* disease model for CPVT were studied. For the cell model of CPVT, human iPSC-derived cardiomyocytes were obtained from CPVT patients carrying *RyR2* mutations. These iPSCs disease models were used to study the disease mechanisms of CPVT, mutation-specific differences in intracellular calcium cycling and the effect of antiarrhythmic treatment of the cells. Mechanistic insights regarding CPVT arrhythmias and drug responses were also validated in the index patients. Additionally, a new calcium cycling analysis software tool was developed for characterizing abnormal intracellular calcium transients of disease-specific cardiomyocytes.

The results of this work demonstrate that patient-specific iPSC-derived cardiomyocytes corresponded to the clinical phenotype in both the pathophysiology and drug responses of CPVT and encourages the continuation of disease modeling utilizing iPSCs. These studies also presented a new mechanism for arrhythmias in CPVT. These findings encourage the translation of findings in basic research to benefit patients in clinical practice, e.g., in the form of potentially new medications.

Acknowledgements

These studies were performed at the BioMediTech, University of Tampere during the years 2009-2015. I am grateful to the former and the present directors of our institute, Riitta Seppänen and Hannu Hanhijärvi for providing the research facilities for my studies. I want to thank Tampere Graduate Programme in Biomedicine and Biotechnology (TGPBB) for the education and for financially supporting my journeys to international conferences.

I have been financially supported by research and travel grants from TEKES, The Academy of Finland, the Finnish Concordia Fund, The Finnish Cultural Foundation and Pirkanmaa Regional Fund, the Finnish Foundation for Cardiovascular Research, the Paavo Nurmi Foundation, the Aarne Koskelo Foundation, the Ida Montin Foundation, Aarne and Aili Turunen Foundation, the Orion-Farmos Research Foundation and the City of Tampere. The support of the funders is sincerely acknowledged.

My deepest gratitude is due to my two kind and sympathetic supervisors, Professor Katriina Aalto-Setälä MD, PhD and Mari Pekkanen Mattila, PhD. Katriina, I thank you for giving me the opportunity to work in this project under your supervision. I am very grateful for your guidance in my work, and all your help and advices. Thank you for supporting and having faith in me. Thank you Mari for all your advices and for being so encouraging and positive. Your door has always been open for me, and I want to thank you for all your time and effort in guiding and teaching me throughout the years.

I am grateful for the comments and positive feedback of my TGPBB thesis commitee, Professor Olli Silvennoinen, MD, PhD and Professor Jari Hyttinen. Professor Hyttinen is also greatly acknowledged as the supervisior of my studies in Tampere University of Tehcnology and the guidance throughout this work.

I also wish to thank the official pre-examiners, Winston Shim, PhD and Professor Timo Mäkikallio, MD, PhD of the careful evaluation of this thesis.

The contribution of co-authors Antti Ahola, Mari Pekkanen-Mattila, Liisa Ikonen, Erja Kerkelä, Jari Hyttinen, Katriina Aalto-Setälä, Jere Paavola, Anna Kiviaho, Kim Larsson, Matti Viitasalo,

Annukka Lahtinen, Lauri Toivonen, Kimmo Kontula, Heikki Swan, Mika Laine, Olli Silvennoinen, Sari Vanninen, Harri Siirtola, Jorge Ávalos-Salguero, Tiina Vainio and Martti Juhola is gratefully acknowledged. Special thanks for the Bachelors of Laboratory Services Henna Venäläinen, Markus Haponen and Merja Lehtinen for their valuable technical help.

I would also like to thank my colleagues and the personnel of BioMediTech for the pleasant work atmosphere and particularly the whole Heart group and its past and present members for providing such a nice work environment. I am grateful for everyone who has helped and advised me in the lab during these years. Special thanks for Liisa Ikonen, Marisa Ojala, Henna Venäläinen and Anna Kiviaho for your friendship, support and all the fun moments during these years. Special thanks to Marisa for sharing an office as well as the ups and downs related to work and life in general.

I want to thank all my dear friends and family for many joyful moments and just being there for me. Especially thanks to my parents, Maire and Kalevi Kujala, for the help, support and encouragement throughout my life and this thesis project.

Thanks to Nooa for literally kicking me through the writing process of this thesis during spring 2015 and for taking long naps so I could finalize this thesis after the pre-examination. Thank you Vesa for being you, my rock, and for tolerating me during my times of stress. Your care, and also expertise in science has helped me during this work. But most of all, thank you Vesa and Nooa for teaching me what is really important in life and for reminding me every once in a while to distance myself from this thesis.

Nokia, 1.3.2016

Table of Contents

List of original publications

This thesis is based on the following original publications that are referred as Study I-IV in the text. The publications are reprinted with permissions from the publishers.

I. **Kujala K**[#], Ahola A, Pekkanen-Mattila M, Ikonen L, Kerkelä E, Hyttinen J, Aalto-Setälä K. Electrical Field Stimulation with a Novel Platform: Effect on Cardiomyocyte Gene Expression but not on Orientation. **International Journal of Biomedical Science** 2012 Jun;8(2):109-20.

II. **Kujala K**[#,*], Paavola J[*], Lahti A, Larsson K, Pekkanen-Mattila M, Viitasalo M, Lahtinen AM, Toivonen L, Kontula K, Swan H, Laine M, Silvennoinen O, Aalto-Setälä K. Cell Model of Catecholaminergic Polymorphic Ventricular Tachycardia Reveals Early and Delayed Afterdepolarizations. **PLoS One** 2012 Sep 4:7(9):e44660 [**]

III. **Penttinen K**[*], Swan H[*], Vanninen S, Paavola J, Lahtinen AM, Kontula K, Aalto-Setälä K. Antiarrhythmic Effects of Dantrolene in Patients with Catecholaminergic Polymorphic Ventricular Tachycardia and Replication of the Responses Using iPSC Models. **PLoS One** 2015 May 8;10(5):e0125366.

IV. **Penttinen K**, Siirtola H, Ávalos-Salguero J, Vainio T, Juhola M, Aalto-Setälä K. Novel Analysis Software for Detecting and Classifying Ca^{2+} Transient Abnormalities in Stem Cell-Derived Cardiomyocytes. **PLoS One** 2015 Aug 26;10(8):e0135806.

[#] Penttinen, née Kujala

[*] These authors contributed equally to this work.

[**] Publication has been previously included in the doctoral dissertation "Aberrant Intracellular Calcium Cycling in the Heart" by Jere Paavola in the Faculty of Medicine, University of Helsinki, Finland, 2014.

Author's contribution

I. The first author designed and performed the cell culture and cell stimulation experiments. The first author analyzed the data and wrote the major part of the manuscript.

II. The first author designed and performed the *in vitro* iPSC and cardiomyocyte culturing and characterizations. The first author performed the Ca^{2+} cycling studies and analyzed and interpreted the data with the other first author. The other first author analyzed the *in vivo* data. Both first authors wrote the manuscript.

III. The first author designed and performed all the *in vitro* cell experiments and analyzed and interpreted the data. The other first author performed and analyzed the *in vivo* data. The first author wrote the major part of the manuscript.

IV. The first author designed and performed all the cell culture experiments and provided the data and analysis criteria for the development of the software. The first author tested and provided the feedback for the software development and compared the analysis efficacy of the software to the manual analysis. The first author wrote the major part of the manuscript.

List of Symbols and Abbreviations

AA	amino acid
APA	action potential amplitude
AFP	α-fetoprotein
AFM	atomic force microscope
AM	acetoxymethyl
ALP	alkaline phosphatase
AP	action potential
APD	action potential duration
APD50	action potential duration at 50 % of the amplitude
APD90	action potential duration at 90 % of the amplitude
ATP	adenosine triphosphate
AVN	atrioventricular node
β-AR	β-adrenergic receptor
bFGF	basic fibroblast growth factor
BMP4	bone morphogenetic protein 4
BPM	beats per minute
BSA	bovine serum albumine
$[Ca^{2+}]_i$	intracellular calcium concentration
calstabin2	FKBP12.6 protein
CaMKII	Ca^{2+}/calmodulin-dependent protein kinase II
cAMP	cyclic adenosine monophosphate
CASQ2	calsequestrin2
cDNA	complementary DNA
CHIR99021	specific glycogen synthase kinase 3 (GSK-3) inhibitor
CICR	Ca^{2+}-induced Ca^{2+} release
CM	cardiomyocyte
CMI	culture medium I
cMyBP-C	myosin biding protein C
c-Myc	myelocytomatosis viral oncogene homolog
CPC	cardiac progenitor cell
CPVT	catecholaminergic polymorphic ventricular tachycardia

CRISPR	clustered regularly interspaced short palindromic repeats
CSFM	complete serum free medium
cTnI	cardiac troponin I
cTnT	cardiac troponin T
Cx-43	connexin 43
DAD	delayed afterdepolarization
DAPI	4’,6-diamidino-2-phenylindole
Dkk1	dickkopf WNT signaling pathway inhibitor
DMEM	Dulbecco’s Modified Eagle -medium
EAD	early afterdepolarization
EB	embryoid body
ECC	excitation–contraction coupling
ECG	electrocardiograph
ECM	extracellular matrix
EFS	electrical field stimulation
END-2	mouse endodermal-like cell line
EpCAM	epithelial cell adhesion molecule
FBS	fetal bovine serum
FP	field potential
FPD	field potential duration
Gata4	GATA binding protein 4
GMT	combination of transcription factors Gata4, Mef2c, Tbx5
GMHT	combination of transcription factors Gata4, Mef2c, Tbx5, Hand2
GSK-3β	glycogen synthase kinase 3β
GTP	guanosine diphosphate
Hand2	basic helix-loop-helix transcription factor
hESC	human embryonic stem cell
HF	heart failure
HL-1	atrial tumor cells
HSA	human serum albumin
I_{CaL}	depolarizing L-type inward Ca^{2+} current
I_{CaT}	T-type Ca^{2+} current
I_f	inward pacemaker current
I_{K1}	inward rectifying potassium K^+ current

I_{Kr}	rapid delayed rectifying K^+ -current
I_{Ks}	slow delayed rectifying K^+ -current
I_{Na}	inward Na^+ current
I_{to}	transient outward K^+ currents
ICD	implantable cardioverter-defibrillators
iCM	induced cardiomyocytes
IP3R	inositol 1,4,5-trisphosphate
Isl1	insulin gene enhancer protein 1
ITS	insulin-transferrin-sodium selenite media supplement
hiPSC	human induced pluripotent stem cell
KDR	kinase insert domain receptor
Klf4	Kruppel-like factor 4
KO	knockout
LIN28	lin-28 homolog A
LQT	long QT syndrome
LTCC	L-type calcium channel
MAP	monophasic action potential
MDP	maximum diastolic potential
MEA	microelectrode array
MEF	mouse embryonic fibroblast
Mef2C	myocyte-specific enhancer factor 2C
Mesp1, 2	mesoderm posterior 1 or 2
MHC α, β	myosin heavy chain (MYH)
MI	myocardial infarction
miRNA	microRNA
MIXL1	homeodomain protein
MLC1, 2	myosin light chain 1, 2
mRNA	messenger RNA
MYH6	myosin heavy chain 6 gene encoding MHC-α
MYH7	myosin heavy chain 7 gene encoding MHC-β
NANOG	Nanog homeobox
NADPH	nicotinamide adenine dinucleotide phosphate
NCAM	neuronal cell adhesion molecule
NCX	Na^+/Ca^{2+} -exchanger

NKX2.5	NK2 transcription factor related gene, locus 5
NEAA	nonessential amino acids
NRC	neonatal rat cardiomyocytes
NSVT	non-sustained ventricular tachycardia
Oct4	octamer-binding transcription factor 4
PC2	polycystin-2
PDE4D3	phosphodiesterase 4D3
PDGFR	platelet-derived growth factor receptor
PFA	paraformaldehyde
PGI2	prostaglandin I2
PKA	protein kinase A
Plat-E	Platinum-E cell line
PLB	phospholamban
PSC/hPSC	pluripotent stem cell/human PSC
PVC	premature ventricular contraction
qPCR	quantitative polymerase chain reaction
Rex1	RNA exonuclease 1
RT-PCR	reverse transcription polymerase chain reaction
RyR2	ryanodine receptor 2
SAN	sinoatrial node
SCD	sudden cardiac death
SCF	stem cell factor
SERCA2a	sarcoplasmic reticulum Ca^{2+} -ATPase
SIRPA	signal regulatory protein-α
SOICR	store overload-induced Ca^{2+} release
Sox1, 2 or 17	sex determining region Y-box 1, 2 or 17
SR	sarcoplasmic reticulum
SSEA3 or 4	stage-specific embryonic antigen 3 or 4
T_3	3,3',5-Triiodo-L-thyronine sodium salt
TALEN	transcription activator-like effector nucleases
Tbx4, 6, 20	T-box transcription factor 4, 6, 20
TGF-β	transforming growth factor β
TNNT1	gene encoding cardiac troponin I (cTnI)
TNNT2	gene encoding cardiac troponin T (cTnT)

TRA1-60	tumor-related antigen 1-60
TRA1-81	tumor-related antigen 1-81
TRDN	triadin
T-tubules	transverse tubules
VCAM	vascular cell adhesion molecule
VEGF	vascular endothelial growth factor
VT	ventricular tachycardia
Wnt	abbreviated combination from Wingless and Integrase-1
WT	wild type
ZFN	zinc finger nucleases

1 Introduction

Cardiac diseases including heart failure (HF) are continuously increasing global health issues that impose a significant medical and economic burden. Currently, cardiac biotechnology is focused on studying the mechanisms, pathophysiology and treatment options of cardiac arrhythmias and diseases as well as the development, physiology and maturity of cardiomyocytes (CMs). Human pluripotent stem cell (hPSC)-derived CMs serve as an important tool in these studies. Other cell and animal models have also been used, but they may fail to recapitulate human physiology. One major problem in culturing hPSC-derived CMs has been the immature phenotype; however, primary CMs have a tendency to dedifferentiate quickly in culture. These limitations interfere with the functional and morphological stability of the cells and are therefore continuously studied by altering and optimizing the culture conditions and environment of the CMs.

Human induced pluripotent stem cells (hiPSCs) (Takahashi et al., 2007; Yu et al., 2007) derived from differentiated somatic cells have a great potential for cardiac research. iPSCs can be differentiated into the desired cell type while retaining the original genotype. Therefore, with this technology, patient-specific stem cell lines and CMs can be created, providing a way to model and study the pathophysiology of various cardiac disorders in human cells. iPSC technology is expected to be utilized in studies of cell development and diseases, in regenerative medicine, in drug-testing platforms and in patient-specific drug therapy optimization. Before iPSCs can be used in clinical applications, these cells need to overcome various challenges. Nevertheless, cardiac disease models and drug testing platforms exploiting iPSC technology have already been established by several research groups with some promising results (Caspi et al., 2009; Moretti et al., 2010; Braam et al., 2010; Itzhaki et al., 2011b; Yazawa et al., 2011; Jung et al., 2012; Itzhaki et al., 2012), including the results presented in this thesis.

The main objective of this work was the development and functional characterization of cardiac cell models. In addition, techniques to improve electrical field stimulation (EFS) and to analyze the calcium (Ca^{2+}) cycling of CMs were developed. Neonatal rat cardiomyocytes (NRCs) were exposed to EFS to study the morphological and functional properties of these cells using a novel EFS platform. An *in vitro* cell model for catecholaminergic polymorphic ventricu-

lar tachycardia (CPVT), a potentially lethal inherited cardiac syndrome, was generated with iPSC-derived CMs generated from CPVT patients carrying cardiac ryanodine receptor gene (*RyR2*) mutations. With these CMs, the mechanisms of arrhythmias, the role of intracellular Ca^{2+} cycling and mutation-specific differences in intracellular Ca^{2+} cycling were studied. Mechanistic insights regarding CPVT arrhythmias in iPSC-derived CMs were also studied in the index patients. The antiarrhythmic potential of dantrolene, an inhibitor of Ca^{2+} release from the sarcoplasmic reticulum (SR), was assessed in the clinical treatment of CPVT patients carrying various *RyR2* mutations, and results were compared to *in vitro* studies using iPSC-derived CMs generated from the same patients. Additionally, Ca^{2+} cycling analysis software was developed to analyze the abnormal intracellular Ca^{2+} cycling of these CMs.

In this thesis, molecular and cellular research exploiting iPSC-derived CMs is compared to clinical patient data to provide important insight regarding how these cells resemble the clinical phenotype of the patients. This relationship has not yet been widely shown by others, and this report is the first to demonstrate mutation-specific differences both in patients and in iPSCs. Most importantly, these studies will help to translate insights gained in basic research to benefit patients in clinical practice. Additionally, because the abnormal Ca^{2+} transients in CPVT resemble those observed in patients with HF, the results of our studies could be beneficial for other patients in addition to CPVT patients.

2 Literature review

2.1 Human heart and cardiomyocytes

The heart is a muscular organ that pumps blood to all the tissues in the body through a network of blood vessels. The heart consists of four chambers, namely, the right and left atria and ventricles (Figure 1), as well as four heart valves, which control blood flow from the atria to the ventricles and out of the ventricles. The endocardium is the inner layer of the heart and is composed of endothelial cells, which provide a smooth, non-adherent surface for the pumping blood. The myocardium is the muscle tissue of the heart and is composed of CMs, which are able to contract and to conduct electricity. The epicardium is a thin layer that consists of connective tissue and fat, which protect the heart. The pericardium is a fibrous connective tissue layer that covers the heart. The sinoatrial node (SAN) in the right atrium generates impulses to initiate heart contractions, and the atrioventricular node (AVN) between the atria and ventricles conducts impulses from the atria to the ventricles (Figure 1). These nodes consist of self-excitatory pacemaker cells (Figure 1) that, together with electrical conducting cells, are called nodal cells. Electrical conducting cells deliver the cardiac current from the SAN to the distant regions of the heart. (Katz, 2006; Thaler, 1999)

The adult human heart is composed of 30% CMs (atrial, ventricular and nodal cells) and 70% non-myocytes, mainly fibroblasts but also vascular cells such as smooth muscle and endothelial cells (Figure 1) (Porter and Turner, 2009). Cardiac fibroblasts are responsible for homeostatic maintenance of extracellular matrix (ECM) in the normal heart. Cardiac ECM is composed of fibrillar collagens I (80%) and III (10%), with smaller amounts of collagens IV, V, VI; elastin; laminin; proteoglycans; glycosaminoglycans; growth factors and proteases. (Brown et al., 2005) A population of cardiac stem cells called cardiac progenitor cells (CPCs) have also been identified in the hearts of several species; however, the origin of these cells is unclear. They compose less than 1% of the cells in the heart and may be able to differentiate into fully mature CMs. (Bollini et al., 2011; Henning, 2011)

CMs are cylindrical and striated cells that are approximately 10-20 μm in diameter and 100 μm in length; these cells can have multiple centrally located, slightly elongated nuclei. CMs can

be branched and connected to adjacent CMs along the longitudinal axis through the intercalated discs (Figure 1). Intercalated discs include the following components: 1) desmosomes, which help to resist shearing forces of contractions; 2) adherens junctions, which serve as attachment points for the actin filaments of terminal sarcomeres, and 3) gap junctions formed by connexins, which function in ion transport between adjacent CMs. (Katz, 2006; Sarantitis et al., 2012)

Sarcomeres are responsible for the contraction of the CM, and the sarcomeric cytoskeleton consists of thin actin filaments and thick myosin filaments (Figure 1). Sarcomeres are approximately 2.2 μm long during relaxation and 1.6 μm during contraction and are connected serially to form a myofibril. The thin filaments consist of cardiac actin, α-tropomyosin and C-, I- and T-troponin subunits. Thick myosin filaments are found among the actin filaments, and each actin monomer has a binding area for myosin to allow the contraction of the sarcomere. The thick filaments consist primarily of myosin and C-, H- and X-myosin binding proteins. The myosin binding protein C (cMyBP-C), which has structural and regulatory characteristics, plays the most important role. Myosin molecules may be divided into two similar heavy chains (MYH6 and MYH7 genes which enccodes α-MHC and β-MHC) and two pairs of light chains (MLC1 and MLC2). (Katz, 2006; Sarantitis et al., 2012)

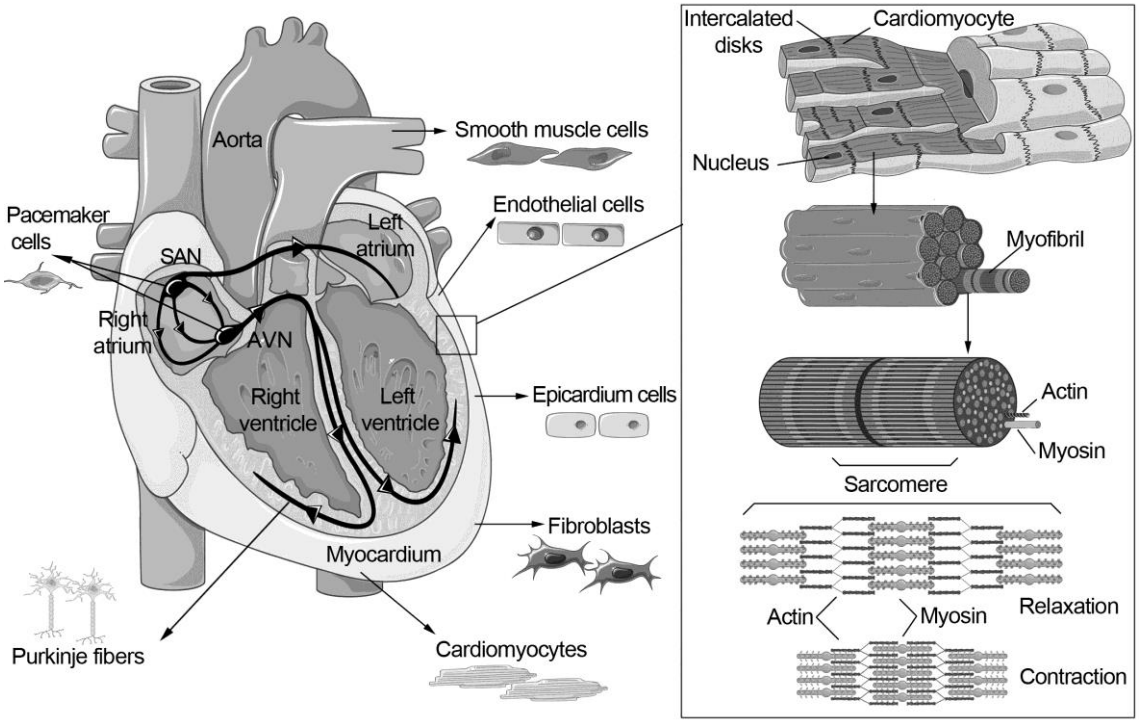

Figure 1. Structure and cell types of the human heart. Cardiac muscle is composed of CMs, which are composed of myofibrils that form the highly organized alignment of sarcomeres. Actin and myosin filaments form the sarcomere structure, which is responsible for the contraction and relaxation of the entire CM. The figure depicting collage is modified from (Xin et al., 2013).

2.2 Electrophysiology of the heart and cardiomyocytes

2.2.1 The cardiac action potential

In excitation–contraction coupling (ECC), the electrical excitation of a CM is translated into mechanical contraction. Continuous cardiac contraction is based on the generation of cyclic action potentials (APs) in the heart. APs result from the transfer of various ions between the outside and inside of the cell through specialized ion channels, which results in changes in the membrane potential. (Grant, 2009) As the membrane potential reaches a certain threshold, ion channels open or close. The direction of the ion currents in or out of the cell is determined by the electrochemical gradient of the corresponding ions. The current amplitude depends on the membrane potential and on the conductivity of the responsible ion channels. (Amin et al., 2010; Bers, 2002)

The AP initiates by the spontaneous excitation of nodal cells in the SAN located in the right atrium. The AP depolarizes adjacent atrial CMs by traveling through the intercellular gap junctions, ultimately resulting in excitation of the atria. The AP propagates via the AVN between the atria and the ventricles and then along Purkinje fibers to the ventricles, where ventricular CMs are depolarized, resulting in excitation of the ventricular myocardium. The shape and duration of the AP varies between nodal, atrial and ventricular CMs because of different ion channel expression (Figure 2). (Amin et al., 2010; Bers, 2002)

The AP is divided into four phases, which are each characterized by tightly controlled ion currents (Figure 2). During phase 4, also called the resting phase, the resting potential of atrial and ventricular myocytes is stable and negative (approximately -85 mV). The negative resting potential results primarily from an inward rectifying potassium (K^+) current (I_{K1}), where K^+ ions flow out of the cell (Figure 2). When an AP reaches the cell, voltage-gated sodium (Na^+) channels open and permit an inward Na^+ current (I_{Na}), which increases the membrane potential and partly depolarizes the cell (phase 0, Figure 2). Simultaneously, the inward rectifying K^+ channels close, which also closes the voltage-gated Na^+ channels and briefly opens transient K^+ channels. The movement of positively charged K^+ ions from the intracellular to the extracellular space results in transient outward K^+ currents (I_{to}), in which the transmembrane voltage decreases and causes early repolarization (phase 1, Figure 2). The plateau phase of the AP (phase 2) results from a balance between the depolarizing L-type inward Ca^{2+} current (I_{CaL}) through voltage-dependent L-type Ca^{2+} channels (LTCCs), and the repolarizing rapid (I_{Kr}) and slow (I_{Ks}) delayed rectifier outward K^+ currents (Figure 2). Phase 2 is absent in nodal cells. At phase 3, LTCCs close while I_{Ks} remain open, and more K^+ channels (I_{Kr} and I_{K1}) open, resulting in K^+ efflux (Figure 2) through the I_{K1} channels, which causes rapid repolarization. When the membrane potential is restored to -85 mV, the delayed rectifier K^+ channels close. Simultaneously, I_{K1} continues passing K^+ ions out of the cell throughout phase 4, which helps to set the resting membrane potential; this potential is also sustained by the sarcolemmal Na^+/Ca^{2+}-exchanger (NCX). In contrast to atrial and ventricular CMs, in nodal CMs, the inward pacemaker current (I_f) and the absence of I_{K1} enable slow depolarization of the resting potential during phase 4. Additionally, in nodal cells, AP depolarization is mainly achieved by I_{CaL} and the T-type Ca^{2+} current (I_{CaT}) (Figure 2). (Amin et al., 2010; Bers, 2002)

AP duration (APD) or phases can be altered by Ca^{2+} ion movements that affect the membrane potential. APD can be prolonged when NCX operates in forward mode by receiving three

Na^+ ions and removing Ca^{2+} ions by creating a positive depolarizing inward current. In return, cell repolarization and APD shortening occur if NCX operates in reverse mode by removing three Na^+ ions for every entered Ca^{2+} ion. For this reason, an increase in the intracellular Ca^{2+} concentration ($[Ca^{2+}]_i$) will usually increase APD. (Casini et al., 2009) High $[Ca^{2+}]_i$ can also increase I_{Ks} and shorten APD, cause a decrease in the maximal upslope velocity of the AP in phase 0 by reducing I_{Na}, and decrease the conduction velocity of APs between cells by closing gap junctions. In addition, it can inactivate LTCC, thus shortening APD. (Laurita and Rosenbaum, 2008; Peracchia, 2004)

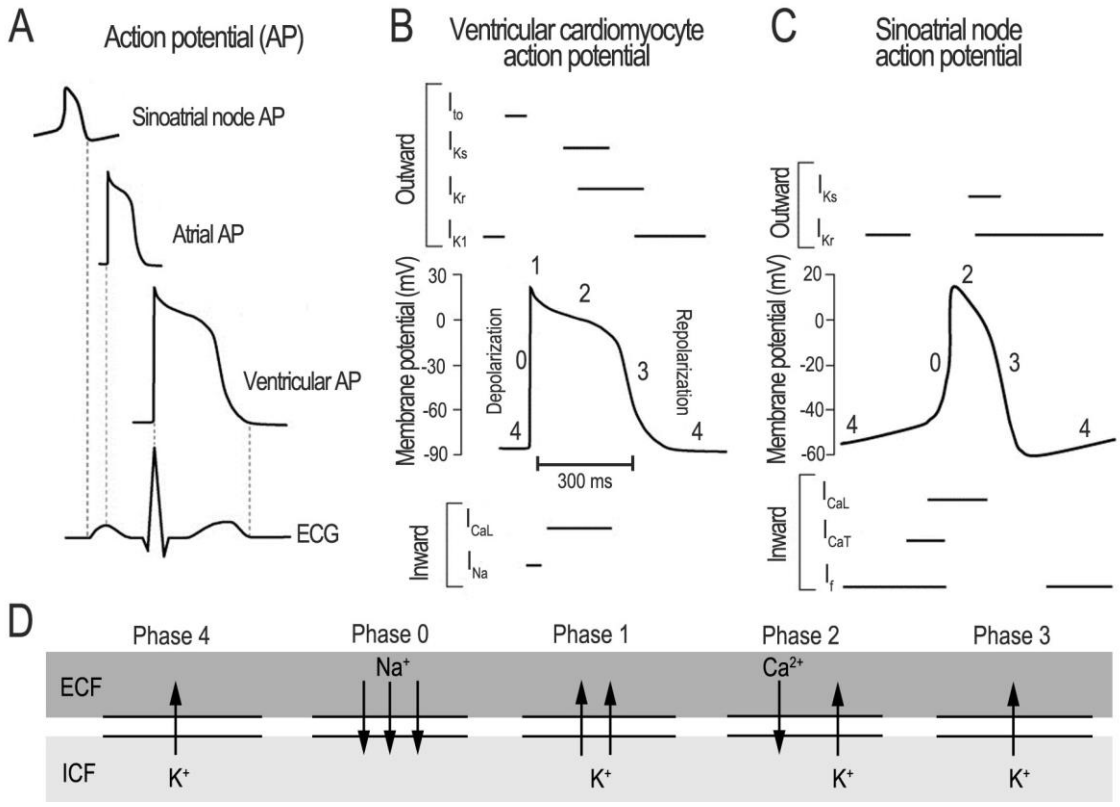

Figure 2. Cardiac APs and electrical activity. A) APs of CMs from different cardiac regions and their correspondence to the clinical electrocardiograph (ECG). Inward and outward currents during different phases of AP in B) ventricular CMs and C) in sinoatrial nodes. D) Active ion movements during different phases of AP in ventricular CMs. ECF, extracellular fluid; ICF, intracellular fluid. Parts A-C are modified from (Amin et al., 2010), and part D is modified from the image at http://www.pathophys.org/physiology-of-cardiac-conduction-and-contractility/.

2.2.2 Calcium cycling

Myofilament activation and cardiac contraction during systole are controlled by cytosolic Ca^{2+} ions. Thus, strict regulation of intracellular Ca^{2+} fluxes is critical for normal cardiac function and mishandling of Ca^{2+} is a central cause of both contractile failure and pathophysiological arrhythmias. (Bers, 2002; Neef and Maier, 2013)

During the plateau phase of an AP, membrane depolarization causes the opening of LTCC and influx of a small amount of Ca^{2+} ions from the extracellular space into the cytosol. This influx subsequently triggers the opening of the SR Ca^{2+} release channel cardiac ryanodine receptor (RyR2) and causes a much greater amount of Ca^{2+} ions being released rapidly from the SR into the cytosol (Figure 3). This entire process is called Ca^{2+}-induced Ca^{2+} release (CICR). (Bers, 2002; Neef and Maier, 2013) SR Ca^{2+} release during AP is also regulated by intracellular Na^{+} ions (Ramirez et al., 2011). The combination of Ca^{2+} influx and outflux raises the free $[Ca^{2+}]_i$ from diastolic values of 0.1 μmol/l up to systolic values of approximately 1 μmol/l and allows Ca^{2+} to bind to the myofilament protein cardiac troponin C (cTnC) in the sarcomere structures. This binding moves tropomyosin aside, allows the binding between actin and myosin filaments, and switches on the shortening and contraction of the entire sarcomere (Figure 3). (Bers, 2002; Neef and Maier, 2013). Transverse tubules (T-tubules), invaginations of the sarcolemma, have an important role in enabling the rapid communication between the sarcolemma and intracellular structures (Ferrantini et al., 2013). Overall, the cardiac contraction strength can be varied by altering the amplitude or duration of the Ca^{2+} transient and the sensitivity of the myofilaments to Ca^{2+} ions, which is dynamically regulated by a number of processes, including Ca^{2+} binding to TnC and de-inhibition of actin-myosin interactions by the thin filament and actin-myosin cross-bridge properties (Venkataraman et al., 2013). Myofilament sensitivity can be enhanced by caffeine or certain inotropic drugs; dynamically affected by stretching the myofilaments; or reduced by acidosis, elevated phosphate and magnesium (Mg^{2+}) concentrations, or adrenergic stimulation. (Bers, 2002; Neef and Maier, 2013) Myofilament Ca^{2+} sensitization has been reported to increase the susceptibility to ventricular tachycardias (VT), and this sensitization is partially due to decreased phosphorylation of cardiac troponin I (cTnI) (Huke and Knollmann, 2010).

For relaxation to occur, Ca^{2+} ions have to be dissociated from cTnC and removed from the cytosol to lower $[Ca^{2+}]_i$. The main mechanisms for this removal are Ca^{2+} reuptake into the SR via SR Ca^{2+}-ATPase (SERCA2a) and Ca^{2+} removal through NCX, which removes one Ca^{2+} ion

in exchange for three Na^+ ions (Figure 3). SERCA2a accounts for approximately 70% and NCX approximately 28% of total Ca^{2+} removal from cytosol. Other rather slow pathways include mitochondrial Ca^{2+} uniport and sarcolemmal Ca^{2+}-ATPase, accounting for approximately 2% of total Ca^{2+} removal. CMs contain an abundance of mitochondria, many of which are near SR Ca^{2+} release sites. (Bers, 2002; Neef and Maier, 2013) Mitochondrial Ca^{2+} is an important regulator of cell metabolism and survival. Mitochondria can influence Ca^{2+} cycling indirectly by changing the concentrations of adenosine triphosphate (ATP), nicotinamide adenine dinucleotide phosphate (NADPH), pyruvate and reactive oxygen species. This change in concentration causes Ca^{2+} buffering, release from internal stores, influx from the extracellular solution, uptake into cellular organelles and extrusion by plasma membrane Ca^{2+} pumps. Mitochondria can directly influence the $[Ca^{2+}]_i$ of the cell by importing Ca^{2+} via the mitochondrial Ca^{2+} uniporter or transporting Ca^{2+} from the interior of the organelle into the cytosol. As a Ca^{2+} buffering system, mitochondria usually display fast Ca^{2+} uptake followed by slow Ca^{2+} extrusion. Mitochondria are thought to be capable of regulating all components of the Ca^{2+} signaling machinery, including Ca^{2+} release via inositol 1,4,5-trisphosphate (IP3R) and RyR, Ca^{2+} influx via store-operated channels, Ca^{2+} uptake and Ca^{2+} extrusion. (Walsh et al., 2009)

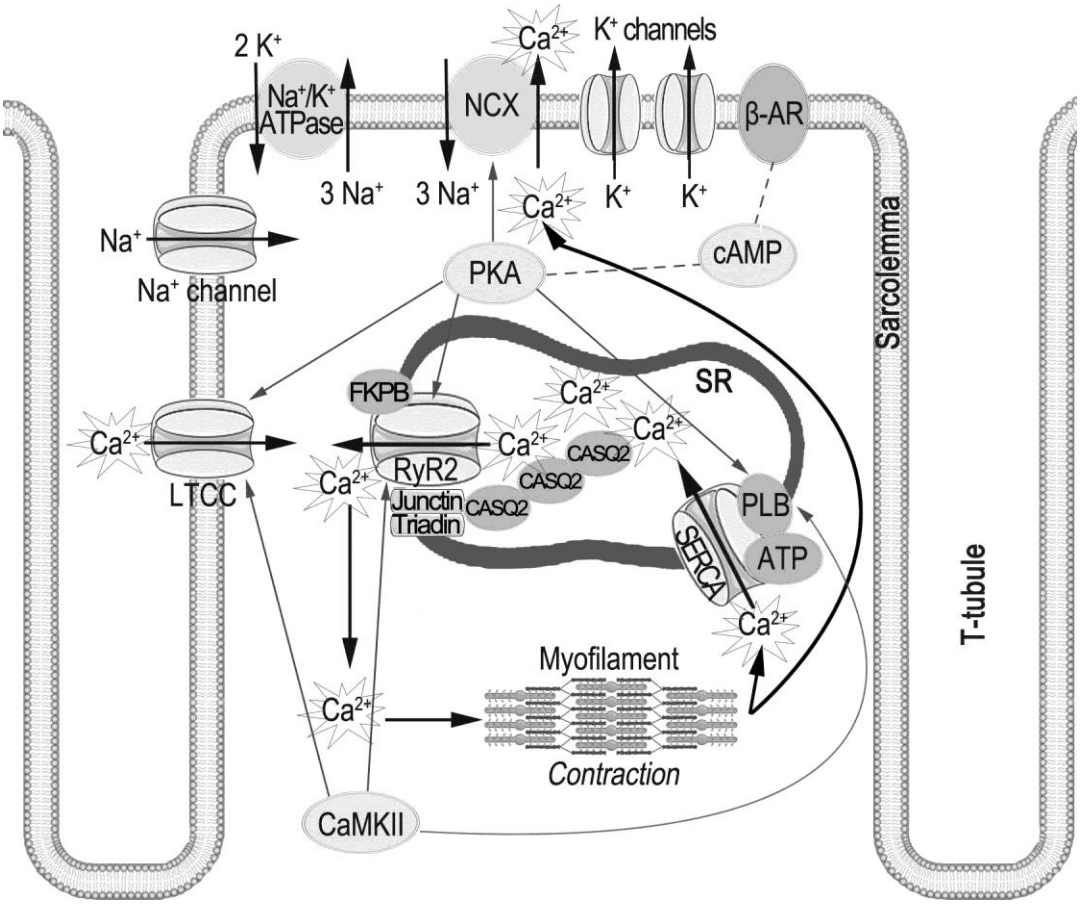

Figure 3. Black arrows allocate the Ca^{2+} cycling in a CM. Gray arrows show the main signaling proteins that affect Ca^{2+} cycling. Abbreviations: L-type Ca^{2+} channel (LTCC), Ca^{2+}/calmodulin-dependent protein kinase II (CaMKII), sodium-calcium exchanger (NCX), calstabin2/FKBP12.6 (FKPB), protein kinase A (PKA), cardiac ryanodine receptor (RyR2), cardiac calsequestrin (CASQ2), sarcoplasmic reticulum Ca^{2+} ATPase (SERCA2a), phospholamban (PLB), cyclic adenosine monophosphate (cAMP), sarcoplasmic reticulum (SR), β-adrenergic receptor (β-AR), transverse tubule (T-tubule). Modified from http://physiologyonline.physiology.org/content/23/1/6/F1 and (Priori and Chen, 2011).

2.2.3 Cardiac ryanodine receptors and intracellular Ca^{2+} release

RyR2 is a large homotetrameric ligand-gated SR Ca^{2+} release channel and a scaffolding protein. This protein is composed of four pore-forming monomers and is often complexed with several accessory proteins. RyRs are arranged in large organized arrays, which are up to 200 nm in diameter, with more than 100 RyRs. The RyR2 monomer contains almost 5000 amino acids and is organized as a series of discrete domains. It has a relatively small carboxyl (C)–terminal, a

transmembrane domain, which crosses the SR membrane. The larger part of the protein (~90%), the N-terminal domain, is in the cytosol between the SR and T-tubule membranes beneath LTCC channels. (Bers, 2002; Camors and Valdivia, 2014)

The cytoplasmic N-region of RyR2 contains multiple regulatory domains, including Ca^{2+} activation and inactivation sites and binding sites for energy sensors (such as ATP), inorganic phosphate, metabolites (such as pyruvate), and ions (such as Mg^{2+}). This region also harbors multiple phosphorylation epitopes and can therefore integrate different cytosolic signals such as Ca^{2+} fluctuations or adrenergic stimulation and transduce these signals to the channel pore to release appropriate amounts of Ca^{2+} ions. Ca^{2+} release is also influenced by intra-SR factors such as Ca^{2+} content and protein interactions and can be regulated by protein–protein interactions when RyR2 binds to smaller and independently regulated accessory proteins. (Bers, 2002; Camors and Valdivia, 2014)

The N-domain of RyR2 is stabilized by the FKBP12.6 (calstabin2) protein, which is essential for receptor closure. The hyper-phosphorylation of RyR2 due to adrenergic stimulation by protein kinase A (PKA) causes calstabin2 dissociation from RyR2, which increases the open probability of RyR2 (Figure 3). This protein also has anchoring sites for regulatory proteins, including calmodulin (inhibits Ca^{2+} release), protein phosphatases 1 and 2A, phosphodiesterase 4D3 (PDE4D3), Ca^{2+}/calmodulin-dependent protein kinase II (CaMKII), S100A1 (regulates RyR2 function) and sorcin (inhibits Ca^{2+} release in a Ca^{2+}-dependent manner). In the C-terminal, at the luminal SR surface, RyRs are coupled to other proteins such as triadin, junctin and calsequestrin2 (CASQ2), which participate in intra-SR Ca^{2+} buffering and modulation of the Ca^{2+} release process (Figure 3). (Bers, 2002; Camors and Valdivia, 2014) Polycystin-2 (PC2), a Ca^{2+}-activated Ca^{2+} channel on the SR membrane, plays an important role in regulating RyR2 function by inhibiting RyR2 channel activity in its open state. PC2 also modulates the channel activity of IP3R, which is a dominant second messenger that leads to the release of Ca^{2+} from SR. (Anyatonwu et al., 2007)

RyR2 is also responsible for Ca^{2+} sparks or spontaneous local Ca^{2+} transients, which reflect the nearly synchronous activation of a cluster of approximately 6–20 RyRs at a single junction. Ca^{2+} sparks SR Ca^{2+} release both at rest and during ECC. During ECC, several thousand Ca^{2+} sparks in each cell are synchronized in time by the AP, making the Ca^{2+} transient appear spatially uniform. Resting Ca^{2+} sparks are normally rare and isolated by the space between couplons but occur when the cellular and SR Ca^{2+} load rise. Then, Ca^{2+} released at one junction can acti-

vate a neighboring junction and lead to propagated Ca^{2+} waves and oscillations. (Bers, 2002; Sauer et al., 2001)

2.2.4 Important signaling proteins related to calcium cycling

ECC is regulated by signaling proteins. PKA is an essential controller of cardiac Ca^{2+} cycling. This protein is activated by adrenergic stimulation, which activates a guanosine diphosphate (GTP)-binding protein through conversion of adenosine triphosphate (ATP) to cyclic adenosine monophosphate (cAMP) (Figure 3). It regulates the effects of catecholamines by phosphorylating key Ca^{2+} cycling proteins, such as RyR2 and LTCC, which leads to increased Ca^{2+}-release into the cytosol. For example, RyR2 phosphorylation can cause the modulation of the channel open probability, leading to increased Ca^{2+} release from the SR to the cytosol. PKA also phosphorylates phospholamban (PLB), which results in accelerated SR Ca^{2+} uptake and increased SR Ca^{2+} loading. Phosphorylation of these proteins increases the heart rate and contractility; therefore, PKA is thought to play a central role in the classic fight or flight response. (Bers, 2002; Neef and Maier, 2013) PKA also phosphorylates myosin binding protein C and cTnI, accelerating the unbinding of Ca^{2+} from cTnC and speeding up the $[Ca^{2+}]_i$ decay and relaxation phase (Li et al., 2000).

CaMKII is another important regulator of Ca^{2+} cycling. CaMKII is activated by a rise in $[Ca^{2+}]_i$, which can be due to reactive adrenergic stimulation (Figure 3). CaMKII phosphorylates RyR2 and increases Ca^{2+} transient magnitude and spontaneous Ca^{2+} release from the SR. CaMKII phosphorylation of PLB prevents its inhibition of SERCA2a, therefore causing SR Ca^{2+} reuptake (Figure 3). CaMKII also phosphorylates LTCC, Na^+ channels, K^+ channels, titin and inositol IP3R. CaMKII is thought to have an important role in the pathophysiology of ECC. Upregulation of CaMKII activity and expression can cause arrhythmias or HF due to the altered cardiac repolarization and Ca^{2+} cycling. (Bers, 2002; Camors and Valdivia, 2014; Neef and Maier, 2013) Inhibition of CaMKII improves cardiac function in HF and may represent a potential novel therapeutic approach of HF and arrhythmias (Sossalla et al., 2010).

2.2.5 Failure of electrical activity and calcium cycling

In the case of ventricular arrhythmias abnormal automaticity and triggered activity of the electrical impulse formation causes early afterdepolarizations (EADs) and delayed afterdepolarizations (DADs). Prolongation of APD can lead to EADs, which are depolarizing oscillations in

membrane potential that occur during repolarization, at phase 2 or 3 of the AP (Figure 4). Electrolyte abnormalities, hypoxia and increased amount of catecholamines may cause EADs, which are also observed in HF. Triggered activity causing EADs may initiate torsades de pointes, a potentially lethal form of VT. At the cellular level, EADs are associated with reduced repolarizing K^+ currents, increased Ca^{2+} current, increased NCX activity, and increased late Na^+ current. EADs are primarily caused by the reactivation of LTCCs, and this reactivation is dependent on the repolarization time. (Volders et al., 2000; Weiss et al., 2010)

DADs are depolarizing oscillations in the membrane potential that follow an AP after completion of repolarization in phase 4 (Figure 4). These oscillations can cause triggered activity if depolarization reaches a threshold and induces an AP (Figure 4). DADs and DAD-induced triggered activity may lead to multiple forms of VT. DADs are associated with high $[Ca^{2+}]_i$, for example, due to catecholamines in CPVT disease. DADs can be a cause of disturbed Ca^{2+} release from the SR, which leads to positive depolarizing inward currents through activation of NCX. (Laurita and Rosenbaum, 2008; Volders et al., 2000)

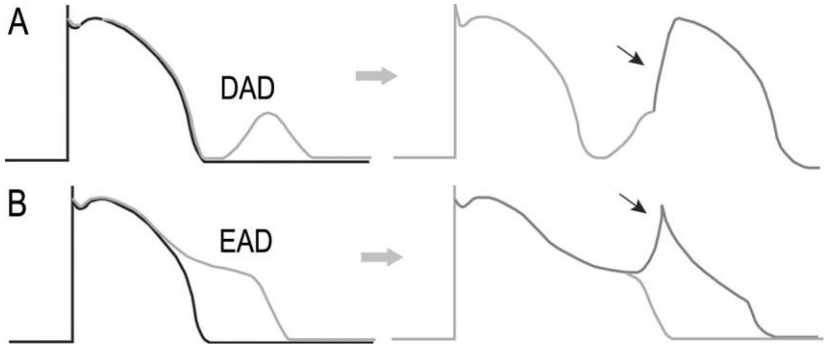

Figure 4. Schematic illustrations of delayed afterdepolarizations (DADs) and early afterdepolarizations (EADs). A) DADs can occur after repolarization (left) and trigger a beat (black arrow, right) if it reaches certain threshold. B) EADs interrupt the repolarization by occurring before the end of the AP (phases 2 and 3) and can lead to the production of a triggered beat (black arrow, right). Figure is modified from (Khan, 2004).

Abnormal Ca^{2+} cycling has been recognized as a key factor behind arrhythmias in the failing heart. In HF, the expression and activity of SERCA2a are often reduced; this reduction is partly counterbalanced by increased NCX activity, causing reduced Ca^{2+} reuptake into the SR. Reduced SR Ca^{2+} content and impaired contractility can cause RyR2 open probability in HF, creating a diastolic SR Ca^{2+} leak that leads to arrhythmias. In addition, PKA and CaMKII have roles

in SR Ca^{2+} leak. (Neef and Maier, 2013) On the sarcomere level, Ca^{2+} leak from the SR has been shown to induce cTnI degradation in skeletal muscle fibers (Li et al., 2009b). Moreover, when studying left ventricular dysfunction of rat hearts, degradation of cTnI has been evident, together with hyperphosphorylation of RyR2, leading to diastolic Ca^{2+} leak (Hall et al., 2005).

High $[Ca^{2+}]_i$ can cause arrhythmias and can alter the expression and activity of different Ca^{2+} cycling proteins. For example, high $[Ca^{2+}]_i$ or spatial heterogeneities in $[Ca^{2+}]_i$ can affect the APD via the NCX. During VT, the rise in the intracellular Na^+ concentration can cause reverse-mode operation of NCX. This action is more rapid than inactivation of LTCC and can therefore cause CICR, which can prolong or aggravate the arrhythmia. In addition, high $[Ca^{2+}]_i$ can cause CaMKII to become particularly activated, which can promote arrhythmias. For example, phosphorylation of LTCCs and Na^+ channels promotes the formation of EADs and exposure to DADs, whereas phosphorylation of RyR2s increases SR Ca^{2+} release and promotes DADs. (Hund and Mohler, 2014; Luo and Anderson, 2013) Dyssyncronous Ca^{2+} release and impaired contractility can cause defective LTCC coupling with RyR2 due to loss of organized T-tubule structure (Song et al., 2006; Wagner et al., 2012).

Arrhythmogenic Ca^{2+} alternans is defined as beat-to-beat alternation of intracellular Ca^{2+} transient amplitude and corresponds to APD alternans (Wang et al., 2014a). Alternans have been thought to be the cause of several, and even contradictory, effects, such as impaired SR Ca^{2+} release (Diaz et al., 2004), slow recovery from RyR2 inactivation (Picht et al., 2006; Restrepo et al., 2008), decreased RyR2 open probability and increased channel refractoriness (Diaz et al., 2002; Xie et al., 2008), increased RyR2 open probability (Lehnart et al., 2006), and weakened SR Ca^{2+} reuptake by SERCA2a (Pieske et al., 1995).

Activation of the SR stress response has been demonstrated to cause mitochondrial dysfunction, triggering oxidative stress and further exacerbating SR stress. Mitochondrial morphology has been shown to be abnormal and ROS generation increased in CPVT compared with wild type (WT) β cells; depletion of SR Ca^{2+} stores due to leaky RyR2 channels reduces glucose-induced mitochondrial Ca^{2+} uptake. These results suggest that chronic SR Ca^{2+} leak triggers SR stress and mitochondrial dysfunction, causing a bioenergetic deficit with decreased ATP synthesis. (Santulli et al., 2015) Mitochondrial Ca^{2+} overload in HF leads to increased production of reactive oxygen species, decreased production of energy, and apoptosis of CMs. (Luo and Anderson, 2013)

2.2.6 Clinical characterization of the electrical activity using ECG and MAP recordings

Electrocardiography (ECG) is a noninvasive clinical recording of the electrical activity of the heart (Figure 5) and is measured by electrodes that are placed on the surface of the body. Normally, 12-lead ECG consists of six precordial leads (V1-6), three limb leads (I-III), and three augmented limb leads (aVR, aVL and aVF). When a wave of depolarization is approaching the positive electrode, a positive deflection occurs on the ECG. The depolarization of the atria results in a P-wave in which the first part corresponds to the right atrial depolarization and the latter part reflects the left atrial depolarization. This atrial depolarization is followed by ventricular depolarization, which is observed on the ECG as the QRS complex. The beginning of the QRS complex reflects the depolarization of the interventricular septum. The latter portion primarily represents the depolarization of the left ventricle because the signal from the right ventricle is covered by the simultaneously depolarizing left ventricle. Atrial repolarization occurs during the QRS complex; however, due to the weakness of the signal, this repolarization is obscured by the electrical activity of the ventricles. The contraction ends by repolarization of the ventricles, which is observed as a T wave on the ECG. Occasionally, the T wave is followed by a small U-wave, which is thought to represent repolarization of the Purkinje fibers and to have the same polarity as the T wave but less than one-third the amplitude of the T wave. (Thaler, 1999)

Monophasic action potentials (MAPs) are extracellularly recorded waveforms from the endocardium and epicardium of the *in situ* beating heart and are therefore suitable for studying the characteristics of local myocardial electrophysiology in a clinical setting. MAPs reflect the repolarization time course of transmembrane APs. MAPs resemble intracellularly recorded AP (Figure 5), and therefore form an important bridge between basic and clinical electrophysiology. APs are recorded with MAP electrode catheters via the femoral vein or artery into the right or left ventricle (Figure 5). Under fluoroscopic guidance, the catheter tip is brought into contact with the endocardium, and APs can be recorded. In clinical settings, MAP recordings can be used to study, for example, the effects of drugs, heart rate and rhythm, and afterdepolarizations, mainly in investigational settings. (Franz, 1999)

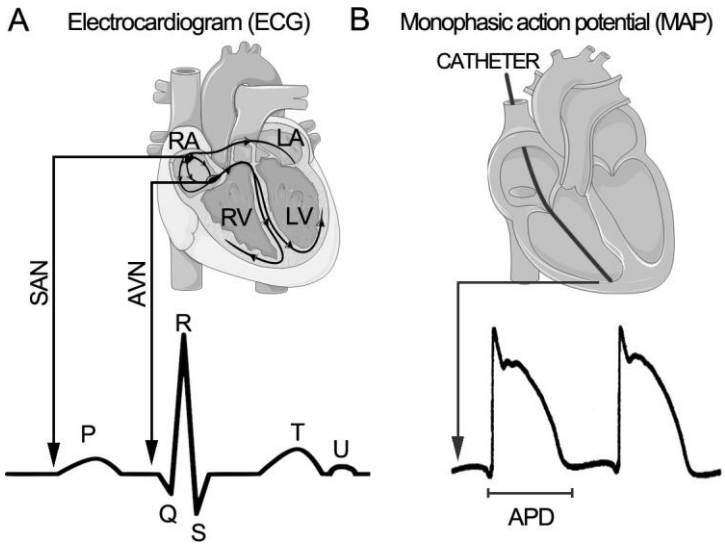

Figure 5. Clinical characterization of the electrical activity of the heart by ECG and MAP recordings. A) Electrical conduction systems of the heart (SAN and AVN), and their corresponding signals on the surface ECG. B) MAP catheter in the right ventricle muscle and the recorded ventricular AP. Figure is modified from (Amin et al., 2010).

2.3 Stem cells

2.3.1 Stem cell renewal and potency

Stem cells are undifferentiated cells and they are capable of self-renewal but can also differentiate into specialized cells. Self-renewal can occur through either symmetrical division, where two identical copies of the original cell are produced, or asymmetrical division, where one daughter cell remains a stem cell and another begins to differentiate toward a certain cell type. (Mountford, 2008; Wolpert et al., 2006)

Stem cell potency defines the cell's ability to differentiate into specialized cell types. The more cell types a cell can differentiate into, the greater its potency is. During the process of stem cell development, the cell gradually loses its differentiation capacity (Figure 6). *Totipotent* stem cells can differentiate into all the cell types of a developing organism, including extraembryonic tissues such as placenta (Figure 6). The only totipotent cells are the fertilized egg and the cells in the embryo until the 8-cell morula stage. After gastrulation, stem cells in the inner cell mass of the blastocyst are *pluripotent* and have the ability to differentiate into cells of the three germ layers, the ecto-, meso-, and endoderm (Figure 6), and these cells are called pluripotent stem

cells (PSCs). (Wolpert et al., 2006; Yamanaka et al., 2008) PSCs can be derived either from a 4-7-day-old blastocyst-stage embryo (Figure 7) (human embryonic stem cells, hESCs) (Thomson et al., 1998) or produced *in vitro* from somatic cells with induction of the expression of genes that are important in embryonic cells (induced pluripotent stem cells, iPSCs) (Takahashi and Yamanaka, 2006; Takahashi et al., 2007; Yu et al., 2007). *Multipotent* or tissue-specific stem cells can only differentiate into a limited number of cell types (Figure 6), usually into the cell types that can be found in the same tissue where the stem cells reside. For example, the bone marrow contains multipotent hematopoietic stem cells that give rise to all the cells of the blood but not to other types of cells. *Unipotent* stem cells can differentiate into only one cell type. For example hepatoblasts, which differentiate into hepatocytes, are unipotent. (Wolpert et al., 2006; Yamanaka et al., 2008)

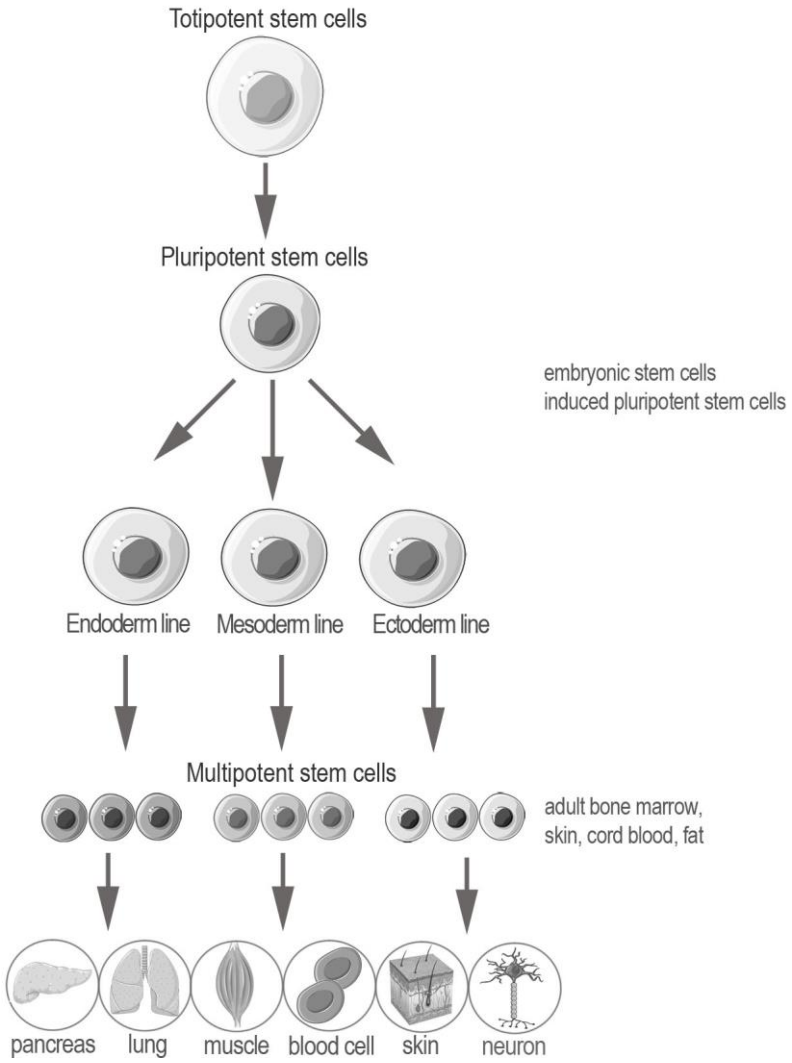

Figure 6. Stem cell potency. During the process of stem cell development, the cell gradually loses its differentiation capacity. Totipotent stem cells can differentiate into all the cell types. PSCs, such as hESCs and iPSCs, have the ability to differentiate in the ecto-, meso-, and endoderm. Multipotent or tissue-specific stem cells differentiate into a limited number of cell types. Figure is modified from the image at http://www.stemcellclinic.com/main-en/klinika/kletochnaya-terapiya/.

2.3.2 Induced pluripotent stem cells

Derivation of the first stable pluripotent hESC lines (Thomson et al., 1998) initiated the widespread research into early human development and regenerative medicine. However, the ethical concerns, limited supply of human embryos and obscurity of the genetic background of the cell lines have been problematic for the application of hESCs. (Yamanaka, 2008) For these reasons

together with the breakthrough insight that somatic cells can be reprogrammed back to PSCs (Figure 7), the discovery of iPSC technology revolutionized the field of biomedical technology (Takahashi et al., 2007; Yu et al., 2007). iPSCs share the characteristics of hESCs, such as pluripotency marker expression and differentiation capacity, as well as a need for supporting matrix. In addition, the cell culture and differentiation methods are similar for both stem cell types (Takahashi et al., 2007).

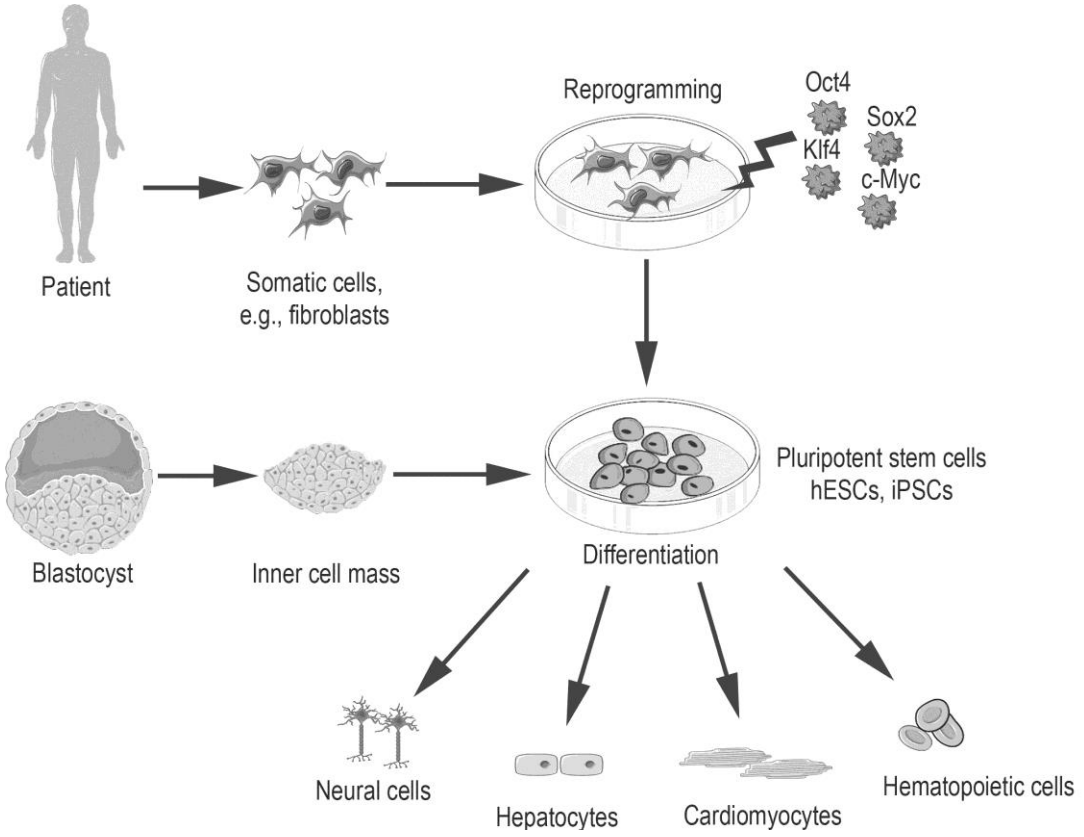

Figure 7. Production of hESCs from the inner cell mass of the early stage embryo blastocyst and of iPSCs from the patient's somatic cells using reprogramming factors. Pluripotent hESCs and iPSCs can be differentiated into various cell types using specific differentiation protocols.

The pioneering work of iPSCs was published in 2006, when the first mouse iPSC lines were generated from mouse embryonic fibroblasts with retroviral transfections (Takahashi and Yamanaka, 2006). The first human iPSCs (hiPSCs) were discovered in two separate studies (Takahashi et al., 2007; Yu et al., 2007). In these studies, human skin fibroblasts were reprogrammed back to a pluripotent state using combinations of retrovirally transfected transgenes of

OCT4 (octamer-binding transcription factor 4), *SOX2* (sex determining region Y-box 2), *c-MYC* (myelocytomatosis viral oncogene homolog) and *KLF4* (Kruppel-like factor 4) (Figure 7) (Takahashi et al., 2007) or of lentivirally transfected factors of *OCT4*, *SOX2*, *NANOG* (Nanog homeobox) and *LIN28* (lin-28 homolog A) (Yu et al., 2007). These genes are involved in maintaining the self-renewal capacity, undifferentiated state, pluripotency and proliferation of PSCs (Takahashi et al., 2007; Yu et al., 2007). Some variations of these gene combinations have been tested for reprogramming. For example, combinations of all six factors, *OCT4*, *SOX2*, *c-MYC*, *KLF4*, *NANOG* and *LIN28*, have increased the reprogramming efficiency (Liao et al., 2008). Reducing the number of reprogramming factors takes advantage of endogenously expressed genes, decreasing the need for ectopic expression of pluripotency factors (Lai et al., 2011). For example, *OCT4* alone has been shown to reprogram human neural stem cells into iPSCs (Kim et al., 2009), and *c-MYC* has been excluded when reprogramming human fibroblasts because these cells express *c-MYC* endogenously (Nakagawa et al., 2008). To date, hiPSCs have been generated from a wide spectrum of somatic cells, including keratinocytes (Aasen et al., 2008), neural stem cells or progenitor cells (Kim et al., 2009), astrocytes (Ruiz et al., 2010), amniotic cells (Li et al., 2009a), adipose tissue (Sun et al., 2009), cord blood cells (Takenaka et al., 2010), T lymphocytes (Seki et al., 2011), skeletal muscle stem cells (Tan et al., 2011), peripheral blood cells (Loh et al., 2010; Staerk et al., 2010), and human urine-derived cells (Zhou et al., 2011).

Originally developed virus-based iPSC technology (Takahashi et al., 2007; Yu et al., 2007) utilizes vectors that can integrate into the genome and that could have harmful consequences, e.g., cell death, residual expression, reprogramming factor re-activation, immunogenicity, uncontrolled transgene silencing, and insertional mutagenesis (Hu, 2014). To overcome these problems, different strategies for iPSC reprogramming have been developed (Figure 8). Transgene reprogramming can be classified into three groups: DNA-based reprogramming, RNA-based reprogramming and protein transduction. Chemical reprogramming with small molecules has also been studied with or without transgene reprogramming (Bayart and Cohen-Haguenauer, 2013; Hu, 2014); for example, the small molecule tranylcypromine and a specific glycogen synthase kinase 3 (GSK-3) inhibitor (CHIR99021), together with *OCT4* and *KLF4* transgenes (Li et al., 2009c), have been used in chemical reprogramming.

DNA-based technologies are the most widely used methods of reprogramming, and they utilize three major forms: virus particles, transposons, and plasmids. Viruses can be retroviruses

(Takahashi et al., 2007), lentiviruses (Yu et al., 2007) or adenoviruses (Stadtfeld et al., 2008), although adenoviruses have not been shown to reprogram human cells. (Hu, 2014) Transposons are mobile genetic elements that can move from one position to another within the genome through an excision/insertion mechanism. For example, a piggyback transposon-based non-viral vector that can induce stable genomic integration and persistent gene expression in mammalian cells quite efficiently has been exploited in iPSC production. (Kaji et al., 2009) Reprogramming plasmids can be linearized to enhance integration into the genome for efficient reprogramming. Non-integrating plasmids include conventional and episomal plasmids, as well as minicircle DNA grouped into plasmids. (Hu, 2014)

Sendai virus is an RNA virus that enables efficient reprogramming of somatic cells and that is already exploited widely in iPSC derivation. It is non-integrating and can therefore be replicated in the host cell cytoplasm without entering the nucleus. (Fusaki et al., 2009) Another non-integrating RNA strategy for iPSC generation is to deliver synthetic messenger RNA (mRNA) encoding reprogramming factors directly into the cells. RNA replicons have also been delivered into cells in the form of packaged virions or as synthetic RNA genomes to avoid the integration of transgenes into the genome. One problem with RNA replicons and Sendai viruses is that they can be converted into complementary DNA (cDNA) by possible reverse transcriptases in the human genome; therefore, they can potentially integrate into the genome. (Hu, 2014) MicroRNAs (miRNAs), short RNA molecules that bind to complementary sequences on messenger RNA and block expression of a gene, have also been used as a reprogramming method. This technique is quite efficient but requires repeated transfection of the miRNAs into the cells (Anokye-Danso et al., 2011; Miyoshi et al., 2011). One method for the generation of transgene-free iPSCs is protein transduction, where reprogramming can be done with mammalian or bacterial recombinant proteins. (Hu, 2014)

iPSCs may hold great promise for regenerative medicine due to the possibility of generating autologic transplantable cells with this technology. iPSC lines generated with methods causing transgene integrations are not applicable for clinical use because of potentially harmful genetic modification. (Ebert et al., 2012) Some studies have also reported substantial differences in genetic or epigenetic profiles of iPSCs versus hESCs, which must be further investigated before therapeutic application of iPSCs in humans (Kim et al., 2010b). Due to these problems, many methods of reduction or complete elimination of transgene integration into genomes have been studied widely. These methods include the use of a polycistron to reduce the number of integra-

tions or the use of the Cre-LoxP system to excise the transgenes (such as lentiviral vectors) from the reprogrammed genome. In addition, transposon transposition of transgenes into the reprogrammed genomes and subsequent excision of transgenes from the reprogrammed genomes have been studied. Repeated transfections of cells with nonreplicating plasmids, the use of non-integrating and replicating episomal plasmids and direct RNA delivery of reprogramming factors (synthetic mRNA, RNA virus, RNA replicon, or miRNA) have also been investigated, and protein transduction and chemical reprogramming methods to eliminate transgene integration into the genome have been studied (Figure 8). (Hu, 2014)

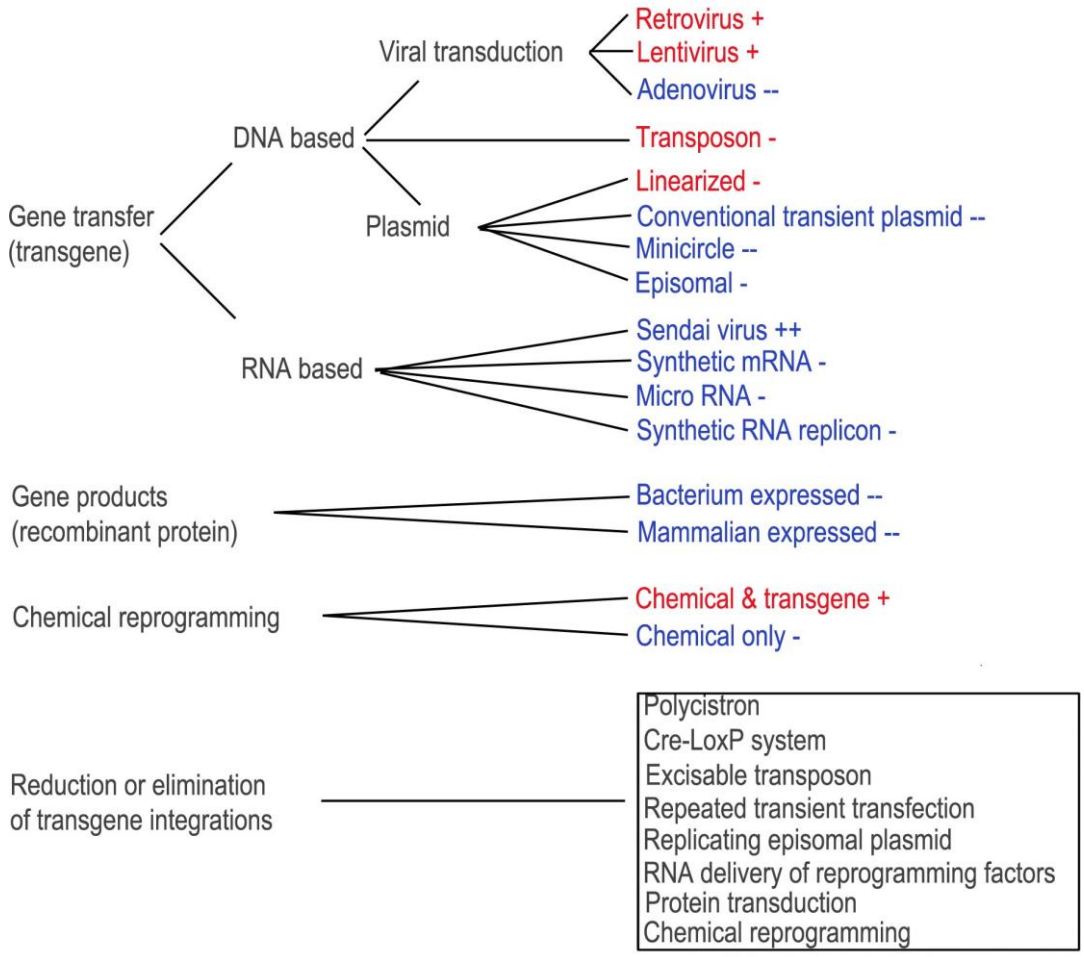

Figure 8. Transgene genome integrating (red) and non-integrating (blue) strategies for iPSC reprogramming and transgene integration reduction methods. The efficiency of each method is categorized as very high (++), high (+), low (-) or very low (--). The figure is modified from (Hu, 2014).

2.3.3 Characterization of induced pluripotent stem cells

iPSCs can be characterized by their morphology because they proliferate in cell culture broadly and form dense colonies with clearly defined edges (Thomson et al., 1998). Despite their clear visual features, the pluripotency of iPSCs must be confirmed using several methods. Teratoma formation is a way to confirm pluripotency by injecting iPSCs into immunodeficient mice to form tumors that include tissues from all three germ layers. *In vitro* differentiation into three-dimensional embryoid bodies (EBs) is another way to characterize the ability of iPSCs to differentiate into cell types of all three germ layers. (Brivanlou et al., 2003; Hoffman and Carpenter, 2005; Thomson et al., 1998) In addition to these methods, pluripotency can be confirmed by studying the expression of genes at the mRNA or protein level. Pluripotency markers that are known to be expressed in iPSCs include Oct4, Nanog, Sox2, RNA exonuclease 1 (Rex1), stage-specific embryonic antigens 3 and 4 (SSEA3 and SSEA4), tumor-related antigens 1-60 and 1-81 (TRA1-60 and TRA1-81) and alkaline phosphatase (ALP). (Adewumi et al., 2007) The expression of the exogenous transgenes in iPSCs must be confirmed and this expression must be fully silenced to demonstrate complete cell reprogramming. (Maherali et al., 2007; Okita et al., 2007) The karyotype of iPSC lines must also be confirmed after the derivation of the lines and repeatedly if the cell lines are kept in culture for longer periods. Telomerase and alkaline phosphate activities are also often studied when pluripotency is evaluated. (Hoffman & Carpenter, 2005).

2.4 Stem cell-differentiated cardiomyocytes and their characterization

2.4.1 Cardiac differentiation

Primary CMs are challenging to obtain from human donors and they easily start to dedifferentiate (Mitcheson et al., 1996). Therefore, primary animal CMs and hPSC-differentiated CMs are widely used for cardiac studies. CM differentiation methods are constantly being improved to increase the differentiation efficiency and the maturation of the hPSC-differentiated CMs. The problems of using these cells compared to primary adult CMs include their immature morphology, structural organization and functionality. (Lieu et al., 2009; Luna et al., 2011) The different cell lines and their differentiation capacities can vary (Osafune et al., 2008; Pekkanen-Mattila et al., 2009), for example, due to epigenetic variation (Kim et al., 2010b).

In vitro differentiation of hPSCs to CMs mimics the stages of embryonic cardiac development. A simplified model of the CM lineage differentiation process and of the transcription factors, cell-surface markers and signaling pathways affecting this process is presented in Table 1.

Table 1. Simplified model shows the differentiation of hPSCs toward the CM lineage and the transcription factors and cell-surface markers identified in this process. Some of the best-characterized signaling pathways that are responsible for the sequential transitions in cell fate are shown. BMP4, bone morphogenetic protein 4; Dkk1, dickkopf Wingless and Integrase-1 (WNT) signaling pathway inhibitor; NKX2.5, NK2 transcription factor-related gene, locus 5; Gata4, GATA binding protein 4; MIXL1, homeodomain protein; Mesp1, mesoderm posterior 1; SSEA, stage-specific embryonic antigen; EpCAM, epithelial cell adhesion molecule; Isl1, Insulin gene enhancer 1; Tbx, T-box transcription factor; NCAM, neuronal cell adhesion molecule; KDR, kinase insert domain receptor; PDGFR, platelet-derived growth factor receptor; SIRPA, signal regulatory protein-α; VCAM, vascular cell adhesion molecule. Table modified from (Mummery et al., 2012).

Signaling pathways	Cell stage	Transcription factors	Cell-surface markers
	hPSC	Oct4, Nanog, Sox2	Tra-1-60, SSEA4, EpCAM
Epithelial-mesenchymal transition	⇩		
	Mesoderm Progenitor	Oct4	NCAM, SSEA1
BMP4, Activin A, FGF2, Wnt3a→ Insulin inhibition→	⇩		
	Precardiac Mesoderm	Brachyury T, MIXL1	
BMP4, Activin A, FGF2, Wnt3a→	⇩		
	Cardiac Mesoderm	Mesp1	KDR, PDGFRα
Dkk1→	⇩		
	Heart Specific Progenitor	Nkx2.5, Gata4 (Tvx5/Isl1/Tbx20)	SIRPA
	⇩		
	Embryonic CM	Nkx2.5, Gata4	SIRPA, VCAM-1

hPSCs can be differentiated into CMs using several techniques. CMs can be derived from hESCs and iPSCs by spontaneous differentiation in EBs, in which cells are cultured in a suspension. Differentiation efficiency has usually been under 10%. (Kehat et al., 2001) The EB protocol has been further tested with different medias such as APEL and STEMPro-34 that include growth factors such as BMP4, basic fibroblast growth factor (bFGF), activin A, vascular endothelial growth factor (VEGF), dickkopf homolog 1 (DKK1), stem cell factor (SCF) and WNT3a (Elliott et al., 2011; Yang et al., 2008). The differentiation process is dependent on the time of addition and on the removal of growth factors. EB formation efficiency has also been enhanced by methods that control EB size. In the spin EB method, hESCs are cultured in a suspension and aggregated by centrifugation to control the aggregate size precisely (Ng et al., 2005). Microfabrication of microwells with defined sizes also provides a way to control the size of the EBs (Khademhosseini et al., 2006), plating cells onto micropatterned ECM (Matrigel) matrix is another option for controlling their size (Bauwens et al., 2008).

hPSCs can be differentiated into CMs by co-culturing stem cells with mouse endodermal-like cells (END-2) in the absence of serum and with ascorbic acid (Mummery et al., 2003; Passier et al., 2005). The role of END-2 cells in this cardiac differentiation method remains unclear; however, the removal of insulin and secretion of prostaglandin I2 (PGI2) by END-2 cells are thought to influence the differentiation process (Xu et al., 2008). Differentiation has also been successful with END-2-conditioned medium instead of co-culturing (Graichen et al., 2008).

Another cardiac differentiation method for hPSCs is monolayer cultures. hESCs are cultured on Matrigel as a monolayer, and activin A and BMP4 induce a cardiogenic fate with a differentiation efficiency of over 30% when used at the beginning of the differentiation protocol (Laflamme et al., 2007). Single-cell dissociated hESCs on Matrigel have been differentiated into CMs with APEL medium containing cytokines such as BMP4, activing A and WNT3a that induce cardiac mesoderm (Ng et al., 2008). In the matrix sandwich differentiation method, hPSCs are differentiated into CMs by layering stem cells that were cultured as monolayers on Matrigel and Matrigel is subsequently overlaid; the matrix sandwich can also be combined with application of growth factors such as Activin A, BMP4 and bFGF (Zhang et al., 2012). Monolayer differentiation methods based on small-molecule activation and canonical Wnt signaling inhibition by treatment with CHIR99021 or IWP2 have been shown to produce high-yield CMs (Lian et al., 2012). CHIR99021 is an aminopyrimidine, which activates Wnt signaling and initiates

mesodermal differentiation by inhibiting glycogen synthase kinase 3β (GSK-3β). After initiation, Wnt signaling is inhibited by some specific Wnt inhibitors (IWP-4, KY02111, XAV939, Wnt-C59), which direct the mesodermal cells toward CMs. (Burridge et al., 2014; Lian et al., 2012; Minami et al., 2012)

In direct reprogramming, transcription factors are used to differentiate cells directly into other differentiated cell types. Direct reprogramming of mouse post-natal cardiac or dermal fibroblasts into functional induced CMs (iCMs) *in vitro* has been achieved by expressing three transcription factors: GATA binding protein 4 (Gata4), myocyte-specific enhancer factor 2C (Mef2c), and T-box transcription factor 5 (Tbx5) (GMT factors) (Ieda et al., 2010). In addition, GMT factors combined with a basic helix-loop-helix transcription factor (Hand2) (GMHT factors) have been able to convert fibroblasts into functional beating iCMs (Song et al., 2012) as well as a combination of miRNAs (Jayawardena et al., 2012). Upon cardiac injury, resident non-myocytes in the murine heart can be reprogrammed into CM-like cells *in vivo* by retroviral delivery of GMT factors (Qian et al., 2012). With human cells, neither GMT nor GHMT have been able to reprogram human fibroblasts into iCMs alone; however, combinations of these factors with other factors have seemed more promising (Fu et al., 2013; Nam et al., 2013; Wada et al., 2013). For example, GHT factors without Mef2C but with myocardin and two muscle-specific miRNAs could reprogram human fibroblasts into iCMs (Nam et al., 2013).

2.4.2 Properties and maturation markers of cardiomyocytes

Functional hPSC-derived CMs can be detected by their ability to form spontaneously beating cells (Kehat et al., 2002; Mummery et al., 2003). Sarcomere markers, myofilament striation detection, myocyte morphology, Ca^{2+} cycling and action potential shape are often characterized (Kehat et al., 2001; Lundy et al., 2013; Pekkanen-Mattila et al., 2009; Radisic et al., 2004) when determining the maturation stage of the cells.

The gene expression pattern of differentiating CMs reflects that of the early embryogenesis, where the first up-regulated genes are primary mesodermal and continue with the activation of the cardiac progenitor genes and the fetal CM genes (Beqqali et al., 2006; Synnergren et al., 2008). Because CMs originate from the mesoderm an early mesodermal marker, Brachyury T, is traditionally used in cardiac cell lineage characterization (Beqqali et al., 2006; Kispert and Herrmann, 1994). Brachyury T belongs to a family of transcription factors that are encoded by the T-box genes and is an endogenous activator of mesodermal genes that are induced by trans-

forming growth factor β (TGF-β) and FGF signaling (Showell et al., 2004). During CM differentiation, several cardiac transcription factor genes are expressed, including Islet-1 (*ISL-1*), mesoderm posterior 1 and 2 (*MESP1* and *MESP2*), *NKX2.5*, *Gata4* and T-box transcription factor 6 (*Tbx6*) (Brand, 2003; Graichen et al., 2008; Yang et al., 2008).

One major challenge in translating hPSC-derived CMs to therapeutic use is that these cells are quite immature when compared to primary adult CMs (Ieda et al., 2010; Qian et al., 2012). Morphologically, these cells are smaller than adult cells, and their intracellular structures are deficiently organized (Luna et al., 2011). Additionally, the lack of clear T-tubules (Li et al., 2013; Lieu et al., 2009; Novak et al., 2012; van den Heuvel et al., 2014), which usually occurs relatively late in mammalian CM development, may affect the fast spread of an electrical signal inside the CMs, causing problems in Ca^{2+} release and contraction of the cell (Ferrantini et al., 2013). Long-term cultivation (80–120 days) of hPSC-derived CMs has been considered one way to achieve the properties of adult CMs because these cells have shown more mature functional and morphological properties following long-term cultivation compared to cells following short-term cultivation of 20-40 days (Lundy et al., 2013). In addition, the modification of functional properties occurring over the maturation process of 15-40 and 50-110-day-old hESC-CMs has been able to be simulated with a computational modeling tool (Paci et al., 2012).

Thus far, no clear agreement exists regarding which marker can accurately track the differentiation status of hPSC-derived CMs. Structural protein cTnT (encoded by the *TNNT2* gene) (Thierfelder et al., 1994) has been widely used in cardiac lineage characterization (Chan et al., 2013; Hazeltine et al., 2014; Kawamura et al., 2013; Park et al., 2014; Rebuzzini et al., 2013), but is also expressed in non-cardiac cells such as smooth muscle cells (Bedada et al., 2014; Lundy et al., 2013). cTnI (encoded by *TNNI1* gene) has been proposed as a good marker for tracking CM maturation (Bedada et al., 2014; Kehat et al., 2001). Nevertheless, in continuously beating hPSC-derived CMs, cTnI was shown to retain a fetal-like state regardless of differentiation conditions and culture duration (Bedada et al., 2014). Cardiac α-actinin has also been used as a marker for a more mature cardiac phenotype (Kehat et al., 2001; Mummery et al., 2003). The structural protein α-myosin heavy chain (α-MHC) is more highly expressed in fast-beating CMs and atrial samples, and this expression increases during the aging process. β-MHC is subsequently expressed at higher levels in ventricular samples. However, a transition in the myosin isoform content in disease complicates its use for lineage or maturation assignment. (Bedada et al., 2014; Nakao et al., 1997; Reiser et al., 2001; Sasse et al., 1993) The cardiac-specific con-

nexin (Cx) proteins of gap junctions (Cx-43, Cx-40 and Cx-45) (Gaborit et al., 2007) are also used as CM markers as well as expression of certain ion channels (Lundy et al., 2013; Sartiani et al., 2007).

2.4.3 Electrical field stimulation of cardiomyocytes

In EFS, cells are imposed to extracellular electric fields that electrically excite active tissue, resulting in transmembrane potential changes. In CMs, this excitation causes a cell to be depolarized on one side and hyperpolarized on the other along the field direction. (Tung and Borderies, 1992) EFS of CMs has been primarily studied with NRCs (Boudou et al., 2012; Chiu et al., 2008; Hirt et al., 2014; Radisic et al., 2004; Sathaye et al., 2006), but has more recently been studied with hESC- and hiPSC-derived CMs (Serena et al., 2009; Chan et al., 2013; Nunes et al., 2013; Xiao et al., 2014; Hirt et al., 2014). Electrical fields have also been used to induce cardiac differentiation of mouse embryonic stem cells (Sauer et al., 1999) and to modify cardiac progenitor cells toward a cardiogenic phenotype (Llucia-Valldeperas et al., 2014).

EFS has been considered an option to generate more mature cardiac constructs by improving contractile and electrophysiological functionality as well as cell alignment and mechanical stability. Previous studies have shown that EFS improves CM functionality (Boudou et al., 2012; Chan et al., 2013; Chiu et al., 2008; Hirt et al., 2014; Miklas et al., 2014; Radisic et al., 2004; Sathaye et al., 2006), for example, by inducing the ECC and amplitude of synchronous contractions (Chiu et al., 2008; Radisic et al., 2004) and by improving the Ca^{2+} cycling of CMs (Chan et al., 2013; Holt et al., 1997). EFS has also been shown to increase the expression of cardiac-specific genes such as MHC and Cx-43 (Au et al., 2009; Barash et al., 2010; Chan et al., 2013; Chiu et al., 2008; Hirt et al., 2014; Miklas et al., 2014; Radisic et al., 2004). Stimulation has also induced cell elongation (Au et al., 2007; Au et al., 2009; Barash et al., 2010; Chiu et al., 2008; Hirt et al., 2014; Radisic et al., 2004) and orientation (Radisic et al., 2004), which has also been enhanced with topographical cues in many studies (Au et al., 2007; Au et al., 2009; Boudou et al., 2012; Chiu et al., 2012). Well-aligned sarcomeres have also been reported as a result of EFS (Hirt et al., 2014; Miklas et al., 2014; Radisic et al., 2004).

In addition to basic commercial and custom-made EFS platforms, different types of 3D stimulation systems and bioreactors that exploit electrical fields have been generated for CM maturation studies and pharmaceutical testing. The effects of stimulation have been studied on the maturation of 3D cardiac constructs composed of biomaterials combined with CMs such as

engineered heart tissues made of fibrinogen or Matrigel (Hirt et al., 2014), migrogrooved collagen-chitosan hydrogels (Chiu et al., 2012), collagen/fibrin 3D matrices (Boudou et al., 2012) and collagen gel around a template suture (Nunes et al., 2013). For high-throughput pharmacological studies, perfusable 3D micro-tissue platforms exploiting EFS have been generated (Agarwal et al., 2013; Xiao et al., 2014), in addition to possibile cyclic stretch (Lu et al., 2013). EFS has also been exploited with disease modeling of iPSC-derived CMs to study the effect of stimulation on the disease phenotype (Siu et al., 2012; Jung et al., 2012; Ji et al., 2013).

2.4.4 Methods to study the functionality of cardiomyocytes

2.4.4.1 Microelectrode array

Microelectrode arrays (MEAs) or multielectrode arrays are platforms than can be used to measure the functionality of electrically active cell aggregates and sheets. These arrays provide platforms for electrophysiological studies of CMs and allow the recordings of the changes in the field potential (FP). FP resembles an ECG measurement (Reppel et al., 2004). The field potential duration (FPD) can be measured from MEA recordings; the FPD correlates closely with the QT interval in the ECG. MEA signals reflect rapid depolarization, a plateau phase, and repolarization of the AP. (Halbach et al., 2006; Meyer et al., 2004)

The MEA platform consists of an MEA plate, which has a cell culture well that allows long-term cell culturing, and electrodes for recording electrical activity. MEA plates are manufactured with different electrode configurations, which can be used for different applications. The contact between the cells and the MEA electrode affects the signal, and current MEA electrodes are not sensitive enough to record signals from single CMs. The MEA method is usually used for cell aggregates or sheets, and it is a rather easy and fast method that is suitable for larger scale screenings.

CMs of various origins have been investigated with MEAs, e.g., NRCs (Berdondini et al., 2005), hESC-derived CMs (Binah et al., 2007; Kehat et al., 2001; Pekkanen-Mattila et al., 2009) and iPSC-derived CMs (Itzhaki et al., 2011a; Itzhaki et al., 2012; Lahti et al., 2012; Mehta et al., 2011). The MEA method has also been used extensively in in vitro drug testing (Braam et al., 2010; Caspi et al., 2009; Liang et al., 2010; Reppel et al., 2004).

2.4.4.2 Patch clamp method

Electrophysiology of single cells can be studied using a patch clamp, which is regarded as the gold standard method of cellular electrophysiology (Hamill et al., 1981; Sakmann and Neher, 1984). With this technique, a cardiac AP can be recorded from a single CM. To measure ion currents, a glass micropipette containing an electrode with ionic solution is brought into tightly sealed contact with the cell membrane. The tight gigaohm seal is formed between the cell membrane and the recording electrode by applying suction to the micropipette. This isolates the membrane patch from the external environment electronically and allows the measurement of changes in the membrane potential or ion channel currents at the level of single cells or even single channels across this patch of membrane. (Molleman, 2002)

Many variations of the patch clamp technique exist. In the whole-cell patch technique, current or voltage changes can be studied. In the voltage clamp method, the ion currents through the membranes of excitable cells are measured, and in the current-clamp method, changes in voltage across the plasma membrane are measured while the current is held constant. Another technique is the perforated patch method, where the cell membrane is ruptured with chemical agents such as amphotericin-B, thus generating many small holes in the membrane. (Hamill et al., 1981; Molleman, 2002) Traditional patch clamp is a very time consuming method, and in recent years, automated planar patch clamp technology has been developed to generate high-quality data with high-throughput capabilities (Milligan and Moller, 2013). Many automated patch clamp platforms have been developed during last years but this method is not yet selective enough to study iPSC-derived CMs accurately.

The patch clamp method have been utilized in studying the maturation of both hESC and IPSC derived CMs (Sartiani et al., 2007; Pekkanen-Mattila et al., 2010; Ma et al., 2011; Lundy et al., 2013). It has also been widely used in disease modeling studies to characterize the phenotype of iPSC-derived CMs (Moretti et al., 2010; Yazawa et al., 2011; Itzhaki et al., 2011a; Novak et al., 2012; Lahti et al., 2012; Jung et al., 2012; Itzhaki et al., 2012; Di Pasquale et al., 2013) as well as drug responses of these cells (Yazawa et al., 2011; Itzhaki et al., 2011a; Itzhaki et al., 2012).

2.4.4.3 Calcium imaging

Ca^{2+} imaging is a technique that quantitatively measures the fast cyclic increases and decreases in $[Ca^{2+}]_i$ which causes the Ca^{2+} transients. The intracellular free Ca^{2+} levels are measured using cytoplasmic Ca^{2+} indicator dyes, which are fluorescent molecules that respond to the binding of Ca^{2+} ions by emitting fluorescent light. (Adams, 2010; Paredes et al., 2008)

Ca^{2+} indicators can be non-ratiometric or ratiometric. Non-ratiometric dyes such as Fluo-4 utilize only one wavelength and are optimal for detecting more than one fluorophore. One advantage of non-ratiometric indicators is that an increase in fluorescence signal can be related directly to an increase in $[Ca^{2+}]_i$. However, fluorescence intensity depends on many factors such as probe concentration and acquisition conditions not related to $[Ca^{2+}]_i$. Ratiometric indicators such as Fura-2 utilize two wavelengths, and the amount of intracellular Ca^{2+} can be determined by the ratio between the two emission amplitudes, which show Ca^{2+} free- and Ca^{2+}-bound -forms of the indicator. The benefit of ratiometric indicators is that those indicators can be calibrated precisely to minimize the problems associated with uneven dye loading, dye leakage, photobleaching and cell volume variability. (Grynkiewicz et al., 1985; Paredes et al., 2008)

Indicator dyes usually contain an acetoxymethyl (AM) ester group, which makes the molecule lipophilic and which allows easy entrance into the cell. Once the indicator is in the cell, esterases cleave off the AM group, the dye is captured inside the cell, and carboxyl groups are exposed, which will be able to bind Ca^{2+}. (Paredes et al., 2008)

Ca^{2+} imaging method have been utilized widely when studying CMs, for example to investigate the basic Ca^{2+} cycling properties and maturity of hESC and iPSC-derived CMs (Itzhaki et al., 2011b; Lee et al., 2011; Lundy et al., 2013). Ca^{2+} cycling of iPSC-derived CMs has also been characterized in disease modeling of long QT syndrome (LQT) (Spencer et al., 2014) and more widely in CPVT disease with Ca^{2+} cycling defects (Di Pasquale et al., 2013; Fatima et al., 2011; Itzhaki et al., 2012; Jung et al., 2012; Zhang et al., 2013). In addition, the drug effects of diseased CMs have been evaluated with this method (Jung et al., 2012; Yazawa et al., 2011).

2.4.4.4 Analysis of the mechanical beating behavior

It has been shown that in addition to defective electrophysiology of a CM, genetic cardiac diseases alter also the mechanical beating behavior, like beating motion or contractile force (Chang et al., 2013; Kiviaho et al., 2015; Lahti et al., 2012). Therefore, novel approaches for analyzing

the mechanical beating of the CMs have been developed. The electrophysiology, contractile force and mechanical beating behavior of a CM are connected, and the comparison of this data has been under investigation.(Laurila et al., 2015)

Mechanical beating behavior can be analyzed with different non-invasive methods. The force exerted by hPSC derived CMs during a contraction has been estimated with a traction force microscopy, where fluorescent beads are embedded in a cell culture substrate. Cell activity can be tracked with optical methods from the displacement of the fluorescent beads due to the cell contraction. (Hazeltine et al., 2012) Atomic force microscopy (AFM), where a small cantilever is brought in contact with the beating CM to measure the vertical movement of the cell membrane, has also been used to measure beating behavior of hPSC derived CMs(Liu et al., 2012). Impedance assays, where cells are seeded on a plate containing electrodes, can detect the beating of CMs indirectly from the varying impedance signal based on mechanical movement of the cells (Peters et al., 2015). The video microscopy is a new and fast method for the analysis of mechanical CM beating behavior. Different light microscopy methods have been published in recent years, which all are based on a video recording of a beating cell or area, which is then analyzed by different computational methods. (Kamgoue et al., 2009; Hayakawa et al., 2012; Ahola et al., 2014; Maddah et al., 2015; Laurila et al., 2015)

2.5 Catecholaminergic polymorphic ventricular tachycardia

2.5.1 Clinical features of CPVT

CPVT is a severe autosomally inherited cardiac disorder that is characterized by physical activity or intense emotion -induced premature ventricular contractions (PVCs) and polymorphic VT in a structrually normal heart (Figure 9). In CPVT, stress-induced release of catecholamines causes dysfunction of Ca^{2+} cycling in CMs, which induces ventricular arrhythmias that can cause ventricular fibrillation. (Coumel et al., 1978; Leenhardt et al., 1995; Swan et al., 1999) In many cases, the first clinical outcome of CPVT is syncope, and spontaneous recovery from the arrhythmia is possible; however, in the worst cases, sudden cardiac death (SCD) can be the first symptom. Approximately 30% of CPVT patients have symptoms even before the age of 10. (Cerrone et al., 2009) The mortality of CPVT can reach 30–35% by the age of 30 years (Swan et al., 1999). CPVT equally affects men and women and the prevalence of the disease is estimated

to be 1:10000 (Liu et al., 2008). Penetrance of CPVT is estimated at 60–70%, and asymptomatic individuals are a minority (Napolitano et al., 2014). However, current insights into disease penetrance and expression are limited.

The diagnosis of CPVT may be challenging because the resting ECG and structure of the heart appear to be normal. Therefore, the diagnosis is frequently missed unless patient undergoes an exercise stress test (Figure 9), or the electrical activity of the heart is continuously monitored, usually for 24 hours with a Holter ECG-device, to catch the ventricular arrhythmias. (Liu et al., 2008) Diagnosis can be complicated due to the variable disease penetrance, the lack of established genotype-phenotype correlations, and the high amount of *de novo* mutations (Leenhardt et al. 2012). Current therapeutic options include beta-antiadrenergic drugs, flecainide ($Na_v1.5$ sodium channel blocker), implantable cardioverter-defibrillators (ICDs) (Leenhardt et al., 2012; Priori et al., 2013; van der Werf and Wilde, 2013) and left cardiac sympathetic denervation (Hayashi et al., 2009; Wilde et al., 2008). However, these treatments often fail to prevent even fatal arrhythmias.

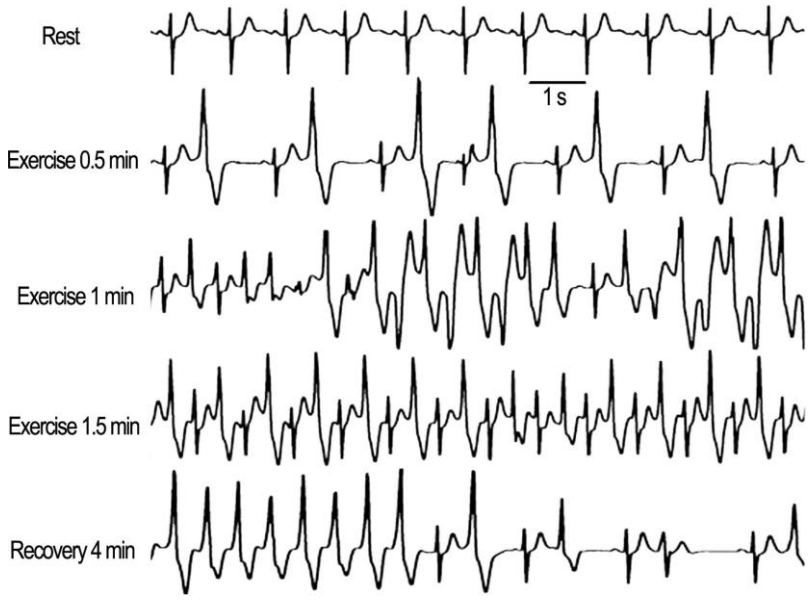

Figure 9. Exercise stress test of a CPVT patient with RyR2 mutation. The occurrence of ventricular arrhythmias increases during exercise but decreases during recovery. Modified from (Liu et al., 2008).

2.5.2 Genetic background of CPVT

Even before CPVT disease was identified and linked to specific genes, several reports introduced patient cases with polymorphic ventricular arrhythmias in the absence of structural heart disease. (Coumel et al., 1978; Leenhardt et al., 1995) In 1999, Swan and his coworkers linked the CPVT phenotype to a disease locus on chromosome 1q42-q43, suggesting an autosomal dominant inheritance pattern of this CPVT form in two Finnish families (Swan et al., 1999). The disease-causing gene on this locus was the *RyR2* gene (Laitinen et al., 2001; Priori et al., 2001). *RyR2* gene mutations are detected in approximately 70% of patients with CPVT, and over a hundred different *RyR2* gene mutations have been identified (Liu et al., 2008; Medeiros-Domingo et al., 2009). The disease-causing mutations are primarily point mutations in which a single nucleotide has changed. Clustering and hotspots of these RyR2 mutations appear to be relatively common in CPVT. RyR2 mutations cluster in four specific regions of the protein (Figure 10) that are on the N-terminal region, calstabin2-protein binding domain, and transmembrane C-terminal domain. However, approximately 24% of mutations occur outside these clusters. (Cerrone et al., 2009; Napolitano and Priori, 2007)

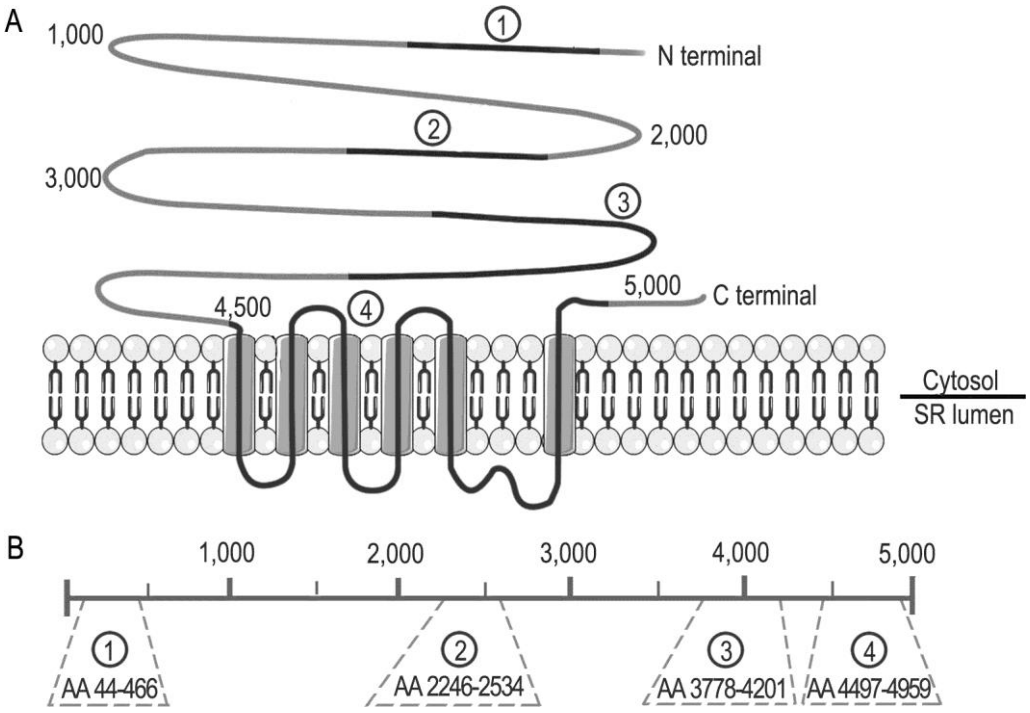

Figure 10. RyR2 mutations cluster in specific regions of the protein. A) Clusters are represented as black lines numbered from 1 to 4. Clusters from 1 to 3 are located in the N-terminal and central regions of the protein, and they form the cytoplasmic domain. Cluster 4 forms the transmembrane domain, which is located in the C-terminal region. B) Cluster 1 includes amino acids (AA) 44-466, cluster 2 AA 2246-2534, cluster 3 AA 3778-4201, and cluster 4 AA 4497-4959. This figure is modified from (Priori and Chen, 2011).

The CPVT phenotype can also be caused by mutations in the *CASQ2* gene in the chromosome 1p13-21 (Lahat et al., 2001). CASQ2 is the major Ca^{2+} storage protein in the SR and is capable of binding luminal Ca^{2+} during diastole to prevent Ca^{2+} precipitation and to reduce the Ca^{2+} concentration (Bers, 2002). *CASQ2* gene mutations have been detected in approximately 3-5% of CPVT patients. These mutations are recessively inherited, and over twenty mutations have been identified, of which half of them are point mutations and half of them are nonsense mutations. (Ackerman et al., 2011; Leenhardt et al., 2012) Mutations in triadin (TRDN), a transmembrane SR protein, and another component of Ca^{2+} homeostasis, have been found to underlie an autosomal recessive form of CPVT (Roux-Buisson et al., 2012). One autosomal recessive form of CPVT in an Arabic family was mapped to chromosome 7p14-p22; however, the disease-causing gene is unknown (Bhuiyan et al., 2007).

2.5.3 Disease pathophysiology

All different CPVT-causing mutations involve proteins associated with intracellular Ca^{2+} release, and it is thought that these mutations result in increased release, or leak, of Ca^{2+} from the SR, which leads to diastolic oscillations of intracellular Ca^{2+}, DADs, and polymorphic VT (Wehrens, 2007). However, the understanding of the detailed pathomechanisms behind these mutations remains incomplete.

In the case of *RyR2* gene mutations, these mutations are thought to lose the capability to control Ca^{2+} release. At the molecular level, three different mechanisms for why RyR2 mutations lead to abnormal diastolic Ca^{2+} release have been hypothesized. (Cerrone et al., 2009) Reduced binding affinity of the RyR2-stabilizing calstabin2 protein has been presumed to be a reason for Ca^{2+} leak. Marx and coworkers suggested that increased dissociation of calstabin2 from RyR2 might cause triggered activity. They stated that mutant RyR2 channels have a weak calstabin2-RyR2 interaction that is further worsened by PKA phosphorylation during adrenergic stimulation (Marx et al., 2000) However, there has also been conflicting evidence that mutant RyR2 can interact normally with calstabin2 at baseline and during adrenergic stimulation (George et al., 2003; Jiang et al., 2005). The complexity of understanding this mechanism has been increased due to new findings, which indicate that SR Ca^{2+} leak is worsened by RyR2 dephosphorylation, which is in conflict with previous studies that implicate increased RyR2 phosphorylation in SR Ca^{2+} leak (Liu et al., 2014). Conflicting results may be the cause of mutation-specific mechanism differences.

One hypothesis implicates defective interdomain interactions as the cause of spontaneous Ca^{2+} leak in CPVT. Unzipping between the N-terminal and central regions of the RyR2 protein can hyperactivate RyR2 and cause diastolic Ca^{2+} leak. (Ikemoto and Yamamoto, 2002) RyR2 mutations may also cause an unstable channel structure through different mechanisms depending on their location (George et al., 2003; Suetomi et al., 2011). This possibility also supports the hypothesis of mutation-specific mechanisms in the molecular pathophysiology of CPVT.

Some studies have suggested that RyR2 and CASQ2 mutations cause the Ca^{2+} release unit to open spontaneously without being triggered by voltage-gated Ca^{2+} influx (Jiang et al., 2002; Priori and Chen, 2011). RyR2 may have increased open probability to luminal or cytosolic Ca^{2+} at a given Ca^{2+} concentration, which can lead to abnormal Ca^{2+} release. This is particularly enhanced under conditions of adrenergic stimulation and is thought to cause spontaneous store overload-induced Ca^{2+} release (SOICR) (Figure 11). (Jiang et al., 2002; Jiang et al., 2005) For

example, activation of β-adrenergic receptors leads to increased expression of cAMP, which activates PKA and leads to phosphorylation of LTCC and PLB. Phosphorylation of LTCC increases Ca^{2+} influx, whereas phosphorylation of PLB relieves its inhibition on SERCA2a and consequently increases SR Ca^{2+} uptake, which may result in SR Ca^{2+} overload and subsequent SOICR. This can activate NCX and thereby generate a transient inward, which can depolarize the surface membrane after the AP is ended and trigger intracellular Ca^{2+} alternans and sudden changes in APD or EADs and DADs (Figure 11). These changes may then trigger premature ventricular beats and ventricular arrhythmias, which are called triggered activity (Figure 11). (Priori and Chen, 2011)

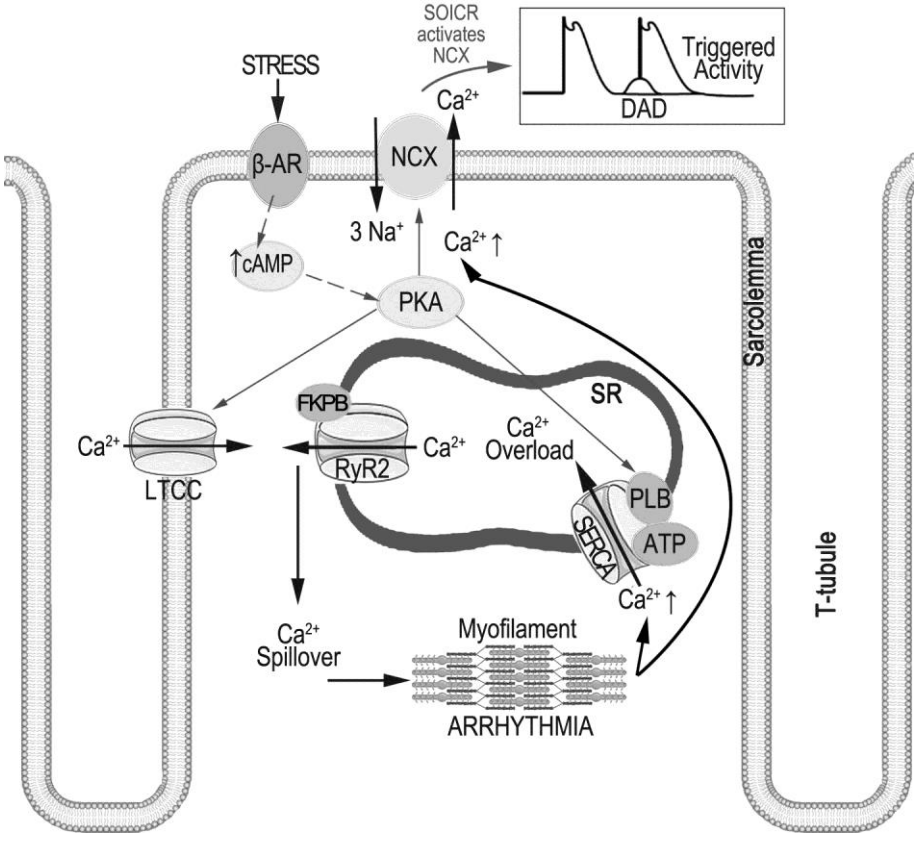

Figure 11. The mechanism of SOICR, in which spontaneous SR Ca^{2+} release or Ca^{2+} spillover occurs under conditions of SR Ca^{2+} overload caused, for example, by stress via the β-AR/cAMP/PKA/LTCC/PLB signaling pathway. SOICR can activate NCX, which can lead to DADs and triggered activities. Modified from (Priori and Chen, 2011).

Mutations in CASQ2 are thought to cause CPVT by several independent mechanisms. CASQ2 may lead to a reduced direct inhibitory effect on RyR2, leading to spontaneous Ca^{2+} release. Other hypotheses are that mutated CASQ2 can result in a loss of Ca^{2+} buffering or that CASQ loss may lead to remodeling of the SR structure and proteins, particularly a reduction of the CASQ2 binding proteins triadin and junctin. Triadin mutations may cause CPVT by an impaired calstabin2–RyR2 interaction or CASQ2 reduction. (Knollmann et al., 2006; Kornyeyev et al., 2012) The absence of triadin has also been linked to CPVT symptoms (Roux-Buisson et al., 2012).

2.5.4 Modeling of CPVT

Although the pathomechanisms of CPVT have been clinically studied in patients with exercise stress tests (Lehnart et al., 2004), genetically engineered mouse models have been of significance to the mechanistic understanding of the disease. Most of the RyR2 mutation-related CPVT studies have been performed in transgenic knock-in mouse models expressing mutations and have shown that Ca^{2+} leaks to the cytosol mediated the arrhythmogenesis (Cerrone et al., 2005; Liu et al., 2006). These models have been pivotal to the understanding of both autosomal-dominant and recessive forms of CPVT. However, the observed phenotypes have not always resembled the human disease (Cerrone et al., 2005; Kannankeril et al., 2006; Liu et al., 2006; Knollmann et al., 2006; Song et al., 2007; Lehnart et al., 2008). CPVT has also been studied by expressing mutations in human embryonic kidney cells (HEK 293) (Jiang et al., 2002; Paavola et al., 2007) and in atrial tumor (HL-1) cells (George et al., 2003). However, these expression systems lack a cardiac intracellular environment that includes accessory proteins and cell structure, which complicate the understanding of how mutations induce cardiac arrhythmias in native CMs.

Different experimental drugs have been tested with CPVT mouse models. The affinity of RyR2 to calstabin2 has been increased with the 1,4-benzothiazepine derivative K201, which has been shown to reduce RyR2 opening and to prevent the onset of arrhythmias in mouse models of CPVT or HF (Wehrens et al., 2004). Treatment with another RyR2-specific compound, the 1,4-benzothiazepine derivative S107, restored the interaction between RyR2 and calstabin2 in a mouse model (Lehnart et al., 2008). The CaMKII inhibitor KN-93 has been able to prevent catecholamine-induced sustained ventricular tachyarrhythmia in RyR2-mutated mouse models both *in vivo* and *in vitro* (Liu et al., 2011). Flecainide has reduced stress-induced arrhythmias in

a CASQ2 knockout mouse model as well in humans (Watanabe et al., 2009). In addition, stabilization of RyR2 by JTV-519 has been shown to reduce CPVT-triggered arrhythmias at the cellular level (Sedej et al., 2010).

Novel iPSC technology has increased the study of CPVT pathophysiology and cardiac arrhythmias in human CM models in recent years. Several groups have reported the generation of CPVT patient-specific iPSCs from individuals carrying a *CASQ2* gene mutation (Novak et al., 2012) and *RyR2* gene mutations (Di Pasquale et al., 2013; Fatima et al., 2011; Itzhaki et al., 2012; Jung et al., 2012; Zhang et al., 2013) with the physiological characteristics of the disease. The similarities and differences in the pathophysiological consequences of RyR2 versus *CASQ2* mutations have also been studied with iPSC-CMs (Novak et al., 2015). In some of these studies, the phenotype of CPVT could be rescued with drugs. These drugs include dantrolene, an inhibitor of Ca^{2+} release through RyR channels (Jung et al., 2012), flecainide, thapsigargin, an inhibitor of the SERCA2a, (Itzhaki et al., 2012) and KN-93 (Di Pasquale et al., 2013).

2.6 The potential use and challenges of iPSC-derived cardiomyocytes in disease modeling and drug screening

Despite the immature nature of iPSC-derived CMs, the possibility of generating disease- and patient-specific CMs with iPSC technology has opened new possibilities for cardiac research. These cells can be used to study the developmental process of the heart as well as to model diseases *in vitro*, studying the basic pathology of cardiac diseases, drug screening, designing personalized medications for patients, and developing and screening new drugs (Figure 12). Previously, non-cardiac human cells, animal cells or transgenic mouse models have been studied to understand the functional changes of genetic mutations identified in patients with inherited diseases. However, these animal organisms or animal cell models do not always demonstrate the same phenotypes as those observed in humans, primarily because of species differences. (Ebert et al., 2012) Additionally, obtaining primary human CMs from cardiac biopsies and maintaining them *in vitro* are challenging (Mitcheson et al., 1996).

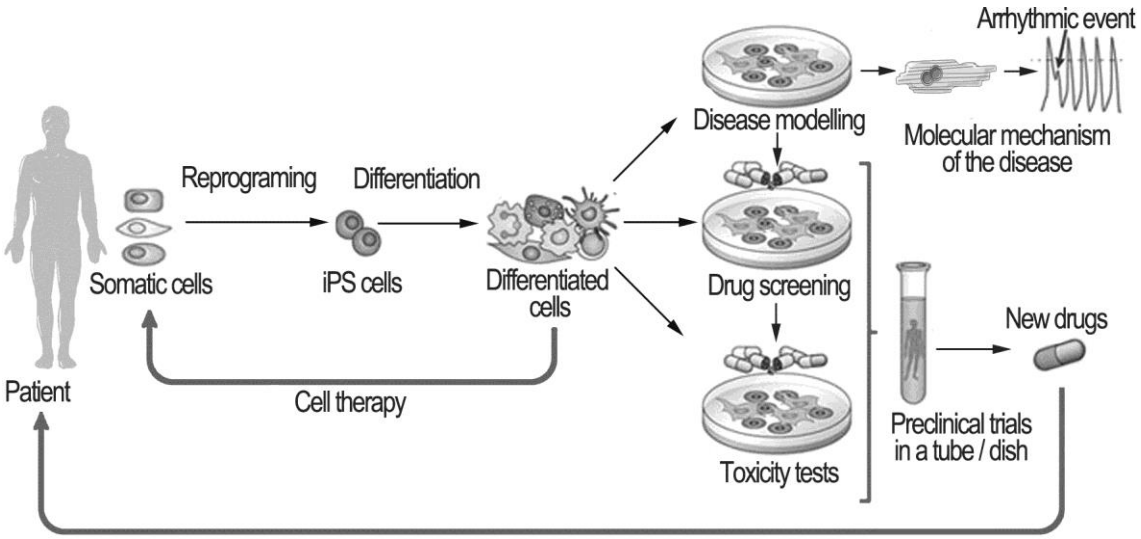

Figure 12. Potential use of iPSC-derived CMs. Figure modified from (Bellin et al., 2012).

After the discovery of iPSC technology, the potential of this technology for creating disease models from patients with complex genetic defects has been studied increasingly. Several genetic diseases have been studied with iPSCs, including hematopoietic, hepatic, endothelial, neurological, and cardiovascular diseases. (Ebert et al., 2012) Disease modelling with iPSCs has been successfully exploited to study multiple cardiac diseases recapitulating the characteristic phenotype of each specific disease: CPVT (Fatima et al., 2011; Jung et al., 2012; Novak et al., 2012; Itzhaki et al., 2012; Zhang et al., 2013; Di Pasquale et al., 2013), LQT1 (Moretti et al., 2010), LQT2 (Itzhaki et al., 2011a; Matsa et al., 2011; Lahti et al., 2012), LQT3 (Ma et al., 2013), dilated cardiomyopathy (Sun et al., 2012), hypertrophic cardiomyopathy (Han et al., 2014; Lan et al., 2013), Timothy syndrome (Yazawa et al., 2011) and LEOPARD syndrome (Carvajal-Vergara et al., 2010).

In addition to disease modeling, iPSC-derived CMs could offer a safe potential platform for cardiovascular drug evaluation for early stage drug screening and pharmacokinetic studies (Figure 12). The heart has been shown to be particularly sensitive to the toxic effects of non-cardiovascular drugs, and several of those types of drugs have been withdrawn from clinical use because they prolonged the QT interval. (Ebert et al., 2012) Prolonged QT intervals and other clinically relevant drug responses have been demonstrated from iPSC-derived CMs with differ-

ent drugs (Itzhaki et al., 2011a; Lahti et al., 2012; Matsa et al., 2011); therefore, iPSC-CMs could also be used in non-cardiovascular drug studies where they could reveal possible cardiac side effects.

The greatest challenges of iPSC technology are related to the safety, efficiency and kinetics of the method, and more knowledge of the reprogramming process is needed. Optimal and efficient non-integrating reprogramming factors need to be found to avoid problems related to genetic alterations, such as risk of mutagenesis and tumors, and possible re-activation of silenced reprogramming genes. Challenges for iPSC technology also include the high costs of iPSC line derivation and culturing, as well as the efficiency of the derivation methods, which would need to be higher for larger scale applications. Especially for clinical cell therapy applications, iPSC derivation and differentiation techniques need to be developed toward xenofree production, and genomic alterations and chromosomal abnormalities during reprogramming and culturing need to be avoided.

The differentiation of CMs from iPSCs has its own challenges, including the efficiency of differentiation, together with complex and expensive differentiation protocols. The epigenetic memory of iPSCs can also influence the differentiation capacity of the cells (Kim et al, 2010b). In addition, cardiac differentiation protocols produce a heterogenous population of CMs and non-cardiac cells, and the sorting and enrichment of CMs is challenging and time-consuming. Currently, all cardiac differentiation methods produce a mixture of all types of cardiomyocytes (ventricular, atrial and conduction types of CMs). Immaturity of iPSC-derived CMs may result in an incomplete phenotype of the cells, which can distort the actual disease characteristics. Immaturity of iPSC-derived CMs has been observed as inadequate sarcomeric structures (Lieu et al., 2009; Luna et al., 2011), changes in ion channel expression (Sartiani et al., 2007), fluctuating electrophysiological properties (Doss et al., 2012), a lack of clear t-tubule structures (Lieu et al., 2009; Novak et al., 2012) and a reduced repolarization reserve (Paci et al., 2014).

3 Aims of the study

The main objective of this work was functional characterization of differentiated CMs and generation of an iPSC-derived CPVT disease cell model to study and characterize the arrhythmic events of these CMs both *in vivo* and *in vitro*. To achieve the main objective, the following specific aims were set:

1. Investigate whether EFS with a novel EFS platform could enhance CM orientation and maturation as well as improve functional properties of NRCs. (Study I)

2. Generate a disease model of CPVT patients carrying a RyR2 mutation with iPSC-derived CMs and clarify the cellular level pathomechanisms of the disease by studying electrophysiology and intracellular Ca^{2+} cycling of these cells. (Studies II-III)

3. Characterize mutation-specific differences of iPSC-derived CPVT CMs and study the antiarrhythmic potential of dantrolene in the treatment of CPVT by assessing the efficacy of intravenously administered dantrolene in patients carrying various RyR2 mutations and compare these effects to *in vitro* studies using iPSC-derived CMs generated from the same patients. (Study III)

4. To analyze Ca^{2+} cycling of iPSC-derived CPVT CMs and abnormal Ca^{2+} transients. (Studies II-IV)

5. To develop and test an automatic Ca^{2+} cycling analysis software tool based on interactive visualization and to compare the results with a visually performed manual analysis. (Study IV)

4 Materials and methods

4.1 Stimulation experiments with neonatal rat cardiomyocytes (I)

4.1.1 Neonatal rat cardiomyocytes

NRCs were harvested from the hearts of 2- to 5-day-old rats' as described previously (Uusimaa et al., 1992). Briefly, the hearts were removed, enzymatically dissociated with collagenase type II and seeded at a cell density of 282 000 cells/cm^2 onto collagen gel or 0.1% gelatin-coated MEA plates. First, cells were cultured in Culture Medium I [CMI, Dulbecco's modified Eagle's medium/Ham's Nutrient Mixture F12 (DMEM/F-12, Sigma-Aldrich, Germany), 10% fetal bovine serum (FBS, Gibco, Finland), 100 IU/ml penicillin/0.1 mg/ml streptomycin (P/S, Gambrex, Belgium), and 2.56 mM L-glutamine (Sigma-Aldrich, Germany)]. After the first day, the cells were precultured in 1 ml of complete serum-free medium [CSFM, DMEM/F-12, 10% bovine serum albumin (BSA, Sigma-Aldrich, Germany), 2.8 mM sodium pyruvate (Cambrex, Belgium), 2.56 mM L-glutamine, insulin-transferrin-sodium selenite media supplement (ITS, Cambrex, Belgium; 1 µM insulin, 5.64 µg/ml transferrin, 32 nM selenium), 100 IU/ml P/0.1 mg/ml S, 0.1 nM 3,3',5-triiodo-L-thyronine sodium salt (T3, Sigma-Aldrich, Germany)] in a 37 °C/5% CO_2 to allow the cells to attach to MEA chambers. The animals were sacrificed according to the guidelines of the Animal Unit, Medical School, University of Tampere, and the Ethical Committee of the Animal Unit has accepted the method to obtain the cells.

4.1.2 Collagen gel

The collagen was isolated from adult Sprague-Dawley rat tails as described previously (Eschenhagen et al., 2002) with some modifications. Briefly, tails were cut into pieces, and the collagen fibers were pulled out and dissolved into 0.1% acetic acid. Then, collagen was precipitated using 25 v-% sodium chloride, the solution was centrifuged, and the collagen pellet was dissolved again in 0.1% acetic acid. The solution was dialyzed at 4 °C to balance the salinity. The concentration of the collagen solution was determined using a Pierce® BCA Protein Assay kit (Thermo Scientific, USA) using BSA as a standard. The gelation of the collagen was performed as described previously (Mather and Roberts, 1998), with two different neutralizing buffers, 12

mg/ml $NaHCO_3$ (Sigma-Aldrich, Germany) in 0.1 N NaOH (Merck, Germany) and 1.3 M NaCl (Baker, The Netherlands) in 0.2 M Na_2HPO_4 (Baker, The Netherlands). The solution was incubated at 37 °C for 30 minutes to allow the gel to form.

4.1.3 Stimulation setup

The stimulation system consisted of electronics for stimulation waveform generation and amplification, a MEA plate container with electrodes, and stimulation software running on a PC laptop. The container was manufactured from polymethyl methacrylate and designed to house six MEA plates. For each MEA plate, stainless steel plate electrodes were placed to generate a homogeneous field for stimulation. The container also included air exchange and water pools to counteract evaporation.

The stimulation system was USB powered, and the electronics of the system were able to create a field strength of at least 5 V/cm with an output frequency ranging from 0.5 to 40 Hz. The shortest pulses capable of being produced were 2 ms wide. The electronics consisted of a single-sided supply operational amplifier circuit, which amplified the signal created by a PC-controlled National Instruments USB-6008 Data Acquisition device and produced voltage-based stimulus. The stimulation voltage and waveforms, frequency, total stimulation time, pulse duration and delays between pulses could be operated by the user. The electrical output of the stimulator was verified with an oscilloscope. In long-term stimulation testing, the effect of the EFS on pH levels of cell culture medium was also studied.

4.1.4 Stimulation protocols

First, cells on gelatin-coated MEA chambers were paced with both monophasic and biphasic pulses at 2.5 and 5 V/cm and frequencies of 1, 2 and 3 Hz with pulse durations of 2 ms, 4 ms and 10 ms to visually confirm the effect of EFS on the cell culture and beating frequency. For long-term stimulation, the cells were precultivated for 48 to 72 h to allow the cells to attach to MEA plates. This precultivation was followed by EFS for an additional 48 to 72 h using either monophasic or biphasic pulses at 5 V/cm or 5.3 V/cm, 2 ms, 4 ms or 200 ms pulse duration and a frequency of 1 Hz. Cell samples cultured without EFS were used as controls. Different stimulation parameters were tested in four different stimulation experiments (n=3-6 per experiment).

4.1.5 Characterization of stimulated cells

Total RNA was isolated from the stimulated cells using a NucleoSpin® RNA II kit (Machery-Nagel, Duren, Germany) and transcribed to cDNA using a High Capacity cDNA Reverse Transcription Kit (Applied Biosystems). The expression levels of β-actin, MYH-6, MYH-7 and Cx-43 were evaluated by PCR. Quantitative RT-PCR (qPCR) was performed according to the standard protocols on an Abi Prism 7300 instrument (Applied Biosystems, Foster City, CA, USA) with the above-mentioned primers.

Stimulated cells were fixed in 4% paraformaldehyde (PFA), stained with the primary antibodies anti-troponin I (Santa Cruz) (1:500) and anti-cardiac troponin T (Abcam) (1:1500) and mounted with Vectashield (Vector Laboratories, USA) containing 4',6-diamidino-2-phenylindole (DAPI) for staining nuclei. Live/dead staining of CMs was performed using a LIVE/DEAD® Viability/Cytotoxity Kit for mammalian cells (Molecular Probes, Inc, Invitrogen) with 0.1 µM calcein AM and 0.5 µM ethidium homodimer-1.

The electrical activity of stimulated and control NRCs was monitored using the MEA system (Multi Channel Systems MCS GmbH, Reutlingen, Germany) before and after the stimulation. The sampling frequency of the MEA measurements was 20 kHz. Measurements were made at 37 °C, and signals were recorded for two minutes via every microelectrode. A Park Systems XE-100 AFM was used to study the surface and electrode wires of the MEA plates.

4.2 Human induced pluripotent stem cell-derived cardiomyocytes (II-IV)

4.2.1 Generation of patient-specific iPSCs (II-IV)

The iPSC study was approved by the ethical committee of Pirkanmaa Hospital District (R08070). Primary fibroblasts for iPSC induction were harvested from skin biopsies of patients and healthy volunteers. The research protocol was approved by the Ethics Committee of the Pirkanmaa Hospital District. All study subjects provided written informed consent. Table 2 summarizes the studied cell lines.

Table 2. iPSC-derived CPVT cell lines used in Studies II-IV; see Figure 10 for RyR2 clusters. *Cell lines generated from the same patient.

Cell line	Mutation	RyR2 cluster	Study
UTA.04602.WT	WT	-	II-IV
UTA.00112.HFF	WT	-	II
UTA.05605.CPVT	exon 3 deletion	1	III, IV
UTA.05203.CPVT*	P2328S	2	II-IV
UTA.05208.CPVT*	P2328S	2	II-IV
UTA.07001.CPVT	T2538R	between 2-3	III, IV
UTA.03701.CPVT	L4115F	3	III, IV
UTA.05503.CPVT	Q4201R	3	III, IV
UTA.05404.CPVT	V4653F	4	III, IV

Patient-specific iPSC lines were established as described previously (Takahashi et al., 2007). Culture medium for primary fibroblasts was composed of DMEM (Lonza, Switzerland) supplemented with 10% FBS (Lonza), 2 mM L-glutamine, and 50 U/mL penicillin/streptomycin. To generate iPSC lines, primary fibroblasts were infected with lentiviruses followed by retroviral infection using 293FT and Platinum-E (Plat-E) cells as packaging cells along with the following plasmids and reagents: pLenti6/UbC/mSlc7a1-vector (Addgene, Cambridge, MA, USA), ViraPower packaging mix (Invitrogen), Lipofectamine 2000 (Invitrogen), pMX retroviral vector (with hOCT3/4/3, hSOX2, hKLF4, or hc-MYC; Addgene), and Fugene (Roche Diagnostics, Mannheim, Germany). The medium for 293FT cells (Invitrogen, Carlsbad, CA, USA) was additionally supplemented with 1% non-essential amino acids (NEAA, Cambrex, NJ, USA). Mouse embryonic fibroblasts (MEFs, Millipore, MA, USA) and Plat-E cells were cultured without penicillin/streptomycin.

4.2.2 Characterization of iPSC lines (II, III)

All the CPVT-iPSC lines were characterized for their karyotypes, mutations, pluripotency, and immunocytochemistry as well as EB and teratoma formation. RT-PCR was used to de-

termine endogenous and exogenous gene expression of the iPSC lines. To study endogenous pluripotency markers at the protein level, 4% PFA fixed iPSCs were stained with at least four primary antibodies directed against the following proteins or antigens: SOX2, NANOG, OCT3/4, stage-specific embryonic antigen (SSEA-4), and tumor-related antigens TRA-1-60 and TRA-1-81.

The presence of heterozygous RyR2 mutations in the CPVT iPSC lines was studied by sequencing or direct RyR2 exon sequencing of PCR-amplified DNA. DNA was isolated using a DNA Tissue XS kit (Macherey-Nagel GmbH & Co., Düren, Germany). The genomic region containing the expected mutation was amplified using PCR. Each PCR product was directly sequenced in both directions using BigDye Terminator v3.1 and an ABI 3730xl DNA Analyzer (Applied Biosystems, Carlsbad, CA, USA). In addition to direct sequencing, exon 3 deletion (1128 nucleotides) was also confirmed using PCR and agarose gel electrophoresis.

Karyotypes of the cell lines were determined using either standard G-banding chromosome analysis (Medix Laboratories, Espoo, Finland) or KaryoLite™ BoBs™ assay (Perkin Elmer) based on BACs-on-Beads™ technology (Molecular and Systems Immunology and Stem Cell Biology, Turku Centre for Biotechnology, University of Turku, Finland).

The expression of markers characteristic of the development of the three embryonic germ layers, ectoderm (*Nestin* or *SOX-1*), endoderm (α-fetoprotein *AFP* or *SOX-17*), and mesoderm (*VEGF-R2*), were studied from EBs maintained in EB medium (knockout (KO)-DMEM with 20% FBS, NEAA, L-glutamine and penicillin/streptomycin) for 5 weeks. The teratoma study was approved by ELLA-Animal Experiment Board of Regional State Administrative Agency for Southern Finland (ESAVI/6543/04.10.03/2011). Nude mice were injected with iPSCs under the testis capsule, and tumor samples were collected eight weeks later, followed by fixation and staining with hematoxylin and eosin.

4.2.3 Differentiation and characterization of cardiomyocytes (II-IV)

iPSC differentiation into CMs was performed by co-culture with END-2 cells. Briefly, undifferentiated iPSC colonies were dissected mechanically into small aggregates and plated on mitomycin C-treated END-2 cells in hESC medium without serum (Mummery et al., 2003; Passier et al., 2005). Differentiation medium was changed on days 5, 8, and 12, and after two weeks,

10% serum was added to the medium. END-2 cells were cultured as described previously (Mummery et al., 1991).

For single cell CM characterization, beating cell colonies were excised mechanically and dissociated with collagenase. RNA from CMs was isolated and used to study the expression of troponin T, RyR2, SERCA2a, LTCC, PLB, and NCX (Study II). In addition, CMs were stained with antibodies for the cardiac markers troponin T and Cx-43 (Studies II and III).

4.2.4 Calcium imaging (II-IV)

Dissociated CMs were loaded with 4 µmol/L Fura-2 AM (Life Technologies, Molecular Probes) for 30 minutes in HEPES-based medium. The cells were perfused with pre-heated extracellular solution consisting of 137 mM NaCl, 5 mM KCl, 0.44 mM KH_2PO_4, 20 mM HEPES, 4.2 mM $NaHCO_3$, 5 mM D-glucose, 2 mM $CaCl_2$, 1.2 mM $MgCl_2$ and 1 mM Na-pyruvate. The pH was adjusted to 7.4 with NaOH. Ca^{2+} cycling measurements were conducted on an inverted IX70 microscope (Olympus Corporation, Hamburg, Germany) with a UApo/340 x20 air objective (Olympus) and an ANDOR iXon 885 CCD camera (Andor Technology, Belfast, Northern Ireland). Fura-2 AM was excited at 340 nm and 380 nm light with a Polychrome V light source, and the emission recorded at 505 nm with TILLvisION or LiveAcquisition software (TILL Photonics, Munich, Germany). For Ca^{2+} analysis, regions of interests were selected for spontaneously beating cells, and background noise was subtracted before further analysis. The Ca^{2+} levels are presented as fura-2 ratio units F340/F380 or as $\Delta F/F0$.

Ca^{2+} cycling was measured during spontaneous baseline beating (Studies II-IV), and beating rhythm was induced with EFS (DS3 Constant Current/Voltage Isolated Stimulators, Digitimer LTD, USA) (Study II) and/or 1 µM adrenaline (Sigma-Aldrich) (Studies II-III) and with 1 µM adrenaline together with 10 µM dantrolene (Sigma) (Study III). The SR Ca^{2+} content was estimated by releasing SR Ca^{2+} instantaneously with 40 mM caffeine (Sigma-Aldrich) (Study II). Data analysis was performed with Clampfit software (Molecular Devices, USA) (Studies II, III). Ca^{2+} signals were also analyzed manually with visual recognition by dividing the signals as normal or abnormal (Studies II-IV), and Ca^{2+} cycling patterns were categorized into different subgroups (Studies II, IV). Ca^{2+} cycling patterns were also analyzed with AnomalyExplorer software (see below, Study IV). Drug responses of dantrolene were categorized depending on the effect of dantrolene on Ca^{2+} abnormalities, and differences in responders, semi-responders and non-responders were compared between *in vivo* and *in vitro* studies (Study III).

4.2.5 Ca^{2+} abnormality analysis software (IV)

In Study IV, AnomalyExplorer, an interactive Ca^{2+} abnormality analysis software, was used to assist in visual classification of Ca^{2+} signals. AnomalyExplorer was designed to detect the abnormalities in the same fashion as a human observer, i.e., to define whether the signal is normal, and to further analyze the quality and distribution of detected Ca^{2+} abnormalities. In Study IV, in addition to visual manual analysis, Ca^{2+} signals were analyzed with AnomalyExplorer where suitable user-defined percentage limits for each abnormality type were selected for two recording software (TillVision and LiveAcquisition, referred to as recording software 1 and 2, respectively) data groups.

AnomalyExplorer exploits the height of the Ca^{2+} signals as well as sections and regression lines, which act as points of reference for the rules defining the Ca^{2+} abnormality types. A section reflects the Ca^{2+} rise or decay and allows a small amount of noise in the signal. The noise threshold determines how much the signal may exhibit direction changes without regarding it as a change in monotonous movement. The regression lines are needed as references for the abnormalities if the amplitude of a Ca^{2+} signal fades over time. Abnormalities are detected by predefined and user-defined limits that can be manipulated via the user interface to correspond to Ca^{2+} measurement settings such as the frame rate of the recordings.

AnomalyExplorer detects six abnormality types. The low peak or middle peak abnormalities are detected if the amplitude of the Ca^{2+} signal does not reach the normal Ca^{2+} signal amplitude level. Oscillation of the Ca^{2+} signal is detected if the signal does not descend low enough before ascending to the next peak for at least three peaks. A double peak is detected if the signal does not descend low enough before ascending to the next peak. An irregular phase is detected if the distances of peaks differ from a user-defined percentage for the median peak distances. Plateau abnormality is detected if the signal changes its rise or decay rate more than a user-defined percentage within a section.

4.2.6 Patch-clamp measurements (II)

APs were recorded in current-clamp mode using amphotericin B with the perforated patch technique. Extracellular perfusate consisted of 143 mM NaCl, 5 mM KCl, 1.8 mM $CaCl_2$, 1.2 mM $MgCl_2$, 5 mM glucose, and 10 mM HEPES, and the pH was adjusted to 7.4 with NaOH. The osmolarity set to 300±2 mOsm (Gonotec, Osmomat 030, Labo Line Oy, Helsinki, Finland) with

sucrose. The intracellular solution included 122 mM $KMeSO_4$, 30 mM KCl, 1 mM $MgCl_2$, and 10 mM HEPES; the pH was adjusted to 7.15 with KOH; and the osmolarity set to 295 ±2 mOsm. Spontaneously beating CMs were patched under similar conditions as during Ca^{2+} imaging. Patch pipettes (model PG150T, Harvard Apparatus, UK) were pulled and flame polished (Narishige, UK) to a resistance of 2.0-2.5 MΩ. APs were recorded in gab-free mode with pClamp 10.2 software. Current-clamp recordings were digitally sampled at 20 kHz and filtered at 5 kHz with a lowpass Bessel filter. AP durations at 50% and 90% of repolarization (APD_{50} and APD_{90}), AP amplitude (APA), maximum diastolic potential (MDP) and beats per minute (BPM) were analyzed from AP recordings with Microcal OriginTM 8.6.

4.3 Clinical data (II, III)

4.3.1 Monophasic action potential and 24-h-ECG recordings (II)

Monophasic action potentials (MAPs) were previously recorded from CPVT patients and healthy controls as reported (Paavola et al., 2007). The data were recorded during sinus rhythm and atrial pacing at a constant cycle length of 600 ms during both baseline and adrenaline infusion. Analysis was performed with custom-made software. EADs were defined as low-amplitude depolarizations during phase 2 or 3 of the AP, with an amplitude of ≥3% of the preceding AP. DADs were defined as low-amplitude depolarizations after completion of repolarization and had an amplitude of ≥3% of the preceding AP. (Vos et al., 2000)

Twenty-four-hour ECGs were previously recorded from CPVT patients and healthy controls with commercial tape recorders (model 8500; Marquette Electronics Inc., Milwaukee, WI, USA). The data were initially analyzed with a Marquette 8000 Holter Analysis system. T1-, T2-, and U-waves were defined as previously reported (Viitasalo et al., 2006; Viitasalo et al., 2008).

4.3.2 Exercise-stress test and dantrolene infusion (III)

In Study III, the antiarrhythmic potential of dantrolene was studied in the treatment of CPVT with both patients and iPSC-derived CMs generated from the same individuals. The clinical tests and the iPSC studies were performed separately and blinded.

The study was approved by the Ethical Review Committee of the Helsinki University Hospital (HUS 396/13/03/01/12) and was performed in accordance with the institutional guidelines

and the Declaration of Helsinki. Written informed consent was obtained from all patients. The clinical trial was registered with EudraCT (2012-005292-14). The follow-up time of the patients was three days after the dantrolene infusion.

Six patients (mean age 50±10 years, range 37–59 years, 5 females) with exon 3 deletion, P2328S, T2538R, L4115F, Q4201R or V4653F RyR2 mutations (same as in Table 2) causing CPVT were associated with exercise-induced ventricular arrhythmias and syncopal spells. Patients used a beta-adrenergic blocking agent during all study phases and no other medications were in use. Patients underwent the exercise stress test with a bicycle ergometer three times with an initial load of 30 W, followed by load increases of 15 W each minute. In the latter phases of the study, the workload target was equal to that achieved in the first study. The first baseline study was carried out in the morning, and later in the afternoon after intravenous infusion of dantrolene sodium (Dantrium®, 1.5 mg per kg of body weight), the second exercise test was repeated. The third exercise test was carried out on the second day to study the effects after dantrolene washout. ECG was recorded continuously throughout the exercise test and the first 8 minutes after the test. Numbers of PVCs and the maximum number of consecutive PVCs during exercise and at the recovery phase were calculated.

4.4 Statistical analysis (I-III)

In Study I, at least two replicates from both stimulated and control groups from each qPCR experiment were analyzed as triplicates. The relative quantification was defined using the $2^{-\Delta\Delta C\tau}$ -method (Livak and Schmittgen, 2001). The data were normalized to the expression of the housekeeping gene β-actin, and the unstimulated sample for each test series was used as the calibrator. The statistical significance for each EFS experimental group was determined with the t-test.

In Studies II and III, the significance of *in vitro* differences between two groups was evaluated with the unpaired Student's *t*-test. The significance of changes within a group was evaluated with the paired Student's *t*-test. The data are expressed as the average±S.E.M.; n refers to the number of cells or experiments.

Statistical analysis of *in vivo* studies (Study III) was performed using SPSS 21.0 statistical software package (SPSS, Chicago, IL). The data are presented as the average+1 SD. Comparisons between phases were performed by the non-parametric Wilcoxon test.

5 Results

5.1 The effect of electrical stimulation on primary cardiomyocytes (I)

5.1.1 The effect of stimulator on cardiomyocytes

The difference in medium pH levels in control and stimulated medium samples after long-term stimulation was 0.10%, suggesting that stimulation had no effect on the pH levels. Different stimulation protocols did not cause degradation of the electrodes or any gas formation. The effect of the EFS on cell beating was characterized visually by a pacing experiment with varying parameters. Stimulation paced the beating rhythm, which returned to its spontaneous frequency after the stimulation.

5.1.2 Cell viability, morphology and functionality

NRC viability was determined with live/dead staining, which revealed no observable differences in cell viability between the stimulated and control samples; approximately 50% of the cells were viable in both groups. However, the number of NRCs decreased similarly during the culture in both the control and stimulated samples. Stimulation did not change the morphology of NRCs, and EFS did not elongate or orientate the cells. Instead, the orientation of the NRCs was observed to be parallel to the MEA plate electrode wires in both the control and stimulation samples where cells were cultured on gelatin (Figure 13). To estimate the effect of MEA surface abrasions on the orientation of cells, the height of the electrode wires was measured with AFM to be 600 nm.

The spontaneous beating rate of NRCs was measured with MEA and was found to vary between 0.5 and 2 Hz, although it was commonly 1.0 Hz. The culturing time decreased the beating rate, which also became irregular during the experiment. This phenomenon was evident in both stimulation and control samples. MEA measurements could not be carried out on NRCs on collagen gel due to the thickness of the gel. However, microscopy revealed that the culturing time also affected the number of beating areas in these samples, and the beating frequency of stimulation and control samples decreased.

5.1.3 Gene and protein expressions

RT-PCR showed that the MYH-7 mRNA levels were higher in the 3-day stimulation experiments than in the control samples and that Cx-43 expression levels were slightly elevated. qPCR analysis confirmed that stimulation increased MYH-7 and Cx-43 expression levels in two experiments ($p<0.05$) when compared to controls (Figure 13). In two other experiments, MYH-7 and Cx-43 expression levels had slightly higher expression, but these levels did not reach statistical significance.

The stimulated cells stained positive for troponin T or I similar to the controls. Stimulation caused no visible changes in the sarcomeric structure of the NRCs.

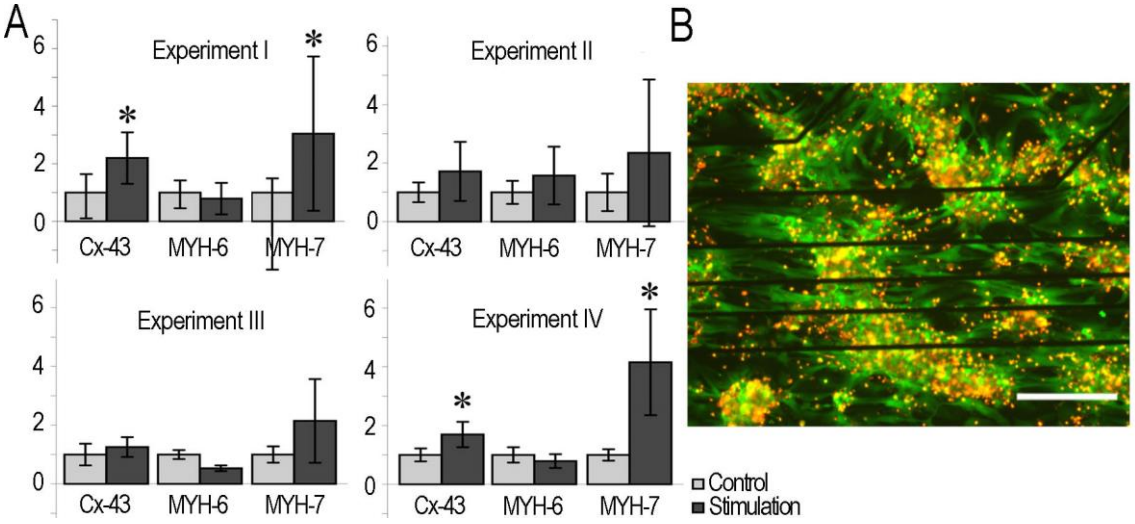

Figure 13. A) Expression levels of Cx-43, MYH-6, and MYH-7 after different stimulation experiments at the end of culturing. Error bars are SD. * indicates statistical significance of $p<0.05$. B) The orientation of NRCs parallel to the electrode lines of the MEA plate was evident in the live/dead stainings.

5.2 Characterization of iPSC and iPSC-derived cardiomyocytes (II, III)

The iPSC lines generated from a CPVT patient and from healthy control subjects were morphologically and karyotypically normal (Figure 14). Retrovirally encoded reprogramming factors were silenced, and endogenous pluripotency genes were turned on and expressed at the protein

level (Figure 14). The pluripotency of the cell lines was further confirmed with *in vivo* teratoma formation and with *in vitro* EB formation as well as with the expression of all three germ layers. The presence of the RyR2 mutations was verified for all the CPVT-iPSC lines by DNA sequence analysis (Figure 14) or by PCR.

iPSC lines were differentiated into spontaneously beating CMs that expressed troponin T and Cx-43 cardiac markers at the protein level. In Study II, expression of troponin T, RyR2, SERCA2a, LTCC, PLB and NCX were confirmed by RT-PCR. No differences in the studied gene or protein expression levels were observed between control and CPVT CMs.

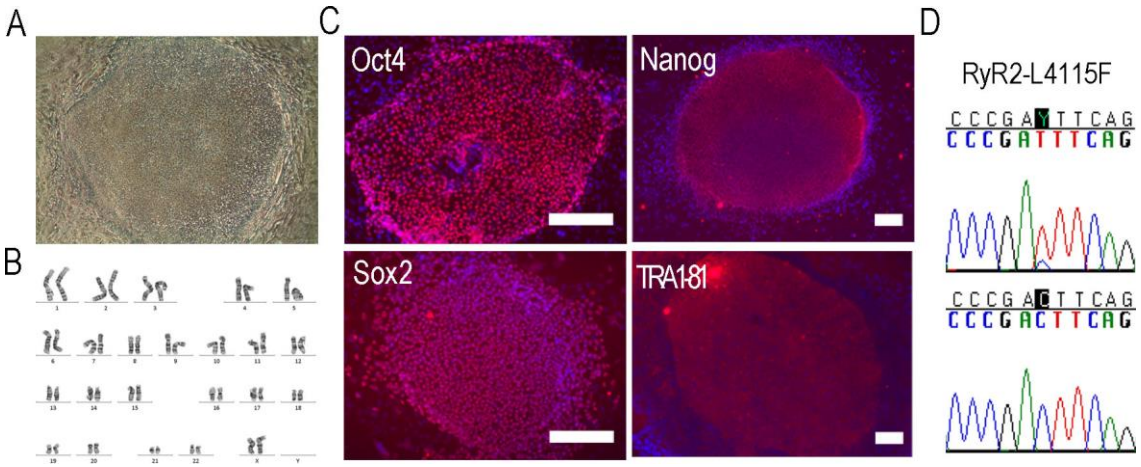

Figure 14. Characterization of CPVT iPSCs. A) Morphology of an iPSC colony. B) Normal karyotype. C) Expression of pluripotency markers at the protein level. Scale bars 200 µm. (E) Sequencing analysis confirming the correct RyR2 mutation of the CPVT iPSC line.

5.3 Functionality of iPSC-derived CMs (II-IV)

5.3.1 Ca^{2+} cycling (II, III)

Ca^{2+} cycling properties of spontaneously beating CPVT-P2328S and control CMs were compared in Study II. The beating rhythm of the cells was induced with electrical pacing and adrenaline perfusion, and the effect of a high-dose caffeine puff was studied. Ca^{2+} transients were categorized into four different categories, with abnormal Ca^{2+} cycling in three of the categories based on irregularity of the rhythm and/or transient amplitude. In spontaneously beating CPVT-

P2328S CMs, 14% of cells showed abnormal Ca^{2+} cycling, which was slightly diminished to 10% during electrical pacing. When beating rhythm was induced with adrenaline (Figure 15), abnormalities increased to 29% and to 32% together with electrical pacing. In control CMs, spontaneously beating cells had only 8% abnormalities, and adrenaline increased the amount to 11%. Electrical pacing completely abolished abnormal Ca^{2+} cycling in control cells. During spontaneous baseline beating and electrical pacing, CPVT-P2328S and control CMs had similar diastolic intracellular Ca^{2+} levels. Adrenaline and electrical pacing induced the intracellular Ca^{2+} to significantly higher levels in CPVT-P2328S cells compared to controls. The SR Ca^{2+} load was measured as the transient amplitude of high-dose caffeine-induced Ca^{2+} release, which was significantly lower in CPVT-P2328S CMs at baseline and in the presence of adrenaline pacing compared to controls. Fractional Ca^{2+} release indicated the amount of Ca^{2+} released from the SR during normal beating in proportion to the total SR Ca^{2+} store. Fractional SR Ca^{2+} release was significantly higher in CPVT CMs during spontaneous beating and during electrical pacing with and without adrenaline perfusion compared to controls.

In Study III, Ca^{2+} cycling of CMs from six different RyR2 mutations were compared to control cell lines. Generally, Ca^{2+} transient abnormalities such as multiple peaks/double peaks (Figure 15) composed of two peaks, irregular phases, oscillations (Figure 15), and varying amplitude manifested as low peaks were more incommon in CPVT CMs than in control CMs at baseline and in response to adrenaline (Figure 15). Although these abnormalities were common with all six mutations examined, some differences between RyR2 mutations were also observed. Accordingly, Ca^{2+} transient abnormalities were somewhat more common in the cluster 4 mutation than in cluster 1, 2 and 3 mutations. Adrenaline increased the beating frequency of each cell line studied. All RyR2-mutated CMs had lower beating frequencies at baseline and during adrenaline perfusion than control CMs. Adrenaline produced significantly elevated diastolic Ca^{2+} levels only in P2328S CMs, while diastolic Ca^{2+} levels were lower or similar in other mutant CMs compared to control CMs. Exon 3 deletion CMs had both lower beating frequency and diastolic Ca^{2+} levels compared to other mutations.

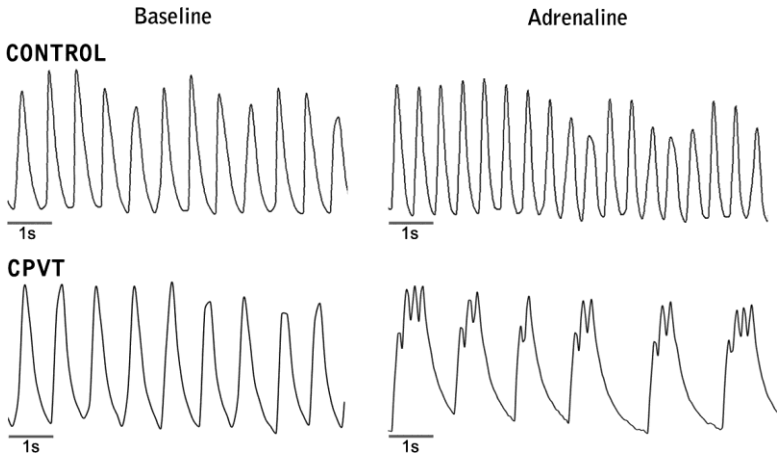

Figure 15. Ca^{2+} cycling transients of control and CPVT CMs during the spontaneous baseline beating and after adrenaline perfusion, which provoked double peaks and oscillating Ca^{2+} abnormalities in CPVT CMs.

5.3.2 Analysis of Ca^{2+} cycling abnormalities (IV)

In Study IV, AnomalyExplorer software was developed and used to analyze visual patterns of Ca^{2+} cycling data independent of observers. The data were generated with two different Ca^{2+} signal recording software. Signals generated with recording software 1 had frequencies from 9 to 10 Hz and signals generated recording software 2 had frequencies from 23 to 26 Hz. This affected the noise level of the recordings; therefore, optimal user-defined parameter settings were selected for both recording software data groups.

Each Ca^{2+} signal was analyzed manually with visual recognition and compared with the results obtained from AnomalyExplorer. With recording software 1 signals, there was 2% inconsistency between manual and AnomalyExplorer analyses, and these were specified as false abnormal (false positive) stating that they were categorized as normal manually but the software categorized them as abnormal. With recording software 2 signals, there was 9% inconsistency with the manual analysis where 4% were false abnormal and 5% were false normal (false negative) stating that they were categorized manually as abnormal but the software categorized them as normal.

The majority of the spontaneously beating CMs were categorized as normal in the manual and AnomalyExplorer analyses. Table 3 shows the percentage of abnormally categorized signals and the percentage of detected abnormality patterns of the data generated with both recording software and with both manual and AnomalyExplorer analyses. Comparison of the analyses and

the consistency of the manual and AnomalyExplorer analysis of different RyR2 mutated CPVT cell lines revealed mutation-specific differences in the Ca^{2+} transient abnormalities with both analysis methods (Table 4).

Table 3. Comparison of detected Ca^{2+} cycling abnormalities analyzed manually and with AnomalyExplorer software in Study IV.

	Recording software 1		**Recording software 2**	
	Manual analysis, abnormalities (n=171)	**AnomalyExplorer analysis, abnormalities (n=157)**	**Manual analysis, abnormalities (n=301)**	**AnomalyExplorer, analysis abnormalities (n=284)**
Double peaks	29%	30%	33%	34%
Low peaks	20%	15%	15%	6%
Middle peaks	5%	6%	9%	9%
Oscillations	26%	30%	26%	28%
Plateau abn.	6%	6%	7%	15%
Irregular phase	14%	13%	13%	8%
Signals categorized as abnormal	34% (n=132)	36% (n=132)	43% (n=212)	42% (n=212)

Table 4. Comparison of AnomalyExplorer and manual Ca^{2+} signal analysis of the different RyR2-mutated CPVT cell lines. AE denotes AnomalyExplorer analyzed data, and M denotes manually analyzed data. Replicates of the analyzed data: exon 3 del, n=46; P2328S, n=32; T2538R, n=51; L4115F, n=106; Q4291R, n=57; V4653F, n=29.

	Oscillation		**Double peaks**		**Low peaks**		**Middle peaks**		**Plateau abn.**		**Irregular phase**	
	AE	**M**	**AE**	**M**	**AE**	**M**	**AE**	**M**	**AE**	**M**	**AE**	**M**
exon 3 del	19%	16%	38%	38%	0%	6%	3%	3%	37%	28%	3%	9%
P2328S	16%	11%	45%	43%	16%	21%	9%	10%	8%	5%	6%	10%
T2538R	52%	51%	31%	17%	0%	7%	4%	4%	2%	4%	11%	17%
L4115F	29%	27%	35%	34%	11%	15%	7%	4%	5%	5%	13%	15%
Q4201R	21%	17%	22%	29%	23%	38%	4%	1%	25%	7%	5%	8%
V4653F	47%	44%	26%	21%	2%	17%	8%	11%	3%	3%	14%	4%

5.3.3 Electrophysiology (II)

In Study II, CPVT-P2328S and control CMs showed similar AP characteristics, and adrenaline caused a similar increase in the beating rate and decreases in APD_{50} and APD_{90}. Three of 16 control cells showed random single DADs at baseline, but no DADs were observed during adrenaline perfusion in five measured control cells. Six of 14 CPVT-P2328S cells showed random DADs at baseline. Eleven CPVT-P2328S cells were exposed to adrenaline, and five of them showed DADs (Figure 16) and a subsequent decrease in the beating rate. During spontaneous baseline beating, three CPVT-P2328S cells showed singular EADs (Figure 16), which were initiated above -25 mV, and the maximum EAD amplitude was 45 mV. One cell with EADs also showed DADs and a phase 3 burst episode. During the burst, the MDP was -50 mV

and the maximum upstroke amplitude 95 mV. No EADs or burst episodes were observed in control CMs.

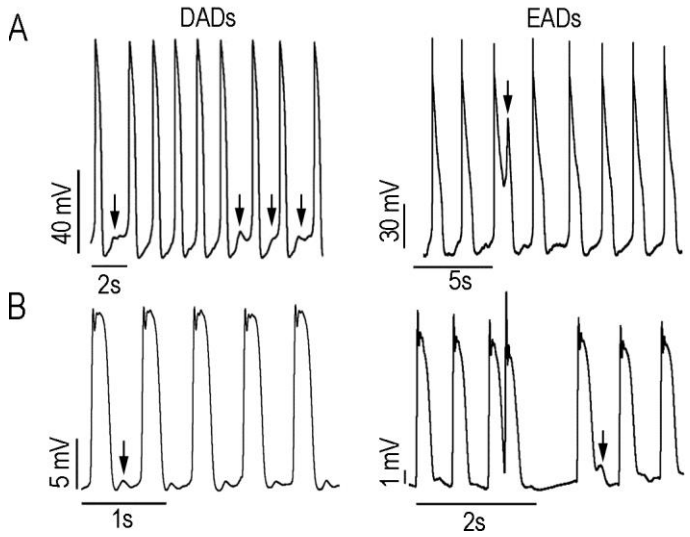

Figure 16. DADs and EADs in electrophysiological measurements of CPVT CMs and in clinical patient recordings. A) *In vitro* patch clamp measurements showing DADs and EADs, and B) *in vivo* MAP recordings of the corresponding phenomena.

5.3.4 Antiarrhythmic effect of dantrolene on Ca^{2+} cycling (III)

Effects of dantrolene were divided into three groups based on their Ca^{2+} responses on iPSC-derived CPVT CMs. In the "responder" group, dantrolene abolished all the Ca^{2+} cycling abnormalities (Figure 17); in the "semi-responder" group, dantrolene reduced them by more than 50%; and in the "non-responder" group, dantrolene reduced them by less than 50%. In CPVT CMs with the mutation in the N terminal or central region of the RyR2 protein (clusters 1-3), dantrolene abolished or reduced the majority of Ca^{2+} cycling abnormalities (Table 4). With exon 3 deletion, P2328S, T2538R or L4115F, dantrolene abolished or reduced Ca^{2+} abnormalities by more than 50% in 65-97% of cells. With the mutation at the end of cluster 3 (Q4201R) or in the transmembrane region (V4653F), the effect of dantrolene was only minimal (Table 4). Dantrolene had no effect on the Ca^{2+} transients in control CMs. Dantrolene did not significantly affect the diastolic Ca^{2+} levels of CMs in which Ca^{2+} transient abnormalities were abolished, which were significantly increased in control and Q4201R CMs where Ca^{2+} transients were unaltered

by the drug. No correlation between the antiarrhythmic effect of dantrolene and its effect on beating frequency was observed.

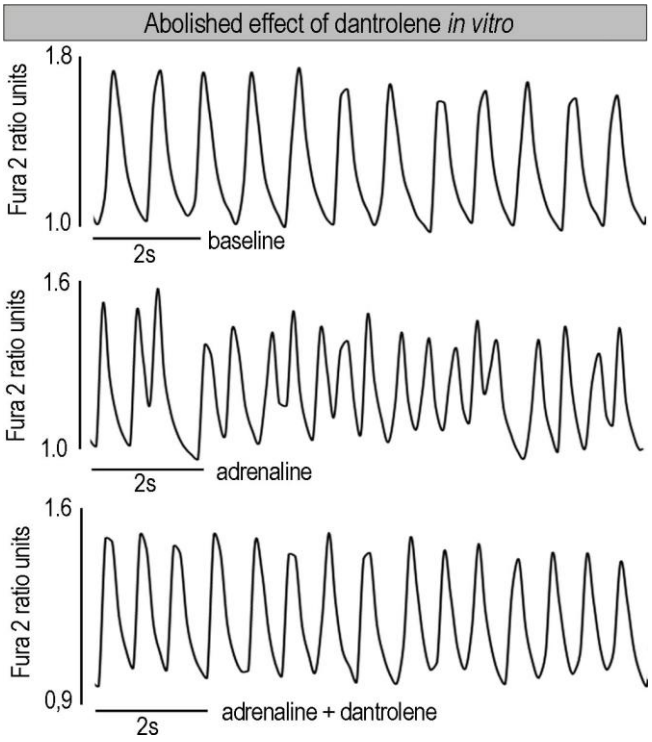

Figure 17. Representative Ca^{2+} transients of CPVT CMs, where dantrolene abolishes adrenaline-induced Ca^{2+} cycling abnormalities.

5.4 Clinical features of CPVT (II, III)

5.4.1 MAP and ECG (II)

In Study II, MAP recordings of CPVT patient demonstrated DADs and occasional EADs (Figure 16), which were absent in MAP recordings of healthy controls. Additionally, 24-h ECGs of 19 CPVT patients and 19 matched healthy controls showed occasional simultaneous T1-, T2- (corresponding to EAD) and U-waves (corresponding to DAD) only in CPVT patients.

5.4.2 Antiarrhythmic effects of dantrolene in patients (III)

In the baseline study, exercise bicycle testing induced polymorphic PVCs in all patients and non-sustained ventricular tachycardia (NSVT, episodes of 3 to 4 consecutive PVCs) in three of them. The average threshold sinus rate for the appearance of PVCs was 105±9 min^{-1}. The total count of PVCs during the workload was 172±119.

All patients tolerated the intravenous infusion of dantrolene but reported considerable muscle weakness as a side effect. Dantrolene abolished from 67% to 97% of PVCs in patients with the mutation in the N-terminal or central region of the RyR2 protein (exon 3 deletion, P2328S, T2538R and L4115F) (Table 4). In contrast, dantrolene abolished only 1 to 2% of PVCs in patients carrying the mutation closer to or within the transmembrane region (Q4201R and V4653F) (Table 5). iPSC-derived CMs markedly reproduced the varying individual clinical responses of dantrolene (Table 4). Dantrolene significantly increased the threshold at which the arrhythmias appeared in patients from 105±9 to 120±17 min^{-1}. After the dantrolene was washed out, the prevalence of PVCs approached the baseline results.

Table 5. *In vivo* and *in vitro* effects of dantrolene corresponding with each RyR2 mutation. *In vitro* drug effects were categorized into three groups depending on how dantrolene affected the amount of Ca^{2+} abnormalities compared to the adrenaline responses. The *in vivo* responder group shows the percentage of the abolished PVCs compared to the baseline. Numbers of cells analyzed in exon 3 del, n=16; P2328S, n=32; T2538R, n=17; L4115F, n=36; Q4201R, n=22; V4653F, n=13.

		Drug effects		
		Non-responder	**Semi-responder**	**Responder**
exon 3 del.	***in vivo***	3%		97%
	in vitro	19%	-	81%
P2328S	***in vivo***	12%		88%
	in vitro	3%	28%	69%
T2538R	***in vivo***	33%		67%
	in vitro	35%	30%	35%
L4115F	***in vivo***	23%		77%
	in vitro	22%	25%	53%
Q4201R	***in vivo***	98%		2%
	in vitro	68%	18%	14%
V4653F	***in vivo***	99%		1%
	in vitro	77%	15%	8%

6 Discussion

The main goal of this thesis was the development and functional characterization of cardiac cell models. NRCs were exposed to EFS with a novel device to study different stimulation protocols and their effects on morphological and functional properties of the cells. A disease model for CPVT was produced with hiPSC-derived CMs generated from CPVT patients carrying various *RyR2* gene mutations to characterize and treat the arrhythmic events of these cells *in vitro* as well as to validate the results in the index patients *in vivo*. With these *RyR2* gene-mutated CMs, the role- and mutation-specific differences in intracellular Ca^{2+} cycling were studied. Based on the findings showing abnormal Ca^{2+} transients in these CMs, a Ca^{2+} cycling analysis software tool based on interactive visualization was developed to facilitate and accelerate the analysis compared to manual analysis with visual recognition.

The main findings of this work are summarized in Figure 18. Stimulation studies showed that EFS could be used to affect the gene expression of cardiac proteins and utilized as a tool for short-term pacing. CPVT studies indicated that molecular and cellular level research exploiting hiPSC-derived CMs correspond to the clinical phenotypes of the patients in studying both path-ophysiological and drug responses of the disease and encourage the continuation of disease modeling utilizing iPSCs even in a mutation- or patient-specific manner. Impaired Ca^{2+} cycling was evident in CPVT-specific CMs and was shown as an essential mechanism of cardiac dys-function in these patients. In future studies, these abnormal Ca^{2+} transients can be analyzed and categorized with the new Ca^{2+} cycling analysis software tool developed in this thesis.

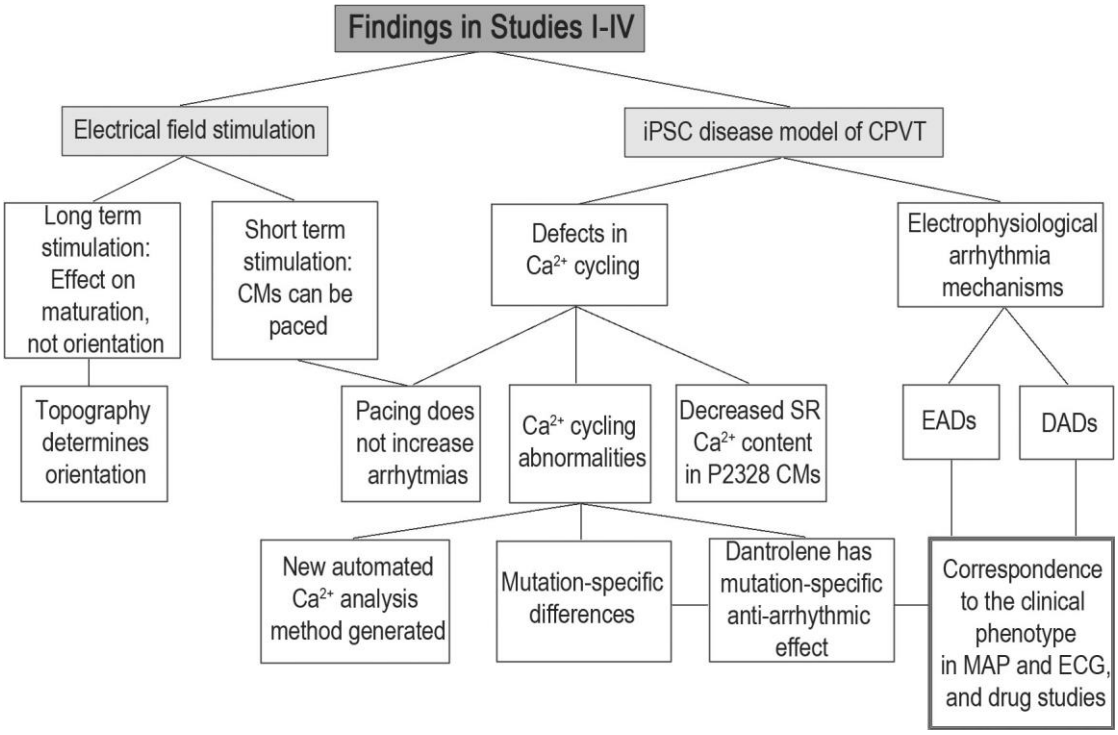

Figure 18. Summary of the findings in Studies I-IV highlighting the correspondence of the CPVT disease model phenotype to the clinical phenotype.

6.1 Electrical field stimulation (I, II)

A novel platform for the EFS of cells was designed in Study I, which had a programmable stimulation platform and the possibility of stimulating several cell culture plates for a long-term period on MEA plates as a benefit compared to other existing stimulation systems. The aim of this study was to determine whether EFS affects cell functionality, morphology and maturation when different stimulation parameters were applied to NRCs cultured on top of gelatin or collagen gel.

EFS and its duration seemed to affect the cardiac gene expression profile. The expression level of MYH-7 increased after three days of stimulation but not after two days stimulation. This increase in MYH-7 could indicate that most isolated and cultured NRCs were ventricular CMs (Asp et al., 2010; Sharma et al., 2003) or that mechanical stress caused by EFS induced a shift from α-MHC toward β-MHC composition (Krenz and Robbins, 2004), which can reduce the contractile efficiency of the CMs. However, EFS was previously shown to increase the ratio

of the sarcomeric proteins MYH-6 and MYH-7, which benefits cardiac contractility and indicates the maturation of the CMs (Radisic et al., 2004). In our study, Cx-43 levels were significantly higher in two stimulation experiments compared to the controls, which could indicate both electrical and metabolic coupling of CMs due to EFS. These results suggest that this stimulation system may prove useful in the future to enhance the cardiac differentiation and maturation of CMs. Because differentiation protocols are constantly improving and more mature and functional CMs are sought, stimulations have already been tested to enhance CM maturation with EFS mimicking the heart environmental stimuli. (Nunes et al., 2013) Electrical pacing has increased the maturation of Ca^{2+} cycling and contractile properties as well as the expression of Ca^{2+} cycling proteins and T-tubule proteins in hESC-derived CMs (Li et al., 2013; Liu et al., 2007).

Although previous studies have shown that EFS influences CM functionality (Chiu et al., 2008; Radisic et al., 2004; Sathaye et al., 2006), and although stimulation increased Cx-43 expression, no long-term effects of EFS on the electrophysiological behavior of the CMs was observed. Instead, the beating rate of the NRCs decreased in all samples and cells detached from the MEA plates, causing the loss of cell-to-cell contacts necessary for signal induction. However, live/dead stainings revealed no significant differences in cell viability between the stimulated and control samples. This decrease in the beating rhythm could be due to the tendency of primary cells to dedifferentiate and eventually stop beating in culture (Montessuit et al., 2004).

In earlier studies, the CMs have been shown to elongate and orientate parallel to the EFS (Au et al., 2007; Hedgepath et al., 1997; Radisic et al., 2004), which was not evident in Study I for this thesis. Instead, the surface topography of MEA electrode wires was a stronger determinant of CM orientation than EFS in both the control and stimulation samples. Electrode wires of the MEA plates had a height of 600 nm, which was in line with previous studies, where topographical cues of a height of several hundred nanometers have been shown to induce cell orientation (Au et al., 2007; Au et al., 2009; Kim et al., 2010a). Consequently, the surface topography should be designed carefully when CM orientation is desired.

Short-term stimulation experiments were able to pace the NRCs, and in the absence of stimulation, the beating returned to the spontaneous rhythm. This observation can be exploited in various cardiac-related studies requiring the electromechanical stimulation of CMs. Because of this phenomenon, iPSC-derived CMs were exposed to EFS in Study II to determine the effect of pacing on intracellular Ca^{2+} cycling. In this study, a commercial stimulation device and plat-

form were used. Electrical pacing has also been exploited with disease modeling of iPSC-derived CMs, e.g., for studying Ca^{2+} cycling of non-beating CPVT CMs (Jung et al., 2012), as well as for studying the effect of stimulation on nuclear senescence and cellular apoptosis of lamin A/C-related dilated cardiomyopathy (Siu et al., 2012). Stimulation has also been used for modeling atrial fibrillation with primary atrial myocytes (Ji et al., 2013).

6.2 iPSC-differentiated cardiomyocytes in disease modeling (II-IV)

In Studies II-IV, several iPSC lines carrying different RyR2 mutations were used. iPSC lines were established with an efficient and original technique utilizing lenti- and retroviruses (Takahashi et al., 2007). This method excluded the use of these cell lines for clinical purposes; however, for disease modeling studies, these cell lines were sufficient after their successful characterization. The characterization of the cell lines proved their pluripotency by the expression of certain pluripotency markers at the mRNA and protein levels as well as their ability to form three embryonic germ layers as shown by EB and *in vivo* teratoma forming assays. Most importantly, the iPSCs lines carried the same RyR2 mutations as the fibroblast donor patients.

All the iPSC lines were able to differentiate into functional CMs. The electrophysiology of CPVT iPSC-CMs appeared fairly mature in Study II based on their AP characteristics, such as AP amplitude, APD90 and resting membrane potential. In addition, CMs expressed several key Ca^{2+} cycling proteins: troponin T, NCX, SERCA2a, RyR2, LTCC and PLB. In addition, in Studies II and III, Ca^{2+} cycling abnormalities were substantially more consistent in CPVT CMs than in control CMs, and drug responses corresponded to the clinical phenotype. This finding indicated that Ca^{2+} cycling of the iPSC-derived CMs was mature based on the differences between control and CPVT cells and similarities between the cell and patient phenotypes. CMs also expressed troponin T and Cx-43 at the protein level, and some cells were multinucleated, which corresponded to the adult CM morphology. However, the round shape of the CMs indicated immature morphological properties. Stem cell-differentiated CMs have been considered immature because of their Ca^{2+} cycling (Fu et al., 2010; Liu et al., 2007; Liu et al., 2009) and electrical properties (Moore et al., 2005; Cao et al., 2008) and because they resemble neonatal CMs with their small cell size and lack of clear T-tubules (Lundy et al., 2013). However, slow maturation does occur with these cells during prolonged culture (Acimovic et al., 2014; Lundy

et al., 2013). The immaturity of iPSC-derived CMs may complicate the analysis of these cells or even cause incorrect phenotypes of the cells. Therefore, comparing results between similarly produced iPSCs and having valid control cells for these studies are important.

Despite the large usage of control iPSCs lines generated from healthy individuals, those lines have been occasionally criticized due to possible genetic variations between diseased and control iPSCs, which can cause false conclusions regarding the underlying mechanisms of the disease (Kim et al., 2014). Disease-causing mutations of the iPSCs can be corrected by generation of genetically identical (isogenic) sibling iPSC lines where nucleotides causing the mutation are altered. These isogenic corrected cell lines have been thought to be optimal controls for *in vitro* disease modeling as they represent the same genetic background except for the mutation. Methods based on zinc finger nucleases (ZFNs) (Soldner et al., 2011), transcription activator-like effector nucleases (TALENs) (Ding et al., 2013) or clustered regularly interspaced short palindromic repeats (CRISPRs) (Li et al., 2015) have been utilized with iPSCs; however, the generation of corrected isogenic iPSC lines is laborious (Kim et al., 2014). In the work for this thesis, control iPSC lines were generated from healthy individuals and compared to the results of disease-specific iPSC-derived CMs, and some clear differences were observed. The benefit of Studies II and III were that the *in vitro* results were also compared and confirmed in the index patients *in vivo*.

6.3 Modeling of CPVT with iPSCs and comparison of the results to the clinical phenotype (II-IV)

6.3.1 Functional properties of iPSC-derived CPVT cardiomyocytes (II, III)

After the discovery of iPSCs, disease modeling with CPVT patient-specific cells has been widely studied. Several groups have reported the generation of CPVT specific CMs from individuals carrying a CASQ2 mutation (Novak et al., 2012; Novak et al., 2015) and RyR2 mutations (Fatima et al., 2011; Jung et al., 2012; Itzhaki et al., 2012; Zhang et al., 2013; Di Pasquale et al., 2013; Novak et al., 2015). In Studies II-IV, iPSC disease models from CPVT patients were generated, and the benefit of these studies was that various *RyR2* gene mutations were characterized, and the results were compared to the clinical phenotype of the patients.

6.3.1.1 Defects in Ca^{2+} cycling and electrophysiology *in vitro* and correspondence with the clinical phenotype (II)

In Study II, an iPSC line from CPVT-P2328S mutation was generated, and the results were compared to iPSC lines generated from healthy controls and to clinical data of the same CPVT-P2328S mutation-carrying patient. No changes were observed between control and P2328S CMs in the morphology or in the expression of cardiac markers in the immunocytochemical stainings. This observation seems natural because CPVT is a disease with a structurally normal heart (Swan et al., 1999). However, in the literature, immature ultrastructures with a disorganized contractile apparatus have been reported with iPSC-derived CMs with CASQ2-D307H mutation (Novak et al., 2012), which was contradictory to the normal heart morphology observed in CPVT mouse models (Faggioni et al., 2012) and in CPVT patients (Leenhardt et al., 1995; Swan et al., 1999).

The new finding of Study II was the identification of EADs in CPVT-P2328S CMs as a novel mechanistic insight in CPVT, and this finding was validated in the clinical data of the index patient. DADs, which can give rise to the polymorphic VT in CPVT, were identified in patch clamp studies of P2328S CMs. Corresponding electrical instability manifested as EADs and DADs were detected in clinical MAP and ECG recordings, which highlight the clinically correct phenotype of the CPVT-P2328S iPSC model. In control CMs, rare single DADs, but no EADs, were detected. Both EADs and DADs were absent in clinical MAP recordings of control patients.

At baseline, Ca^{2+} transients were similar in control and P2328S CMs. Defective intracellular Ca^{2+} release with Ca^{2+} cycling abnormalities were observed in CPVT-P2328S cells in response to catecholaminergic stimulation with adrenaline. These observations correlate with the clinical phenotype of CPVT where arrhythmias and VT are detectable under conditions of physical or mental stress (Swan et al., 1999). Adrenaline produced significantly elevated diastolic Ca^{2+} levels, increased the amplitude of Ca^{2+} transients, decreased the SR Ca^{2+} content and increased fractional SR Ca^{2+} release in P2328S CMs compared to control CMs. Taken together, these results demonstrate that catecholaminergic stimulation caused increased sensitivity of Ca^{2+} release from SR in the CPVT-P2328S CMs. This increased diastolic SR Ca^{2+} leak may lead to DADs and to the generation of triggered arrhythmias (Schlotthauer and Bers, 2000) and explains the aforementioned results of patch clamp and clinical studies. Surprisingly, stimulation

with adrenaline caused occasionally slowing in the beating rate of CMs. Nevertheless, this finding was in line with a previous study (Novak et al., 2012) and was thought to be a cause of adrenaline-induced frequent DADs, which can suppress the following AP and therefore prevent the increase in the beating rate. Interestingly, electrical pacing did not increase the arrhythmogenicity of the P2328S CMs. At baseline, pacing stabilized Ca^{2+} cycling in both control and CPVT CMs and adrenaline together with electrical pacing did not increase Ca^{2+} abnormalities. This result is opposite of previous findings of some other CPVT iPSC studies (Novak et al., 2012; Jung et al., 2012) and could suggest mutation-specific differences in CPVT disease.

The Ca^{2+} cycling results of Study II suggest Ca^{2+} mediated mechanisms behind EAD-formation. EADs have been thought to result from spontaneous reactivation of LTCCs under conditions of APD prolongation, when LTCCs recover from inactivation but reactivate while the membrane is still depolarized (January and Moscucci, 1992). However, later, the roles of cytoplasmic Ca^{2+} overload and spontaneous Ca^{2+} release were thought to be the triggers behind EAD formation (Volders et al., 2000; Xie and Weiss, 2009). This phenomenon is a result of NCX activation due to spontaneous release of Ca^{2+} from the SR, which causes a depolarizing current that reactivates the LTCC and leads to an EAD. EADs arising from membrane potentials that are more negative than the threshold potential of LTCC have been shown to be NCX-mediated and to share similar properties with DADs (Patterson et al., 1990; Spencer and Sham, 2003; Xu et al., 1996). These mechanistic explanations indicate that EADs and DADs somewhat resemble each other; therefore, the observation of both afterdepolarization types in CPVT-P2328S CMs was not contradictory to the previous hypothesis. In addition, the possibility of EAD-mediated triggered activity in CPVT patients has been suggested based on previous findings in ECG recordings (Viitasalo et al., 2008).

Compared to other CPVT disease modeling studies where *RyR2* gene mutations have been studied with iPSC-derived CMs (Fatima et al., 2011; Jung et al., 2012; Itzhaki et al., 2012; Zhang et al., 2013; Di Pasquale et al., 2013; Novak et al., 2015), all of these studies have shown similar results, including abnormal Ca^{2+} cycling and DADs, and some of them have shown reduced SR Ca^{2+} content (Jung et al., 2012; Zhang et al., 2013). No clinical data were available in any of these studies to corroborate the validity of the iPSC-derived CM phenotype, and no other previous study suggested novel mechanistic insight regarding CPVT. Taken together, the results of the iPSC model of CPVT in Study II showed disturbances in intracellular Ca^{2+} cycling and recapitulated the arrhythmic changes observed clinically in patients with CPVT. Overall, this

study confirmed the usefulness of the CPVT model in pathophysiological studies and suggested its applicability to drug screening, which was studied and verified in Study III.

Because Study II raised questions about mutation-specific differences between CPVT mutations, six *RyR2* gene mutations were investigated in Study III, and the results were compared to a healthy control cell line. RyR2 mutations are clustered in four hotspots, one-third of the reported mutations can be found in clusters 1 and 2, and the rest can be found between clusters 3 and 4. Only 10% of RyR2 mutations have been detected outside of these clusters. (Priori and Chen, 2011)

6.3.1.2 RyR2 mutation-specific differences in the Ca^{2+} cycling *in vitro* (III, IV)

In Study III, RyR2 mutations from all four mutation clusters were investigated, and both similarities and differences in the CPVT *in vitro* phenotypes were observed depending on the nature of the mutation. All the CPVT CMs showed similar disturbances in intracellular Ca^{2+} cycling consisting of variable abnormality patterns, including multiple peaks/double peaks, oscillation, varying amplitude such as low peaks, irregular beating rhytmn and prolonged rise or decay time (plateau abnormality). These abnormalities were somewhat more common in the cluster 4 mutation than in cluster 1, 2 and 3 mutations, and in all cases, were more common compared to control cells. Surprisingly, abnormalities were also observed in baseline recordings of the CPVT CMs, although arrhythmias in patients are usually provoked by catecholaminergic stimulation. When comparing the baseline Ca^{2+} transient abnormality patterns of different CPVT cell lines in Study IV, mutation-specific differences were shown. These types of differences could reflect the mutation-specific pathology of the disease and indicate that the location of the mutation could affect the disease phenotype. Further Ca^{2+} cycling experiments combined with electrophysiological studies are needed to assess how different Ca^{2+} cycling abnormality patterns reflect the mechanism of the disease. In Study III, adrenaline did not increase the amount of Ca^{2+} cycling abnormalities significantly in all mutations because the amount of abnormalities was already high in the baseline. This phenomenon could be explained by the single-cell level Ca^{2+} cycling measurements, where the abnormalities might be more easily detected from single cells than from cell aggregates or the whole hearts, where the surrounding healthy CMs can pace the abnormally beating cells. In other CPVT iPSC studies, Ca^{2+} cycling abnormalities have already been detected at the baseline, and abnormalities have been somewhat exacerbated due to cate-

cholaminergic stimulation (Itzhaki et al., 2012; Zhang et al., 2013; Di Pasquale et al., 2013). In addition, baseline conditions in HEK293 cells expressing RyR2 mutations showed frequent spontaneous Ca^{2+} oscillations (Jiang et al., 2002). Thus, the susceptibility of different RyR2 mutations to Ca^{2+} cycling abnormalities can be mutation specific.

The beating frequency of CPVT CMs was lower than that in control CMs in Study III. This finding was in line with CPVT patients (Postma et al., 2005; van der Werf and Wilde, 2013). A lower beating frequency could be a cause of Ca^{2+} cycling abnormalities detected in CPVT CMs, which decreases the amount of regular spiking and causes irregular and abnormal spiking. Exon 3 deletion CMs differed from all the other mutated CMs by having lower diastolic Ca^{2+} levels and beating frequencies at baseline and in response to adrenaline. Exon 3 encodes secondary structure elements that are crucial for folding of the N-terminal domain. RyR2 with exon 3 deletion may regulate Ca^{2+} release by altering the conformation of the domain (Lobo et al., 2011), which could explain the observed differences between this deletion and the point mutations.

With the RyR2 point mutations presenting descending trends for the beating frequency and diastolic Ca^{2+} levels, increased Ca^{2+} abnormalities observed when moving from P2328S toward transmembrane area mutations. Mutations other than P2328S had lower or similar diastolic Ca^{2+} levels compared with control CMs. At the molecular level, different mechanisms explaining why RyR2 mutations lead to abnormal diastolic Ca^{2+} release have been hypothesized, which most likely could explain these mutation-specific phenotypes observed in basic Ca^{2+} cycling characterization and in drug response studies discussed in the next chapter. RyR2 sensitivity to low cytosolic Ca^{2+} concentrations and increased SR Ca^{2+} uptake, leading to SR Ca^{2+} overload and SOICR, (Jiang et al., 2002; Priori and Chen, 2011) could explain why diastolic Ca^{2+} levels were lower in some mutations and still cause abnormal Ca^{2+} release. Some RyR2 mutations change the receptor to be inappropriately activated at low diastolic levels of cytosolic Ca^{2+}, thereby inducing a diastolic SR Ca^{2+} leak (Meli et al., 2011). Diastolic Ca^{2+} levels were not significantly elevated with adrenaline in mutations other than P2328S, which could indicate that $[Ca^{2+}]_i$ alone was unlikely to account for the increase in spontaneous Ca^{2+} release. Overall, further conclusions regarding the mutation-specific mechanism behind abnormal Ca^{2+} release require further electrophysiological and Ca^{2+} cycling studies of these RyR2 mutations, including investigation of SR Ca^{2+} levels.

6.3.2 Pharmacological responses of dantrolene (III)

Due to detected defective Ca^{2+} cycling of CPVT iPSC-derived CMs and similarities between the *in vivo* and *in vitro* phenotypes of CPVT observed in Study II, the goal in Study III was to test the antiarrhythmic effect of dantrolene on both patients and iPSC-derived CMs. Dantrolene is a muscle relaxant that can prevent or reduce severe high body temperature and is therefore a specific, and currently the only, effective treatment for malignant hyperthermia. Dantrolene reduces ECC in muscles by binding to ryanodine receptors and decreasing free $[Ca^{2+}]_i$. (Krause et al., 2004) Dantrolene is also thought to inhibit Ca^{2+} leak from RyR2 because it has shown antiarrhythmic effects in experimental animal models of CPVT (Kobayashi et al., 2009; Kobayashi et al., 2010; Suetomi et al., 2011; Uchinoumi et al., 2010; Xu et al., 2010) and in iPSC-derived CMs (Jung et al., 2012).

The location of the RyR2 mutation is thought to be critical for a favorable effect of dantrolene. The binding site for dantrolene has been localized to the N-terminus of RyR2 between amino acids 601 and 620 (Kobayashi et al., 2009; Paul-Pletzer et al., 2005), and this binding sequence is considered to constitute part of the domain switch region. Therefore, dantrolene may participate in the correction of defective unzipping and allosteric stabilization of interdomain interactions between the N-terminal and central regions of RyR2 by restoring interdomain interactions critical for the closed state of the RyR2 Ca^{2+} channel, which causes the inhibition of Ca^{2+} leak from RyR2 (Kobayashi et al., 2005; Suetomi et al., 2011; Wang et al., 2011). This hypothesis has been demonstrated in previous studies (Kobayashi et al., 2005; Kobayashi et al., 2009; Paul-Pletzer et al., 2005).

6.3.2.1 Antiarrhythmic effects of dantrolene *in vitro* and *in vivo*

In Study III, the antiarrhythmic effect of dantrolene was shown only with RyR2 mutations of exon 3 deletion, P2328S, T2538R and L4115F located in the N-terminal or central regions of the RyR2 protein (clusters 1-3). This effect was evident both *in vivo* and *in vitro* and could indicate that a defective inter-domain interaction within RyR2 could be the underlying arrhythmogenic mechanism for these mutations. In the case of the T2538R mutation, dantrolene did not suppress the arrhythmias to the same extent as in other central region mutations. This finding could be explained by differences in the mode of interdomain interaction in dantrolene binding regions, which could cause differences in its antiarrhythmic efficacy (Suetomi et al., 2011).

Furthermore, it is possible, that other additional dantrolene binding regions in the carboxyl-terminal half or in the N-terminal area of the RyR2 exist (Kobayashi et al., 2009).

Interestingly, minimal or no antiarrhythmic effect of dantrolene was observed *in vivo* or *in vitro* with mutations Q4201R or V4653F located at the end of cluster 3 or in the transmembrane region of cluster 4. Although the Q4201R mutation is located in the cytosolic portion of RyR2 and in cluster 3, no antiarrhythmic effect of dantrolene was observed in its terminal part. This result suggests that the antiarrhythmic response of dantrolene is not necessarily cluster specific. Because the antiarrhythmic effect of dantrolene was evidently similar *in vivo* and *in vitro*, iPSC-derived CMs can be used to model individual responses. Although a dose-dependent effect of dantrolene cannot be excluded for certain, the antiarrhythmic effect of dantrolene appeared to be mutation specific. Similar observations on mutation-specific drug responses have been obtained for other genetic disorders, including LQT3 (Ruan et al., 2007) and cystic fibrosis (O'Reilly and Elphick, 2013), as well as for certain neoplastic diseases (Willyard, 2011). In our work, the *in vitro* studies showed that dantrolene had no effect on normally beating control or CPVT CMs, which was in line with previous reports showing that dantrolene inhibits only abnormal Ca^{2+} release. This inhibition has been thought to be a cause of the native conformation of RyR2, which may restrict binding of the drug. Alternatively, dantrolene binding to RyR2 may be dependent on a specific conformational state present only in mutated cells. (Kobayashi et al., 2009; Paul-Pletzer et al., 2005) Dantrolene has also been shown to restore defective calmodulin binding caused by RyR2 domain unzipping (Ono et al., 2010; Xu et al., 2010), which could be the reason why dantrolene inhibits only abnormal Ca^{2+} releases.

Overall, Study III showed the proof of principle that dantrolene suppresses ventricular arrhythmias in various patients with RyR2-mutated CPVT and has clinical benefit. In addition, iPSC-derived patient-specific CMs correctly predicted the clinical response of the drug. In addition, both *in vivo* and *in vitro* results consistently showed that the location of the RyR2 mutation affects the antiarrhythmic effect of dantrolene in CPVT. The results of Study III indicate that iPSC-derived CMs could serve as a platform for drug development and for the design of personalized medication, which would allow an individual's medication to be tailored in cell culture without predisposing the individual to the potentially serious side effects of a drug.

6.3.2.2 New insights into the treatment of CPVT

At present, risk stratification for the occurrence of arrhythmic events in CPVT patients is poorly defined, and these patients are advised to abstain from competitive sports and not to swim unsupervised (van der Werf and Wilde, 2013). Beta-antiadrenergic drugs are the first-line drug treatment for CPVT and have been shown to reduce the risk of arrhythmic events. Carvedilol, both α- and β-blocker, could be optimal choice due to its RyR2 blocking properties. (Hayashi et al., 2009; Hayashi et al., 2012) Flecainide together with β-blocker treatment has also been suggested to be beneficial. Based on preclinical data, which has shown direct RyR2 blocking properties of flecainide (Watanabe et al., 2009), the use of flecainide in the treatment of CPVT patients has increased; however, its mechanism remains under debate (Hilliard et al., 2010). A placebo-controlled randomized, crossover trial (NCT01117454) of flecainide together with standard beta-blocker therapy in CPVT treatment is currently going on in Europe and the USA (van der Werf and Wilde, 2013). A RyR2-specific compound, S107 (Lehnart et al., 2008; Hwang et al., 2011), is currently in phase 2 trials for the treatment of ventricular arrhythmias in CPVT and HF (van der Werf and Wilde, 2013). The efficacy of verapamil in CPVT patients has also been studied, but its long-term efficacy has been disappointing (Rosso et al., 2007). Current therapeutic options for CPVT also include ICDs; however, several case reports have shown that they may be proarrhythmic in CPVT because ICD shocks and the subsequent catecholamine release may trigger ventricular storms (Mohamed et al., 2006). In some earlier iPSC studies, the phenotype of CPVT has also been rescued with drugs. Dantrolene was shown to restore normal Ca^{2+} spark properties and the arrhythmogenic phenotype of CMs carrying an N-terminal S406L mutation (Jung et al., 2012). Flecainide and thapsigargin have been shown to eliminate afterdepolarizations, and beta-blockers have improved Ca^{2+} abnormalities worsened with adrenergic stimulation (Itzhaki et al., 2012). Treatment with KN-93, a methoxybenzenesulfonamide that is an effective inhibitor of CaMKII phosphorylating activity, has been shown to reduce DADs in CVPT-CMs (Di Pasquale et al., 2013). However, all of these studies were conducted only with iPSC-derived CMs; therefore, whether these findings will translate into a clinical benefit cannot be stated, although the drugs were found to be beneficial in the patient-derived iPSC differentiated CMs.

Our study suggests that at least a subset of patients would benefit from the antiarrhythmic potential of dantrolene. Intravenously administered dantrolene could be beneficial for CPVT

patients in emergencies such as incessant VT. However, further drug development is needed because dantrolene would not be suitable for long-term treatment of CPVT patients due to muscle weakness as a side effect. Overall, in the case of further drug development, the recognition of potential mutation-specific responses will be important because our results indicate that one drug may not work for all patients even if the disease is the same. The existence of defective RyR2-mediated Ca^{2+} leak in patients with HF has been reported previously (George, 2008); therefore, the results of these findings could also be beneficial for these patients.

6.3.3 Ca^{2+} cycling abnormalities and novel Ca^{2+}-analysis software (II-IV)

As shown in Studies II and III, RyR2-mutated iPSC-derived CMs show defective and abnormal Ca^{2+} cycling, which can be observed as variations in the beating rhythm and amplitude and manifested as multiple peaks/double peaks, oscillations, irregular rhythm and/or low amplitude peaks. As reviewed previously, Ca^{2+} cycling has a central role in CM ECC, and disturbances in this process can have fatal consequences. As shown in Study II, other studies have shown that disease-specific iPSC-derived CMs with Ca^{2+} cycling abnormalities also manifest arrhythmic features such as DADs in their AP (Fatima et al., 2011; Itzhaki et al., 2012; Jung et al., 2012; Lan et al., 2013; Novak et al., 2012; Yazawa et al., 2011). Simultaneous AP and Ca^{2+} recordings of LQT-specific CMs have revealed that abnormal Ca^{2+} cycling is involved in prolonging the AP duration as well as in forming EADs (Spencer et al., 2014). These results indicate that disease phenotype-specific changes in electrophysiology can be mirrored by changes in Ca^{2+} cycling, highlighting the importance of Ca^{2+} cycling abnormality analysis.

In Studies II and III as well as in other previous studies, the detection of Ca^{2+} signal abnormalities has been performed manually with visual recognition. This method is based on how the researchers categorize data based on an individual's experience and observations, which makes the analysis highly subjective. Usually, the signal has been categorized as abnormal if at least one abnormality is detected and the absolute amount or Ca^{2+} abnormalities in one signal is not clarified (Yazawa et al., 2011; Fatima et al., 2011; Novak et al., 2012; Jung et al., 2012; Itzhaki et al., 2012; Lan et al., 2013; Novak et al., 2015). In some previous studies (Itzhaki et al., 2012; Jung et al., 2012) as well as in Studies II and III, Ca^{2+} abnormalities were divided into subgroups, which is challenging in some cases because one signal can express different abnormality patterns. Comparison of disease modeling between different studies is challenging for these aforementioned reasons and because no specific analysis criteria are determined for abnormali-

ties and their definitions are not interchangeable. Unspecified criteria for Ca^{2+} abnormality analysis also complicate the comparison of Ca^{2+} cycling parameters between studies because it is unclear how Ca^{2+} cycling abnormalities have been considered in the numerical analysis of the data. In addition, analysis of drug responses, such as in Study III, would be more accurate with specified criteria for Ca^{2+} abnormality analysis.

In Study IV, novel software for Ca^{2+} cycling abnormality analysis was developed. This AnomalyExplorer tool recognized and categorized abnormalities by the visual features alone, using interactive visualization in a manner similar to traditional manual analysis. However, compared to manual analysis made with visual recognition, AnomalyExplorer is fast, repeatable, person-independent, and capable of screening large datasets. In addition, specific criteria for different types of Ca^{2+} abnormalities can be determined. All of these reasons make the results more comparable between the different studies.

In Study IV, AnomalyExplorer was tested with the Ca^{2+} cycling signals recorded from both CPVT and control iPSC-derived CMs. Data were generated with two different Ca^{2+} recording software programs to test the usability of the AnomalyExplorer with data consisting of varying sampling frequencies. Due to the ability of user-defined analysis criteria in the AnomalyExplorer software, optimal analysis parameters could be found for the data recorded with different software. This setting enables the universal use of software regardless of the recording software utilizes in Ca^{2+} cycling studies. When manual analysis of the test data was compared with AnomalyExplorer analysis, the detection of normal and abnormal signals was reasonably uniform, with inconsistency ranging from 2 to 9%. When the abnormalities were categorized into subgroups, the difference in the amount of different subgroup-specific abnormalities ranged from 0 to 5% between manual and AnomalyExplorer analysis, with the exception of two abnormality subgroups with 8 or 10% difference. The usefulness of AnomalyExplorer for detecting cell line- and mutation-specific variability in the Ca^{2+} transient abnormality patterns was also shown in this study by showing mutation-specific differences in the CPVT cell line.

The differences between manual and AnomalyExplorer analysis could be a cause of the background noise in the high sampling frequency measurements, thus complicating both manual and AnomalyExplorer analyses. In addition, the accuracy of the manual analysis made by visual recognition can vary and make the analysis non-repeatable. Challenges of Ca^{2+} imaging methods such as photobleaching as well as the toxicity of the Ca^{2+} indicator and UV light to CMs can

add interference and noise to the measurements, and these can complicate the analysis and cause differences between these two analysis methods.

In future studies, this software and analysis method can be exploited for Ca^{2+} cycling analysis to study not only basic disease pathology but also different drug responses. AnomalyExplorer does not exclude the need for the numerical analysis of different Ca^{2+} cycling parameters; however, it will clarify the analysis by defining how abnormalities should be considered in the numerical analysis, for example, when calculating the peak duration of multiple peaks/double peaks or oscillations. To understand the mechanism and severity of Ca^{2+} cycling abnormalities, combined electrophysiological measurements and Ca^{2+} imaging measurements are essential in the future.

6.4 Limitations of the study

In Study I, the problem with NRCs was their tendency to dedifferentiate during culture, which caused a lack of functionality and complicated the analysis of the effects of EFS. The amount of stimulated samples per one experiment was restricted due to our stimulation setup, and more replicates and repetition of stimulation protocols would be needed to compare results between different stimulation settings more thoroughly. In addition, comparing our results to those of other stimulation studies is difficult because the stimulation devices, stimulation parameters, and time in culture vary a lot greatly between studies. In the future, to enhance the positive effect of EFS, it would be important to understand the mechanism by which stimulation and different stimulation parameters influences cellular maturation and processes. In addition, more effective ways to quantify this phenomenon at the cellular level are needed.

In Study II, iPSC-derived CMs from two CPVT and two control cell lines were studied, and both CPVT lines were from the same patient. Cell lines of CPVT patients behaved the same way; however, whether the results were typical to this mutation or only to this patient cannot be stated with certainty. Despite the very rare nature of CPVT disease, we were able to extend our research by examining in detail six different disease-causing RyR2 mutations in Study III. However, only one cell line per patient and control was studied, and the results could be cell line-specific. However because the *in vitro* dantrolene responses resembled the *in vivo* responses, the phenotype of the iPSC-derived CMs was highly likely to be at least patient specific in

Study III. Only one fixed concentration of dantrolene was used in Study III, which is why the dose-responsive effect of dantrolene cannot be evaluated although positive effects of dantrolene were observed with four mutations with the same dantrolene concentration. Future studies of disease modeling and different mutations in multiple cell lines per patient as well as in mutation-specific cell lines from several individuals are necessary.

One challenge in disease modeling studies is proper controls for diseased cell lines. The problem with healthy controls is that they might differ from diseased cells lines with disease-causing mutation and may contain several other mutations and polymorphisms that cause phenotypic differences. Therefore, the use of multiple different iPSC lines as controls would be optimal for disease modeling studies. One way to limit the variability between control and diseased cell lines would be to derive control iPSC lines from close relatives of the patient who are not affected by the disease-causing mutation. However, even in studies in which healthy siblings have been used as controls for disease patients, only ∼50% of the genome is shared between any siblings. Furthermore, phenotypic differences could be the result of DNA variants in the other ∼50% of the genome, rather than the disease-associated mutations. (Wang et al., 2014b) In our study, we observed clear phenotypic differences between healthy control CMs and CPVT CMs. However, isogenic controls could more accurately depict non-diseased cellular phenotypes compared to healthy controls. With the help of isogenic controls, the effects of genetic modifiers and epigenetic factors of CPVT disease progression between different individuals could be studied. Addressing whether healthy control cell lines are as suitable for controls in CPVT disease modeling as are isogenic gene-edited iPSC lines is important. However, the generation of isogenic cell lines also needs validation because they are subject to clonal variation.

Abnormal Ca^{2+} cycling was observed in CPVT CMs but rarely in control CMs, which is why at least most of the abnormalities resembled the CPVT disease phenotype. Validation of the *in vitro* results with the patient data indicated the correct phenotype of our CPVT CMs. However, some abnormal Ca^{2+} cycling may still be a consequence of the immature CM gene expression levels or phosphorylating activity of the CMs because some iPSC-derived CMs lack of t-tubules and have low expression levels of the SR Ca^{2+} buffering protein CASQ2, which can disturb RyR2-dependent Ca^{2+} release (Knollmann, 2013). These possibilities, together with possible electrophysiological and structural CM immaturity, may interfere with the normal Ca^{2+} cycling of these cells. Nevertheless, earlier studies have shown that iPSC-CMs display functional and loaded RyR-regulated intracellular Ca^{2+} stores, which can release Ca^{2+} via RyRs and

can reload their content through SR Ca^{2+} uptake. The immaturity of the CMs can be a problem in disease modeling. Their immature phenotype is due to current differentiation technologies, is dependent of culturing time, and can cause significant line-to-line and patient-to-patient variability. This variability complicates comparisons of results where CMs have been generated with different differentiation protocols. Otherwise, immaturity of iPSC-derived CM have been observed as immature morphology, incomplete organization of the sarcomeric structure (Lieu et al., 2009; Luna et al., 2011), changes in the expression of ion channels related to the cardiac AP (Sartiani et al., 2007), varying AP characteristics (Doss et al., 2012), and as a lack of clear t-tubule structures (Lieu et al., 2009; Novak et al., 2012), which all may cause problems in Ca^{2+} cycling due to slower spread of electrical signals and have an effect on the phenotype of the CMs. Additionally, in earlier studies, significant heterogeneity in the subtypes of hiPSC-CMs, including atrial, nodal, and ventricular CMs, has been found with each round of differentiation (Moretti et al., 2010). While this characteristic can be considered an advantage due to the possibility of assessing the physiological properties in all these cell types, the disadvantage is that changes that occur only in one subpopulation of cells cannot be specified when the readout is taken from all cells (Sinnecker et al., 2014). The various CM subtypes express differential sets of transcription factors, structural proteins and ion channels and have distinguishable AP parameters (David and Franz, 2012). Therefore, the arrhythmic events detected in these subtypes can also vary. The development of cardiac differentiation and maturation protocols will hopefully improve the homogeneity of iPSCs; however, clarifying the rules for what should be considered mature CMs and characterizing the effects of various cardiac subtypes with AP measurements will be important.

In Studies II-IV, the type of CMs (nodal, atrial, or ventricular) under investigation was unclear in the Ca^{2+} imaging studies because Ca^{2+} imaging method cannot be used to determine the CM type. The differences between the CM types can affect the Ca^{2+} cycling and future simultaneous recording of APs and Ca^{2+} would help to distinguish the CM type and provide mechanistic information regarding the interplay between Ca^{2+} cycling and the membrane potential. Understanding the electrophysiological mechanism behind different Ca^{2+} cycling abnormalities will also be very important. In Studies III and IV, AP characteristics, SR Ca^{2+} storage or Ca^{2+} sparks indicating Ca^{2+} leak from SR were not studied between different mutations, which would allow more information regarding mutation-specific differences. These differences could be addressed in the future by patch clamp, Ca^{2+} imaging methods and computational models.

Because the nature of abnormal Ca^{2+} analysis has been visual inspection, this analysis was performed subjectively in Studies II-IV and may not be repeatable between two persons. However, this problem occurs for all manual data analyses. Consistent rules for the analysis of Ca^{2+} signal abnormalities are currently lacking, and AnomalyExplorer software was generated for this reason. Because this program does not consider the interplay between AP and Ca^{2+} or quantify the Ca^{2+} cycling parameters, these abnormalities could be studied and improved in the future. The user-defined analysis parameters in AnomalyExplorer might cause differences between two individuals performing the analysis, although those parameters are needed for analyses performed with different software and/or with different sampling frequencies. In addition, AnomalyExplorer was designed and implemented for a specific use case and for specific digitization systems, which can be stated as a limitation of the current prototype. Therefore, some future improvement may be needed, for example, for analysis of high frequency Ca^{2+} signals.

In clinical recordings in Study II, the noise and acquisition frequency of the ECG signal can be limiting factors in the 24-h recordings and affect the results of the recordings. One limitation of the MAP method used in Study II was that it records extracellular activity and can provide only limited information regarding events occurring across the cell membranes. In Study III, we were permitted to study only acute effects of intravenously administered dantrolene and, therefore, cannot state the long-term clinical effects of the drug. Additionally, although the dose of dantrolene was titrated according to the weights of the patients, serum levels of the drug were not measured and could have varied from patient to patient, resulting in concentration-dependent variations in clinical responses.

6.5 Future perspectives

The advantages of iPSCs cannot be ignored in disease modeling, designing personalized medications for patients, preclinical drug testing and regenerative medicine in the future. iPSCs do not have ethical issues like ESCs, and compared to animal models, they mimic the physiological conditions more close to humans and have a possibility of providing consistent phenotypes of the diseases.

Cardiac disease modeling with single-cell iPSC-CM technology is challenging because the CM monolayer environment lacks the cell–cell connections between both CMs and non-

myocytes found *in vivo*, as well as the interactions with the ECM and mechanical forces that are important for maintaining morphology, maturity, and molecular composition. In addition, the CM monolayer does not mimic the native cardiac tissue because impulse propagation in the heart depends on not only the excitability of individual CMs but also impulse transmission between adjacent myocytes and the 3D arrangement of those cells (Smaill et al., 2013), thus constraining the modeling of cardiac diseases in monolayers. Therefore, future cardiac disease modeling, as well as the case of CPVT, could benefit from 3D culture models that resemble native cardiac tissue. For these models, cultures that include other cells should be developed because, for example, endothelial-CM contacts are known to be crucial for maintaining the rhythmic and synchronous contraction of CMs (Smaill et al., 2013). The development of 3D culture models would minimize the immaturity of cultures by enhancing the structural organization of the cells and improving the contractile performance and Ca^{2+} cycling of CMs, which would benefit the disease and arrhythmia modeling of CPVT and the study of Ca^{2+} cycling propagation and abnormalities of these cells.

As iPSCs eliminate the chances of immunorejection, they hold great importance in regenerative medicine and in gene therapy, with the possibility of using isogenic corrected cell lines in complete correction of a genetic deficiency. However, before future clinical applications, more comprehensive knowledge of the reprogramming process is needed. To reach the potential of iPSCs technology, many questions related to safety issues and to the method efficiency need to be solved. Optimal and efficient non-integrating reprogramming factors need to be found due to the problems with genomic integration of the viral transgenes, possible reactivation of even silenced reprogramming genes and the risk of tumorigenesis. Novel nonviral and non-genetic methods for reprogramming are improving quickly, and these methods may resolve these problems. For therapeutic purposes in the future, the culture conditions of iPSCs have to be xeno-free, and genomic alterations and chromosomal abnormalities during reprogramming and culturing have to be avoided. Overall, methods to evaluate the safety of iPSCs in clinical applications must be clarified. Cardiac regenerative medicine holds its own challenges; for example, proper Ca^{2+}-cycling and electrophysiological properties are also essential in these applications because transplantation of cells with improper characteristic could lead to potentially lethal arrhythmias, and proper integration of the transplanted cells into the recipient heart is essential. Derivation of iPSCs is rather slow, which may limit their use in the treatment of acute conditions such as myocardial infarction (MI). One solution for this problem may be direct reprogramming of fibro-

blasts into iCMs, which is already under investigation (Fu et al., 2013; Nam et al., 2013; Wada et al., 2013). Currently, iPSC technology is primarily utilized only with laboratory scale production and testing assays, and its efficiency needs to be increased for the use of these cells in the larger scale in clinical applications. The economic issues related to iPSCs need to be considered because the generation of cell lines and a sufficient amount of CMs for each treatment or drug screening studies is costly.

Currently, clinical cell therapy applications of patient- and disease-specific iPSC-derived CMs are not yet available due to various challenges. However, these cells have potential to be exploited for designing individualized medications and for the diagnostics of genetic cardiac diseases because they provide a great improvement compared to previous animal models and transfected non-cardiac cells (Savla et al., 2014; Sugiyama, 2008). Of course, for reliable studies regarding pathogenesis and for pharmacological testing related to cardiac diseases, the cardiac differentiation methods and maturation need to be improved. Large quantities of more homogenous and adult-like mature populations of CMs are needed with sufficient quality for these applications. Overall, the requirements for the maturation state of the hPSC-derived CMs need to be investigated and determined, and maturation may need to be enhanced, with alterations in culture conditions, for example, with electrical or mechanical stimulation. Additionally, to develop highly efficient differentiation protocols, purification and cell sorting of CMs from a heterogeneous cell population could be beneficial.

The further validation of iPSCs as a drug discovery technology helps the pharmaceutical industry to avoid failed drug development programs and may lead to a new era where preclinical testing in non-predictive animal models can be reduced and where testing can proceed directly from *in vitro* trials to actual clinical trials in patients. As differentiation protocols and high-throughput techniques improve, iPSC technology may play an integral role in developing new pharmacologic agents for genetically based diseases and in screening compounds for potential cardiotoxicity. In addition to identifying new compounds, iPSC-derived disease-specific CMs could be used to test drug responsiveness *in vitro* before administration of the drug to the patient. iPSC-derived cells could prevent drugs with severe cardiac side effects to enter the market. In addition, these cells could be used for screening against druggable targets in cells that recapitulate disease pathology or to determine whether a particular target contributes to the pathogenesis of a specific disease (Sterneckert et al., 2014).

In disease modeling, the combination of iPSC technology together with clinical experiments will help clarify the mechanisms behind the diseases and optimize treatment in a patient-specific manner. Thus, the iPSC disease model can be validated clinically and utilized increasingly in the future as a safe platform for studying therapeutic options for patients. iPSC technology is beneficial especially in diseases such as CPVT, which may arise from hundreds of different mutations, and optimal therapy is likely to be mutation or even patient specific. Therefore, studies of CPVT will likely shift from animal models to iPSC models combined with clinical trials. Of course, with regard to a disease with a high risk of SCD such as CPVT, arrhythmia risk prediction and prevention are extremely crucial for these patients and for the pathophysiology of the disease, and new treatment options need to be studied further.

7 Conclusions and outlook

The aim of this thesis was functional characterization of CMs and generation of a CPVT-disease model with iPSC-derived CMs to study, characterize and treat the arrhythmic events of these cells *in vitro* as well as to validate the results in patients *in vivo*. Based on the four studies presented, the following conclusions can be drawn:

- EFS with a novel device did not enhance functional or morphological properties of NRCs. However, stimulation could be used for short-term pacing. Stimulation affected gene expression of some main cardiac proteins, suggesting that stimulation could be utilized to enhance CM differentiation and maturation.
- Using hiPSC technology, CPVT-specific iPSC lines carrying different RyR2 mutations could be established and differentiated into functional CPVT CMs recapitulating the disease phenotype observed in patients.
- CPVT CMs carrying the P2328S mutation showed abnormalities in electrophysiology in the form of DADs and EADs. Novel mechanistic insight regarding EADs in CPVT was also evident in the index patient.
- CPVT CMs showed defects and abnormalities in Ca^{2+} cycling *in vitro,* which in addition to drug responses, varied between different RyR2 mutations, suggesting patient- or mutation-specific differences in the mechanisms of arrhythmias.
- Dantrolene showed mutation-specific antiarrhythmic effects *in vivo* in CPVT patients and iPSC-derived CPVT CMs generated from the same patients reproduced these drug responses. These findings illustrate the potential of iPSC models to serve as a platform for disease modeling and for design of personalized medication of inherited diseases.
- A novel software for the classification of abnormal Ca^{2+} transient patterns detected in iPSC-derived CMs was developed. This tool, which was based on interactive visualization, will facilitate and speed up the analysis of Ca^{2+} signals by making it more accurate and person-independent compared to traditional visual analysis.

In conclusion, the findings in this thesis show that iPSC disease models can be used to clarify the mechanisms behind the diseases and to optimize treatment in a mutation- or patient-

specific manner. Translational studies provide important insight regarding how the iPSC-derived CMs resemble and predict the clinical phenotype and outcomes of the patient, therefore helping to improve our understanding of CPVT. Most importantly, these findings give proof of concept about how insights gained in basic research can be translated into benefits for patients in clinical practice. Because the deficient Ca^{2+} cycling behavior in CPVT pathophysiology resembles those observed in patients with HF, the results of these mechanistic findings could also be beneficial for patients other than those with CPVT.

References

Aasen, T., Raya, A., Barrero, M.J., Garreta, E., Consiglio, A., Gonzalez, F., Vassena, R., Bilic, J., Pekarik, V., Tiscornia, G., Edel, M., Boue, S., and Izpisua Belmonte, J.C. (2008). Efficient and rapid generation of induced pluripotent stem cells from human keratinocytes. Nat. Biotechnol. *26,* 1276-1284.

Acimovic, I., Vilotic, A., Pesl, M., Lacampagne, A., Dvorak, P., Rotrekl, V., and Meli, A.C. (2014). Human pluripotent stem cell-derived cardiomyocytes as research and therapeutic tools. Biomed. Res. Int. *2014,* 512831.

Ackerman, M.J., Priori, S.G., Willems, S., Berul, C., Brugada, R., Calkins, H., Camm, A.J., Ellinor, P.T., Gollob, M., Hamilton, R., Hershberger, R.E., Judge, D.P., Le Marec, H., McKenna, W.J., Schulze-Bahr, E., Semsarian, C., Towbin, J.A., Watkins, H., Wilde, A., Wolpert, C., and Zipes, D.P. (2011). HRS/EHRA expert consensus statement on the state of genetic testing for the channelopathies and cardiomyopathies this document was developed as a partnership between the Heart Rhythm Society (HRS) and the European Heart Rhythm Association (EHRA). Heart Rhythm *8,* 1308-1339.

Adams, S.R. (2010). How calcium indicators work. Cold Spring Harb Protoc. *2010,* pdb.top70.

Adewumi, O., Aflatoonian, B., Ahrlund-Richter, L., Amit, M., Andrews, P.W., Beighton, G., Bello, P.A., Benvenisty, N., Berry, L.S., Bevan, S., Blum, B., Brooking, J., Chen, K.G., Choo, A.B., Churchill, G.A., Corbel, M., Damjanov, I., Draper, J.S., Dvorak, P., Emanuelsson, K., Fleck, R.A., Ford, A., Gertow, K., Gertsenstein, M., Gokhale, P.J., Hamilton, R.S., Hampl, A., Healy, L.E., Hovatta, O., Hyllner, J., Imreh, M.P., Itskovitz-Eldor, J., Jackson, J., Johnson, J.L., Jones, M., Kee, K., King, B.L., Knowles, B.B., Lako, M., Lebrin, F., Mallon, B.S., Manning, D., Mayshar, Y., McKay, R.D., Michalska, A.E., Mikkola, M., Mileikovsky, M., Minger, S.L., Moore, H.D., Mummery, C.L., Nagy, A., Nakatsuji, N., O'Brien, C.M., Oh, S.K., Olsson, C., Otonkoski, T., Park, K.Y., Passier, R., Patel, H., Patel, M., Pedersen, R., Pera, M.F., Piekarczyk, M.S., Pera, R.A., Reubinoff, B.E., Robins, A.J., Rossant, J., Rugg-Gunn, P., Schulz, T.C., Semb, H., Sherrer, E.S., Siemen, H., Stacey, G.N., Stojkovic, M., Suemori, H., Szatkiewicz, J., Turetsky, T., Tuuri, T., van den Brink, S., Vintersten, K., Vuoristo, S., Ward, D., Weaver, T.A., Young, L.A., and Zhang, W. (2007). Characterization of human embryonic stem cell lines by the International Stem Cell Initiative. Nat. Biotechnol. *25,* 803-816.

Agarwal, A., Goss, J.A., Cho, A., McCain, M.L., and Parker, K.K. (2013). Microfluidic heart on a chip for higher throughput pharmacological studies. Lab. Chip *13,* 3599-3608.

Ahola, A., Kiviaho, A.L., Larsson, K., Honkanen, M., Aalto-Setala, K., and Hyttinen, J. (2014). Video image-based analysis of single human induced pluripotent stem cell derived cardiomyocyte beating dynamics using digital image correlation. Biomed. Eng. Online *13,* 39-925X-13-39.

Amin, A.S., Tan, H.L., and Wilde, A.A. (2010). Cardiac ion channels in health and disease. Heart Rhythm *7*, 117-126.

Anokye-Danso, F., Trivedi, C.M., Juhr, D., Gupta, M., Cui, Z., Tian, Y., Zhang, Y., Yang, W., Gruber, P.J., Epstein, J.A., and Morrisey, E.E. (2011). Highly efficient miRNA-mediated reprogramming of mouse and human somatic cells to pluripotency. Cell. Stem Cell. *8*, 376-388.

Anyatonwu, G.I., Estrada, M., Tian, X., Somlo, S., and Ehrlich, B.E. (2007). Regulation of ryanodine receptor-dependent calcium signaling by polycystin-2. Proc. Natl. Acad. Sci. U. S. A. *104*, 6454-6459.

Asp, J., Steel, D., Jonsson, M., Ameen, C., Dahlenborg, K., Jeppsson, A., Lindahl, A., and Sartipy, P. (2010). Cardiomyocyte clusters derived from human embryonic stem cells share similarities with human heart tissue. J Mol Cell Biol *2*, 276-83.

Au, H.T., Cheng, I., Chowdhury, M.F., and Radisic, M. (2007). Interactive effects of surface topography and pulsatile electrical field stimulation on orientation and elongation of fibroblasts and cardiomyocytes. Biomaterials *28*, 4277-93.

Au, H.T., Cui, B., Chu, Z.E., Veres, T., and Radisic, M. (2009). Cell culture chips for simultaneous application of topographical and electrical cues enhance phenotype of cardiomyocytes. Lab Chip *9*, 564-75.

Barash, Y., Dvir, T., Tandeitnik, P., Ruvinov, E., Guterman, H., and Cohen, S. (2010). Electric field stimulation integrated into perfusion bioreactor for cardiac tissue engineering. Tissue Eng Part C Methods *16*, 1417-26.

Bauwens, C.L., Peerani, R., Niebruegge, S., Woodhouse, K.A., Kumacheva, E., Husain, M., and Zandstra, P.W. (2008). Control of human embryonic stem cell colony and aggregate size heterogeneity influences differentiation trajectories. Stem Cells *26*, 2300-2310.

Bayart, E., and Cohen-Haguenauer, O. (2013). Technological overview of iPS induction from human adult somatic cells. Curr. Gene Ther. *13*, 73-92.

Bedada, F.B., Chan, S.S., Metzger, S.K., Zhang, L., Zhang, J., Garry, D.J., Kamp, T.J., Kyba, M., and Metzger, J.M. (2014). Acquisition of a quantitative, stoichiometrically conserved ratiometric marker of maturation status in stem cell-derived cardiac myocytes. Stem Cell. Reports *3*, 594-605.

Bellin, M., Marchetto, M.C., Gage, F.H., and Mummery, C.L. (2012). Induced pluripotent stem cells: the new patient? Nat. Rev. Mol. Cell Biol. *13*, 713-726.

Beqqali, A., Kloots, J., Ward-van Oostwaard, D., Mummery, C., and Passier, R. (2006). Genome-wide transcriptional profiling of human embryonic stem cells differentiating to cardiomyocytes. Stem Cells *24*, 1956-1967.

Berdondini, L., van der Wal, P.D., Guenat, O., de Rooij, N.F., Koudelka-Hep, M., Seitz, P., Kaufmann, R., Metzler, P., Blanc, N., and Rohr, S. (2005). High-density electrode array for imaging in vitro electrophysiological activity. Biosens. Bioelectron. *21,* 167-174.

Bers, D.M. (2002). Cardiac excitation-contraction coupling. Nature *415,* 198-205.

Bhuiyan, Z.A., Hamdan, M.A., Shamsi, E.T., Postma, A.V., Mannens, M.M., Wilde, A.A., and Al-Gazali, L. (2007). A novel early onset lethal form of catecholaminergic polymorphic ventricular tachycardia maps to chromosome 7p14-p22. J. Cardiovasc. Electrophysiol. *18,* 1060-1066.

Binah, O., Dolnikov, K., Sadan, O., Shilkrut, M., Zeevi-Levin, N., Amit, M., Danon, A., and Itskovitz-Eldor, J. (2007). Functional and developmental properties of human embryonic stem cells-derived cardiomyocytes. J. Electrocardiol. *40,* S192-6.

Bollini, S., Smart, N., and Riley, P.R. (2011). Resident cardiac progenitor cells: at the heart of regeneration. J. Mol. Cell. Cardiol. *50,* 296-303.

Boudou, T., Legant, W.R., Mu, A., Borochin, M.A., Thavandiran, N., Radisic, M., Zandstra, P.W., Epstein, J.A., Margulies, K.B., and Chen, C.S. (2012). A microfabricated platform to measure and manipulate the mechanics of engineered cardiac microtissues. Tissue Eng. Part A. *18,* 910-919.

Braam, S.R., Tertoolen, L., van de Stolpe, A., Meyer, T., Passier, R., and Mummery, C.L. (2010). Prediction of drug-induced cardiotoxicity using human embryonic stem cell-derived cardiomyocytes. Stem Cell. Res. *4,* 107-116.

Brand, T. (2003). Heart development: molecular insights into cardiac specification and early morphogenesis. Dev. Biol. *258,* 1-19.

Brivanlou, A.H., Gage, F.H., Jaenisch, R., Jessell, T., Melton, D., and Rossant, J. (2003). Stem cells. Setting standards for human embryonic stem cells. Science *300,* 913-916.

Brown, R.D., Ambler, S.K., Mitchell, M.D., and Long, C.S. (2005). The cardiac fibroblast: therapeutic target in myocardial remodeling and failure. Annu. Rev. Pharmacol. Toxicol. *45,* 657-687.

Burridge, P.W., Matsa, E., Shukla, P., Lin, Z.C., Churko, J.M., Ebert, A.D., Lan, F., Diecke, S., Huber, B., Mordwinkin, N.M., Plews, J.R., Abilez, O.J., Cui, B., Gold, J.D., and Wu, J.C. (2014). Chemically defined generation of human cardiomyocytes. Nat. Methods *11,* 855-860.

Camors, E., and Valdivia, H.H. (2014). CaMKII regulation of cardiac ryanodine receptors and inositol triphosphate receptors. Front. Pharmacol. *5,* 101.

Cao, F., Wagner, R.A., Wilson, K.D., Xie, X., Fu, J.D., Drukker, M., Lee, A., Li, R.A., Gambhir, S.S., Weissman, I.L., Robbins, R.C., and Wu, J.C. (2008). Transcriptional and func-

tional profiling of human embryonic stem cell-derived cardiomyocytes. PLoS One *3*, e3474.

Carvajal-Vergara, X., Sevilla, A., D'Souza, S.L., Ang, Y.S., Schaniel, C., Lee, D.F., Yang, L., Kaplan, A.D., Adler, E.D., Rozov, R., Ge, Y., Cohen, N., Edelmann, L.J., Chang, B., Waghray, A., Su, J., Pardo, S., Lichtenbelt, K.D., Tartaglia, M., Gelb, B.D., and Lemischka, I.R. (2010). Patient-specific induced pluripotent stem-cell-derived models of LEOPARD syndrome. Nature *465*, 808-12.

Casini, S., Verkerk, A.O., van Borren, M.M., van Ginneken, A.C., Veldkamp, M.W., de Bakker, J.M., and Tan, H.L. (2009). Intracellular calcium modulation of voltage-gated sodium channels in ventricular myocytes. Cardiovasc. Res. *81*, 72-81.

Caspi, O., Itzhaki, I., Kehat, I., Gepstein, A., Arbel, G., Huber, I., Satin, J., and Gepstein, L. (2009). In vitro electrophysiological drug testing using human embryonic stem cell derived cardiomyocytes. Stem Cells Dev. *18*, 161-172.

Cerrone, M., Colombi, B., Santoro, M., di Barletta, M.R., Scelsi, M., Villani, L., Napolitano, C., and Priori, S.G. (2005). Bidirectional ventricular tachycardia and fibrillation elicited in a knock-in mouse model carrier of a mutation in the cardiac ryanodine receptor. Circ Res *96*, e77-82.

Cerrone, M., Napolitano, C., and Priori, S.G. (2009). Catecholaminergic polymorphic ventricular tachycardia: A paradigm to understand mechanisms of arrhythmias associated to impaired Ca(2+) regulation. Heart Rhythm *6*, 1652-9.

Chan, Y.C., Ting, S., Lee, Y.K., Ng, K.M., Zhang, J., Chen, Z., Siu, C.W., Oh, S.K., and Tse, H.F. (2013). Electrical stimulation promotes maturation of cardiomyocytes derived from human embryonic stem cells. J. Cardiovasc. Transl. Res. *6*, 989-999.

Chang, W.T., Yu, D., Lai, Y.C., Lin, K.Y., and Liau, I. (2013). Characterization of the mechanodynamic response of cardiomyocytes with atomic force microscopy. Anal. Chem. *85*, 1395-1400.

Chiu, L.L., Iyer, R.K., King, J.P., and Radisic, M. (2008). Biphasic electrical field stimulation aids in tissue engineering of multicell-type cardiac organoids. Tissue Eng Part A *17*, 1465-77.

Chiu, L.L., Janic, K., and Radisic, M. (2012). Engineering of oriented myocardium on three-dimensional micropatterned collagen-chitosan hydrogel. Int. J. Artif. Organs *35*, 237-250.

Coumel, P., Fidelle, J., Lucet, V., Attuel, P., and Bouvrain, Y. (1978). Catecholaminergic-induced severe ventricular arrhythmias with Adams-Stokes syndrome in children: report of four cases. Br Heart J. *40*, 28-37.

David, R., and Franz, W.M. (2012). From pluripotency to distinct cardiomyocyte subtypes. Physiology (Bethesda) *27*, 119-129.

Di Pasquale, E., Lodola, F., Miragoli, M., Denegri, M., Avelino-Cruz, J.E., Buonocore, M., Nakahama, H., Portararo, P., Bloise, R., Napolitano, C., Condorelli, G., and Priori, S.G. (2013). CaMKII inhibition rectifies arrhythmic phenotype in a patient-specific model of catecholaminergic polymorphic ventricular tachycardia. Cell. Death Dis. *4,* e843.

Diaz, M.E., Eisner, D.A., and O'Neill, S.C. (2002). Depressed ryanodine receptor activity increases variability and duration of the systolic Ca2+ transient in rat ventricular myocytes. Circ. Res. *91,* 585-593.

Diaz, M.E., O'Neill, S.C., and Eisner, D.A. (2004). Sarcoplasmic reticulum calcium content fluctuation is the key to cardiac alternans. Circ. Res. *94,* 650-656.

Ding, Q., Lee, Y.K., Schaefer, E.A., Peters, D.T., Veres, A., Kim, K., Kuperwasser, N., Motola, D.L., Meissner, T.B., Hendriks, W.T., Trevisan, M., Gupta, R.M., Moisan, A., Banks, E., Friesen, M., Schinzel, R.T., Xia, F., Tang, A., Xia, Y., Figueroa, E., Wann, A., Ahfeldt, T., Daheron, L., Zhang, F., Rubin, L.L., Peng, L.F., Chung, R.T., Musunuru, K., and Cowan, C.A. (2013). A TALEN genome-editing system for generating human stem cell-based disease models. Cell. Stem Cell. *12,* 238-251.

Doss, M.X., Di Diego, J.M., Goodrow, R.J., Wu, Y., Cordeiro, J.M., Nesterenko, V.V., Barajas-Martinez, H., Hu, D., Urrutia, J., Desai, M., Treat, J.A., Sachinidis, A., and Antzelevitch, C. (2012). Maximum diastolic potential of human induced pluripotent stem cell-derived cardiomyocytes depends critically on I(Kr). PLoS One *7,* e40288.

Ebert, A.D., Liang, P., and Wu, J.C. (2012). Induced pluripotent stem cells as a disease modeling and drug screening platform. J. Cardiovasc. Pharmacol. *60,* 408-416.

Elliott, D.A., Braam, S.R., Koutsis, K., Ng, E.S., Jenny, R., Lagerqvist, E.L., Biben, C., Hatzistavrou, T., Hirst, C.E., Yu, Q.C., Skelton, R.J., Ward-van Oostwaard, D., Lim, S.M., Khammy, O., Li, X., Hawes, S.M., Davis, R.P., Goulburn, A.L., Passier, R., Prall, O.W., Haynes, J.M., Pouton, C.W., Kaye, D.M., Mummery, C.L., Elefanty, A.G., and Stanley, E.G. (2011). NKX2-5(eGFP/w) hESCs for isolation of human cardiac progenitors and cardiomyocytes. Nat. Methods *8,* 1037-1040.

Eschenhagen, T., Didie, M., Munzel, F., Schubert, P., Schneiderbanger, K., and Zimmermann, W.H. (2002). 3D engineered heart tissue for replacement therapy. Basic Res Cardiol *97 Suppl 1,* I146-52.

Faggioni, M., Kryshtal, D.O., and Knollmann, B.C. (2012). Calsequestrin mutations and catecholaminergic polymorphic ventricular tachycardia. Pediatr. Cardiol. *33,* 959-967.

Fatima, A., Xu, G., Shao, K., Papadopoulos, S., Lehmann, M., Arnaiz-Cot, J.J., Rosa, A.O., Nguemo, F., Matzkies, M., Dittmann, S., Stone, S.L., Linke, M., Zechner, U., Beyer, V., Hennies, H.C., Rosenkranz, S., Klauke, B., Parwani, A.S., Haverkamp, W., Pfitzer, G., Farr, M., Cleemann, L., Morad, M., Milting, H., Hescheler, J., and Saric, T. (2011). In vitro Modeling of Ryanodine Receptor 2 Dysfunction Using Human Induced Pluripotent Stem Cells. Cell Physiol Biochem *28,* 579-92.

Ferrantini, C., Crocini, C., Coppini, R., Vanzi, F., Tesi, C., Cerbai, E., Poggesi, C., Pavone, F.S., and Sacconi, L. (2013). The transverse-axial tubular system of cardiomyocytes. Cell Mol. Life Sci. *70*, 4695-4710.

Franz, M.R. (1999). Current status of monophasic action potential recording: theories, measurements and interpretations. Cardiovasc. Res. *41*, 25-40.

Fu, J.D., Jiang, P., Rushing, S., Liu, J., Chiamvimonvat, N., and Li, R.A. (2010). Na+/Ca2+ exchanger is a determinant of excitation-contraction coupling in human embryonic stem cell-derived ventricular cardiomyocytes. Stem Cells Dev. *19*, 773-782.

Fu, J.D., Stone, N.R., Liu, L., Spencer, C.I., Qian, L., Hayashi, Y., Delgado-Olguin, P., Ding, S., Bruneau, B.G., and Srivastava, D. (2013). Direct reprogramming of human fibroblasts toward a cardiomyocyte-like state. Stem Cell. Reports *1*, 235-247.

Fusaki, N., Ban, H., Nishiyama, A., Saeki, K., and Hasegawa, M. (2009). Efficient induction of transgene-free human pluripotent stem cells using a vector based on Sendai virus, an RNA virus that does not integrate into the host genome. Proc. Jpn. Acad. Ser. B. Phys. Biol. Sci. *85*, 348-362.

Gaborit, N., Le Bouter, S., Szuts, V., Varro, A., Escande, D., Nattel, S., and Demolombe, S. (2007). Regional and tissue specific transcript signatures of ion channel genes in the non-diseased human heart. J. Physiol. *582*, 675-693.

George, C.H. (2008). Sarcoplasmic reticulum Ca2+ leak in heart failure: mere observation or functional relevance? Cardiovasc. Res. *77*, 302-314.

George, C.H., Higgs, G.V., and Lai, F.A. (2003). Ryanodine receptor mutations associated with stress-induced ventricular tachycardia mediate increased calcium release in stimulated cardiomyocytes. Circ. Res. *93*, 531-540.

Graichen, R., Xu, X., Braam, S.R., Balakrishnan, T., Norfiza, S., Sieh, S., Soo, S.Y., Tham, S.C., Mummery, C., Colman, A., Zweigerdt, R., and Davidson, B.P. (2008). Enhanced cardiomyogenesis of human embryonic stem cells by a small molecular inhibitor of p38 MAPK. Differentiation *76*, 357-370.

Grant, A.O. (2009). Cardiac ion channels. Circ. Arrhythm Electrophysiol. *2*, 185-194.

Grynkiewicz, G., Poenie, M., and Tsien, R.Y. (1985). A new generation of Ca2+ indicators with greatly improved fluorescence properties. J. Biol. Chem. *260*, 3440-3450.

Halbach, M., Pillekamp, F., Brockmeier, K., Hescheler, J., Muller-Ehmsen, J., and Reppel, M. (2006). Ventricular slices of adult mouse hearts--a new multicellular in vitro model for electrophysiological studies. Cell. Physiol. Biochem. *18*, 1-8.

Hall, S.R., Wang, L., Milne, B., and Hong, M. (2005). Left ventricular dysfunction after acute intracranial hypertension is associated with increased hydroxyl free radical production,

cardiac ryanodine hyperphosphorylation, and troponin I degradation. J. Heart Lung Transplant. *24,* 1639-1649.

Hamill, O.P., Marty, A., Neher, E., Sakmann, B., and Sigworth, F.J. (1981). Improved patch-clamp techniques for high-resolution current recording from cells and cell-free membrane patches. Pflugers Arch *391,* 85-100.

Han, L., Li, Y., Tchao, J., Kaplan, A.D., Lin, B., Li, Y., Mich-Basso, J., Lis, A., Hassan, N., London, B., Bett, G.C., Tobita, K., Rasmusson, R.L., and Yang, L. (2014). Study familial hypertrophic cardiomyopathy using patient-specific induced pluripotent stem cells. Cardiovasc. Res.

Hayakawa, T., Kunihiro, T., Dowaki, S., Uno, H., Matsui, E., Uchida, M., Kobayashi, S., Yasuda, A., Shimizu, T., and Okano, T. (2012). Noninvasive evaluation of contractile behavior of cardiomyocyte monolayers based on motion vector analysis. Tissue Eng. Part C. Methods *18,* 21-32.

Hayashi, M., Denjoy, I., Extramiana, F., Maltret, A., Buisson, N.R., Lupoglazoff, J.M., Klug, D., Hayashi, M., Takatsuki, S., Villain, E., Kamblock, J., Messali, A., Guicheney, P., Lunardi, J., and Leenhardt, A. (2009). Incidence and risk factors of arrhythmic events in catecholaminergic polymorphic ventricular tachycardia. Circulation *119,* 2426-2434.

Hayashi, M., Denjoy, I., Hayashi, M., Extramiana, F., Maltret, A., Roux-Buisson, N., Lupoglazoff, J.M., Klug, D., Maury, P., Messali, A., Guicheney, P., and Leenhardt, A. (2012). The role of stress test for predicting genetic mutations and future cardiac events in asymptomatic relatives of catecholaminergic polymorphic ventricular tachycardia probands. Europace *14,* 1344-1351.

Hazeltine, L.B., Badur, M.G., Lian, X., Das, A., Han, W., and Palecek, S.P. (2014). Temporal impact of substrate mechanics on differentiation of human embryonic stem cells to cardiomyocytes. Acta Biomater. *10,* 604-612.

Hazeltine, L.B., Simmons, C.S., Salick, M.R., Lian, X., Badur, M.G., Han, W., Delgado, S.M., Wakatsuki, T., Crone, W.C., Pruitt, B.L., and Palecek, S.P. (2012). Effects of substrate mechanics on contractility of cardiomyocytes generated from human pluripotent stem cells. Int. J. Cell. Biol. *2012,* 508294.

Hedgepath, K.R., Mukherjee, R., Wang, Z., and Spinale, F.G. (1997). The relation between changes in myocyte orientation and contractile function with electrical field stimulation. Basic Res Cardiol *92,* 385-90.

Henning, R.J. (2011). Stem cells in cardiac repair. Future Cardiol. *7,* 99-117.

Hilliard, F.A., Steele, D.S., Laver, D., Yang, Z., Le Marchand, S.J., Chopra, N., Piston, D.W., Huke, S., and Knollmann, B.C. (2010). Flecainide inhibits arrhythmogenic Ca2+ waves by open state block of ryanodine receptor Ca2+ release channels and reduction of Ca2+ spark mass. J. Mol. Cell. Cardiol. *48,* 293-301.

Hirt, M.N., Boeddinghaus, J., Mitchell, A., Schaaf, S., Bornchen, C., Muller, C., Schulz, H., Hubner, N., Stenzig, J., Stoehr, A., Neuber, C., Eder, A., Luther, P.K., Hansen, A., and Eschenhagen, T. (2014). Functional improvement and maturation of rat and human engineered heart tissue by chronic electrical stimulation. J. Mol. Cell. Cardiol. *74,* 151-161.

Hoffman, L.M., and Carpenter, M.K. (2005). Characterization and culture of human embryonic stem cells. Nat. Biotechnol. *23,* 699-708.

Holt, E., Lunde, P.K., Sejersted, O.M., and Christensen, G. (1997). Electrical stimulation of adult rat cardiomyocytes in culture improves contractile properties and is associated with altered calcium handling. Basic Res Cardiol *92,* 289-98.

Hu, K. (2014). All roads lead to induced pluripotent stem cells: the technologies of iPSC generation. Stem Cells Dev. *23,* 1285-1300.

Huke, S., and Knollmann, B.C. (2010). Increased myofilament Ca2+-sensitivity and arrhythmia susceptibility. J. Mol. Cell. Cardiol. *48,* 824-833.

Hund, T.J., and Mohler, P.J. (2014). Role of CaMKII in cardiac arrhythmias. Trends Cardiovasc. Med.

Hwang, H.S., Hasdemir, C., Laver, D., Mehra, D., Turhan, K., Faggioni, M., Yin, H., and Knollmann, B.C. (2011). Inhibition of cardiac Ca2+ release channels (RyR2) determines efficacy of class I antiarrhythmic drugs in catecholaminergic polymorphic ventricular tachycardia. Circ. Arrhythm Electrophysiol. *4,* 128-135.

Ieda, M., Fu, J.D., Delgado-Olguin, P., Vedantham, V., Hayashi, Y., Bruneau, B.G., and Srivastava, D. (2010). Direct reprogramming of fibroblasts into functional cardiomyocytes by defined factors. Cell *142,* 375-386.

Ikemoto, N., and Yamamoto, T. (2002). Regulation of calcium release by interdomain interaction within ryanodine receptors. Front. Biosci. *7,* d671-83.

Itzhaki, I., Maizels, L., Huber, I., Gepstein, A., Arbel, G., Caspi, O., Miller, L., Belhassen, B., Nof, E., Glikson, M., and Gepstein, L. (2012). Modeling of catecholaminergic polymorphic ventricular tachycardia with patient-specific human-induced pluripotent stem cells. J. Am. Coll. Cardiol. *60,* 990-1000.

Itzhaki, I., Maizels, L., Huber, I., Zwi-Dantsis, L., Caspi, O., Winterstern, A., Feldman, O., Gepstein, A., Arbel, G., Hammerman, H., Boulos, M., and Gepstein, L. (2011a). Modelling the long QT syndrome with induced pluripotent stem cells. Nature *471,* 225-9.

Itzhaki, I., Rapoport, S., Huber, I., Mizrahi, I., Zwi-Dantsis, L., Arbel, G., Schiller, J., and Gepstein, L. (2011b). Calcium handling in human induced pluripotent stem cell derived cardiomyocytes. PLoS One *6,* e18037.

January, C.T., and Moscucci, A. (1992). Cellular mechanisms of early afterdepolarizations. Ann N Y Acad Sci *644*, 23-32.

Jayawardena, T.M., Egemnazarov, B., Finch, E.A., Zhang, L., Payne, J.A., Pandya, K., Zhang, Z., Rosenberg, P., Mirotsou, M., and Dzau, V.J. (2012). MicroRNA-mediated in vitro and in vivo direct reprogramming of cardiac fibroblasts to cardiomyocytes. Circ. Res. *110*, 1465-1473.

Ji, Q., Liu, H., Mei, Y., Wang, X., Feng, J., and Ding, W. (2013). Expression changes of ionic channels in early phase of cultured rat atrial myocytes induced by rapid pacing. J. Cardiothorac. Surg. *8*, 194-8090-8-194.

Jiang, D., Wang, R., Xiao, B., Kong, H., Hunt, D.J., Choi, P., Zhang, L., and Chen, S.R. (2005). Enhanced store overload-induced Ca2+ release and channel sensitivity to luminal Ca2+ activation are common defects of RyR2 mutations linked to ventricular tachycardia and sudden death. Circ. Res. *97*, 1173-1181.

Jiang, D., Xiao, B., Zhang, L., and Chen, S.R. (2002). Enhanced basal activity of a cardiac Ca2+ release channel (ryanodine receptor) mutant associated with ventricular tachycardia and sudden death. Circ. Res. *91*, 218-225.

Jung, C.B., Moretti, A., Mederos y Schnitzler, M., Iop, L., Storch, U., Bellin, M., Dorn, T., Ruppenthal, S., Pfeiffer, S., Goedel, A., Dirschinger, R.J., Seyfarth, M., Lam, J.T., Sinnecker, D., Gudermann, T., Lipp, P., and Laugwitz, K.L. (2012). Dantrolene rescues arrhythmogenic RYR2 defect in a patient-specific stem cell model of catecholaminergic polymorphic ventricular tachycardia. EMBO Mol. Med. *4*, 180-191.

Kaji, K., Norrby, K., Paca, A., Mileikovsky, M., Mohseni, P., and Woltjen, K. (2009). Virus-free induction of pluripotency and subsequent excision of reprogramming factors. Nature *458*, 771-775.

Kamgoue, A., Ohayon, J., Usson, Y., Riou, L., and Tracqui, P. (2009). Quantification of cardiomyocyte contraction based on image correlation analysis. Cytometry A. *75*, 298-308.

Kannankeril, P.J., Mitchell, B.M., Goonasekera, S.A., Chelu, M.G., Zhang, W., Sood, S., Kearney, D.L., Danila, C.I., De Biasi, M., Wehrens, X.H., Pautler, R.G., Roden, D.M., Taffet, G.E., Dirksen, R.T., Anderson, M.E., and Hamilton, S.L. (2006). Mice with the R176Q cardiac ryanodine receptor mutation exhibit catecholamine-induced ventricular tachycardia and cardiomyopathy. Proc Natl Acad Sci U S A *103*, 12179-84.

Katz, A.M. (2006). Physiology of the heart (Philadelphia, Pa. ; London: Lippincott Williams & Wilkins).

Kawamura, M., Miyagawa, S., Fukushima, S., Saito, A., Miki, K., Ito, E., Sougawa, N., Kawamura, T., Daimon, T., Shimizu, T., Okano, T., Toda, K., and Sawa, Y. (2013). Enhanced survival of transplanted human induced pluripotent stem cell-derived cardiomyocytes by

the combination of cell sheets with the pedicled omental flap technique in a porcine heart. Circulation *128,* S87-94.

Kehat, I., Gepstein, A., Spira, A., Itskovitz-Eldor, J., and Gepstein, L. (2002). High-resolution electrophysiological assessment of human embryonic stem cell-derived cardiomyocytes: a novel in vitro model for the study of conduction. Circ. Res. *91,* 659-661.

Kehat, I., Kenyagin-Karsenti, D., Snir, M., Segev, H., Amit, M., Gepstein, A., Livne, E., Binah, O., Itskovitz-Eldor, J., and Gepstein, L. (2001). Human embryonic stem cells can differentiate into myocytes with structural and functional properties of cardiomyocytes. J Clin Invest *108,* 407-14.

Khademhosseini, A., Ferreira, L., Blumling, J.,3rd, Yeh, J., Karp, J.M., Fukuda, J., and Langer, R. (2006). Co-culture of human embryonic stem cells with murine embryonic fibroblasts on microwell-patterned substrates. Biomaterials *27,* 5968-5977.

Khan, R. (2004). Identifying and understanding the role of pulmonary vein activity in atrial fibrillation. Cardiovasc. Res. *64,* 387-394.

Kim, D.H., Lipke, E.A., Kim, P., Cheong, R., Thompson, S., Delannoy, M., Suh, K.Y., Tung, L., and Levchenko, A. (2010a). Nanoscale cues regulate the structure and function of macroscopic cardiac tissue constructs. Proc Natl Acad Sci U S A *107,* 565-70.

Kim, H.S., Bernitz, J.M., Lee, D.F., and Lemischka, I.R. (2014). Genomic editing tools to model human diseases with isogenic pluripotent stem cells. Stem Cells Dev. *23,* 2673-2686.

Kim, J.B., Greber, B., Arauzo-Bravo, M.J., Meyer, J., Park, K.I., Zaehres, H., and Scholer, H.R. (2009). Direct reprogramming of human neural stem cells by OCT4. Nature *461,* 649-643.

Kim, K., Doi, A., Wen, B., Ng, K., Zhao, R., Cahan, P., Kim, J., Aryee, M.J., Ji, H., Ehrlich, L.I., Yabuuchi, A., Takeuchi, A., Cunniff, K.C., Hongguang, H., McKinney-Freeman, S., Naveiras, O., Yoon, T.J., Irizarry, R.A., Jung, N., Seita, J., Hanna, J., Murakami, P., Jaenisch, R., Weissleder, R., Orkin, S.H., Weissman, I.L., Feinberg, A.P., and Daley, G.Q. (2010b). Epigenetic memory in induced pluripotent stem cells. Nature *467,* 285-290.

Kispert, A., and Herrmann, B.G. (1994). Immunohistochemical analysis of the Brachyury protein in wild-type and mutant mouse embryos. Dev. Biol. *161,* 179-193.

Kiviaho, A.L., Ahola, A., Larsson, K., Penttinen, K., Swan, H., Pekkanen-Mattila, M., Venäläinen, H., Paavola, K., Hyttinen, J., and Aalto-Setala, K. (2015). Distinct electrophysiological and mechanical beating phenotypes of long QT syndrome type 1-specific cardiomyocytes carrying different mutations. Dis. Model. Mech. *8,* 19-31.

Knollmann, B.C. (2013). Induced pluripotent stem cell-derived cardiomyocytes: boutique science or valuable arrhythmia model? Circ. Res. *112,* 969-76; discussion 976.

Knollmann, B.C., Chopra, N., Hlaing, T., Akin, B., Yang, T., Ettensohn, K., Knollmann, B.E., Horton, K.D., Weissman, N.J., Holinstat, I., Zhang, W., Roden, D.M., Jones, L.R., Franzini-Armstrong, C., and Pfeifer, K. (2006). Casq2 deletion causes sarcoplasmic reticulum volume increase, premature Ca2+ release, and catecholaminergic polymorphic ventricular tachycardia. J. Clin. Invest. *116*, 2510-2520.

Kobayashi, S., Bannister, M.L., Gangopadhyay, J.P., Hamada, T., Parness, J., and Ikemoto, N. (2005). Dantrolene stabilizes domain interactions within the ryanodine receptor. J. Biol. Chem. *280*, 6580-6587.

Kobayashi, S., Yano, M., Suetomi, T., Ono, M., Tateishi, H., Mochizuki, M., Xu, X., Uchinoumi, H., Okuda, S., Yamamoto, T., Koseki, N., Kyushiki, H., Ikemoto, N., and Matsuzaki, M. (2009). Dantrolene, a therapeutic agent for malignant hyperthermia, markedly improves the function of failing cardiomyocytes by stabilizing interdomain interactions within the ryanodine receptor. J. Am. Coll. Cardiol. *53*, 1993-2005.

Kobayashi, S., Yano, M., Uchinoumi, H., Suetomi, T., Susa, T., Ono, M., Xu, X., Tateishi, H., Oda, T., Okuda, S., Doi, M., Yamamoto, T., and Matsuzaki, M. (2010). Dantrolene, a therapeutic agent for malignant hyperthermia, inhibits catecholaminergic polymorphic ventricular tachycardia in a RyR2(R2474S/+) knock-in mouse model. Circ. J. *74*, 2579-2584.

Kornyeyev, D., Petrosky, A.D., Zepeda, B., Ferreiro, M., Knollmann, B., and Escobar, A.L. (2012). Calsequestrin 2 deletion shortens the refractoriness of Ca(2)(+) release and reduces rate-dependent Ca(2)(+)-alternans in intact mouse hearts. J. Mol. Cell. Cardiol. *52*, 21-31.

Krause, T., Gerbershagen, M.U., Fiege, M., Weisshorn, R., and Wappler, F. (2004). Dantrolene--a review of its pharmacology, therapeutic use and new developments. Anaesthesia *59*, 364-373.

Krenz, M., and Robbins, J. (2004). Impact of beta-myosin heavy chain expression on cardiac function during stress. J Am Coll Cardiol *44*, 2390-7.

Laflamme, M.A., Chen, K.Y., Naumova, A.V., Muskheli, V., Fugate, J.A., Dupras, S.K., Reinecke, H., Xu, C., Hassanipour, M., Police, S., O'Sullivan, C., Collins, L., Chen, Y., Minami, E., Gill, E.A., Ueno, S., Yuan, C., Gold, J., and Murry, C.E. (2007). Cardiomyocytes derived from human embryonic stem cells in pro-survival factors enhance function of infarcted rat hearts. Nat. Biotechnol. *25*, 1015-1024.

Lahat, H., Pras, E., Olender, T., Avidan, N., Ben-Asher, E., Man, O., Levy-Nissenbaum, E., Khoury, A., Lorber, A., Goldman, B., Lancet, D., and Eldar, M. (2001). A missense mutation in a highly conserved region of CASQ2 is associated with autosomal recessive catecholamine-induced polymorphic ventricular tachycardia in Bedouin families from Israel. Am J Hum Genet *69*, 1378-84.

Lahti, A.L., Kujala, V.J., Chapman, H., Koivisto, A.P., Pekkanen-Mattila, M., Kerkela, E., Hyttinen, J., Kontula, K., Swan, H., Conklin, B.R., Yamanaka, S., Silvennoinen, O., and Aal-

to-Setala, K. (2012). Model for long QT syndrome type 2 using human iPS cells demonstrates arrhythmogenic characteristics in cell culture. Dis. Model. Mech. *5*, 220-230.

Lai, M.I., Wendy-Yeo, W.Y., Ramasamy, R., Nordin, N., Rosli, R., Veerakumarasivam, A., and Abdullah, S. (2011). Advancements in reprogramming strategies for the generation of induced pluripotent stem cells. J. Assist. Reprod. Genet. *28*, 291-301.

Laitinen, P.J., Brown, K.M., Piippo, K., Swan, H., Devaney, J.M., Brahmbhatt, B., Donarum, E.A., Marino, M., Tiso, N., Viitasalo, M., Toivonen, L., Stephan, D.A., and Kontula, K. (2001). Mutations of the cardiac ryanodine receptor (RyR2) gene in familial polymorphic ventricular tachycardia. Circulation *103*, 485-90.

Lan, F., Lee, A.S., Liang, P., Sanchez-Freire, V., Nguyen, P.K., Wang, L., Han, L., Yen, M., Wang, Y., Sun, N., Abilez, O.J., Hu, S., Ebert, A.D., Navarrete, E.G., Simmons, C.S., Wheeler, M., Pruitt, B., Lewis, R., Yamaguchi, Y., Ashley, E.A., Bers, D.M., Robbins, R.C., Longaker, M.T., and Wu, J.C. (2013). Abnormal calcium handling properties underlie familial hypertrophic cardiomyopathy pathology in patient-specific induced pluripotent stem cells. Cell. Stem Cell. *12*, 101-113.

Laurila, E., Ahola, A., Hyttinen, J., and Aalto-Setala, K. (2015). Methods for in vitro functional analysis of iPSC derived cardiomyocytes - Special focus on analyzing the mechanical beating behavior. Biochim. Biophys. Acta

Laurita, K.R., and Rosenbaum, D.S. (2008). Cellular mechanisms of arrhythmogenic cardiac alternans. Prog. Biophys. Mol. Biol. *97*, 332-347.

Lee, Y.K., Ng, K.M., Lai, W.H., Chan, Y.C., Lau, Y.M., Lian, Q., Tse, H.F., and Siu, C.W. (2011). Calcium homeostasis in human induced pluripotent stem cell-derived cardiomyocytes. Stem Cell. Rev. *7*, 976-986.

Leenhardt, A., Denjoy, I., and Guicheney, P. (2012). Catecholaminergic polymorphic ventricular tachycardia. Circ. Arrhythm Electrophysiol. *5*, 1044-1052.

Leenhardt, A., Lucet, V., Denjoy, I., Grau, F., Ngoc, D.D., and Coumel, P. (1995). Catecholaminergic polymorphic ventricular tachycardia in children. A 7-year follow-up of 21 patients. Circulation *91*, 1512-9.

Lehnart, S.E., Mongillo, M., Bellinger, A., Lindegger, N., Chen, B.X., Hsueh, W., Reiken, S., Wronska, A., Drew, L.J., Ward, C.W., Lederer, W.J., Kass, R.S., Morley, G., and Marks, A.R. (2008). Leaky Ca2+ release channel/ryanodine receptor 2 causes seizures and sudden cardiac death in mice. J. Clin. Invest. *118*, 2230-2245.

Lehnart, S.E., Terrenoire, C., Reiken, S., Wehrens, X.H., Song, L.S., Tillman, E.J., Mancarella, S., Coromilas, J., Lederer, W.J., Kass, R.S., and Marks, A.R. (2006). Stabilization of cardiac ryanodine receptor prevents intracellular calcium leak and arrhythmias. Proc. Natl. Acad. Sci. U. S. A. *103*, 7906-7910.

Lehnart, S.E., Wehrens, X.H., Laitinen, P.J., Reiken, S.R., Deng, S.X., Cheng, Z., Landry, D.W., Kontula, K., Swan, H., and Marks, A.R. (2004). Sudden death in familial polymorphic ventricular tachycardia associated with calcium release channel (ryanodine receptor) leak. Circulation *109,* 3208-14.

Li, C., Zhou, J., Shi, G., Ma, Y., Yang, Y., Gu, J., Yu, H., Jin, S., Wei, Z., Chen, F., and Jin, Y. (2009a). Pluripotency can be rapidly and efficiently induced in human amniotic fluid-derived cells. Hum. Mol. Genet. *18,* 4340-4349.

Li, H.L., Fujimoto, N., Sasakawa, N., Shirai, S., Ohkame, T., Sakuma, T., Tanaka, M., Amano, N., Watanabe, A., Sakurai, H., Yamamoto, T., Yamanaka, S., and Hotta, A. (2015). Precise correction of the dystrophin gene in duchenne muscular dystrophy patient induced pluripotent stem cells by TALEN and CRISPR-Cas9. Stem Cell. Reports *4,* 143-154.

Li, L., Desantiago, J., Chu, G., Kranias, E.G., and Bers, D.M. (2000). Phosphorylation of phospholamban and troponin I in beta-adrenergic-induced acceleration of cardiac relaxation. Am. J. Physiol. Heart Circ. Physiol. *278,* H769-79.

Li, Q., Wang, Y.Y., Li, H., Jiao, B., and Yu, Z.B. (2009b). Calcium leak of sarcoplasmic reticulum induces degradation of troponin I in skeletal muscle fibers. Sheng Li Xue Bao *61,* 223-229.

Li, S., Chen, G., and Li, R.A. (2013). Calcium signalling of human pluripotent stem cell-derived cardiomyocytes. J. Physiol. *591,* 5279-5290.

Li, W., Zhou, H., Abujarour, R., Zhu, S., Young Joo, J., Lin, T., Hao, E., Scholer, H.R., Hayek, A., and Ding, S. (2009c). Generation of human-induced pluripotent stem cells in the absence of exogenous Sox2. Stem Cells *27,* 2992-3000.

Lian, X., Hsiao, C., Wilson, G., Zhu, K., Hazeltine, L.B., Azarin, S.M., Raval, K.K., Zhang, J., Kamp, T.J., and Palecek, S.P. (2012). Robust cardiomyocyte differentiation from human pluripotent stem cells via temporal modulation of canonical Wnt signaling. Proc. Natl. Acad. Sci. U. S. A. *109,* E1848-57.

Liang, H., Matzkies, M., Schunkert, H., Tang, M., Bonnemeier, H., Hescheler, J., and Reppel, M. (2010). Human and murine embryonic stem cell-derived cardiomyocytes serve together as a valuable model for drug safety screening. Cell. Physiol. Biochem. *25,* 459-466.

Liao, J., Wu, Z., Wang, Y., Cheng, L., Cui, C., Gao, Y., Chen, T., Rao, L., Chen, S., Jia, N., Dai, H., Xin, S., Kang, J., Pei, G., and Xiao, L. (2008). Enhanced efficiency of generating induced pluripotent stem (iPS) cells from human somatic cells by a combination of six transcription factors. Cell Res. *18,* 600-603.

Lieu, D.K., Liu, J., Siu, C.W., McNerney, G.P., Tse, H.F., Abu-Khalil, A., Huser, T., and Li, R.A. (2009). Absence of transverse tubules contributes to non-uniform Ca(2+) wavefronts in mouse and human embryonic stem cell-derived cardiomyocytes. Stem Cells Dev. *18,* 1493-1500.

Liu, B., Ho, H.T., Velez-Cortes, F., Lou, Q., Valdivia, C.R., Knollmann, B.C., Valdivia, H.H., and Gyorke, S. (2014). Genetic ablation of ryanodine receptor 2 phosphorylation at Ser-2808 aggravates Ca(2+)-dependent cardiomyopathy by exacerbating diastolic Ca2+ release. J. Physiol. *592,* 1957-1973.

Liu, J., Fu, J.D., Siu, C.W., and Li, R.A. (2007). Functional sarcoplasmic reticulum for calcium handling of human embryonic stem cell-derived cardiomyocytes: insights for driven maturation. Stem Cells *25,* 3038-3044.

Liu, J., Sun, N., Bruce, M.A., Wu, J.C., and Butte, M.J. (2012). Atomic force mechanobiology of pluripotent stem cell-derived cardiomyocytes. PLoS One *7,* e37559.

Liu, N., Colombi, B., Memmi, M., Zissimopoulos, S., Rizzi, N., Negri, S., Imbriani, M., Napolitano, C., Lai, F.A., and Priori, S.G. (2006). Arrhythmogenesis in catecholaminergic polymorphic ventricular tachycardia: insights from a RyR2 R4496C knock-in mouse model. Circ Res *99,* 292-8.

Liu, N., Rizzi, N., Boveri, L., and Priori, S.G. (2009). Ryanodine receptor and calsequestrin in arrhythmogenesis: what we have learnt from genetic diseases and transgenic mice. J Mol Cell Cardiol *46,* 149-59.

Liu, N., Ruan, Y., Denegri, M., Bachetti, T., Li, Y., Colombi, B., Napolitano, C., Coetzee, W.A., and Priori, S.G. (2011). Calmodulin kinase II inhibition prevents arrhythmias in RyR2(R4496C+/-) mice with catecholaminergic polymorphic ventricular tachycardia. J. Mol. Cell. Cardiol. *50,* 214-222.

Liu, N., Ruan, Y., and Priori, S.G. (2008). Catecholaminergic polymorphic ventricular tachycardia. Prog Cardiovasc Dis *51,* 23-30.

Livak, K.J., and Schmittgen, T.D. (2001). Analysis of relative gene expression data using real-time quantitative PCR and the 2(-Delta Delta C(T)) Method. Methods *25,* 402-8.

Llucia-Valldeperas, A., Sanchez, B., Soler-Botija, C., Galvez-Monton, C., Roura, S., Prat-Vidal, C., Perea-Gil, I., Rosell-Ferrer, J., Bragos, R., and Bayes-Genis, A. (2014). Physiological conditioning by electric field stimulation promotes cardiomyogenic gene expression in human cardiomyocyte progenitor cells. Stem Cell. Res. Ther. *5,* 93.

Lobo, P.A., Kimlicka, L., Tung, C.C., and Van Petegem, F. (2011). The deletion of exon 3 in the cardiac ryanodine receptor is rescued by beta strand switching. Structure *19,* 790-798.

Loh, Y.H., Hartung, O., Li, H., Guo, C., Sahalie, J.M., Manos, P.D., Urbach, A., Heffner, G.C., Grskovic, M., Vigneault, F., Lensch, M.W., Park, I.H., Agarwal, S., Church, G.M., Collins, J.J., Irion, S., and Daley, G.Q. (2010). Reprogramming of T cells from human peripheral blood. Cell. Stem Cell. *7,* 15-19.

Lu, L., Mende, M., Yang, X., Korber, H.F., Schnittler, H.J., Weinert, S., Heubach, J., Werner, C., and Ravens, U. (2013). Design and validation of a bioreactor for simulating the cardiac

niche: a system incorporating cyclic stretch, electrical stimulation, and constant perfusion. Tissue Eng. Part A. *19,* 403-414.

Luna, J.I., Ciriza, J., Garcia-Ojeda, M.E., Kong, M., Herren, A., Lieu, D.K., Li, R.A., Fowlkes, C.C., Khine, M., and McCloskey, K.E. (2011). Multiscale biomimetic topography for the alignment of neonatal and embryonic stem cell-derived heart cells. Tissue Eng. Part C. Methods *17,* 579-588.

Lundy, S.D., Zhu, W.Z., Regnier, M., and Laflamme, M.A. (2013). Structural and functional maturation of cardiomyocytes derived from human pluripotent stem cells. Stem Cells Dev. *22,* 1991-2002.

Luo, M., and Anderson, M.E. (2013). Mechanisms of altered Ca(2)(+) handling in heart failure. Circ. Res. *113,* 690-708.

Ma, D., Wei, H., Zhao, Y., Lu, J., Li, G., Sahib, N.B., Tan, T.H., Wong, K.Y., Shim, W., Wong, P., Cook, S.A., and Liew, R. (2013). Modeling type 3 long QT syndrome with cardiomyocytes derived from patient-specific induced pluripotent stem cells. Int. J. Cardiol. *168,* 5277-5286.

Ma, J., Guo, L., Fiene, S.J., Anson, B.D., Thomson, J.A., Kamp, T.J., Kolaja, K.L., Swanson, B.J., and January, C.T. (2011). High purity human-induced pluripotent stem cell-derived cardiomyocytes: electrophysiological properties of action potentials and ionic currents. Am. J. Physiol. Heart Circ. Physiol. *301,* H2006-17.

Maddah, M., Heidmann, J.D., Mandegar, M.A., Walker, C.D., Bolouki, S., Conklin, B.R., and Loewke, K.E. (2015). A non-invasive platform for functional characterization of stem-cell-derived cardiomyocytes with applications in cardiotoxicity testing. Stem Cell. Reports *4,* 621-631.

Maherali, N., Sridharan, R., Xie, W., Utikal, J., Eminli, S., Arnold, K., Stadtfeld, M., Yachechko, R., Tchieu, J., Jaenisch, R., Plath, K., and Hochedlinger, K. (2007). Directly reprogrammed fibroblasts show global epigenetic remodeling and widespread tissue contribution. Cell. Stem Cell. *1,* 55-70.

Marx, S.O., Reiken, S., Hisamatsu, Y., Jayaraman, T., Burkhoff, D., Rosemblit, N., and Marks, A.R. (2000). PKA phosphorylation dissociates FKBP12.6 from the calcium release channel (ryanodine receptor): defective regulation in failing hearts. Cell *101,* 365-376.

Mather, J.P., and Roberts, P.E. (1998). Introduction to cell and tissue culture theory and technique (New York: Plenum Press).

Matsa, E., Rajamohan, D., Dick, E., Young, L., Mellor, I., Staniforth, A., and Denning, C. (2011). Drug evaluation in cardiomyocytes derived from human induced pluripotent stem cells carrying a long QT syndrome type 2 mutation. Eur Heart J *32,* 952-62.

Medeiros-Domingo, A., Bhuiyan, Z.A., Tester, D.J., Hofman, N., Bikker, H., van Tintelen, J.P., Mannens, M.M., Wilde, A.A., and Ackerman, M.J. (2009). The RYR2-encoded ryanodine receptor/calcium release channel in patients diagnosed previously with either catecholaminergic polymorphic ventricular tachycardia or genotype negative, exercise-induced long QT syndrome: a comprehensive open reading frame mutational analysis. J. Am. Coll. Cardiol. *54,* 2065-2074.

Mehta, A., Chung, Y.Y., Ng, A., Iskandar, F., Atan, S., Wei, H., Dusting, G., Sun, W., Wong, P., and Shim, W. (2011). Pharmacological response of human cardiomyocytes derived from virus-free induced pluripotent stem cells. Cardiovasc. Res. *91,* 577-586.

Meli, A.C., Refaat, M.M., Dura, M., Reiken, S., Wronska, A., Wojciak, J., Carroll, J., Scheinman, M.M., and Marks, A.R. (2011). A novel ryanodine receptor mutation linked to sudden death increases sensitivity to cytosolic calcium. Circ. Res. *109,* 281-290.

Meyer, T., Boven, K.H., Gunther, E., and Fejtl, M. (2004). Micro-electrode arrays in cardiac safety pharmacology: a novel tool to study QT interval prolongation. Drug Saf. *27,* 763-772.

Miklas, J.W., Nunes, S.S., Sofla, A., Reis, L.A., Pahnke, A., Xiao, Y., Laschinger, C., and Radisic, M. (2014). Bioreactor for modulation of cardiac microtissue phenotype by combined static stretch and electrical stimulation. Biofabrication *6,* 024113-5082/6/2/024113. Epub 2014 May 30.

Milligan, C.J., and Moller, C. (2013). Automated planar patch-clamp. Methods Mol. Biol. *998,* 171-187.

Minami, I., Yamada, K., Otsuji, T.G., Yamamoto, T., Shen, Y., Otsuka, S., Kadota, S., Morone, N., Barve, M., Asai, Y., Tenkova-Heuser, T., Heuser, J.E., Uesugi, M., Aiba, K., and Nakatsuji, N. (2012). A small molecule that promotes cardiac differentiation of human pluripotent stem cells under defined, cytokine- and xeno-free conditions. Cell. Rep. *2,* 1448-1460.

Mitcheson, J.S., Hancox, J.C., and Levi, A.J. (1996). Action potentials, ion channel currents and transverse tubule density in adult rabbit ventricular myocytes maintained for 6 days in cell culture. Pflugers Arch. *431,* 814-827.

Miyoshi, N., Ishii, H., Nagano, H., Haraguchi, N., Dewi, D.L., Kano, Y., Nishikawa, S., Tanemura, M., Mimori, K., Tanaka, F., Saito, T., Nishimura, J., Takemasa, I., Mizushima, T., Ikeda, M., Yamamoto, H., Sekimoto, M., Doki, Y., and Mori, M. (2011). Reprogramming of mouse and human cells to pluripotency using mature microRNAs. Cell. Stem Cell. *8,* 633-638.

Mohamed, U., Gollob, M.H., Gow, R.M., and Krahn, A.D. (2006). Sudden cardiac death despite an implantable cardioverter-defibrillator in a young female with catecholaminergic ventricular tachycardia. Heart Rhythm *3,* 1486-1489.

Molleman, A. (2002). Patch clamping : an introductory guide to patch clamp electrophysiology (New York: J. Wiley).

Montessuit, C., Rosenblatt-Velin, N., Papageorgiou, I., Campos, L., Pellieux, C., Palma, T., and Lerch, R. (2004). Regulation of glucose transporter expression in cardiac myocytes: p38 MAPK is a strong inducer of GLUT4. Cardiovasc Res *64*, 94-104.

Moore, J.C., van Laake, L.W., Braam, S.R., Xue, T., Tsang, S.Y., Ward, D., Passier, R., Tertoolen, L.L., Li, R.A., and Mummery, C.L. (2005). Human embryonic stem cells: genetic manipulation on the way to cardiac cell therapies. Reprod. Toxicol. *20*, 377-391.

Moretti, A., Bellin, M., Welling, A., Jung, C.B., Lam, J.T., Bott-Flugel, L., Dorn, T., Goedel, A., Hohnke, C., Hofmann, F., Seyfarth, M., Sinnecker, D., Schomig, A., and Laugwitz, K.L. (2010). Patient-specific induced pluripotent stem-cell models for long-QT syndrome. N Engl J Med *363*, 1397-409.

Mountford, J.C. (2008). Human embryonic stem cells: origins, characteristics and potential for regenerative therapy. Transfus. Med. *18*, 1-12.

Mummery, C., Ward-van Oostwaard, D., Doevendans, P., Spijker, R., van den Brink, S., Hassink, R., van der Heyden, M., Opthof, T., Pera, M., de la Riviere, A.B., Passier, R., and Tertoolen, L. (2003). Differentiation of human embryonic stem cells to cardiomyocytes: role of coculture with visceral endoderm-like cells. Circulation *107*, 2733-40.

Mummery, C.L., van Achterberg, T.A., van den Eijnden-van Raaij, A.J., van Haaster, L., Willemse, A., de Laat, S.W., and Piersma, A.H. (1991). Visceral-endoderm-like cell lines induce differentiation of murine P19 embryonal carcinoma cells. Differentiation *46*, 51-60.

Mummery, C.L., Zhang, J., Ng, E.S., Elliott, D.A., Elefanty, A.G., and Kamp, T.J. (2012). Differentiation of human embryonic stem cells and induced pluripotent stem cells to cardiomyocytes: a methods overview. Circ. Res. *111*, 344-358.

Nakagawa, M., Koyanagi, M., Tanabe, K., Takahashi, K., Ichisaka, T., Aoi, T., Okita, K., Mochiduki, Y., Takizawa, N., and Yamanaka, S. (2008). Generation of induced pluripotent stem cells without Myc from mouse and human fibroblasts. Nat. Biotechnol. *26*, 101-106.

Nakao, K., Minobe, W., Roden, R., Bristow, M.R., and Leinwand, L.A. (1997). Myosin heavy chain gene expression in human heart failure. J Clin Invest *100*, 2362-70.

Nam, Y.J., Song, K., Luo, X., Daniel, E., Lambeth, K., West, K., Hill, J.A., DiMaio, J.M., Baker, L.A., Bassel-Duby, R., and Olson, E.N. (2013). Reprogramming of human fibroblasts toward a cardiac fate. Proc. Natl. Acad. Sci. U. S. A. *110*, 5588-5593.

Napolitano, C., Bloise, R., Memmi, M., and Priori, S.G. (2014). Clinical utility gene card for: Catecholaminergic polymorphic ventricular tachycardia (CPVT). Eur. J. Hum. Genet. *22*, 10.1038/ejhg.2013.55. Epub 2013 Apr 3.

Napolitano, C., and Priori, S.G. (2007). Diagnosis and treatment of catecholaminergic polymorphic ventricular tachycardia. Heart Rhythm *4,* 675-8.

Neef, S., and Maier, L.S. (2013). Novel aspects of excitation-contraction coupling in heart failure. Basic Res. Cardiol. *108,* 360-013-0360-2. Epub 2013 Jun 6.

Ng, E.S., Davis, R., Stanley, E.G., and Elefanty, A.G. (2008). A protocol describing the use of a recombinant protein-based, animal product-free medium (APEL) for human embryonic stem cell differentiation as spin embryoid bodies. Nat. Protoc. *3,* 768-776.

Ng, E.S., Davis, R.P., Azzola, L., Stanley, E.G., and Elefanty, A.G. (2005). Forced aggregation of defined numbers of human embryonic stem cells into embryoid bodies fosters robust, reproducible hematopoietic differentiation. Blood *106,* 1601-1603.

Novak, A., Barad, L., Lorber, A., Gherghiceanu, M., Reiter, I., Eisen, B., Eldor, L., Itskovitz-Eldor, J., Eldar, M., Arad, M., and Binah, O. (2015). Functional abnormalities in iPSC-derived cardiomyocytes generated from CPVT1 and CPVT2 patients carrying ryanodine or calsequestrin mutations. J. Cell. Mol. Med. *19,* 2006-2018.

Novak, A., Barad, L., Zeevi-Levin, N., Shick, R., Shtreichman, R., Lorber, A., Itskovitz-Eldor, J., and Binah, O. (2012). Cardiomyocytes generated from CPVT(D307H) patients are arrhythmogenic in response to beta-adrenergic stimulation. J Cell Mol Med *3,* 468-82.

Nunes, S.S., Miklas, J.W., Liu, J., Aschar-Sobbi, R., Xiao, Y., Zhang, B., Jiang, J., Masse, S., Gagliardi, M., Hsieh, A., Thavandiran, N., Laflamme, M.A., Nanthakumar, K., Gross, G.J., Backx, P.H., Keller, G., and Radisic, M. (2013). Biowire: a platform for maturation of human pluripotent stem cell-derived cardiomyocytes. Nat. Methods *10,* 781-787.

Okita, K., Ichisaka, T., and Yamanaka, S. (2007). Generation of germline-competent induced pluripotent stem cells. Nature *448,* 313-317.

Ono, M., Yano, M., Hino, A., Suetomi, T., Xu, X., Susa, T., Uchinoumi, H., Tateishi, H., Oda, T., Okuda, S., Doi, M., Kobayashi, S., Yamamoto, T., Koseki, N., Kyushiki, H., Ikemoto, N., and Matsuzaki, M. (2010). Dissociation of calmodulin from cardiac ryanodine receptor causes aberrant Ca(2+) release in heart failure. Cardiovasc. Res. *87,* 609-617.

O'Reilly, R., and Elphick, H.E. (2013). Development, clinical utility, and place of ivacaftor in the treatment of cystic fibrosis. Drug Des. Devel. Ther. *7,* 929-937.

Osafune, K., Caron, L., Borowiak, M., Martinez, R.J., Fitz-Gerald, C.S., Sato, Y., Cowan, C.A., Chien, K.R., and Melton, D.A. (2008). Marked differences in differentiation propensity among human embryonic stem cell lines. Nat. Biotechnol. *26,* 313-315.

Paavola, J., Viitasalo, M., Laitinen-Forsblom, P.J., Pasternack, M., Swan, H., Tikkanen, I., Toivonen, L., Kontula, K., and Laine, M. (2007). Mutant ryanodine receptors in catecholaminergic polymorphic ventricular tachycardia generate delayed afterdepolarizations due to increased propensity to Ca2+ waves. Eur Heart J *28,* 1135-42.

Paci, M., Hyttinen, J., and Severi, S. (2014). The Reduced Repolarization Reserve Enhances the LQT1 Effects in Human Induced Pluripotent Stem Cell-Derived Cardiomyocytes: A Simulation Study. Biophysical Journal *106,* Supplement 1, p721a–722a.

Paci, M., Sartiani, L., Del Lungo, M., Jaconi, M., Mugelli, A., Cerbai, E., and Severi, S. (2012). Mathematical modelling of the action potential of human embryonic stem cell derived cardiomyocytes. Biomed. Eng. Online *11,* 61-925X-11-61.

Paredes, R.M., Etzler, J.C., Watts, L.T., Zheng, W., and Lechleiter, J.D. (2008). Chemical calcium indicators. Methods *46,* 143-151.

Park, H., Larson, B.L., Kolewe, M.E., Vunjak-Novakovic, G., and Freed, L.E. (2014). Biomimetic scaffold combined with electrical stimulation and growth factor promotes tissue engineered cardiac development. Exp. Cell Res. *321,* 297-306.

Passier, R., Oostwaard, D.W., Snapper, J., Kloots, J., Hassink, R.J., Kuijk, E., Roelen, B., de la Riviere, A.B., and Mummery, C. (2005). Increased cardiomyocyte differentiation from human embryonic stem cells in serum-free cultures. Stem Cells *23,* 772-780.

Patterson, E., Szabo, B., Scherlag, B.J., and Lazzara, R. (1990). Early and delayed afterdepolarizations associated with cesium chloride-induced arrhythmias in the dog. J Cardiovasc Pharmacol *15,* 323-31.

Paul-Pletzer, K., Yamamoto, T., Ikemoto, N., Jimenez, L.S., Morimoto, H., Williams, P.G., Ma, J., and Parness, J. (2005). Probing a putative dantrolene-binding site on the cardiac ryanodine receptor. Biochem. J. *387,* 905-909.

Pekkanen-Mattila, M., Chapman, H., Kerkela, E., Suuronen, R., Skottman, H., Koivisto, A.P., and Aalto-Setala, K. (2010). Human embryonic stem cell-derived cardiomyocytes: demonstration of a portion of cardiac cells with fairly mature electrical phenotype. Exp. Biol. Med. (Maywood) *235,* 522-530.

Pekkanen-Mattila, M., Kerkela, E., Tanskanen, J.M., Pietila, M., Pelto-Huikko, M., Hyttinen, J., Skottman, H., Suuronen, R., and Aalto-Setala, K. (2009). Substantial variation in the cardiac differentiation of human embryonic stem cell lines derived and propagated under the same conditions--a comparison of multiple cell lines. Ann. Med. *41,* 360-370.

Peracchia, C. (2004). Chemical gating of gap junction channels; roles of calcium, pH and calmodulin. Biochim. Biophys. Acta *1662,* 61-80.

Peters, M.F., Lamore, S.D., Guo, L., Scott, C.W., and Kolaja, K.L. (2015). Human stem cell-derived cardiomyocytes in cellular impedance assays: bringing cardiotoxicity screening to the front line. Cardiovasc. Toxicol. *15,* 127-139.

Picht, E., DeSantiago, J., Blatter, L.A., and Bers, D.M. (2006). Cardiac alternans do not rely on diastolic sarcoplasmic reticulum calcium content fluctuations. Circ. Res. *99,* 740-748.

Pieske, B., Kretschmann, B., Meyer, M., Holubarsch, C., Weirich, J., Posival, H., Minami, K., Just, H., and Hasenfuss, G. (1995). Alterations in intracellular calcium handling associated with the inverse force-frequency relation in human dilated cardiomyopathy. Circulation *92*, 1169-1178.

Porter, K.E., and Turner, N.A. (2009). Cardiac fibroblasts: at the heart of myocardial remodeling. Pharmacol. Ther. *123*, 255-278.

Postma, A.V., Denjoy, I., Kamblock, J., Alders, M., Lupoglazoff, J.M., Vaksmann, G., Dubosq-Bidot, L., Sebillon, P., Mannens, M.M., Guicheney, P., and Wilde, A.A. (2005). Catecholaminergic polymorphic ventricular tachycardia: RYR2 mutations, bradycardia, and follow up of the patients. J. Med. Genet. *42*, 863-870.

Priori, S.G., and Chen, S.R. (2011). Inherited dysfunction of sarcoplasmic reticulum Ca2+ handling and arrhythmogenesis. Circ. Res. *108*, 871-883.

Priori, S.G., Napolitano, C., Tiso, N., Memmi, M., Vignati, G., Bloise, R., Sorrentino, V., and Danieli, G.A. (2001). Mutations in the cardiac ryanodine receptor gene (hRyR2) underlie catecholaminergic polymorphic ventricular tachycardia. Circulation *103*, 196-200.

Priori, S.G., Wilde, A.A., Horie, M., Cho, Y., Behr, E.R., Berul, C., Blom, N., Brugada, J., Chiang, C.E., Huikuri, H., Kannankeril, P., Krahn, A., Leenhardt, A., Moss, A., Schwartz, P.J., Shimizu, W., Tomaselli, G., and Tracy, C. (2013). Executive summary: HRS/EHRA/APHRS expert consensus statement on the diagnosis and management of patients with inherited primary arrhythmia syndromes. Heart Rhythm *10*, e85-108.

Qian, L., Huang, Y., Spencer, C.I., Foley, A., Vedantham, V., Liu, L., Conway, S.J., Fu, J.D., and Srivastava, D. (2012). In vivo reprogramming of murine cardiac fibroblasts into induced cardiomyocytes. Nature *485*, 593-598.

Radisic, M., Park, H., Shing, H., Consi, T., Schoen, F.J., Langer, R., Freed, L.E., and Vunjak-Novakovic, G. (2004). Functional assembly of engineered myocardium by electrical stimulation of cardiac myocytes cultured on scaffolds. Proc Natl Acad Sci U S A *101*, 18129-34.

Ramirez, R.J., Sah, R., Liu, J., Rose, R.A., and Backx, P.H. (2011). Intracellular [Na(+)] modulates synergy between Na(+)/Ca (2+) exchanger and L-type Ca (2+) current in cardiac excitation-contraction coupling during action potentials. Basic Res. Cardiol. *106*, 967-977.

Rebuzzini, P., Fassina, L., Mulas, F., Bellazzi, R., Redi, C.A., Di Liberto, R., Magenes, G., Adjaye, J., Zuccotti, M., and Garagna, S. (2013). Mouse embryonic stem cells irradiated with gamma-rays differentiate into cardiomyocytes but with altered contractile properties. Mutat. Res. *756*, 37-45.

Reiser, P.J., Portman, M.A., Ning, X.H., and Schomisch Moravec, C. (2001). Human cardiac myosin heavy chain isoforms in fetal and failing adult atria and ventricles. Am. J. Physiol. Heart Circ. Physiol. *280*, H1814-20.

Reppel, M., Pillekamp, F., Lu, Z.J., Halbach, M., Brockmeier, K., Fleischmann, B.K., and Hescheler, J. (2004). Microelectrode arrays: a new tool to measure embryonic heart activity. J. Electrocardiol. *37 Suppl*, 104-109.

Restrepo, J.G., Weiss, J.N., and Karma, A. (2008). Calsequestrin-mediated mechanism for cellular calcium transient alternans. Biophys. J. *95*, 3767-3789.

Rosso, R., Kalman, J.M., Rogowski, O., Diamant, S., Birger, A., Biner, S., Belhassen, B., and Viskin, S. (2007). Calcium channel blockers and beta-blockers versus beta-blockers alone for preventing exercise-induced arrhythmias in catecholaminergic polymorphic ventricular tachycardia. Heart Rhythm *4*, 1149-1154.

Roux-Buisson, N., Cacheux, M., Fourest-Lieuvin, A., Fauconnier, J., Brocard, J., Denjoy, I., Durand, P., Guicheney, P., Kyndt, F., Leenhardt, A., Le Marec, H., Lucet, V., Mabo, P., Probst, V., Monnier, N., Ray, P.F., Santoni, E., Tremeaux, P., Lacampagne, A., Faure, J., Lunardi, J., and Marty, I. (2012). Absence of triadin, a protein of the calcium release complex, is responsible for cardiac arrhythmia with sudden death in human. Hum. Mol. Genet. *21*, 2759-2767.

Ruan, Y., Liu, N., Bloise, R., Napolitano, C., and Priori, S.G. (2007). Gating properties of SCN5A mutations and the response to mexiletine in long-QT syndrome type 3 patients. Circulation *116*, 1137-1144.

Ruiz, S., Brennand, K., Panopoulos, A.D., Herrerias, A., Gage, F.H., and Izpisua-Belmonte, J.C. (2010). High-efficient generation of induced pluripotent stem cells from human astrocytes. PLoS One *5*, e15526.

Sakmann, B., and Neher, E. (1984). Patch clamp techniques for studying ionic channels in excitable membranes. Annu. Rev. Physiol. *46*, 455-472.

Santulli, G., Pagano, G., Sardu, C., Xie, W., Reiken, S., D'Ascia, S.L., Cannone, M., Marziliano, N., Trimarco, B., Guise, T.A., Lacampagne, A., and Marks, A.R. (2015). Calcium release channel RyR2 regulates insulin release and glucose homeostasis. J. Clin. Invest. *125*, 1968-1978.

Sarantitis, I., Papanastasopoulos, P., Manousi, M., Baikoussis, N.G., and Apostolakis, E. (2012). The cytoskeleton of the cardiac muscle cell. Hellenic J. Cardiol. *53*, 367-379.

Sartiani, L., Bettiol, E., Stillitano, F., Mugelli, A., Cerbai, E., and Jaconi, M.E. (2007). Developmental changes in cardiomyocytes differentiated from human embryonic stem cells: a molecular and electrophysiological approach. Stem Cells *25*, 1136-1144.

Sasse, S., Brand, N.J., Kyprianou, P., Dhoot, G.K., Wade, R., Arai, M., Periasamy, M., Yacoub, M.H., and Barton, P.J. (1993). Troponin I gene expression during human cardiac development and in end-stage heart failure. Circ. Res. *72*, 932-938.

Sathaye, A., Bursac, N., Sheehy, S., and Tung, L. (2006). Electrical pacing counteracts intrinsic shortening of action potential duration of neonatal rat ventricular cells in culture. J Mol Cell Cardiol *41,* 633-41.

Sauer, H., Rahimi, G., Hescheler, J., and Wartenberg, M. (1999). Effects of electrical fields on cardiomyocyte differentiation of embryonic stem cells. J Cell Biochem *75,* 710-23.

Sauer, H., Theben, T., Hescheler, J., Lindner, M., Brandt, M.C., and Wartenberg, M. (2001). Characteristics of calcium sparks in cardiomyocytes derived from embryonic stem cells. Am. J. Physiol. Heart Circ. Physiol. *281,* H411-21.

Savla, J.J., Nelson, B.C., Perry, C.N., and Adler, E.D. (2014). Induced pluripotent stem cells for the study of cardiovascular disease. J. Am. Coll. Cardiol. *64,* 512-519.

Schlotthauer, K., and Bers, D.M. (2000). Sarcoplasmic reticulum Ca(2+) release causes myocyte depolarization. Underlying mechanism and threshold for triggered action potentials. Circ Res *87,* 774-80.

Sedej, S., Heinzel, F.R., Walther, S., Dybkova, N., Wakula, P., Groborz, J., Gronau, P., Maier, L.S., Vos, M.A., Lai, F.A., Napolitano, C., Priori, S.G., Kockskamper, J., and Pieske, B. (2010). Na+-dependent SR Ca2+ overload induces arrhythmogenic events in mouse cardiomyocytes with a human CPVT mutation. Cardiovasc. Res. *87,* 50-59.

Seki, T., Yuasa, S., and Fukuda, K. (2011). Derivation of induced pluripotent stem cells from human peripheral circulating T cells. Curr. Protoc. Stem Cell. Biol. *Chapter 4,* Unit4A.3.

Serena, E., Figallo, E., Tandon, N., Cannizzaro, C., Gerecht, S., Elvassore, N., and Vunjak-Novakovic, G. (2009). Electrical stimulation of human embryonic stem cells: cardiac differentiation and the generation of reactive oxygen species. Exp Cell Res *315,* 3611-9.

Sharma, S., Razeghi, P., Shakir, A., Keneson, B.J.,2nd, Clubb, F., and Taegtmeyer, H. (2003). Regional heterogeneity in gene expression profiles: a transcript analysis in human and rat heart. Cardiology *100,* 73-9.

Showell, C., Binder, O., and Conlon, F.L. (2004). T-box genes in early embryogenesis. Dev. Dyn. *229,* 201-218.

Sinnecker, D., Laugwitz, K.L., and Moretti, A. (2014). Induced pluripotent stem cell-derived cardiomyocytes for drug development and toxicity testing. Pharmacol. Ther. *143,* 246-252.

Siu, C.W., Lee, Y.K., Ho, J.C., Lai, W.H., Chan, Y.C., Ng, K.M., Wong, L.Y., Au, K.W., Lau, Y.M., Zhang, J., Lay, K.W., Colman, A., and Tse, H.F. (2012). Modeling of lamin A/C mutation premature cardiac aging using patient-specific induced pluripotent stem cells. Aging (Albany NY) *4,* 803-822.

Smaill, B.H., Zhao, J., and Trew, M.L. (2013). Three-dimensional impulse propagation in myocardium: arrhythmogenic mechanisms at the tissue level. Circ. Res. *112,* 834-848.

Soldner, F., Laganiere, J., Cheng, A.W., Hockemeyer, D., Gao, Q., Alagappan, R., Khurana, V., Golbe, L.I., Myers, R.H., Lindquist, S., Zhang, L., Guschin, D., Fong, L.K., Vu, B.J., Meng, X., Urnov, F.D., Rebar, E.J., Gregory, P.D., Zhang, H.S., and Jaenisch, R. (2011). Generation of isogenic pluripotent stem cells differing exclusively at two early onset Parkinson point mutations. Cell *146*, 318-331.

Song, K., Nam, Y.J., Luo, X., Qi, X., Tan, W., Huang, G.N., Acharya, A., Smith, C.L., Tallquist, M.D., Neilson, E.G., Hill, J.A., Bassel-Duby, R., and Olson, E.N. (2012). Heart repair by reprogramming non-myocytes with cardiac transcription factors. Nature *485*, 599-604.

Song, L., Alcalai, R., Arad, M., Wolf, C.M., Toka, O., Conner, D.A., Berul, C.I., Eldar, M., Seidman, C.E., and Seidman, J.G. (2007). Calsequestrin 2 (CASQ2) mutations increase expression of calreticulin and ryanodine receptors, causing catecholaminergic polymorphic ventricular tachycardia. J. Clin. Invest. *117*, 1814-1823.

Song, L.S., Sobie, E.A., McCulle, S., Lederer, W.J., Balke, C.W., and Cheng, H. (2006). Orphaned ryanodine receptors in the failing heart. Proc. Natl. Acad. Sci. U. S. A. *103*, 4305-4310.

Sossalla, S., Fluschnik, N., Schotola, H., Ort, K.R., Neef, S., Schulte, T., Wittkopper, K., Renner, A., Schmitto, J.D., Gummert, J., El-Armouche, A., Hasenfuss, G., and Maier, L.S. (2010). Inhibition of elevated Ca2+/calmodulin-dependent protein kinase II improves contractility in human failing myocardium. Circ. Res. *107*, 1150-1161.

Spencer, C.I., Baba, S., Nakamura, K., Hua, E.A., Sears, M.A., Fu, C.C., Zhang, J., Balijepalli, S., Tomoda, K., Hayashi, Y., Lizarraga, P., Wojciak, J., Scheinman, M.M., Aalto-Setala, K., Makielski, J.C., January, C.T., Healy, K.E., Kamp, T.J., Yamanaka, S., and Conklin, B.R. (2014). Calcium Transients Closely Reflect Prolonged Action Potentials in iPSC Models of Inherited Cardiac Arrhythmia. Stem Cell. Reports *3*, 269-281.

Spencer, C.I., and Sham, J.S. (2003). Effects of Na+/Ca2+ exchange induced by SR Ca2+ release on action potentials and afterdepolarizations in guinea pig ventricular myocytes. Am J Physiol Heart Circ Physiol *285*, H2552-62.

Stadtfeld, M., Nagaya, M., Utikal, J., Weir, G., and Hochedlinger, K. (2008). Induced pluripotent stem cells generated without viral integration. Science *322*, 945-949.

Staerk, J., Dawlaty, M.M., Gao, Q., Maetzel, D., Hanna, J., Sommer, C.A., Mostoslavsky, G., and Jaenisch, R. (2010). Reprogramming of human peripheral blood cells to induced pluripotent stem cells. Cell. Stem Cell. *7*, 20-24.

Sterneckert, J.L., Reinhardt, P., and Scholer, H.R. (2014). Investigating human disease using stem cell models. Nat. Rev. Genet. *15*, 625-639.

Suetomi, T., Yano, M., Uchinoumi, H., Fukuda, M., Hino, A., Ono, M., Xu, X., Tateishi, H., Okuda, S., Doi, M., Kobayashi, S., Ikeda, Y., Yamamoto, T., Ikemoto, N., and Matsuzaki,

M. (2011). Mutation-linked defective interdomain interactions within ryanodine receptor cause aberrant Ca(2)(+)release leading to catecholaminergic polymorphic ventricular tachycardia. Circulation *124*, 682-694.

Sugiyama, A. (2008). Sensitive and reliable proarrhythmia in vivo animal models for predicting drug-induced torsades de pointes in patients with remodelled hearts. Br. J. Pharmacol. *154*, 1528-1537.

Sun, N., Panetta, N.J., Gupta, D.M., Wilson, K.D., Lee, A., Jia, F., Hu, S., Cherry, A.M., Robbins, R.C., Longaker, M.T., and Wu, J.C. (2009). Feeder-free derivation of induced pluripotent stem cells from adult human adipose stem cells. Proc. Natl. Acad. Sci. U. S. A. *106*, 15720-15725.

Sun, N., Yazawa, M., Liu, J., Han, L., Sanchez-Freire, V., Abilez, O.J., Navarrete, E.G., Hu, S., Wang, L., Lee, A., Pavlovic, A., Lin, S., Chen, R., Hajjar, R.J., Snyder, M.P., Dolmetsch, R.E., Butte, M.J., Ashley, E.A., Longaker, M.T., Robbins, R.C., and Wu, J.C. (2012). Patient-specific induced pluripotent stem cells as a model for familial dilated cardiomyopathy. Sci. Transl. Med. *4*, 130ra47.

Swan, H., Piippo, K., Viitasalo, M., Heikkila, P., Paavonen, T., Kainulainen, K., Kere, J., Keto, P., Kontula, K., and Toivonen, L. (1999). Arrhythmic disorder mapped to chromosome 1q42-q43 causes malignant polymorphic ventricular tachycardia in structurally normal hearts. J Am Coll Cardiol *34*, 2035-42.

Synnergren, J., Akesson, K., Dahlenborg, K., Vidarsson, H., Ameen, C., Steel, D., Lindahl, A., Olsson, B., and Sartipy, P. (2008). Molecular signature of cardiomyocyte clusters derived from human embryonic stem cells. Stem Cells *26*, 1831-1840.

Takahashi, K., Tanabe, K., Ohnuki, M., Narita, M., Ichisaka, T., Tomoda, K., and Yamanaka, S. (2007). Induction of pluripotent stem cells from adult human fibroblasts by defined factors. Cell *131*, 861-72.

Takahashi, K., and Yamanaka, S. (2006). Induction of pluripotent stem cells from mouse embryonic and adult fibroblast cultures by defined factors. Cell *126*, 663-676.

Takenaka, C., Nishishita, N., Takada, N., Jakt, L.M., and Kawamata, S. (2010). Effective generation of iPS cells from CD34+ cord blood cells by inhibition of p53. Exp. Hematol. *38*, 154-162.

Tan, K.Y., Eminli, S., Hettmer, S., Hochedlinger, K., and Wagers, A.J. (2011). Efficient generation of iPS cells from skeletal muscle stem cells. PLoS One *6*, e26406.

Thaler, M.S. (1999). The only EKG book you'll ever need (Philadelphia ; London: Lippincott Williams & Wilkins).

Thierfelder, L., Watkins, H., MacRae, C., Lamas, R., McKenna, W., Vosberg, H.P., Seidman, J.G., and Seidman, C.E. (1994). Alpha-tropomyosin and cardiac troponin T mutations cause familial hypertrophic cardiomyopathy: a disease of the sarcomere. Cell *77*, 701-712.

Thomson, J.A., Itskovitz-Eldor, J., Shapiro, S.S., Waknitz, M.A., Swiergiel, J.J., Marshall, V.S., and Jones, J.M. (1998). Embryonic stem cell lines derived from human blastocysts. Science *282*, 1145-1147.

Tung, L., and Borderies, J.R. (1992). Analysis of electric field stimulation of single cardiac muscle cells. Biophys. J. *63*, 371-386.

Uchinoumi, H., Yano, M., Suetomi, T., Ono, M., Xu, X., Tateishi, H., Oda, T., Okuda, S., Doi, M., Kobayashi, S., Yamamoto, T., Ikeda, Y., Ohkusa, T., Ikemoto, N., and Matsuzaki, M. (2010). Catecholaminergic polymorphic ventricular tachycardia is caused by mutation-linked defective conformational regulation of the ryanodine receptor. Circ. Res. *106*, 1413-1424.

Uusimaa, P.A., Hassinen, I.E., Vuolteenaho, O., and Ruskoaho, H. (1992). Endothelin-induced atrial natriuretic peptide release from cultured neonatal cardiac myocytes: the role of extracellular calcium and protein kinase-C. Endocrinology *130*, 2455-64.

van den Heuvel, N.H., van Veen, T.A., Lim, B., and Jonsson, M.K. (2014). Lessons from the heart: mirroring electrophysiological characteristics during cardiac development to in vitro differentiation of stem cell derived cardiomyocytes. J. Mol. Cell. Cardiol. *67*, 12-25.

van der Werf, C., and Wilde, A.A. (2013). Catecholaminergic polymorphic ventricular tachycardia: from bench to bedside. Heart *99*, 497-504.

Venkataraman, R., Baldo, M.P., Hwang, H.S., Veltri, T., Pinto, J.R., Baudenbacher, F.J., and Knollmann, B.C. (2013). Myofilament calcium de-sensitization and contractile uncoupling prevent pause-triggered ventricular tachycardia in mouse hearts with chronic myocardial infarction. J. Mol. Cell. Cardiol. *60*, 8-15.

Viitasalo, M., Oikarinen, L., Swan, H., Glatter, K.A., Vaananen, H., Fodstad, H., Chiamvimonvat, N., Kontula, K., Toivonen, L., and Scheinman, M.M. (2006). Ratio of late to early T-wave peak amplitude in 24-h electrocardiographic recordings as indicator of symptom history in patients with long-QT Syndrome types 1 and 2. J Am Coll Cardiol *47*, 112-20.

Viitasalo, M., Oikarinen, L., Vaananen, H., Kontula, K., Toivonen, L., and Swan, H. (2008). U-waves and T-wave peak to T-wave end intervals in patients with catecholaminergic polymorphic ventricular tachycardia, effects of beta-blockers. Heart Rhythm *5*, 1382-8.

Volders, P.G., Vos, M.A., Szabo, B., Sipido, K.R., de Groot, S.H., Gorgels, A.P., Wellens, H.J., and Lazzara, R. (2000). Progress in the understanding of cardiac early afterdepolarizations and torsades de pointes: time to revise current concepts. Cardiovasc Res *46*, 376-92.

Vos, M., de Groot, S., and Wellens, H. (2000). Delayed afterdepolarizations in the in situ canine heart: The role of the diastolic upslope. In: Franz MR, editor. Monophasic Action Potentials: Bridging Cell and Bedside (New York: Futura Publishing Company).

Wada, R., Muraoka, N., Inagawa, K., Yamakawa, H., Miyamoto, K., Sadahiro, T., Umei, T., Kaneda, R., Suzuki, T., Kamiya, K., Tohyama, S., Yuasa, S., Kokaji, K., Aeba, R., Yozu, R., Yamagishi, H., Kitamura, T., Fukuda, K., and Ieda, M. (2013). Induction of human cardiomyocyte-like cells from fibroblasts by defined factors. Proc. Natl. Acad. Sci. U. S. A. *110*, 12667-12672.

Wagner, E., Lauterbach, M.A., Kohl, T., Westphal, V., Williams, G.S., Steinbrecher, J.H., Streich, J.H., Korff, B., Tuan, H.T., Hagen, B., Luther, S., Hasenfuss, G., Parlitz, U., Jafri, M.S., Hell, S.W., Lederer, W.J., and Lehnart, S.E. (2012). Stimulated emission depletion live-cell super-resolution imaging shows proliferative remodeling of T-tubule membrane structures after myocardial infarction. Circ. Res. *111*, 402-414.

Walsh, C., Barrow, S., Voronina, S., Chvanov, M., Petersen, O.H., and Tepikin, A. (2009). Modulation of calcium signalling by mitochondria. Biochim. Biophys. Acta *1787*, 1374-1382.

Wang, L., Myles, R.C., De Jesus, N.M., Ohlendorf, A.K., Bers, D.M., and Ripplinger, C.M. (2014a). Optical mapping of sarcoplasmic reticulum Ca2+ in the intact heart: ryanodine receptor refractoriness during alternans and fibrillation. Circ. Res. *114*, 1410-1421.

Wang, R., Zhong, X., Meng, X., Koop, A., Tian, X., Jones, P.P., Fruen, B.R., Wagenknecht, T., Liu, Z., and Chen, S.R. (2011). Localization of the dantrolene-binding sequence near the FK506-binding protein-binding site in the three-dimensional structure of the ryanodine receptor. J. Biol. Chem. *286*, 12202-12212.

Wang, Y., Liang, P., Lan, F., Wu, H., Lisowski, L., Gu, M., Hu, S., Kay, M.A., Urnov, F.D., Shinnawi, R., Gold, J.D., Gepstein, L., and Wu, J.C. (2014b). Genome editing of isogenic human induced pluripotent stem cells recapitulates long QT phenotype for drug testing. J. Am. Coll. Cardiol. *64*, 451-459.

Watanabe, H., Chopra, N., Laver, D., Hwang, H.S., Davies, S.S., Roach, D.E., Duff, H.J., Roden, D.M., Wilde, A.A., and Knollmann, B.C. (2009). Flecainide prevents catecholaminergic polymorphic ventricular tachycardia in mice and humans. Nat. Med. *15*, 380-383.

Wehrens, X.H. (2007). The molecular basis of catecholaminergic polymorphic ventricular tachycardia: what are the different hypotheses regarding mechanisms? Heart Rhythm *4*, 794-7.

Wehrens, X.H., Lehnart, S.E., Reiken, S.R., Deng, S.X., Vest, J.A., Cervantes, D., Coromilas, J., Landry, D.W., and Marks, A.R. (2004). Protection from cardiac arrhythmia through ryanodine receptor-stabilizing protein calstabin2. Science *304*, 292-296.

Weiss, J.N., Garfinkel, A., Karagueuzian, H.S., Chen, P.S., and Qu, Z. (2010). Early afterdepolarizations and cardiac arrhythmias. Heart Rhythm *7*, 1891-1899.

Wilde, A.A., Bhuiyan, Z.A., Crotti, L., Facchini, M., De Ferrari, G.M., Paul, T., Ferrandi, C., Koolbergen, D.R., Odero, A., and Schwartz, P.J. (2008). Left cardiac sympathetic denervation for catecholaminergic polymorphic ventricular tachycardia. N. Engl. J. Med. *358,* 2024-2029.

Willyard, C. (2011). Companies compete over mutation-specific melanoma drugs. Nat. Med. *17,* 268-268a.

Wolpert, L., Jessell, T., Lawrence, P., Meyerowitz, E., Robertson, E., and Smith, J. (2006). Principles of development (Oxford: Oxford University Press).

Xiao, Y., Zhang, B., Liu, H., Miklas, J.W., Gagliardi, M., Pahnke, A., Thavandiran, N., Sun, Y., Simmons, C., Keller, G., and Radisic, M. (2014). Microfabricated perfusable cardiac biowire: a platform that mimics native cardiac bundle. Lab. Chip *14,* 869-882.

Xie, L.H., Sato, D., Garfinkel, A., Qu, Z., and Weiss, J.N. (2008). Intracellular Ca alternans: coordinated regulation by sarcoplasmic reticulum release, uptake, and leak. Biophys. J. *95,* 3100-3110.

Xie, L.H., and Weiss, J.N. (2009). Arrhythmogenic consequences of intracellular calcium waves. Am J Physiol Heart Circ Physiol *297,* H997-H1002.

Xin, M., Olson, E.N., and Bassel-Duby, R. (2013). Mending broken hearts: cardiac development as a basis for adult heart regeneration and repair. Nat. Rev. Mol. Cell Biol. *14,* 529-541.

Xu, J., Zaim, S., and Pelleg, A. (1996). Effects of pinacidil, verapamil, and heart rate on afterdepolarizations in the guinea-pig heart in vivo. Heart Vessels *11,* 289-302.

Xu, X., Yano, M., Uchinoumi, H., Hino, A., Suetomi, T., Ono, M., Tateishi, H., Oda, T., Okuda, S., Doi, M., Kobayashi, S., Yamamoto, T., Ikeda, Y., Ikemoto, N., and Matsuzaki, M. (2010). Defective calmodulin binding to the cardiac ryanodine receptor plays a key role in CPVT-associated channel dysfunction. Biochem. Biophys. Res. Commun. *394,* 660-666.

Xu, X.Q., Graichen, R., Soo, S.Y., Balakrishnan, T., Rahmat, S.N., Sieh, S., Tham, S.C., Freund, C., Moore, J., Mummery, C., Colman, A., Zweigerdt, R., and Davidson, B.P. (2008). Chemically defined medium supporting cardiomyocyte differentiation of human embryonic stem cells. Differentiation *76,* 958-970.

Yamanaka, S. (2008). Pluripotency and nuclear reprogramming. Philos. Trans. R. Soc. Lond. B. Biol. Sci. *363,* 2079-2087.

Yamanaka, S., Li, J., Kania, G., Elliott, S., Wersto, R.P., Van Eyk, J., Wobus, A.M., and Boheler, K.R. (2008). Pluripotency of embryonic stem cells. Cell Tissue Res. *331,* 5-22.

Yang, L., Soonpaa, M.H., Adler, E.D., Roepke, T.K., Kattman, S.J., Kennedy, M., Henckaerts, E., Bonham, K., Abbott, G.W., Linden, R.M., Field, L.J., and Keller, G.M. (2008). Human

cardiovascular progenitor cells develop from a KDR+ embryonic-stem-cell-derived population. Nature *453,* 524-528.

Yazawa, M., Hsueh, B., Jia, X., Pasca, A.M., Bernstein, J.A., Hallmayer, J., and Dolmetsch, R.E. (2011). Using induced pluripotent stem cells to investigate cardiac phenotypes in Timothy syndrome. Nature *471,* 230-4.

Yu, J., Vodyanik, M.A., Smuga-Otto, K., Antosiewicz-Bourget, J., Frane, J.L., Tian, S., Nie, J., Jonsdottir, G.A., Ruotti, V., Stewart, R., II, S., and Thomson, J.A. (2007). Induced pluripotent stem cell lines derived from human somatic cells. Science *318,* 1917-20.

Zhang, J., Klos, M., Wilson, G.F., Herman, A.M., Lian, X., Raval, K.K., Barron, M.R., Hou, L., Soerens, A.G., Yu, J., Palecek, S.P., Lyons, G.E., Thomson, J.A., Herron, T.J., Jalife, J., and Kamp, T.J. (2012). Extracellular matrix promotes highly efficient cardiac differentiation of human pluripotent stem cells: the matrix sandwich method. Circ. Res. *111,* 1125-1136.

Zhang, X.H., Haviland, S., Wei, H., Saric, T., Fatima, A., Hescheler, J., Cleemann, L., and Morad, M. (2013). Ca2+ signaling in human induced pluripotent stem cell-derived cardiomyocytes (iPS-CM) from normal and catecholaminergic polymorphic ventricular tachycardia (CPVT)-afflicted subjects. Cell Calcium *54,* 57-70.

Zhou, T., Benda, C., Duzinger, S., Huang, Y., Li, X., Li, Y., Guo, X., Cao, G., Chen, S., Hao, L., Chan, Y.C., Ng, K.M., Ho, J.C., Wieser, M., Wu, J., Redl, H., Tse, H.F., Grillari, J., Grillari-Voglauer, R., Pei, D., and Esteban, M.A. (2011). Generation of induced pluripotent stem cells from urine. J. Am. Soc. Nephrol. *22,* 1221-1228.

Original publications

Study I

Kujala K, Ahola A, Pekkanen-Mattila M, Ikonen L, Kerkelä E, Hyttinen J, Aalto-Setälä K

Electrical Field Stimulation with a Novel Platform: Effect on Cardiomyocyte Gene Expression but not on Orientation

International Journal of Biomedical Science 2012 Jun; 8(2):109-20

ORIGINAL ARTICLE

Electrical Field Stimulation with a Novel Platform: Effect on Cardiomyocyte Gene Expression but not on Orientation

Kirsi Kujala[1, 2], Antti Ahola[2, 3], Mari Pekkanen-Mattila[1, 2], Liisa Ikonen[1, 2], Erja Kerkelä[1, 4], Jari Hyttinen[2, 3], Katriina Aalto-Setälä[1, 2, 5]

[1]Institute of Biomedical Technology, University of Tampere, FIN-33014 University of Tampere, Tampere, Finland; [2]BioMediTech, Tampere, Finland; [3]Department of Biomedical Engineering, Tampere University of Technology, P.O. Box 692, FIN-33101 Tampere, Finland; [4]Finnish Red Cross, Blood Service, Helsinki, Finland; [5]Heart Center, Tampere University Hospital, Teiskontie 35, 33520 Tampere, Finland

ABSTRACT

Electrical field stimulation has been shown to improve cardiac cell alignment and functional properties. In this study, neonatal rat cardiomyocytes were exposed to both long-term and short-term stimulation with the goal of investigating whether it is possible to achieve cell orientation and the maturation of cardiomyocytes with a novel, microelectrode array (MEA)-compatible electrical stimulation platform. Cells were viable after electrical stimulation, but no orientation or other morphological changes were observed. However, the electrode wires in MEA dishes affected the cell orientation. Cell contractions synchronized with pacing, but settled back to their original frequency in the absence of stimulation. The expression of genes encoding a gap junction protein connexin-43 (Cx-43), and contractile cardiac protein beta myosin heavy chain 7, was stronger in stimulated cells than in controls ($p<0.05$). In summary, the surface topography influenced to cardiomyocyte orientation, suggesting that the micro architecture of the biomaterials should be carefully designed for cell applications. However, as electrical stimulation and its duration affected gene expression of some main cardiac proteins, the stimulation system may prove useful to enhance the cardiac differentiation of stem cells. (*Int J Biomed Sci* 2012; 8 (2): 109-120)

Keywords: cardiomyocytes; collagen gel; connexin-43; electrical stimulation; orientation; beta myosin heavy chain 7; gene expression

Corresponding author: Katriina Aalto-Setälä, Institute of Biomedical Technology, University of Tampere, Biokatu 12, 33520 Tampere, Finland. Tel: +358-40-582-9567; Fax: +358-3-3551-8498. Email: katriina.aalto-setala@uta.fi. Website: www.uta.fi/ibt/.

Note: This study was funded by the Pirkanmaa Hospital District, the Academy of Finland, the Finnish Cardiovascular Foundation, and Biocenter Finland.

Received March 6, 2012**; Accepted** April 5, 2012

INTRODUCTION

The ultimate goal in cardiac tissue engineering is to generate heart muscle with the morphological and functional properties of natural myocardium. Pluripotent human embryonic stem cells (hESC) and human induced pluripotent stem cells (hiPS) can differentiate into cardiomyocytes (CM) (14, 34), and with the help of stem cell technology, it could be possible to generate a tissue model for cardiac studies and eventually to create a graft to re-

place damaged heart tissue. However, one major problem in culturing CMs has been the lack of cell orientation and immature phenotype.

Contractile and electrophysiological functionality as well as cell alignment, mechanical stability and the expression of cardiac cell markers are among the most important characteristics of engineered cardiac constructs. Electrical field stimulation has proposed to improve cell differentiation, alignment and functional properties, and is therefore considered a crucial parameter for the generation of synchronously contracting cardiac cells. Even though electrical field stimulation studies have been carried out mostly on neonatal rat CMs (NRCs), electrical fields have also served in the cardiac differentiation of mouse embryonic stem cells (27) and hESCs (28). Electrical stimulation has been shown to induce cell elongation (3-5, 9, 24) and alignment (3, 11, 24), both affecting cell functionality. In addition, reports indicate that electrically stimulated CMs have a preferred orientation in response to field stimulation. Namely, it has been demonstrated that CMs are more excitable when the long axis of the cell is oriented parallel to the electrical field (30). Also, a marked level of ultra structural organization has been observed due to stimulation by means of centrally positioned elongated nuclei and well-aligned registers of sarcomeres (24). As for functional properties, stimulation has induced regular excitation-contraction coupling between electrical pacing signals and macroscopic contractions, which is necessary for the development of contractile behavior (9, 24). In addition, stimulation has induced other functional properties such as low excitation threshold (9), amplitude of synchronous contractions (24), stabilization of action potential duration (26) and an increase in the calcium current peak (6). Electrical stimulation has also led to enhanced calcium transients (12) and the development of more organized myofibrils (20), while stimulated CMs have demonstrated well-developed contractile apparatuses (3, 24). On the molecular level, electrical stimulation has induced a rise in myosin heavy chain (MHC) levels (24), which correlates with the contractile velocity of cardiac muscle (22). Electrical stimulation has also increased the production of gap junction protein Connexin-43 (Cx-43) (4, 5, 9, 24) as well as expression of the cardiac genes of myosin light chain-2 and atrial natriuretic factor (20).

Electrical stimulation has been studied with various stimulation systems using current- or voltage-based stimulation. Optimization of the stimulation parameters is based on those found in both the developing and the native heart (i.e., in the hearts of one-week-old rats) (3, 9). The frequency of 1 Hz has been used because it is physiological for humans and at the low end of the physiological regime for rats (3). In earlier studies, rat CMs have typically been stimulated with a field strength of around 5 V/cm with monophasic or biphasic waveforms (3, 9, 12, 24).

The main objective of this study was to investigate whether electrical field stimulation with our novel platform could enhance CM orientation and maturation as well as improve functional properties. NRCs were cultured as monolayers on collagen gel or gelatin-coated micro electrode array (MEA) chambers and stimulated. The cell viability, electrophysiological and morphological properties, as well as protein and gene expression of cardiac cell markers were analyzed to determine the effect of this novel device on functional and molecular properties of NRCs.

MATERIALS AND METHODS

Cell culture

NRCs were chosen to this study because they are easy to obtain in large amounts and they provide a suited cell model of beating CMs. NRCs were harvested from the whole-hearts of two- to five-day-old rats as described earlier (31). The hearts were removed and enzymatically dissociated with collagenase type II solution and seeded as cell density of 282 000 cells/cm^2 onto collagen gel or 0.1% gelatin-coated MEA chambers in Culture Medium I [CMI, Dulbecco's Modified Eagle's Medium/Ham's Nutrient Mixture F12 (DMEM/F-12, Sigma-Aldrich, Germany), 10% Fetal bovine serum (FBS, Gibco, Finland), 100 IU/ml Penicillin/ 0.1 mg/ml Streptomycin (P/S, Gambrex, Belgium), 2.56 mM L-glutamine (Sigma-Aldrich, Germany)]. After first day and thereafter cells were precultured in 1 ml of Complete Serum Free Medium [CSFM, DMEM/F-12, 10% Bovine serum albumin (BSA, Sigma-Aldrich, Germany), 2.8 mM Sodium Pyruvate (Cambrex, Belgium), 2.56 mM L-glutamine, Insulin-transferrin-sodium selenite media supplement (ITS, Cambrex, Belgium; 1 µM insulin, 5.64 µg/ml transferring, 32 nM selenium), 100 IU/ml P/ 0.1 mg/ml S, 0.1 nM 3,3',5-Triiodo-L-thyronine sodium salt (T3, Sigma-Aldrich, Germany)] in a 37°C/5% CO_2 to allow the cells to attach to MEA chambers. Culture medium was changed every or every second day. Cells serving as controls were cultured in the same way as electrically stimulated cells were. The animals were sacrificed according to guidelines of the Animal Unit, Medical School, University of Tampere and the Ethical Committee of the Animal Unit has accepted the method to obtain the cells.

Collagen gel

The collagen was isolated from adult Sprague Dawley rat tails (10) and stored at -20°C. In brief, tails were thawed and cut into pieces, the skin was then removed, and the collagen fibers were pulled out and placed into 0.1% acetic acid. The fibers were dissolved into acetic acid, and the collagen was precipitated with 25 v-% sodium chloride. The solution was then centrifuged, and the collagen pellet was again dissolved in 0.1% acetic acid. To balance the salinity, the solution was dialyzed at 4°C. Finally, the concentration of the collagen was determined with a Pierce® BCA Protein Assay kit (Thermo Scientific, USA) using BSA as the standard. The concentration was 1.043 mg/ml.

The gelation of the collagen (19) was performed as described earlier, with some modifications. At first the collagen solution was placed on ice, and two different neutralizing buffers [12 mg/ml $NaHCO_3$ (Sigma-Aldrich, Germany) in 0.1 N NaOH (Merck, Germany) and 1.3 M NaCl (Baker, the Netherlands) in 0.2 M Na_2HPO_4 (Baker, the Netherlands)] were added. The solution was then incubated at 37°C for 30 min to allow for gel formation.

Electrical stimulation setup

The in-house designed and developed system comprised three parts: electronics for stimulation waveform generation and amplification, an MEA dish container with electrodes, and stimulation software running on a PC laptop (Figure 1A and 1D). The functionality of the system was tested electrically, and its effects on the cells were observed with a microscope.

The electrode holder manufactured from polymethyl methacrylate also worked as a container and was designed to serve as a petri-dish as well. The container was designed to house six MEA dishes. For each MEA dish, two 10-mm-wide stainless steel plate electrodes were placed 5 mm apart to create a homogeneous field for stimulation. The electrode setup and the stimulus field were simulated with the finite element method using Comsol Multiphysics software to assess the homogeneity of the field across the whole cell culture (Figure 1B and 1C). To ensure that the stimulation field is as uniform as possible, the electrodes were set to 0.5 mm from the bottom. Air exchange was enabled via a small space between the container and the lid, which was designed to feature a 10 mm protruding rim to keep the container closed. To counteract evaporation,

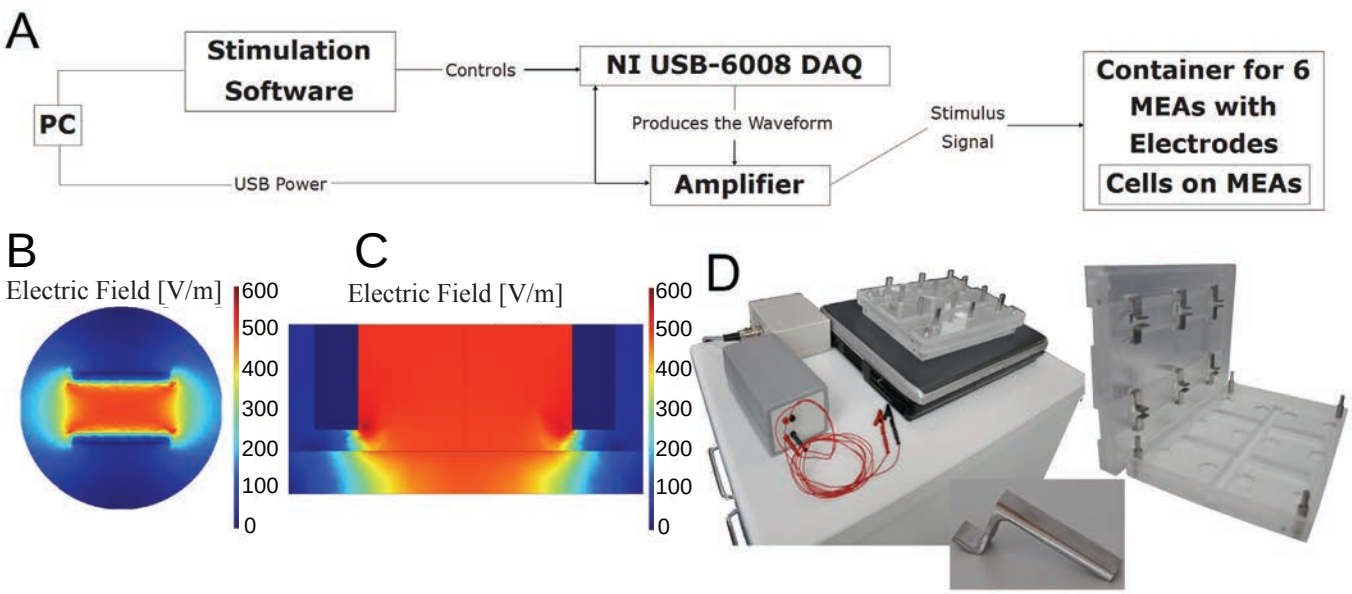

Figure 1. (A) The stimulation system. The stimulation sequence is designed with PC software that controls the NI USB-6008 DAQ device. The waveform that the device produces is amplified and delivered to the MEA container, where the cells reside on MEA dishes; **(B, C)** The simulated result of the electrical field on an MEA dish; **(B)** If the cells to be stimulated are placed on the MEA electrodes in the middle of the MEA dish, they will experience a fairly uniform 500 V/m electrical field. The image is plotted at the height of 0.1 mm; **(C)** A lateral view from the center line shows that the electrical field diminishes at the bottom of the MEA close to the electrodes. The MEA dish has been included in the simulation as an insulator at the bottom; **(D)** The designed stimulation system, consisting of the stimulation electronics, PC, and the MEA dish container; the MEA dish container appears in detail on right, with an individual electrode shown in detail at the bottom.

the bottom part of the container was designed to provide pools for sterile water. The lid and the bottom part featured small glass windows which allow the user to observe the cell cultures on the MEAs with a microscope.

The electronics of the system were designed to yield a field strength of at least 5 V/cm, as similar field strengths had proved effective (23). The electronics consisted of a single-sided supply operational amplifier circuit which amplifies the signal created by a PC-controlled National Instruments USB-6008 Data Acquisition (DAQ) device and produces a voltage-based stimulus. The system was designed to be USB powered. The user can set the stimulation voltage, frequency, total stimulation time, pulse duration, and delays between pulses. The software allows users to design stimulation waveforms, thus enabling them to use uncommon pulse shapes. The system produces electrical fields with a maximum of 5.3 V/cm and an output frequency ranging from 0.5 to 40 Hz. The shortest pulses produced were 2 ms wide. Two clips and wiring connected the electronics to the electrodes. Waveform production using the DAQ device was controlled with the software, which allows the user to adjust the required stimulation parameters and to queue different stimulation sequences.

The electrical output of the stimulator, from both the stimulation electrodes and the MEA electrodes, was verified with an oscilloscope. In addition, the effect of stimulation on medium pH levels was measured with pH electrode (AMANI-1000, Innovative Instruments, Inc, Tampa, USA) from stimulated and control samples after a long-term stimulation with the same parameters used in experiment I (Table 1).

Stimulation protocols

Pacing experiment. Delivery of the stimulation pulses to the cells and the effect of stimulation on the cell culture and beating frequency was tested by observing the behavior of NRCs with a microscope (Olympus IX51, Olympus Corporation, Tokyo, Japan). The cells were seeded on gelatin-coated MEA chambers and paced for 20 s with both monophasic and biphasic pulses at 2.5 and 5 V/cm and a frequency of 1, 2, and 3 Hz with pulse durations of 2 ms, 4 ms, and 10 ms.

Long-term stimulation. After preculture, MEA chambers were transferred to the stimulating chamber. The cells were cultivated for 48 to 72 h without electrical field stimulation in order to allow the cells to attach; electrical field stimulation followed for an additional 48 to 72 h using either monophasic or biphasic pulses at 5 V/cm or 5.3 V/cm with 2 ms, 4 ms or 200 ms pulse durations and a frequency of 1 Hz (Figure 2). Constructs cultured without electrical stimulation served as controls. There were four independent experimental series and three to six samples in both the stimulation and control groups within each experimental series. Electrical field stimulation stopped on days 4 to 6, and cells were processed either for live/dead staining, immunocytochemistry, or for RNA isolation. More detailed information on each experimental series appears in Table 1.

Electrophysiology - microelectrode array (MEA)

The electrical activity of beating NRCs was monitored using the microelectrode array (MEA) system (Multi Channel Systems MCS GmbH, Reutlingen, Germany). Measurements were made of cells on gelatin coating at 37°C, and signals were recorded for 2 min via every microelectrode. The sampling frequency was 20 kHz. Signals were measured before and after stimulation from the first, second, and third experimental samples, and in addition, signals from the second experimental samples were measured twice during the stimulation period. Signals from the control samples were measured at the same time points.

Cell stainings

Live/dead staining. CMs were live/dead stained using a LIVE/DEAD® Viability/Cytotoxity kit for mammalian cells (Molecular Probes, Inc., Invitrogen, USA). Staining

Table 1. Experimental groups

	Pulse form	Pulse duration	Electrical field	Frequency	Duration of stimulation	Culture material	n[a]
Experiment I	Biphasic	100 ms / 100 ms	5.3 V/cm	1 Hz	3 d	2D-coating	3/3
Experiment II	Biphasic	2 ms / 2 ms	5.3 V/cm	1 Hz	2 d	2D-coating	3/5
Experiment III	Monophasic	2 ms	5 V/cm	1 Hz	3 d	2D-coating	4/5
Experiment IV	Monophasic	2 ms	5 V/cm	1 Hz	3 d	collagen gel	6/6

[a]Control/stimulated samples.

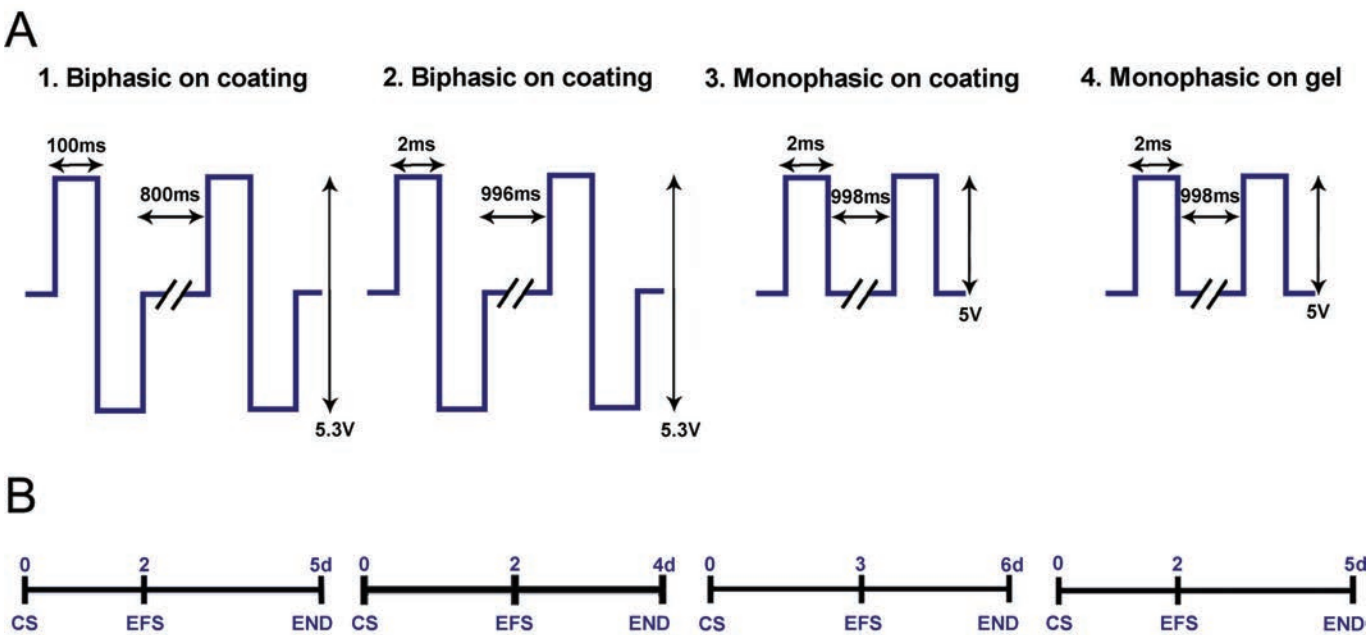

Figure 2. Experimental design. **(A)** Experimental groups for long-term stimulation where NRCs were cultured either on gelatin coating (1-3) or on collagen gel (4). Parameters used for electrical stimulation were biphasic 100-ms square pulses at 5.3 V/cm and 1 Hz (1), biphasic 2-ms square pulses at 5.3 V/cm and 1 Hz (2), and monophasic 2-ms square pulses at 5 V/cm and 1 Hz (3 and 4). **(B)** Experimental timelines for each stimulation group. Control samples were cultured for the same amount of time, but without electrical stimulation. CS, cell seeding; EFS, electrical field stimulation initiation; END, experimental ends.

was carried out according to Molecular Probes' instructions. 0.1 μM Calcein AM staining live cells green and being seen at wavelength of 488 nm and 0.5 μM Ethidium homodimer-1 staining dead cells red and being seen at wavelength of 568 nm were added to the culture medium and incubated at room temperature. The labeled cells were viewed and photographed with a Nikon Eclipse TE2000-S phase contrast microscope with fluorescence optics and a Nikon COOLPIX 5400 camera.

Immunocytochemistry. The cells were fixed in MEA chambers with 4% PFA in phosphate-buffered saline (PBS) (0.01 M, pH7.4) for 20 min at room temperature (RT), followed by washing with PBS (2 × 5 min). The cells were then permeabilized and blocked with 0.1% Triton X-100, 1% BSA (Sigma-Aldrich, Germany), and 10% normal donkey serum (Sigma-Aldrich, Germany) in PBS for 45 min at RT. Primary antibodies anti-troponin I (Santa Cruz, USA) (1:500) and anti-cardiac troponin T (Abcam, UK) (1:1500) were incubated overnight at 4°C. Alexa Fluor 568-conjugated donkey anti-goat served as a secondary antibody (1:800) (Invitrogen, USA) and finally the cells were mounted with Vectashield (Vector Laboratories, USA) containing 4',6-diamidino-2-phenylindole (DAPI) for staining nuclei.

RT-PCR

Total RNA was isolated with a NucleoSpin® RNA II kit (Macherey-Nagel GmbH & Co., Germany). The concentration and quality of the RNA was monitored spectroscopically (Nanodrop, Wilmington, DE, USA) and 100 ng of total RNA was transcribed to cDNA in a total volume of 20 μl with a High Capacity cDNA Reverse Transcription kit (Applied Biosystems, USA). The PCR reaction consisted of 1 μl cDNA, 24 μl of 2 × PCR Mastermix (Applied Biosystems, USA), and 200 nM of each primer. The expressions of three cardiac markers were evaluated: alpha myosin heavy chain 6 (MYH-6), beta myosin heavy chain 7 (MYH-7), and connexin 43 (Cx-43). GAPDH served as a housekeeping gene and calibrator of all cells (Primers: Table 2).

Quantitative RT-PCR

Quantitative RT-PCR was performed according to the standard protocols on an Abi Prism 7300 instrument (Applied Biosystems, Foster City, CA, USA). Total RNA was isolated as described above. Complementary DNA was synthesized from 200 ng of total RNA in a total volume of 20 μl as described above. The PCR reaction consisted of 1 μl cDNA, 7.5 μl of 2 × Power SYBR green PCR mas-

termix (Applied Biosystems, Foster City, CA, USA), 5.3 µl sterile water, and 400 nM of each primer, which were for the same markers as those in RT-PCR (Table 2). Each experiment group was analyzed separately and at least two replicates between both the stimulated and control groups were analyzed as triplicates. Cτ values were determined for every reaction, and the relative quantification was defined with the $2^{-\Delta\Delta C\tau}$ method (18). The data were normalized to the expression of the housekeeping gene Beta actin (β-actin), and the unstimulated sample for each test series served as the calibrator. Statistical significance for each experiment group was determined with the t-test.

Atomic force microscopy

Atomic force microscope (AFM) (XE-100, Park Systems, Korea) with ACTA-50 probe was used in studying the surface of the MEA dish. AFM images of an empty MEA surface were obtained by moving the probe on the sample surface across the measurement area in one direction for each image line in order to create a topographical map of the sample (7).

RESULTS

Stimulator capabilities

The designed system, consisting of the MEA container, stimulation electronics, and the controlling software on a laptop computer, fulfilled the requirements set for the device. To our knowledge, the resulting system is among the first systems to enable the use of the MEA platform in long-term electrical stimulation with homogeneous fields.

The difference of medium pH levels in control and stimulated samples after long term stimulation was 0.10% suggesting stimulation had no effect on pH levels. There were either seen no degradation of the electrodes or any possible gas formation during the different stimulation protocols.

Cardiomyocyte function in a short-term pacing experiment

The effect of short-term stimulation on cell beating was characterized by a pacing experiment in which different stimulation parameters were applied and the pacing of the cells observed visually with a microscope. Initially, the beating rate was about 60 per minute. As the stimulation stopped, beating returned to its original, spontaneous frequency, so the cells did not remain in the paced rhythm after stimulation (data not shown). Visually, the pulse duration or pulse form had no effect on cell beating. When the electrical field was 5 V/cm, the beating was stronger than with the smaller 2.5 V/cm field.

Cell morphology

In the long-term stimulation, cells in experiments I, II, and III (Table 1) were electrically stimulated on gelatin-coated MEA chambers with different parameters (Figure 2). Different parameters based on earlier publications (3, 9, 24) were tested to try to find the optimal parameters for NRC stimulation. The morphology of NRCs was the same during stimulation, and both stimulated and control cells exhibited similar morphological features throughout the ex-

Table 2. Primer sequences

Gene	Forward Primer	Reverse Primer	Size (bp)
RT-PCR			
GAPDH[a]	TGGAAAGCTGTGGCGTGATG	TCCACCACCCTGTTGCTGTAGC	380
MYH6[a] (alpha myosin heavy chain 6)	GGAAGAGCGAGCGGCGCATCAAGG	CTGCTGGACAGGTTATTCCTCA	304
MYH7[a] (beta myosin heavy chain 7)	GCCAACACCAACCTGTCCAAGTTC	TCAAAGGCTCCAGGTCTCAGGGC	201
Cx-43[a] (connexin 43)	CATTGGGGGGAAGGCGTGAGG	AGCGCACGTGAGAGATGGGGAAG	401
Q-PCR			
β-actin[b] (beta actin)	TAAAGACCTCTATGCCAACAC	GATAGAGCCACCAATCCAC	166
MYH6[c] (alpha myosin heavy chain 6)	TTCCGCAAGGTGCAGCACGAG	TCCTCATCGTGCATTTTCTGCTTGG	125
MYH7[c] (beta myosin heavy chain 7)	TTCCGCAAGGTGCAGCACGAG	TACTCTTCATTCAGGCCCTTGGCGC	122
Cx-43[b] (connexin 43)	GTTCTATGTGATGAGGAAGG	ACTTCTTGATTTCAATCTGC	116

[a, b]Primers have been described earlier (24), (9), respectively; [c]Primers have been made with Primer-BLAST of NCBI.

perimental period. The cells were not elongated or oriented parallel to the electrical field. Instead, the orientation of the cells was seen parallel to the MEA electrode wires in both the control and stimulation samples (Figures 3A and 3B). An equal number of cells were plated on each well, and the number of cells decreased similarly during the culture in both the control and stimulated samples. The time in culture also affected the beating frequency, which was evident both microscopically and in MEA measurements as a decrease in the beating rate (Figures 4A and 4B).

In experiment series IV, CMs were cultured on collagen gel (Figures 3C and 3D). The cells contracted nicely and were well spread over the surface of the gel. After three days of stimulation, cell orientation appeared unaltered. Microscope analysis revealed that cells in the control and stimulation samples were similarly shaped. In both the control and stimulated samples, long tube-like structures (Figure 3C and 3D) were observed on the collagen gel in addition to cardiac cells.

Electrophysiology

We monitored the electrical activity of both stimulated and control NRCs with MEA. The spontaneous beating rate varied between 0.5 and 2 Hz, and was usually 1.0 Hz (Figures 4A and 4B). After stimulation, the cells either stopped beating or the beating rate was more irregular than before stimulation; this was also evident in the controls after experiment. In experiment II, the signals were measured before stimulation and 5, 24, and 48 hours after stimulation. The control samples were measured at the same time points. The beating rate decreased both in stimulated and control groups (Figure 4A and B), but less radically than in experiments I, III and IV. The beating was more irregular in the end of the experiment than in the beginning (Figure 4A and 4B).

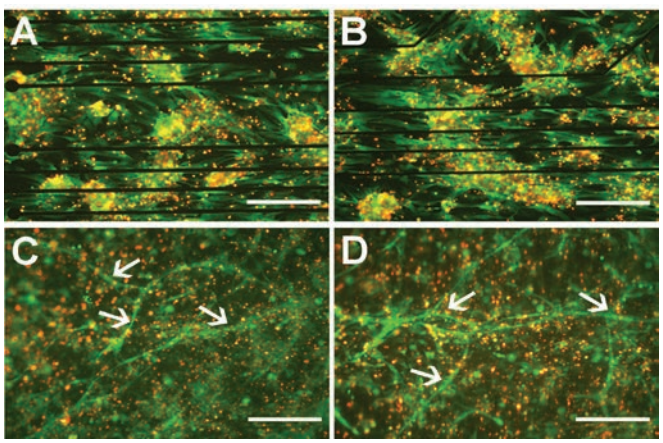

Figure 3. Cell viability. In addition to cell viability, the orientation of NRCs on gelatin coating parallel to the electrode lines of the MEA chambers is evident in the live/dead stainings (live cells green, dead cells red) in both control **(A)** and stimulated **(B)** samples. The tube formation of cells on collagen gel in experiment IV is clearly evident from the live/dead stainings in both control (**C**) and stimulated **(D)** samples. Arrows denote tube-like structures, which were observed in both stimulated and control samples. The direction of the electrical field is horizontal in the pictures. Scale bars are 200 µm.

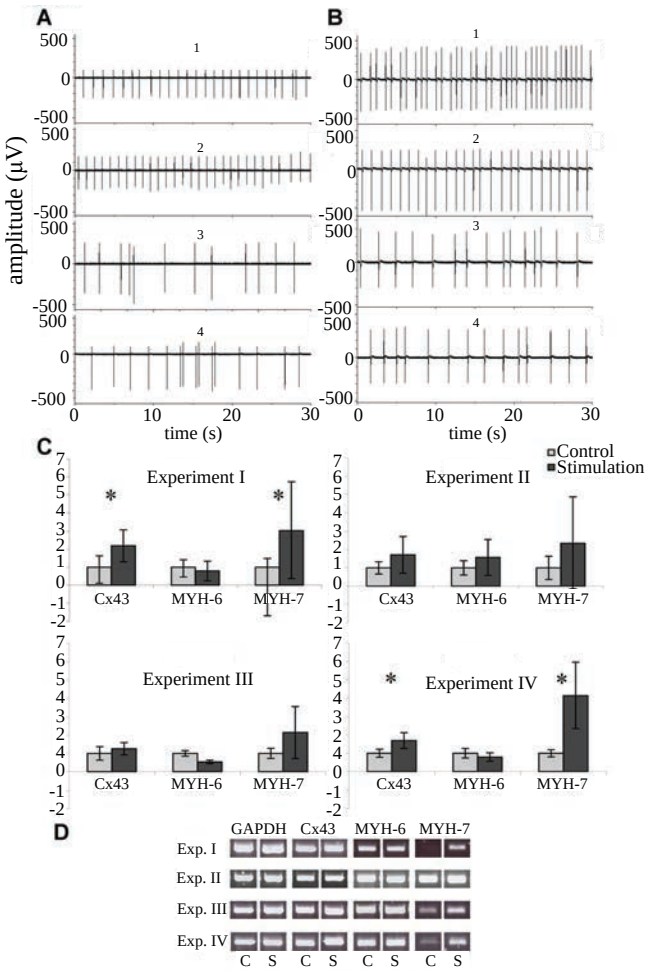

Figure 4. Functional properties of long-term stimulated NRCs. Electrical activity of control NRCs **(A)** and stimulated samples **(B)** in experiment II before stimulation (1) and after 5 hours (2), 24 hours (3), and 48 hours (4) of stimulation. **(C)** Cx-43, MYH-6, and MYH-7 expressions from each experiment determined by qPCR at the end of culturing. Statistical significance is marked with (*p<0.05). Number of control vs stimulated samples analyzed as triplicates: Exp. I n=2 vs n=3, Exp. II n=3 vs n=4, Exp. III n=2 vs n=2, Exp. IV n=3 vs n=3. Error bars are SD. **(D)** Gene expressions from each experiment determined by RT-PCR at the end of culturing. S, electrically stimulated samples; C, control samples.

MEA measurements could not be carried out on cells on collagen gel due to the thickness of the gel, so the beating was observed only visually with a microscope. Before stimulation, the beating rate of the cells on the gel was regular, contractions were clearly observed, and the gel adjusted to the beating. Although the size of the beating area differed between replicates, overall the beating was the same when compared to the samples on gelatin coating. After stimulation, beating areas were fewer in number and smaller in size, and the beating frequency in both sample groups decreased.

Cell viability

Cell viability was determined after each experimental series. Live/dead staining indicated that there were no differences in cell viability between the stimulated and control samples (Figures 3A, 3B, 3C, and 3D) and roughly 50 % of the cells were alive in both conditions. In addition, cell alignment and elongation was more distinguishable with the help of live/dead staining, but we observed no changes due to stimulation. Instead, the orientation of the cells on gelatin coating was parallel to the MEA chamber electrode wires in both the control and stimulation samples (Figures 3A and 3B). The orientation was very clear in experiment II, and cell alignment was precisely paralleled the direction of the electrode wires.

With the help of live/dead staining, we observed the tube-like structures from the collagen gel samples. Tubes were present in every collagen gel sample (Figures 3C and 3D) and showed no orientation in any specific direction.

Gene expression

According to the RT-PCR results, the MYH-7 mRNA level was higher in the 3-day stimulation experiments (I, III, and IV) than in the control samples. Cx-43 expression levels were also slightly elevated in these stimulated samples, but in other genes no differences were evident (Figure 4D).

To ensure the difference in gene expression levels, quantitative RT-PCR was carried out for the same samples as used in RT-PCR. Stimulation increased MYH-7 and Cx-43 expression levels in experiments I and IV ($p<0.05$) when compared to controls (Figure 4C). In experiments II and III, MYH-7 and Cx-43 expression levels had a trend towards higher expression, but it did not reach statistical significance. No significant difference in MYH-6 expression between the control and stimulated samples was observed in any experiment.

Protein expression

Immunocytochemistry served to identify CM structures. The stimulated cells stained positively with troponin T or I similarly to the controls (Figure 5). The stimulated CMs revealed no visible changes in sarcomeric structure.

In experiment IV, narrow and long tube-like structures formed during culture on collagen gel. The tubes were analyzed with antibodies against Vimentin (mesenchymal origin: fibroblasts, endothelial, smooth muscle), α-AS (myotubes in skeletal and cardiac muscles), α-SMA (smooth muscle), VWf1 (endothelial), VWf2 (endothelial), Pax-6 (neural) and MAP-2 (neural), however, no positive staining with any antibodies used was seen (13). Since the origin of tubes were not neural, vascular or muscle-derived the nature of the tubes remains unknown.

Surface measurement using AFM

To estimate the effect of surface abrasions on the orientation of cells, AFM served to measure the height of the

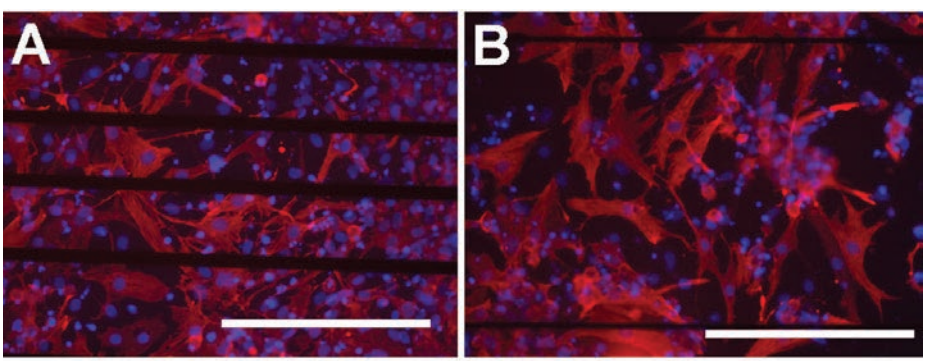

Figure 5. Expression of troponin T (red) in control (**A**) and in stimulated (**B**) samples; blue indicates cell nuclei (scale bars 200 µm).

electrode wires on an MEA dish. The results revealed that the electrode wires on the MEA had a height of 600 nm (Figure 6).

DISCUSSION

A novel platform for the electrical stimulation of cells was designed in this study. When compared with other existing systems for cell culture stimulation, the designed system provides several possibilities which to our knowledge can not all be found in other stimulation platforms: the possibility to stimulate several cell cultures, homogeneous long term electrical field stimulation on MEAs and programmable stimulation platform. In some earlier studies MEAs have been used (8, 16), which have the capability of localized electrical stimuli. However in studies with goal of creating a uniform field, carbon rod electrodes have been more widely used (3, 12, 24) together with commercial cell containers like plates, wells and dishes (3, 12, 24). In waveform creation commercial stimulators are used in several studies (3, 11, 24).

The main objective was to examine whether electrical field stimulation affects synchronous cell contractions and cell alignment, the maturation or functional assembly of CMs. In the present study, stimulation was initiated on either the second or third day after plating. This arrangement was based on previous findings (24), which indicate that if applied on the first day *in vitro*, electrical stimulation yields poor contractile behavior. In contrast, if stimulation was applied on day five, fewer contractile proteins were found in the cells (24). This timing also ensured that the cells had enough time to recover from the cell isolation procedure and to attach properly to the MEA chambers prior to stimulation. In the present study both monophasic and symmetric biphasic square pulses were used. A previous study has reported that the use of biphasic pulses in applications of electrical stimulation maintains biocompatibility better by avoiding tissue injury or electrode damage (25). Biphasic pulses minimize the damage caused by electrodes as a result of the redox reaction on the electrodes, which leads to tissue damage due to pH and metal salts released in the process (25). Biphasic pulses have also been reported to enhance the positive effects of electrical stimulation with regard to functional and structural properties (9). However, we saw no differences between biphasic and monophasic pulses in our set-up.

In the pacing experiments the stimulator served to pace NRCs and in the absence of stimulation the beating returned back to spontaneous rhythm. When the field strength was 2.5 V/cm, the cells failed to contract as uniformly as with the higher 5 V/cm fields, thus demonstrating the efficacy of the system. Previous studies have shown that the higher the field strength, the more likely the cell will reach the depolarization threshold and contract in response to the stimulus (3).

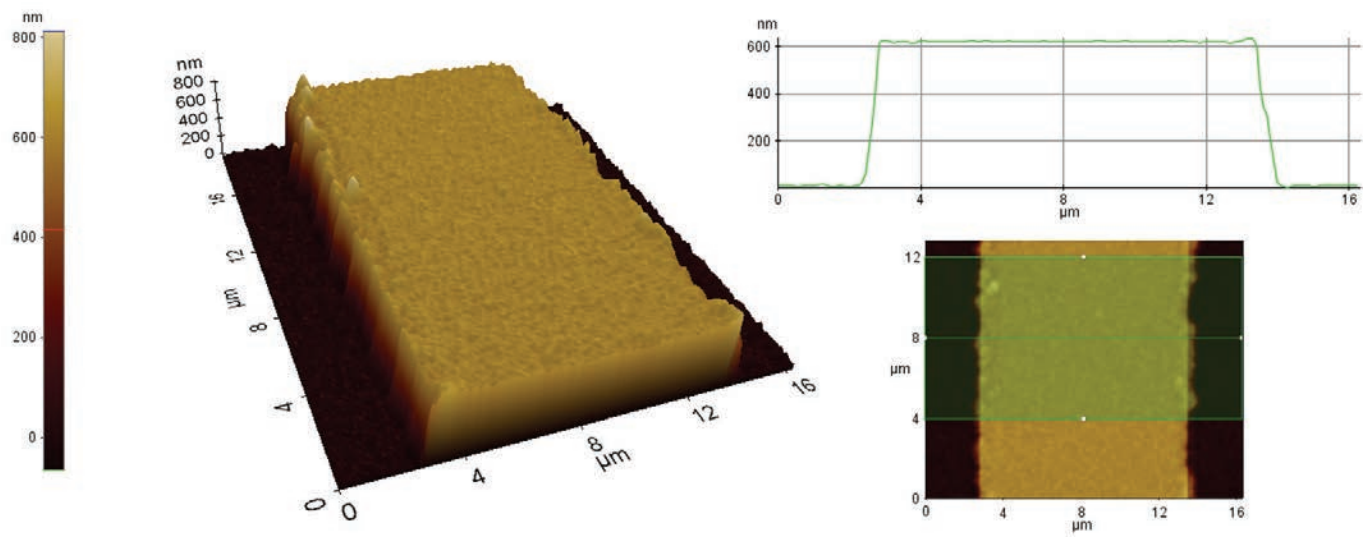

Figure 6. An AFM surface scan of the MEA electrode wiring. The scan shows the height of the electrode wirings to be approximately 600 nm. The height was determined by averaging the height profile from an 8-µm-long wiring track.

The benefit of the new stimulation system is its potential to stimulate cells in MEA chambers and measure the electrical activity of cells both before and after stimulation. In the long-term experiments, the beating rate decreased in all samples. The detachment of the cells affected negatively on the spontaneous beating rate which might be due to the loss of the cell-to-cell contacts necessary for signal induction. CMs isolated from the heart and cultured *in vitro* are known to dedifferentiate and eventually stop beating (21). They also lose many of their surface channels and receptors (2), myofilament equipment, and acquire a round shape (35). All these factors may lower the beating rate, which was evident in the MEA measurements. Previous studies indicate that the number of spontaneously beating cells decreased to 8% after eight days *in vitro* and no spontaneous beating was observed in the stimulated samples, but the beating could be triggered by external stimulus (26).

Live/dead staining revealed that there were no significant differences in cell viability between the stimulated and control samples. In earlier studies, the cells were shown to elongate, couple, and orientate parallel to the electrical field (3, 11, 24) using either a direct (3) or an alternating current field (11). In the present study no such morphological changes in the cells were observed. However, no changes in cell morphology during electrical stimulation has also reported earlier (26). Collagen gel could also provide a more elastic surface to enable cell orientation. However, we found no improvement in the stimulation results, but the cells spread nicely and migrated within the gel, and the gel allowed the cell beating.

In the present study, cells were oriented parallel to the MEA chamber electrode wires in both the control and stimulation samples, so the topography of the cell culture surface was a determinant of cell orientation. The AFM results showed that the electrode wires on the MEA have a height of 600 nm. Previous studies have shown that topographical cues of a height of several hundred nanometers are sufficient to induce cell orientation (3, 4, 15). Au *et al.* used topographical cues from 140 to 700 nm of height (3) as well as microgrooves of 400 nm (4) which were all capable of inducing cellular orientation. Kim *et al.* used nanoscale cues from 200 to 500 nm in height, and these affected the structure and function of cardiac tissue constructs (15). Our findings support those earlier observations that the surface topography is a stronger factor than the electrical field with regards to cell orientation; once cells have orientated towards topographical shapes, they cannot re-orient with electrical stimulation (3, 4). We can therefore conclude that when aiming at cell orientation, it is more worthwhile to model and improve the topography of the cell substrate than to use electrical field stimulation.

Previous studies have shown that electrical field stimulation influences CM functionality (9, 24, 26). Cx-43 molecules form gap junctions, which are intercellular channels located in the intercalated disc and provide both electrical and metabolic coupling for CMs (33). Cx-43 is expressed in virtually all myocytes of the atrial- and ventricular mammalian myocardium regardless of the stage of development (33). According to the qPCR analysis in our study, the expression level of Cx-43 was significantly higher in two stimulation experiments when compared to the controls. This is in line with earlier studies where the expression of Cx-43 increased on both the gene and protein levels due to electrical field stimulation (3, 9, 24). MHC is the major contractile protein of cardiac muscle cells and the primary determinant of the efficiency of muscle contraction (32). MHC genes exist in cardiac cells in two isoforms: α-MHC encoded by the MYH-6 gene, which is upregulated during adult cardiac development, and β-MHC by the MYH-7 gene, which is upregulated during fetal cardiac development (22). In this study, the gene expression level of MYH-7 increased after three days of stimulation, which suggests an increase in the fetal type of cardiac cells due to electrical stimulation. Stimulating the CMs for two days instead of three showed no differences in MYH-7 expression, which may indicate that stimulation should last at least three days to ensure perceptivity of the effects of stimulation. These results are in line with previous studies where the expression of sarcomeric proteins MYH-6 and MYH-7 increased due to electrical stimulation and its duration. However, in the earlier reports the ratio of these two isoforms has changed indicating maturation of the CMs (24). We did not observe this in our study. Other studies have shown that the mRNA level of MYH-7 in CMs derived from hESCs is substantially higher in ventricular tissue (1) which has also been observed in rat hearts (29). This could indicate that most isolated and cultured NRCs were ventricular, and therefore only MYH-7 expression increased. One reason for the increase in MYH-7 expression could be the mechanical stress, in this case due to electrical stimulation, which in earlier studies induced a shift from α-MHC toward β-MHC composition in mice hearts (17). This shift could reduce contractile efficiency, and therefore be one reason for the lower beating rate observed in this study.

As a conclusion our data suggest that surface topog-

raphy was a stronger determinant of CM orientation than electrical field stimulation; consequently, the micro architecture of the materials should be examined carefully when cell orientation is desired. Electrical stimulation and its duration seem to affect gene expression profile, and this stimulation system may prove useful in the future, for example, to enhance cardiac differentiation of stem cells. Our stimulation platform proved capable of pacing cultured cells, and this property can be exploited in various cardiac-related studies requiring the electromechanical stimulation of cardiac cells. However, we did not detect any long-term effects of electrical stimulation on the electrophysiological behavior of the cells even though stimulation increased Cx-43 expression. In the future, it would be important to optimize the stimulation parameters to improve the maturation process and to understand the effect of these parameters at the cellular level. It would also be important to understand better the mechanism of how electrical stimulation influences cell differentiation and maturation and to discover effective ways to quantify this phenomenon at the cellular level.

ACKNOWLEDGEMENTS

We thank Kirsi Nurminen for the technical assistance of pH measurements. This study was funded by the Pirkanmaa Hospital District, the Academy of Finland, the Finnish Cardiovascular Foundation, and Biocenter Finland.

CONFLICT OF INTERESTS

The authors declare that no conflicting interests exist.

REFERENCES

1. Asp J, Steel D, Jonsson M, *et al*. Cardiomyocyte clusters derived from human embryonic stem cells share similarities with human heart tissue. *J. Mol. Cell Biol.* 2010; 2 (5): 276.
2. Atala A. Methods of tissue engineering. *San Diego: Academic Press.* 2002; p1285.
3. Au HT, Cheng I, Chowdhury MF, Radisic M. Interactive effects of surface topography and pulsatile electrical field stimulation on orientation and elongation of fibroblasts and cardiomyocytes. *Biomaterials.* 2007; 28 (29): 4277.
4. Au HT, Cui B, Chu ZE, *et al*. Cell culture chips for simultaneous application of topographical and electrical cues enhance phenotype of cardiomyocytes. *Lab. Chip.* 2009; 9 (4): 564.
5. Barash Y, Dvir T, Tandeitnik P, *et al*. Electric field stimulation integrated into perfusion bioreactor for cardiac tissue engineering. *Tissue Eng. Part C Methods.* 2010; 16 (6): 1417.
6. Berger HJ, Prasad SK, Davidoff AJ, *et al*. Continual electric field stimulation preserves contractile function of adult ventricular myocytes in primary culture. *Am. J. Physiol.* 1994; 266 (1 Pt 2): H341.
7. Binnig G, Quate CF, Gerber C. Atomic force microscope. *Phys. Rev. Lett.* 1986; 56 (9): 930.
8. Chen MQ, Xie X, Hollis Whittington R, *et al*. Cardiac differentiation of embryonic stem cells with point-source electrical stimulation. *Conf. Proc. IEEE Eng. Med. Biol. Soc.* 2008; 2008: 1729.
9. Chiu LL, Iyer RK, King JP, Radisic M. Biphasic electrical field stimulation aids in tissue engineering of multicell-type cardiac organoids. *Tissue Eng. Part A.* 2008; 17 (11-12): 1465.
10. Eschenhagen T, Didie M, Munzel F, *et al*. 3D engineered heart tissue for replacement therapy. *Basic Res. Cardiol.* 2002; 97 Suppl 1: I146.
11. Hedgepath KR, Mukherjee R, Wang Z, Spinale FG. The relation between changes in myocyte orientation and contractile function with electrical field stimulation. *Basic Res. Cardiol.* 1997; 92 (6): 385.
12. Holt E, Lunde PK, Sejersted OM, Christensen G. Electrical stimulation of adult rat cardiomyocytes in culture improves contractile properties and is associated with altered calcium handling. *Basic Res. Cardiol.* 1997; 92 (5): 289.
13. Ikonen L, Kerkelä E, Kujala K, *et al*. Analysis of different natural and synthetic biomaterials to support cardiomyocyte growth. *J. Clinic. Experiment. Cardiol.* 2011; S4-003.
14. Kehat I, Kenyagin-Karsenti D, Snir M, *et al*. Human embryonic stem cells can differentiate into myocytes with structural and functional properties of cardiomyocytes. *J. Clin. Invest.* 2001; 108 (3): 407.
15. Kim DH, Lipke EA, Kim P, *et al*. Nanoscale cues regulate the structure and function of macroscopic cardiac tissue constructs. *Proc. Natl. Acad. Sci. USA.* 2010; 107 (2): 565.
16. Klauke N, Smith GL, Cooper J. Stimulation of single isolated adult ventricular myocytes within a low volume using a planar microelectrode array. *Biophys. J.* 2003; 85 (3): 1766.
17. Krenz M, Robbins J. Impact of beta-myosin heavy chain expression on cardiac function during stress. *J. Am. Coll. Cardiol.* 2004; 44 (12): 2390.
18. Livak KJ, Schmittgen TD. Analysis of relative gene expression data using real-time quantitative PCR and the 2(-Delta Delta C(T)) Method. *Methods.* 2001; 25 (4): 402.
19. Mather JP, Roberts PE. Introduction to cell and tissue culture theory and technique. *New York: Plenum Press.* 1998; p241.
20. McDonough PM, Glembotski CC. Induction of atrial natriuretic factor and myosin light chain-2 gene expression in cultured ventricular myocytes by electrical stimulation of contraction. *J. Biol. Chem.* 1992; 267 (17): 11665.
21. Montessuit C, Rosenblatt-Velin N, Papageorgiou I, *et al*. Regulation of glucose transporter expression in cardiac myocytes: p38 MAPK is a strong inducer of GLUT4. *Cardiovasc. Res.* 2004; 64 (1): 94.
22. Nakao K, Minobe W, Roden R, *et al*. Myosin heavy chain gene expression in human heart failure. *J. Clin. Invest.* 1997; 100 (9): 2362.
23. Radisic M, Park H, Gerecht S, *et al*. Biomimetic approach to cardiac tissue engineering. *Philos Trans. R. Soc. Lond. B Biol. Sci.* 2007; 362 (1484): 1357.
24. Radisic M, Park H, Shing H, *et al*. Functional assembly of engineered myocardium by electrical stimulation of cardiac myocytes cultured on scaffolds. *Proc. Natl. Acad. Sci. USA.* 2004; 101 (52): 18129.
25. Rubinstein JT, Miller CA, Mino H, Abbas PJ. Analysis of monophasic and biphasic electrical stimulation of nerve. *IEEE Trans. Biomed. Eng.* 2001; 48 (10): 1065.
26. Sathaye A, Bursac N, Sheehy S, Tung L. Electrical pacing counteracts intrinsic shortening of action potential duration of neonatal rat ventricular cells in culture. *J. Mol. Cell Cardiol.* 2006; 41 (4): 633.
27. Sauer H, Rahimi G, Hescheler J, Wartenberg M. Effects of electrical fields on cardiomyocyte differentiation of embryonic stem cells. *J. Cell*

Biochem. 1999; 75 (4): 710.
28. Serena E, Figallo E, Tandon N, *et al*. Electrical stimulation of human embryonic stem cells: cardiac differentiation and the generation of reactive oxygen species. *Exp. Cell Res.* 2009; 315 (20): 3611.
29. Sharma S, Razeghi P, Shakir A, *et al*. Regional heterogeneity in gene expression profiles: a transcript analysis in human and rat heart. *Cardiology*. 2003; 100 (2): 73.
30. Tung L, Sliz N, Mulligan MR. Influence of electrical axis of stimulation on excitation of cardiac muscle cells. *Circ. Res.* 1991; 69 (3): 722.
31. Uusimaa PA, Hassinen IE, Vuolteenaho O, Ruskoaho H. Endothelin-induced atrial natriuretic peptide release from cultured neonatal cardiac myocytes: the role of extracellular calcium and protein kinase-C. *Endocrinology*. 1992; 130 (5): 2455.
32. van Rooij E, Quiat D, Johnson BA, *et al*. A family of microRNAs encoded by myosin genes governs myosin expression and muscle performance. *Dev. Cell*. 2009; 17 (5): 662.
33. van Veen AA, van Rijen HV, Opthof T. Cardiac gap junction channels: modulation of expression and channel properties. *Cardiovasc. Res.* 2001; 51 (2): 217.
34. Zhang J, Wilson GF, Soerens AG, *et al*. Functional cardiomyocytes derived from human induced pluripotent stem cells. *Circ. Res.* 2009; 104 (4): e30.
35. Zimmermann WH, Schneiderbanger K, Schubert P, *et al*. Tissue engineering of a differentiated cardiac muscle construct. *Circ. Res.* 2002; 90 (2): 223.

Study II

Kujala K, Paavola J, Lahti A, Larsson K, Pekkanen-Mattila M, Viitasalo M, Lahtinen AM, Toivonen L, Kontula K, Swan H, Laine M, Silvennoinen O, Aalto-Setälä K

Cell Model of Catecholaminergic Polymorphic Ventricular Tachycardia Reveals Early and Delayed Afterdepolarizations

PLoS One. 2012 Sep 4:7(9):e44660

OPEN ACCESS Freely available online

PLOS ONE

Cell Model of Catecholaminergic Polymorphic Ventricular Tachycardia Reveals Early and Delayed Afterdepolarizations

Kirsi Kujala[1,2☯], Jere Paavola[1,2,3☯], Anna Lahti[1,2], Kim Larsson[1,2], Mari Pekkanen-Mattila[1,2], Matti Viitasalo[4], Annukka M. Lahtinen[5], Lauri Toivonen[4], Kimmo Kontula[6], Heikki Swan[6], Mika Laine[3,4], Olli Silvennoinen[1,2,7], Katriina Aalto-Setälä[1,2,8]*

1 Institute of Biomedical Technology, University of Tampere, Tampere, Finland, **2** BioMediTech, Tampere, Finland, **3** Minerva Foundation Institute for Medical Research, Helsinki, Finland, **4** Department of Cardiology, Helsinki University Hospital, Helsinki, Finland, **5** Research Program's Unit Molecular Medicine, University of Helsinki, Helsinki, Finland, **6** Department of Medicine, University of Helsinki, Helsinki, Finland, **7** Tampere University Hospital, Tampere, Finland, **8** Heart Center, Tampere, Finland

Abstract

Background: Induced pluripotent stem cells (iPSC) provide means to study the pathophysiology of genetic disorders. Catecholaminergic polymorphic ventricular tachycardia (CPVT) is a malignant inherited ion channel disorder predominantly caused by mutations in the cardiac ryanodine receptor (RyR2). In this study the cellular characteristics of CPVT are investigated and whether the electrophysiological features of this mutation can be mimicked using iPSC -derived cardiomyocytes (CM).

Methodology/Principal Findings: Spontaneously beating CMs were differentiated from iPSCs derived from a CPVT patient carrying a *P2328S* mutation in RyR2 and from two healthy controls. Calcium (Ca^{2+}) cycling and electrophysiological properties were studied by Ca^{2+} imaging and patch-clamp techniques. Monophasic action potential (MAP) recordings and 24h-ECGs of *CPVT-P2328S* patients were analyzed for the presence of afterdepolarizations. We found defects in Ca^{2+} cycling and electrophysiology in CPVT CMs, reflecting the cardiac phenotype observed in the patients. Catecholaminergic stress led to abnormal Ca^{2+} signaling and induced arrhythmias in CPVT CMs. CPVT CMs also displayed reduced sarcoplasmic reticulum (SR) Ca^{2+} content, indicating leakage of Ca^{2+} from the SR. Patch-clamp recordings of CPVT CMs revealed both delayed afterdepolarizations (DADs) during spontaneous beating and in response to adrenaline and also early afterdepolarizations (EADs) during spontaneous beating, recapitulating the changes seen in MAP and 24h-ECG recordings of patients carrying the same mutation.

Conclusions/Significance: This cell model shows aberrant Ca^{2+} cycling characteristic of CPVT and in addition to DADs it displays EADs. This cell model for CPVT provides a platform to study basic pathology, to screen drugs, and to optimize drug therapy.

Citation: Kujala K, Paavola J, Lahti A, Larsson K, Pekkanen-Mattila M, et al. (2012) Cell Model of Catecholaminergic Polymorphic Ventricular Tachycardia Reveals Early and Delayed Afterdepolarizations. PLoS ONE 7(9): e44660. doi:10.1371/journal.pone.0044660

Editor: Vladimir E. Bondarenko, Georgia State University, United States of America

Received May 25, 2012; **Accepted** August 6, 2012; **Published** September 4, 2012

Funding: This work was supported by Academy of Finland (http://www.aka.fi/en-GB/A/), TEKES (http://www.tekes.fi/en/), Finnish Foundation for Cardiovascular Research (http://www.sydantutkimussaatio.fi), Pirkanmaa Hospital District (www.pshp.fi), Ida Montin Foundation (http://www.idamontininsaatio.fi), Finnish Medical Foundation/The Finnish Medical Society Duodecim (www.duodecim.fi/), Aarne Koskelo Foundation (www.aarnekoskelonsaatio.fi/), Orion-Farmos Research Foundation (http://www.orion.fi/Tutkimus-ja-tuotekehitys/Orion-Farmos-Tutkimussaatio/), Finnish Cultural Foundation (www.skr.fi/), and Oskar Öflund Foundation (www.oskaroflund.fi/). The funders had no role in study design, data collection and analysis, decision to publish, or preparation of the manuscript.

Competing Interests: The authors have declared that no competing interests exist.

* E-mail: katriina.aalto-setala@uta.fi

☯ These authors contributed equally to this work.

Introduction

Catecholaminergic polymorphic ventricular tachycardia (CPVT) is a severe inherited cardiac disorder characterized by stress-induced polymorphic ventricular tachycardia in a structurally normal heart. Approximately 30% of CPVT patients have symptoms before the age of 10 and the mortality rate is 30–35% by the age of 30. β-blockers are recommended for CPVT, but this treatment often fails to prevent even fatal arrhythmias [1].

CPVT is caused by mutations in the cardiac ryanodine receptor (*RyR2*) or calsequestrin (*CASQ2*) gene. RyR2 is involved in the release of calcium (Ca^{2+}) from the sarcoplasmic reticulum (SR) and thus plays a key role in excitation-contraction coupling. Calsequestrin is a regulatory calcium-buffering protein associated with RyR2 in the SR. *RyR2* mutations can be detected in about 70% of patients with CPVT. These mutations are thought to result in increased release, or leak, of Ca^{2+} from the SR potentially leading to diastolic oscillations of intracellular Ca^{2+}, delayed afterdepolarizations (DAD), and polymorphic ventricular tachycardia [1]. However, our understanding of the detailed pathophysiology behind CPVT remains incomplete.

Although the pathomechanisms have been clinically studied in CPVT patients with exercise stress tests, genetically engineered mouse models have been significant to the understanding of CPVT. Most of the CPVT-studies related to *RyR2* mutations have been performed in autosomal dominant transgenic knock-in mouse models expressing mutations which have shown Ca^{2+} -mediated arrhythmogenesis [2].

Induced pluripotent stem cell (iPSC) technology where pluripotent stem cells are generated by reprogramming differentiated cells into a pluripotent state provides a way to study the pathophysiology of various disorders in human cells. iPSCs can be differentiated into the desired cell type, retaining the original genotype. Recently CPVT-specific iPSCs -derived cardiomyocytes (CMs) from individuals carrying *RyR2* mutations [3,4] have demonstrated DADs as the electrical abnormalities.

The *P2328S* mutation in *RyR2* has been found in families with CPVT. Here we introduce a functional cell model for CPVT caused by this mutation. We investigated the mechanistic characteristics of this disease *in vitro* using iPSC –derived CMs. Importantly, we demonstrate the presence of EADs in addition to DADs as a pathophysiological mechanism of CPVT.

Methods

Generation of Patient-Specific iPSCs

The study was approved by the ethical committee of Pirkanmaa Hospital District (R08070) and written informed consent was obtained from all the participants. Patient-specific iPSC lines were established as described earlier [5]. Two CPVT-specific iPSC lines (UTA.05203.CPVT and UTA.05208.CPVT) were generated from a 25-year-old male carrying a *RyR2-P2328S* mutation. iPSC lines UTA.00112.hFF (derived from foreskin fibroblasts) and UTA.04602.WT (from skin fibroblasts of a healthy 55-year-old female) were used as controls.

Characterization of iPSC Lines

Genotyping. The *RyR2-P2328S* mutation was assayed with PCR amplification of genomic DNA with primers for *RyR2* exon 46 (forward: ttt gtt tac tta tct tcc cca ttc, reverse: tat gga tca ctc gtg agg gt) and HaeIII digestion (New England Biolabs, Ipswich, MA, USA). DNA for wild type was 170 and 87 and for *P2328S* heterozygote 257, 170 and 87 base pairs long. For confirmation of the mutation by direct sequencing, the *RyR2* exon 46 PCR products were sequenced with BigDye Terminator v3.1 and ABI 3730xl DNA Analyzer (Applied Biosystems, Carlsbad, CA, USA).

Karyotype analysis. Karyotypes of the cell lines were determined using standard G-banding chromosome analysis (Medix laboratories, Espoo, Finland).

Reverse transcription polymerase chain reaction (RT-PCR). Endogenous and exogenous gene expressions were studied from iPSCs by RT-PCR. The PCR reaction consisted of 1 μl cDNA and 500 nmol/L of each primer. PCR primers for iPSC characterization and detailed reaction conditions have been described earlier [5]. β-actin served as a housekeeping gene.

Immunocytochemistry. The iPSCs were fixed with 4% paraformaldehyde (Sigma-Aldrich, Saint Louis, USA). Primary antibodies anti-SOX2, anti-NANOG, anti-stage-specific embryonic antigen (SSEA)4, and anti-tumour-related antigen (TRA)1–81 (all 1:200, from Santa Cruz Biotechnology, Santa Cruz, CA, USA), anti-OCT3/4 (1:400, R&D Systems) and anti-TRA1–60 (1:200, Millipore) were used. Cells were mounted with Vectashield (Vector Laboratories, USA) containing 4′, 6-diamidino-2-phenylindole (DAPI) for staining nuclei.

Embryoid body (EB) formation. EBs were maintained in EB-medium (KO-DMEM with 20% FBS, NEAA, L-glutamine and penicillin/streptomycin) for 5 weeks. The expression of markers characteristic of ectoderm (*Nestin*), endoderm (*AFP*), and mesoderm (*α-cardiactin*) development in EBs were studied (primers in Table 1).

Teratoma formation. The study was approved by ELLA-Animal Experiment Board of Regional State Administrative Agency for Southern Finland (ESAVI/6543/04.10.03/2011). iPSCs were injected into nude mice under the testis capsule and tumor samples collected 8 weeks after injection. This was followed by fixation with 4% paraformaldehyde and staining of the sections with haematoxylin and eosin.

Cardiomyocyte Differentiation and Characterization

Differentiation into cardiomyocytes (CMs) was carried out by co-culturing iPSCs with murine visceral endoderm-like (END-2)

Table 1. Primer sequences for RT-PCR.

Gene	Forward Primer	Reverse Primer	GenBank ID
Endodermal			
AFP	AGAACCTGTCACAAGCTGTG	GACAGCAAGCTGAGGATGTC	174
Ectodermal			
Nestin	CAGCTGGCGCACCTCAAGATG	AGGGAAGTTGGGCTCAGGACTGG	10763
Mesodermal			
a-cardiactin	GGAGTTATGGTGGGTATGGGTC	AGTGGTGACAAAGGAGTAGCCA	70
Ca^{2+} cycling			
RyR2	TAGATTTATAAGGGGCCTTG	GATTCTTCAGGGCTCGTAGT	6262
Cav1.2	TGACATCGAGGGAGAAAACT	ACATTAGACTTGACTGCGGC	775
Serca2a	GAGAACGCGCACACCAAGA	TTGGAGCCCCATCTCTCCTT	488
Phospholamban	CTGCCAAGGCTACCTAAAAG	AGCTGAGCGAGTGAGGTATT	5350
NCX	TTCCAGAATGATGAAATTGTGAAGAT	TCCTCAAGCACAAGGGAGAAAC	6546
TNTT2	ATCCCCGATGGAGAGAGAGT	TCTTCTTCTTTTCCCGCTCA	7139
GAPDH	AGCCACATCGCTCAGACACC	GTACTCAGCGGCCAGCATCG	2597

doi:10.1371/journal.pone.0044660.t001

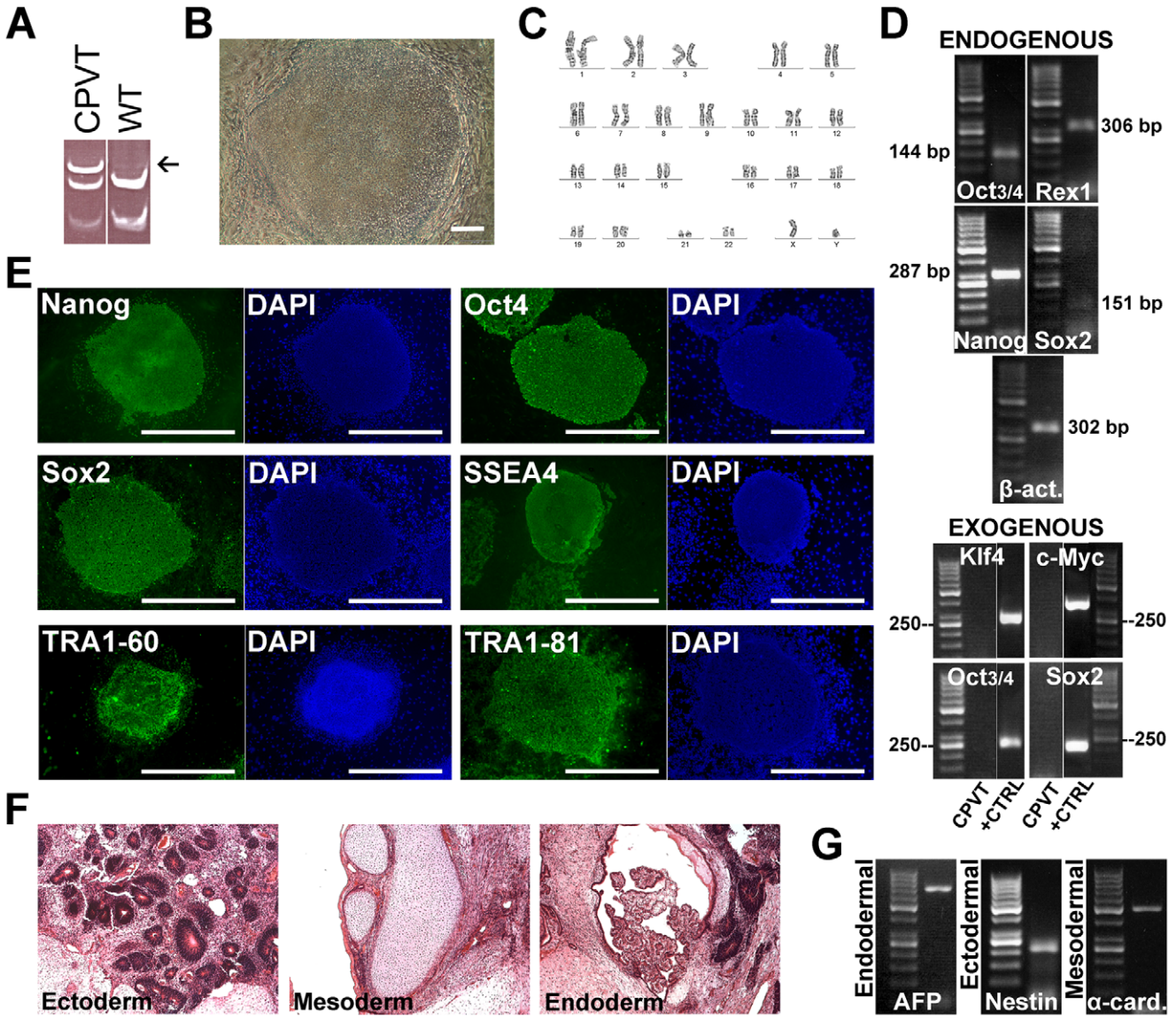

Figure 1. Characterization of CPVT-iPSCs. A, Mutation analysis confirming the RyR2-*P2328S* mutation with altered DNA cleavage (arrow). **B**, Morphology of an iPSC colony. Scale bar 200 μm. **C**, Normal karyotype. **D**, Expression of pluripotency markers at passage 4 shown by RT-PCR, β-actin serving as a housekeeping gene. All studied endogenous pluripotency genes are turned on. None of the exogenous genes are expressed at passage 4. **E**, Immunocytochemical staining showing expression of pluripotency markers. Scale bars 1000 μm. **F**, Teratomas made from a CPVT-iPSC line further confirms pluripotency. **G**, EBs express markers from all the three embryonic germ layers.
doi:10.1371/journal.pone.0044660.g001

cells (Humbrecht Institute, Utrecht, The Netherlands) as described earlier [6]. The beating areas of the cell colonies were mechanically excised and treated with collagenase A (Roche Diagnostics) [6].

Immunocytochemistry. Single beating CMs were immunostained with anti-cardiac-troponin-T (1:1500, Abcam, Cambridge, MA, USA), anti-α-actinin (1:1500, Sigma-Aldrich) and anti-connexin-43 (1:1000, Sigma-Aldrich).

RT-PCR for cardiac Ca^{2+}-cycling protein analysis. RNA was isolated from iPSC-derived CMs. The expression of troponin T (*TNTT2*), *RyR2*, SR Ca^{2+} ATPase (*SERCA2a*), L-type Ca^{2+} channel ($Ca_v1.2$), phospholamban (*PLN*) and sodium-calcium exchanger (*NCX*) were assessed. Primer sequences are listed in Table 1. *GAPDH* served as a housekeeping gene.

Ca^{2+} imaging. Dissociated CMs on a coverslip were loaded with 4 μmol/L Fura-2 AM (Invitrogen, Molecular Probes) for 30 minutes in HEPES based medium, followed by a 30-minute de-esterification. The coverslip was then transferred to an RC-27NE or an RC-25 recording chamber (Warner Instruments Inc., CT, USA) and continuously perfused with 37°C HEPES based perfusate. The perfusate was preheated by an SH-27B inline-heater controlled by a TC-324B unit (Warner Instruments Inc., USA) and consisted of (in mmol/L): 137 NaCl, 5 KCl, 0.44 KH_2PO_4, 20 HEPES, 4.2 $NaHCO_3$, 5 D-glucose, 2 $CaCl_2$, 1.2 $MgCl_2$ and 1 Na-puryvate (pH was adjusted to 7.4 with NaOH).

Ca^{2+} measurements were conducted on an inverted IX70 microscope (Olympus Corporation, Hamburg, Germany) where spontaneously beating CMs were visualized with a UApo/340 x20 air objective (Olympus). Images were acquired with an ANDOR

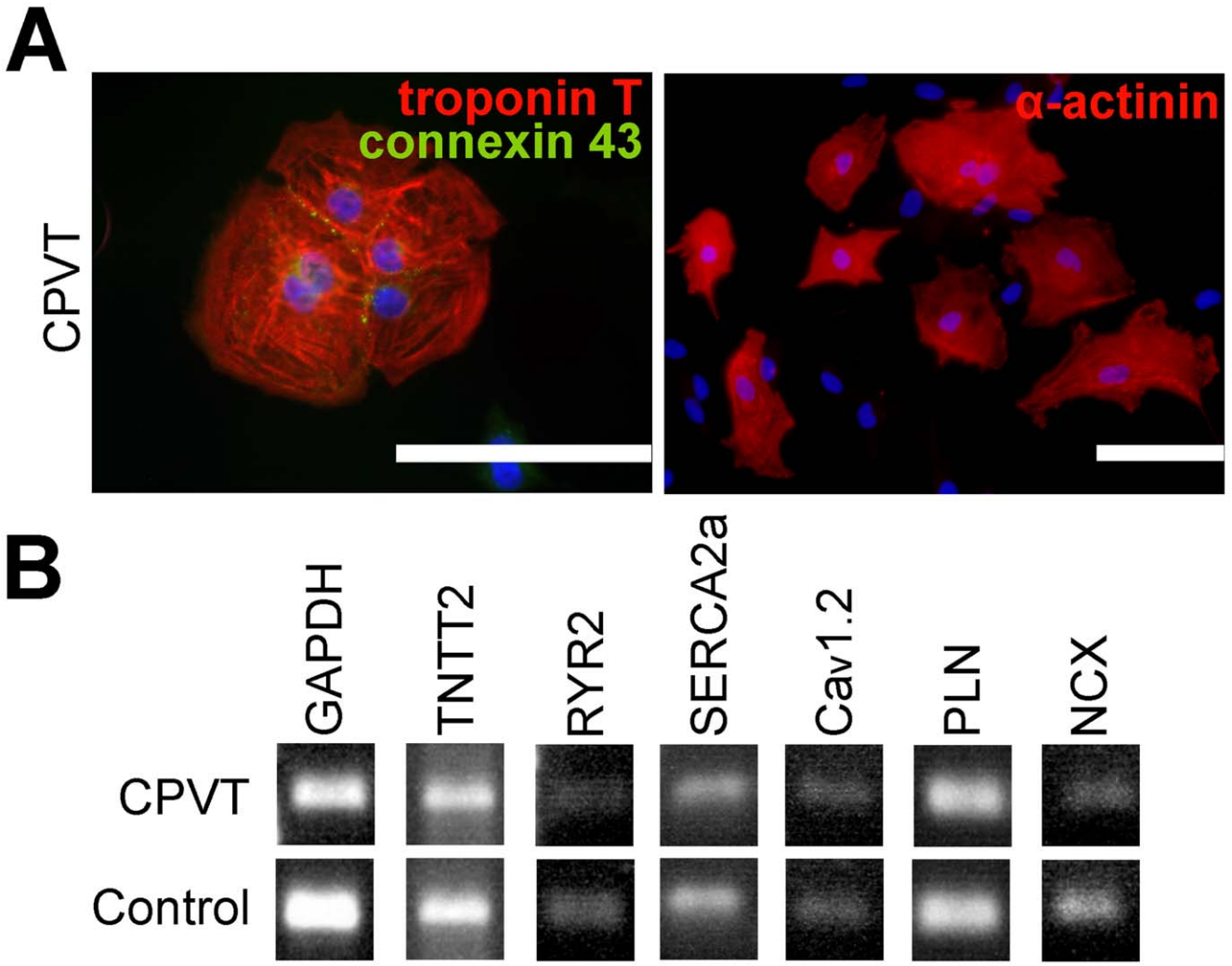

Figure 2. Characterization of iPSC-derived CPVT CMs. A, Immunocytochemical staining of cardiac markers, blue represents DAPI-staining for nuclei. Scale bars 100 μm. **B**, The expression of Ca^{2+} cycling genes in differentiated CMs shown by RT-PCR. GAPDH is used as a housekeeping gene. doi:10.1371/journal.pone.0044660.g002

iXon 885 CCD camera (Andor Technology, Belfast, Northern Ireland) synchronized with a Polychrome V light source by a real time DSP control unit and TILLvisION software (TILL Photonics, Munich, Germany). Fura-2 in CMs was excited at 340 nm and 380 nm light and the emission was recorded at 505 nm. For Ca^{2+} analysis, regions of interests were selected for spontaneously beating cells and background noise was subtracted before further processing. The Ca^{2+} levels are presented as ratiometric values of F340/F380 or as $\Delta F/F_0$.

CMs were paced with 10–50 ms pulses (27–32 mA) (DS3 Constant Current/Voltage Isolated Stimulators, Digitimer LTD, USA) at a frequency of 0.1–0.3 Hz higher than the spontaneous beating rate. The changes in Ca^{2+} were recorded during spontaneous baseline beating, electrical pacing, spontaneous beating during 1 μmol/L adrenaline (Sigma-Aldrich) perfusion and electrical pacing during adrenaline perfusion. The SR Ca^{2+} content was measured by releasing all the SR Ca^{2+} with instantaneous and high concentration (40 mmol/L) caffeine (Sigma-Aldrich) puffs after each measurement, after which the relative amplitude change in calcium release in CPVT versus control CMs was quantified. Viability of CMs was confirmed after the experimental protocol. Amplitudes, beating frequency and caffeine induced Ca^{2+} peaks were analyzed with Clampfit version 9.2 (Molecular devices, USA). Analysis was performed blinded to genotype of CMs.

Measurement of action potentials. Action potentials (APs) were recorded in current-clamp mode using the standard patch-clamp technique in the perforated patch configuration [7]. The HEPES based extracellular perfusate for current-clamp recordings consisted of (in mmol/L): 143 NaCl, 5 KCl, 1.8 $CaCl_2$, 1.2 $MgCl_2$, 5 glucose, 10 HEPES, pH was adjusted to 7.4 with NaOH and the osmolarity set to 300±2 mOsm (Gonotec, Osmomat 030, Labo Line Oy, Helsinki, Finland). The intracellular solution consisted of (in mmol/L): 122 $KMeSO_4$, 30 KCl, 1 $MgCl_2$, 10 HEPES. KOH was used to set pH to 7.15 and the osmolarity was set to 295±2 mOsm. Amphotericin B (Sigma-Aldrich) was used as membrane perforation agent and dissolved in DMSO to a final concentration in the patch pipette of 0.24 mg/ml. Spontaneously beating CMs were patched in same bath conditions as in Ca^{2+} imaging. Patch pipettes (model PG150T, Harvard Apparatus, UK) were pulled with a PC-10 puller and flame polished with Microforge MF-900 (Narishige, UK) to a resistance of 2.0–2.5 MΩ measured in the bath perfusate. APs were recorded in gab-free mode with pClamp 10.2 using the Axopatch 200B patch-clamp amplifier connected to

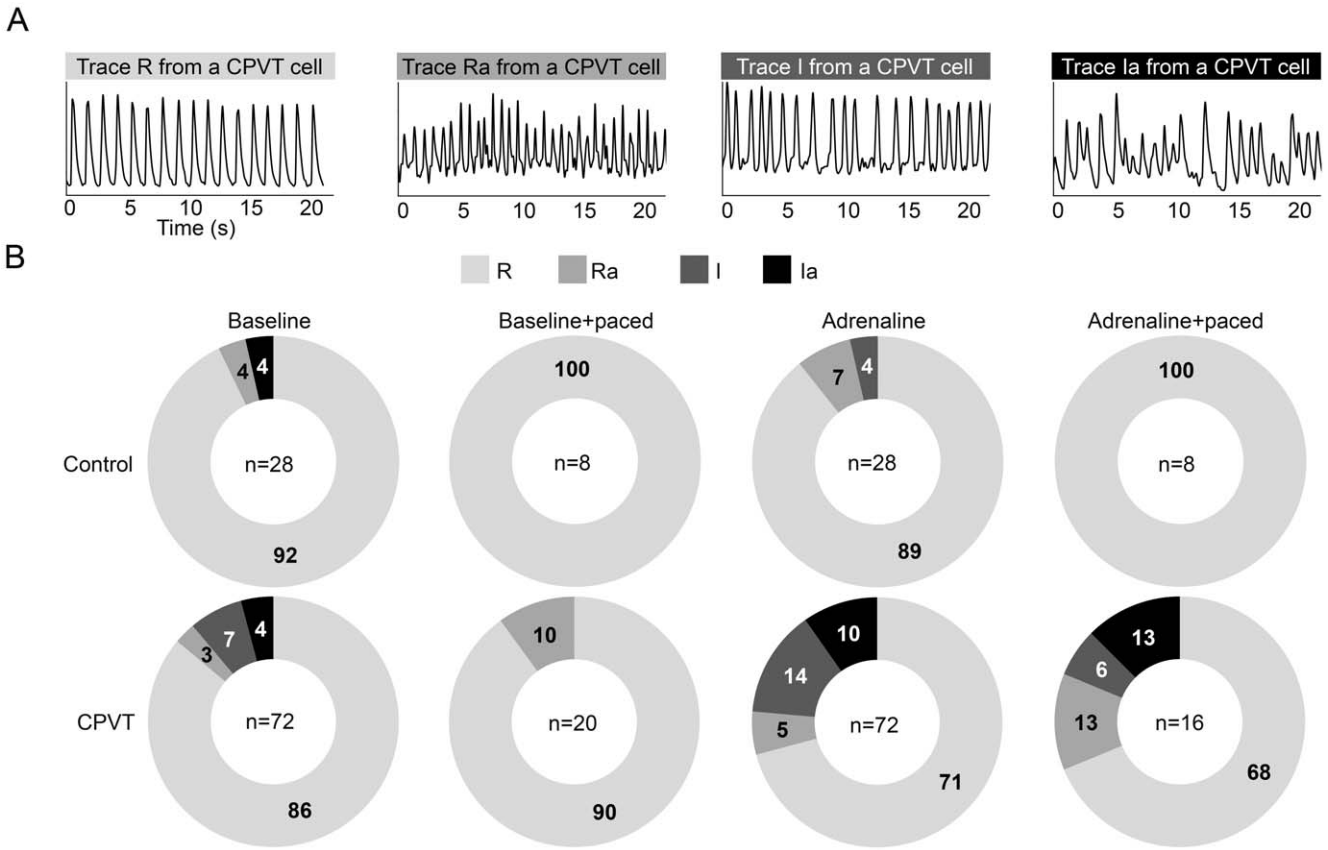

Figure 3. Intracellular Ca^{2+} cycling and analysis of rhythm. A, representative traces of the four different rhythm categories. Regular rhythm of calcium release with stable amplitude R, regular rhythm with varying amplitude Ra, irregular rhythm with stable amplitude I, irregular rhythm with varying amplitude Ia. **B**, doughnut charts indicating the percentage of CPVT and control CMs under each rhythm category.
doi:10.1371/journal.pone.0044660.g003

an acquisition computer via AD/DA Digidata 1440 (Molecular devices, USA). Current-clamp recordings were digitally sampled at 20 kHz and filtered at 5 kHz using the lowpass Bessel filter on the recording amplifier. AP duration at 50% and 90% of repolarization (ADP_{50} and ADP_{90}), AP amplitude (APA), maximum diastolic potential (MDP) and beats per minute (BPM) were extracted from AP recordings using an automated script in Microcal OriginTM 8.6.

Monophasic Action Potential Recordings

Monophasic action potentials (MAPs) were previously recorded from CPVT patients and healthy controls as reported [8]. Briefly, MAPs were recorded from the right ventricular septum with a bipolar silver-silver chloride catheter (model 006248, Bard Inc., Lowell, MA, USA). Data were recorded during sinus rhythm and atrial pacing at a constant cycle length of 600 ms, both during baseline and adrenaline infusion (maximum rate 0.05 μg/kg/min). Custom-made software was used for analysis.

Definition of DADs and EADs

EADs were defined as low-amplitude depolarizations that occur during phase 2 or 3 of the AP, before completion of repolarization, and have an amplitude of ≥3% of the preceding AP. DADs were defined as low-amplitude depolarizations that occur after completion of repolarization, and have an amplitude of ≥3% of the preceding AP [9].

24h-ECG Recordings

24h-ECGs were previously recorded from CPVT patients and healthy controls as reported [10]. Briefly, 24-h ECGs were recorded using commercial tape recorders (model 8500; Marquette Electronics Inc., Milwaukee, WI, USA). The tapes were initially analyzed with a Marquette 8000 Holter Analysis system (version 5.8 software) to label the QRS complexes to normal, ventricular extrasystoles, or aberrant complexes.

Definition of T1-, T2-, and U-waves

The first peak during repolarization was considered as a T1-wave. The second peak was considered as a T2-wave if it occasionally merged with the T1-wave, or as a U-wave if it never merged with the T1-wave. The third peak, which never merged with the T1-wave, was also considered as a U-wave [10,11,12].

Statistical Analysis

The significance of differences between two groups was evaluated with the unpaired Student's *t*-test. The significance of changes within a group was evaluated with the paired Student's *t*-test. $P<0.05$ was considered statistically significant, where (*) represents $P<0.05$ and (**) $P<0.01$. Data are expressed as means ± S.E.M. and n (where indicated) refers to the number of cells or experiments.

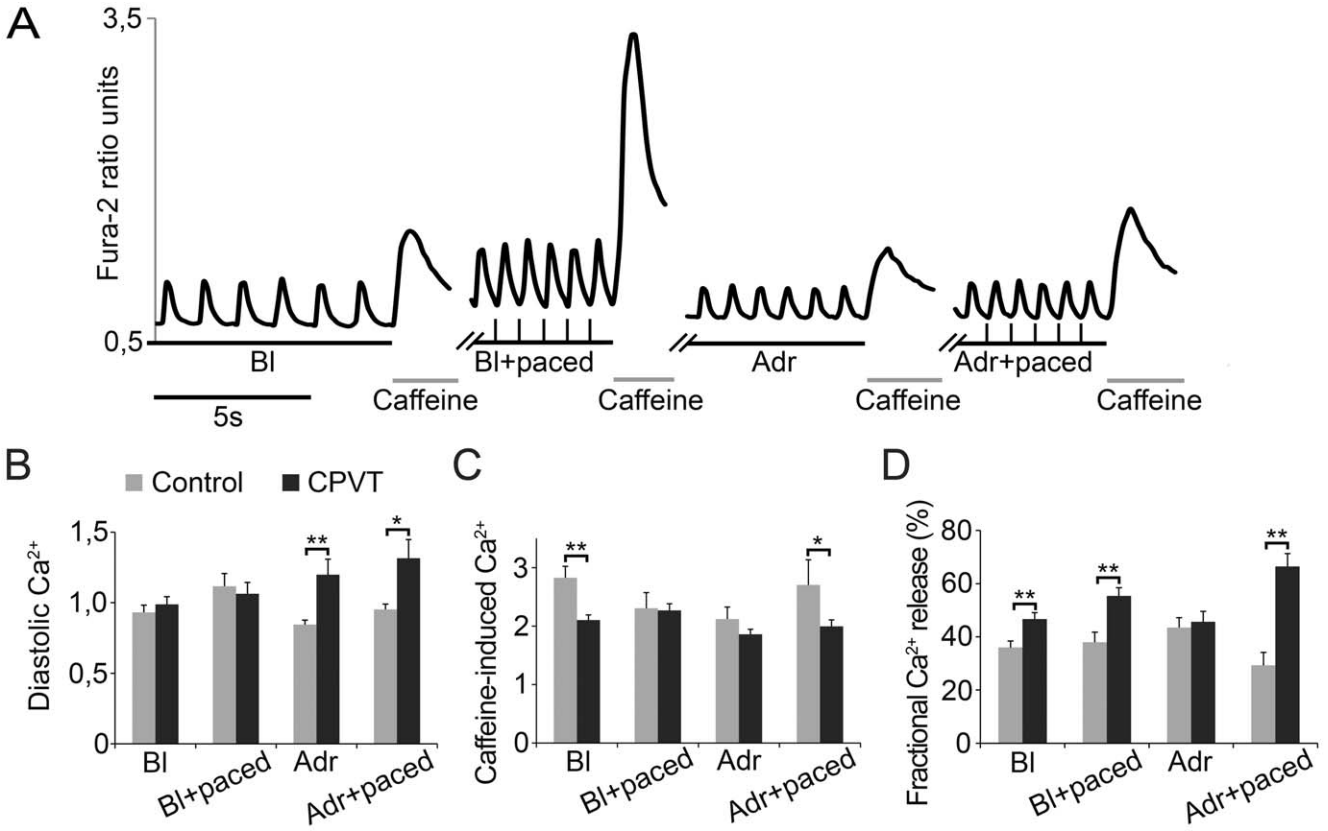

Figure 4. Intracellular Ca^{2+} cycling and SR Ca^{2+} stores. A, representative traces from a single CPVT cell demonstrating the experimental protocol. Bl; spontaneous baseline beating, Adr; adrenaline perfusion. Caffeine was added following 10 spontaneous or paced beats. **B**, diastolic level of intracellular Ca^{2+}. **C**, amplitude of caffeine-induced Ca^{2+} transients. **D**, amplitude of Ca^{2+} transients divided by amplitude of caffeine-induced Ca^{2+} transient, indicating fractional SR Ca^{2+} release. Units in A and B are Fura-2 ratio units, in C $\Delta F/F0$. Numbers of control vs CPVT CMs analyzed: Bl n = 54 vs n = 90, Bl+paced n = 25 vs n = 50, Adr n = 27 vs 47, Adr+paced n = 19 vs n = 35, respectively. Error bars, SEM. *P<0.05, **P<0.01, with student's t-test.
doi:10.1371/journal.pone.0044660.g004

Results

Characterization of iPSC Lines Confirms Pluripotent Stem Cell Characteristics

The presence of the *P2328S* mutation was confirmed in the two *CPVT-P2328S* iPSC lines (Figure 1A). The iPSC colonies were morphologically round-shaped and the iPSC lines had normal karyotype (Figure 1B–C). All studied endogenous pluripotency genes were turned on and expression of retrovirally encoded reprogramming factors was silenced (Figure 1D). iPSC lines expressed endogenous pluripotent markers at the protein level (Figure 1E). Pluripotency was confirmed by teratoma formation and with *in vitro* embryoid body (EB) formation expressing all three germ layers (Figure 1F–G).

iPSC-derived CMs Express Cardiac Markers

iPSCs were differentiated into spontaneously beating cells and the differentiated CMs expressed cardiac markers at the protein level (Figure 2A). RT-PCR was performed to confirm the expression of genes related to Ca^{2+} cycling (Figure 2B).

CPVT-P2328S CMs Display Aberrant Ca^{2+} Cycling

Ca^{2+} cycling properties of CPVT and control CMs were compared in four conditions: spontaneous baseline beating, pacing, spontaneous beating during adrenaline perfusion, and pacing during adrenaline perfusion. Ca^{2+} cycling was categorized into four different rhythm categories in which three of them the Ca^{2+} cycling was characterized abnormal due to varying amplitude and/or irregular rhythm (Figure 3A). Ca^{2+} cycling abnormalities were more common in CPVT CMs than in control CMs in each studied condition (Figure 3B). At baseline a higher percentage of CPVT CMs (14%) showed abnormal Ca^{2+} cycling when compared to control CMs (8%). Pacing stabilized Ca^{2+} cycling partially in CPVT CMs and completely in control CMs. Adrenaline increased Ca^{2+} cycling abnormalities to 30% of the CPVT CMs. In control CMs adrenaline had no effect on Ca^{2+} cycling. Pacing with adrenaline abolished all Ca^{2+} cycling abnormalities in controls but did not have an effect in CPVT CMs.

Under baseline and electrical pacing conditions, CPVT and control CMs presented similar diastolic Ca^{2+} levels (Figure 4B). However, adrenaline with and without pacing produced significantly more elevated diastolic Ca^{2+} levels in CPVT CMs.

In CPVT CMs significantly lower SR Ca^{2+} load was seen at baseline and in the presence of pacing during adrenaline (Figure 4C). Caffeine-induced Ca^{2+} release via RyR2 was studied under the four different aforementioned conditions (Figure 4A). To determine the fractional Ca^{2+} release, the amplitude of the Ca^{2+} transients were divided by the amplitude of the following caffeine-induced Ca^{2+} transient. Fractional SR Ca^{2+} release was significantly higher in CPVT CMs during spontaneous beating

Table 2. Characteristics of spontaneous ventricular-like APs in control and CVPT-CMs during regular beating.

Baseline	**BPM**	**APD50 (ms)**	**APD90 (ms)**	**APA (mV)**	**MDP (mV)**
control (n = 16)	41±6	204.4±20.3	329.7±22.4	117.85±2.61	−68.35±1.87
CPVT (n = 14)	43±5	238.6±22.4	305.4±25.7	114.80±2.70	−67.55±1.51
Adrenaline	**BPM % increase**	**APD50 % decrease**	**APD90 % decrease**	**APA ΔmV**	**MDP ΔmV**
control (n = 5)	23.2±0.9	18.4±1.8	16.8±2.1	−5.82±1.17	+2.55±0.61
CPVT (n = 11)	16.0±12.3	21.5±5.5	24.0±3.5	−8.25±2.15	+4.59±0.82

doi:10.1371/journal.pone.0044660.t002

and during electrical pacing with and without adrenaline perfusion (Figure 4D).

Current-clamp Reveals DADs and EADs in *CPVT-P2328S* CMs

Using the perforated patch technique in current-clamp mode APs of 16/18 control and 14/14 CPVT CMs were ventricular-like. The basic AP characteristics were similar in control and CPVT CMs (Table 2). Eleven CPVT and five control CMs were exposed to adrenaline and a similar increase in beating rate and decrease in APD_{50} and APD_{90} were observed in all of them. In general, control CMs had robust synchronized beating throughout the recordings, but in 3/16 CMs (19%) DADs were randomly observed during baseline recordings (1–2 DADs/60 APs). At baseline DADs were observed in 6/14 (42%) of CPVT CMs. In 6/11 CPVT CMs exposed to adrenaline, wash-out recovered the beating rate to normal as in control CMs. However, in the remaining 5/11 CPVT CMs, adrenaline subsequently evoked DADs and resulted in decreased beating rate (Figure 5A and 5B).

In three other CPVT CMs spontaneous EADs were seen at baseline (Figure 5C and 5D). Additionally phase 3 burst episodes were seen in one cell showing EADs and DADs (Figure 5C). All solitary EAD upstrokes were seen above −25 mV. The MDP of the burst was −50 mV. The maximum upstroke amplitude for solitary EADs was 45 mV and during the bursts 95 mV. No EADs or spontaneous bursting were observed in control CMs.

MAP Recordings of *CPVT-P2328S* Patients Reveal EADs and DADs, ECGs Show Simultaneous T2 and U-waves

We examined MAP recordings for EADs and DADs and 24h-ECGs for their ECG counterparts, T2 and U-waves. MAP recordings demonstrated DADs (Figure 6A) and EADs (Figure 6B). 24h-ECGs showed occasional simultaneous T1, T2, and U-waves (Figure 6C). These changes were observed repeatedly, and no similar changes were seen in healthy controls.

Discussion

We report, for the first time, that in addition to DADs, CPVT patient-specific iPSC-derived CMs display EADs, providing novel insight into the arrhythmogenic mechanisms in CPVT. Our findings demonstrate the applicability of iPSC-derived CMs in studying the pathophysiology of CPVT-causing *RyR2* mutations.

CPVT CMs show disturbances in intracellular Ca^{2+} cycling in response to catecholaminergic stimulation with adrenaline. These changes in Ca^{2+} cycling indicate increased diastolic SR Ca^{2+} leak, which may lead to DADs and the generation of triggered arrhythmias [13]. In accordance with a previous report [14], upon perfusion with adrenaline, CPVT CMs develop frequent DADs, which occasionally suppress the following AP, preventing the increase in the beating frequency.

Adrenaline produced significantly more elevated diastolic Ca^{2+} levels in CPVT CMs. Adrenaline also failed to increase caffeine-induced Ca^{2+} release and fractional Ca^{2+} release compared to control cells. The Ca^{2+} measurements with adrenaline were recorded after 3 minutes of perfusion with the drug. During this time Ca^{2+} leaked from the SR to the cytosol in the CPVT CMs, as indicated by the elevated diastolic Ca^{2+} levels in the cytosol and the reduced caffeine-induced SR Ca^{2+} release.

Fractional SR Ca^{2+} release increases steeply with elevation of SR calcium. [15,16]. Therefore, it is expected that continuous adrenaline perfusion without pacing will only transiently increase fractional SR Ca^{2+} release in the RyR2 mutant CMs, which will soon find a new equilibrium, balanced by increased sensitivity to SR Ca^{2+} and decreased SR Ca^{2+} stores. On the other hand, transient pacing (10 beats) increases SR Ca^{2+} load. When the fractional SR Ca^{2+} release is measured immediately after the pacing, increased values are observed. As expected, in this case the fractional SR Ca^{2+} release is greater in the RyR2 mutant CMs, which are more sensitive to luminal SR Ca^{2+} release.

Traditionally, EADs have been thought to result from spontaneous reactivation of the L-type Ca^{2+} channel (LTCC) during conditions of prolonged APD, such as LQT2 [17]. However, recent understanding highlights the role of Ca^{2+} overload and spontaneous Ca^{2+} release as the main triggers behind EADs [18,19]. Conditions leading to Ca^{2+} overload include heart failure, digitalis toxicity, and CPVT. Under conditions of SR Ca^{2+} overload or leaky RyR2s, spontaneous release of Ca^{2+} from the SR leads to activation of the sodium-calcium-exchanger (NCX), which results in a depolarizing current that reactivates the LTCC, leading to an EAD. It has been shown that early Ca^{2+} aftertransients are the primary events that induce EADs, and not vice versa [20,21]. In addition to early EADs, late EADs arising from membrane potentials more negative than the threshold potential of LTCC (−35 mV), are reported to be NCX-mediated and share similar properties with DADs [22–24]. Further support for the role of cytosolic calcium in EAD induction comes from recent findings that despite prolonging APD, ranolazine suppresses EADs by stabilizing RyR2 [25]. However, ranolazine's ability to prevent EADs is also likely to be mediated by late sodium current inhibition, which decreases cytosolic Ca^{2+} by reducing NCX-mediated Ca^{2+} influx [26,27]. Lower cytosolic Ca^{2+} will less likely cause SR Ca^{2+} leak, which would lead to forward-mode NCX activation and afterdepolarizations. Accordingly, we must acknowledge the potential role of the late sodium current in EAD provocation.

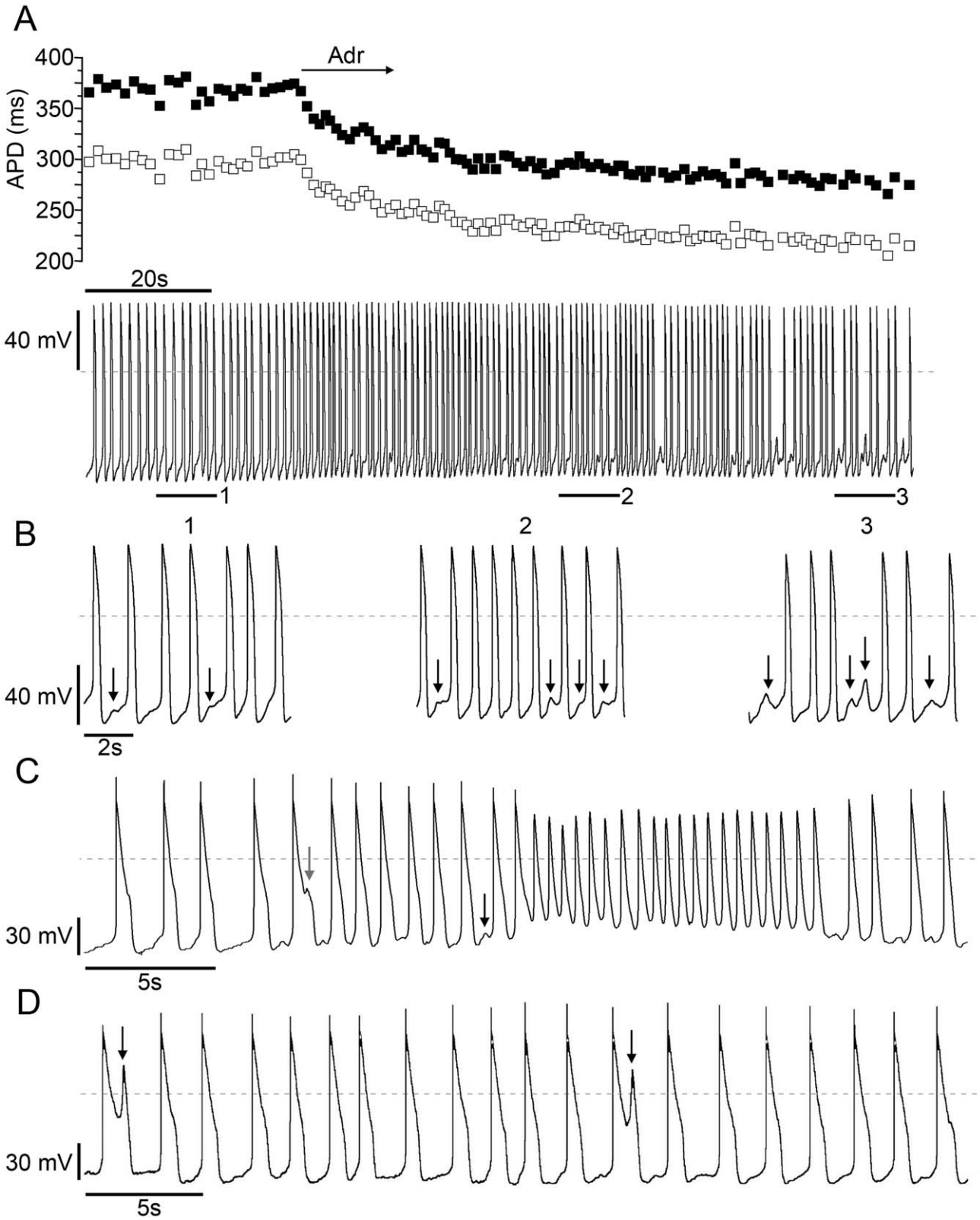

Figure 5. CPVT-*P2328S* CMs display DADs and EADs. A, Time course of APD_{50} (empty squares) and APD_{90} (filled squares) Adr indicates perfusion with adrenaline. **B**, bars 1–3 are 9 sec time courses enlarged from **A**. (1) baseline with DADs, (2) DADs in the presence of adrenaline, (3) DADs continue after adrenaline perfusion. MDP −70 mV. Arrows indicate DADs. **C**, A CPVT-*P2328S* CM showing an EAD (grey arrow) and a DAD (black arrow) followed by a spontaneous burst episode (MDP −50 mV, maximum upstroke amplitude 45 mV). **D**, Current clamp recording of a CPVT-*P2328S* CM showing occasional EADs (arrows). MDP −70 mV. Dashed lines indicate the zero reference potential.
doi:10.1371/journal.pone.0044660.g005

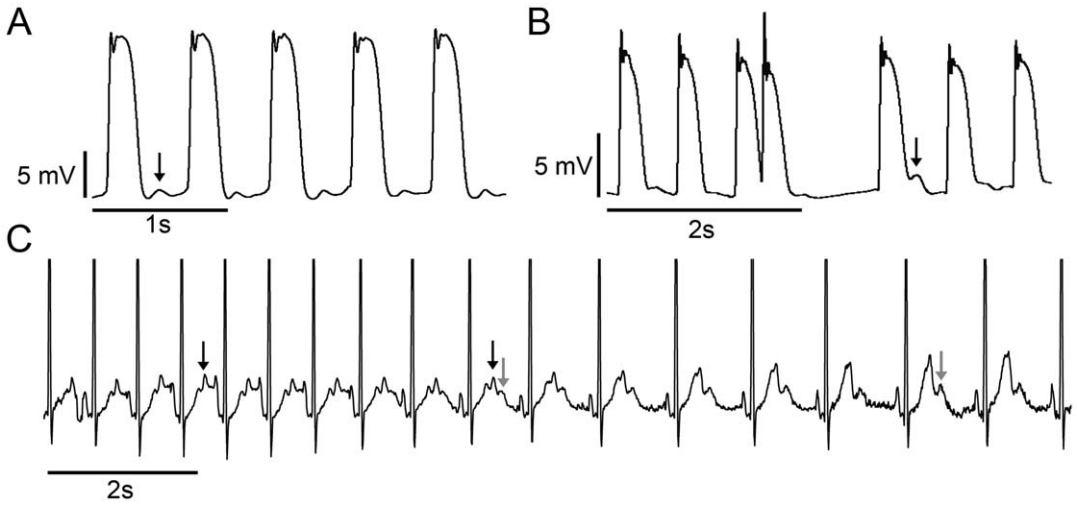

Figure 6. CPVT patients show afterdepolarizations and corresponding ECG changes. A, MAP recording from CPVT-*P2328S* patient showing DADs (arrow). **B**, Example MAP recording from a CPVT-*P2328S* patient showing an extrasystole and the following beat with EAD (arrow). **C**, Example 24-h ECG recording from a CPVT-P2328S patient showing the simultaneous occurrence of T2- (black arrow) and U-waves (grey arrow) representing clinical counterparts to EADs [11,28] and DADs [8], respectively.
doi:10.1371/journal.pone.0044660.g006

Our results support this emerging consensus on the role of NCX-mediated generation of EADs. We found that CPVT CMs display irregular spontaneous calcium release events, DADs, and EADs. Furthermore, MAP recordings in *CPVT-P2328S* patients show both DADs and EADs. Although not experimentally shown, it has previously been suggested that CPVT patients with *RyR2* mutations are susceptible to both EAD and DAD-mediated arrhythmia mechanisms [10]. As shown here, these patients show both T2 and U-waves, the ECG equivalents of EADs and DADs, respectively [10].

We could not demonstrate increased arrhythmogenicity with pacing. At baseline, pacing stabilized beating in both control and CPVT CMs. When arrhythmias were provoked in CPVT CMs with adrenaline, pacing on top of that did not have any affect on the recorded arrhythmias. This is contrary to previous CPVT reports using either spontaneously beating CMs with a CASQ2 mutation [14] or resting CMs with a *RyR2* mutation [4]. This observation suggests that there are mutation-specific differences. Our *P2328S-RyR2* mutation presents arrhythmias only in the presence of catecholaminergic stimulation, but not if increased beating rate is generated by pacing.

Our findings demonstrate that in addition to DADs, *CPVT-P2328S* CMs display EADs which may be involved in arrhythmogenesis in these patients. This broadens the mechanistic understanding of arrhythmias linked to *RyR2* mutations and helps to direct efforts to optimize therapy in these patients. Our iPSC-derived CM model offers a promising platform for further research into the pathophysiological mechanisms of CPVT, as well as a safe tool for screening and optimizing drug therapy with patient-specific CMs.

Study Limitations

We studied iPSC-derived CMs from two CPVT and two control iPS cell lines. However, both CPVT lines were from the same patient. The control lines were from two healthy controls. It is therefore unclear whether the changes we saw are typical of all CPVT patients, of this specific mutation, or only this specific patient. In the future we need to extend our studies, looking at various RyR2 mutations and several cell lines from multiple patients harboring a specific mutation.

The type of CM (nodal, atrial, or ventricular) under investigation was unclear in the Ca^{2+} imaging studies. Part of the variability in the results may stem from differences between the CM types. To address this in the future, simultaneous recording of APs and intracellular Ca^{2+} will help to distinguish cell type and additionally give temporally synchronized info on the interplay between Ca^{2+} handling and APs.

Additionally, further development of cardiac differentiation and maturation procedures will hopefully improve the homogeneity of iPS cell lines.

Acknowledgments

We thank Marisa Ojala, Merja Lehtinen, Henna Venäläinen and Markus Haponen for technical support.

Author Contributions

Conceived and designed the experiments: K. Kujala JP KL K. Kontula OS KAS. Performed the experiments: K. Kujala JP AL KL MV AML. Analyzed the data: K. Kujala JP KL MPM MV LT ML OS KAS. Contributed reagents/materials/analysis tools: OS KAS. Wrote the paper: K. Kujala JP KL KAS. Clinical expertise: LT K. Kontula HS ML. Genetic expertise: K. Kontula HS. Provided genotyped patients: K. Kontula.

References

1. Priori SG, Chen SR (2011) Inherited dysfunction of sarcoplasmic reticulum Ca2+ handling and arrhythmogenesis. Circ Res 108: 871–883.
2. Mohamed U, Napolitano C, Priori SG (2007) Molecular and electrophysiological bases of catecholaminergic polymorphic ventricular tachycardia. J Cardiovasc Electrophysiol 18: 791–797.
3. Fatima A, Xu G, Shao K, Papadopoulos S, Lehmann M, et al. (2011) In vitro Modeling of Ryanodine Receptor 2 Dysfunction Using Human Induced Pluripotent Stem Cells. Cell Physiol Biochem 28: 579–592.
4. Jung CB, Moretti A, Schnitzler MM, Iop L, Storch U, et al. (2011) Dantrolene rescues arrhythmogenic RYR2 defect in a patient-specific stem cell model of catecholaminergic polymorphic ventricular tachycardia. EMBO Mol Med 4: 180–191.

5. Takahashi K, Tanabe K, Ohnuki M, Narita M, Ichisaka T, et al. (2007) Induction of pluripotent stem cells from adult human fibroblasts by defined factors. Cell 131: 861–872.
6. Mummery C, Ward-van Oostwaard D, Doevendans P, Spijker R, van den Brink S, et al. (2003) Differentiation of human embryonic stem cells to cardiomyocytes: role of coculture with visceral endoderm-like cells. Circulation 107: 2733–2740.
7. Hamill OP, Marty A, Neher E, Sakmann B, Sigworth FJ (1981) Improved patch-clamp techniques for high-resolution current recording from cells and cell-free membrane patches. Pflugers Arch 391: 85–100.
8. Paavola J, Viitasalo M, Laitinen-Forsblom PJ, Pasternack M, Swan H, et al. (2007) Mutant ryanodine receptors in catecholaminergic polymorphic ventricular tachycardia generate delayed afterdepolarizations due to increased propensity to Ca2+ waves. Eur Heart J 28: 1135–1142.
9. Vos M, de Groot S, Wellens H (2000) Delayed afterdepolarizations in the in situ canine heart: The role of the diastolic upslope. In: Franz MR, editor. Monophasic Action Potentials: Bridging Cell and Bedside. New York: Futura Publishing Company. 571–582
10. Viitasalo M, Oikarinen L, Vaananen H, Kontula K, Toivonen L, et al. (2008) U-waves and T-wave peak to T-wave end intervals in patients with catecholaminergic polymorphic ventricular tachycardia, effects of beta-blockers. Heart Rhythm 5: 1382–1388.
11. Viitasalo M, Oikarinen L, Swan H, Glatter KA, Vaananen H, et al. (2006) Ratio of late to early T-wave peak amplitude in 24-h electrocardiographic recordings as indicator of symptom history in patients with long-QT Syndrome types 1 and 2. J Am Coll Cardiol 47: 112–120.
12. Aizawa Y, Komura S, Okada S, Chinushi M, Aizawa Y, et al. (2006) Distinct U wave changes in patients with catecholaminergic polymorphic ventricular tachycardia (CPVT). Int Heart J 47: 381–389.
13. Schlotthauer K, Bers DM (2000) Sarcoplasmic reticulum Ca(2+) release causes myocyte depolarization. Underlying mechanism and threshold for triggered action potentials. Circ Res 87: 774–780.
14. Novak A, Barad L, Zeevi-Levin N, Shick R, Shtreichman R, et al. (2011) Cardiomyocytes generated from CPVT(D307H) patients are arrhythmogenic in response to beta-adrenergic stimulation. J Cell Mol Med 3: 468–482
15. Bassani JWM, Yuan W, Bers DM (1995) Fractional SR Ca release is regulated by trigger Ca and SR Ca content in cardiac myocytes. Am J Physiol 268: C1313–C1319.
16. Shannon TR, Ginsburg KS, Bers DM (2000) Potentiation of fractional SR Ca release by total and free intra-SR Ca concentration. Biophys J 78: 334–343.
17. January CT, Moscucci A (1992) Cellular mechanisms of early afterdepolarizations. Ann N Y Acad Sci 644: 23–32.
18. Volders PG, Vos MA, Szabo B, Sipido KR, de Groot SH, et al. (2000) Progress in the understanding of cardiac early afterdepolarizations and torsades de pointes: time to revise current concepts. Cardiovasc Res 46: 376–392.
19. Xie LH, Weiss JN (2009) Arrhythmogenic consequences of intracellular calcium waves. Am J Physiol Heart Circ Physiol 297: H997-H1002.
20. Volders PG, Kulcsar A, Vos MA, Sipido KR, Wellens HJ, et al. (1997) Similarities between early and delayed afterdepolarizations induced by isoproterenol in canine ventricular myocytes. Cardiovasc Res 34: 348–359.
21. Choi BR, Burton F, Salama G (2002) Cytosolic Ca2+ triggers early afterdepolarizations and Torsade de Pointes in rabbit hearts with type 2 long QT syndrome. J Physiol 543: 615–631.
22. Patterson E, Szabo B, Scherlag BJ, Lazzara R (1990) Early and delayed afterdepolarizations associated with cesium chloride-induced arrhythmias in the dog. J Cardiovasc Pharmacol 15: 323–331.
23. Xu J, Zaim S, Pelleg A (1996) Effects of pinacidil, verapamil, and heart rate on afterdepolarizations in the guinea-pig heart in vivo. Heart Vessels 11: 289–302.
24. Spencer CI, Sham JS (2003) Effects of Na+/Ca2+ exchange induced by SR Ca2+ release on action potentials and afterdepolarizations in guinea pig ventricular myocytes. Am J Physiol Heart Circ Physiol 285: H2552–2562.
25. Parikh A, Mantravadi R, Kozhevnikov D, Roche MA, Ye Y, et al. (2012) Ranolazine stabilizes cardiac ryanodine receptors: A novel mechanism for the suppression of early afterdepolarization and torsades de pointes in long QT type 2. Heart Rhythm 9: 953–960.
26. Antzelevitch C, Burashnikov A, Sicouri S, Belardinelli L (2011) Electrophysiologic basis for the antiarrhythmic actions of ranolazine. Heart Rhythm 8: 1281–1290.
27. Morita N, Lee JH, Xie Y, Sovari A, Qu Z, et al. (2011). Suppression of re-entrant and multifocal ventricular fibrillation by the late sodium current blocker ranolazine. Journal of the American College of Cardiology 57: 366–375.
28. Gbadebo TD, Trimble RW, Khoo MS, Temple J, Roden DM, et al. (2002) Calmodulin inhibitor W-7 unmasks a novel electrocardiographic parameter that predicts initiation of torsade de pointes. Circulation 105: 770–774.

Study III

Penttinen K, Swan H, Vanninen S, Paavola J, Lahtinen AM, Kontula K, Aalto-Setälä K
Antiarrhythmic Effects of Dantrolene in Patients with Catecholaminergic Polymorphic Ventricular Tachycardia and Replication of the Responses Using iPSC Models
PLoS One. 2015 May 8;10(5):e0125366

PLOS ONE

RESEARCH ARTICLE

Antiarrhythmic Effects of Dantrolene in Patients with Catecholaminergic Polymorphic Ventricular Tachycardia and Replication of the Responses Using iPSC Models

Kirsi Penttinen[1,2☯], Heikki Swan[3☯], Sari Vanninen[4], Jere Paavola[5], Annukka M. Lahtinen[6], Kimmo Kontula[6], Katriina Aalto-Setälä[1,2,4]*

1 BioMediTech, University of Tampere, Tampere, Finland, **2** School of Medicine, University of Tampere, Tampere, Finland, **3** Heart and Lung Center, Helsinki University Hospital, Helsinki, Finland, **4** Heart Hospital, Tampere University Hospital, Tampere, Finland, **5** Minerva Foundation Institute for Medical Research, Helsinki, Finland, **6** Department of Medicine, University of Helsinki and Helsinki University Hospital, Helsinki, Finland

☯ These authors contributed equally to this work.
* katriina.aalto-setala@uta.fi

OPEN ACCESS

Citation: Penttinen K, Swan H, Vanninen S, Paavola J, Lahtinen AM, Kontula K, et al. (2015) Antiarrhythmic Effects of Dantrolene in Patients with Catecholaminergic Polymorphic Ventricular Tachycardia and Replication of the Responses Using iPSC Models. PLoS ONE 10(5): e0125366. doi:10.1371/journal.pone.0125366

Academic Editor: Larisa G. Tereshchenko, Johns Hopkins University SOM, UNITED STATES

Received: December 10, 2014

Accepted: February 13, 2015

Published: May 8, 2015

Data Availability Statement: All relevant data are within the paper and its Supporting Information files.

Funding: This work was supported by TEKES-Finnish Funding Agency for Innovation (www.tekes.fi/en), Finnish Cultural Foundation (https://www.skr.fi/en), Ida Montin Foundation (www.idamontininsaatio.fi/), Aarne Koskelo Foundation (www.aarnekoskelonsaatio.fi/), Pirkanmaa Hospital District (www.pshp.fi), Orion-Farmos Research Foundation (http://www.orion.fi/fi/tutkimus/orionin-tutkimussaatio/), The Finnish Foundation for Cardiovascular Research

Abstract

Catecholaminergic polymorphic ventricular tachycardia (CPVT) is a highly malignant inherited arrhythmogenic disorder. Type 1 CPVT (CPVT1) is caused by cardiac ryanodine receptor (*RyR2*) gene mutations resulting in abnormal calcium release from sarcoplasmic reticulum. Dantrolene, an inhibitor of sarcoplasmic Ca^{2+} release, has been shown to rescue this abnormal Ca^{2+} release in vitro. We assessed the antiarrhythmic efficacy of dantrolene in six patients carrying various *RyR2* mutations causing CPVT. The patients underwent exercise stress test before and after dantrolene infusion. Dantrolene reduced the number of premature ventricular complexes (PVCs) on average by 74% (range 33-97) in four patients with N-terminal or central mutations in the cytosolic region of the *RyR2* protein, while dantrolene had no effect in two patients with mutations in or near the transmembrane domain. Induced pluripotent stem cells (iPSCs) were generated from all the patients and differentiated into spontaneously beating cardiomyocytes (CMs). The antiarrhythmic effect of dantrolene was studied in CMs after adrenaline stimulation by Ca^{2+} imaging. In iPSC derived CMs with *RyR2* mutations in the N-terminal or central region, dantrolene suppressed the Ca^{2+} cycling abnormalities in 80% (range 65-97) of cells while with mutations in or near the transmembrane domain only in 23 or 32% of cells. In conclusion, we demonstrate that dantrolene given intravenously shows antiarrhythmic effects in a portion of CPVT1 patients and that iPSC derived CM models replicate these individual drug responses. These findings illustrate the potential of iPSC models to individualize drug therapy of inherited diseases.

Trial Registration

EudraCT Clinical Trial Registry 2012-005292-14

(www.sydantutkimussaatio.fi/?lang = en), and The Sigrid Juselius Foundation (www.sigridjuselius.fi/foundation). The funders had no role in study design, data collection and analysis, decision to publish, or preparation of the manuscript.

Competing Interests: The authors have declared that no competing interests exist.

Introduction

Catecholaminergic polymorphic ventricular tachycardia (CPVT) is one of the most malignant inherited arrhythmogenic disorders. It manifests with exercise-induced premature ventricular complexes (PVCs), polymorphic or bidirectional ventricular tachycardia, or sudden death, usually associated with vigorous physical exercise or mental stress.[1–3] Current therapeutic options include beta-antiadrenergic drugs, flecainide, implantable cardioverter-defibrillators (ICD) [4–6] and left cardiac sympathetic denervation.[7,8] Better antiarrhythmic medication is still needed to minimize the need for ICD shock therapies. The most common subtype, type 1 of CPVT (CPVT1) is a dominantly inherited disease caused by mutations in the cardiac ryanodine receptor (*RyR2*) gene.[9,10] The gain-of-function mutations of *RyR2* cause increased calcium (Ca^{2+}) sensitivity which can lead to spontaneous Ca^{2+} release from sarcoplasmic reticulum, generation of afterdepolarizations, and triggered activity.[4,5,11]

The ryanodine receptor isoform *RyR1* is the skeletal muscle counterpart in the gene family. Mutations of *RyR1* result in malignant hyperthermia, a rare but life-threatening complication of general anesthesia occurring upon administration of volatile anesthetics or depolarizing muscle relaxants. Dantrolene is a specific and currently the only effective treatment for malignant hyperthermia.[12] Interestingly, dantrolene has also shown to exert antiarrhythmic effects in animal models of CPVT1.[13–15] Dantrolene has been proposed to act through binding to the N-terminal parts of *RyR1* and *RyR2* and restoring inter-domain interactions critical for the closed state of the *RyR2* Ca^{2+} channel.[16]

Several studies using induced pluripotent stem cell (iPSC) technology [17] have indicated the ability of CPVT1 patient-specific iPSC derived cardiomyocytes (CMs) to replicate the disease phenotype in cell culture.[18–24] Dantrolene was reported to rescue the disease phenotype in iPSCs derived CMs from a single *RyR2* mutation carrier [20] but no *in vivo* data exists on its effects on CPVT1 patients.

In the present study, we report the proof of principle of the antiarrhythmic activity of dantrolene in a cohort of CPVT1 patients. In addition, we demonstrate that the in vivo drug effects are closely reproduced in iPSC-derived patient-specific CMs, and provide evidence for mutation-specific effects of dantrolene in CPVT1.

Materials and Methods

The protocol for this trial is available as supporting information; see S1 Protocol and S2 Protocol.

Clinical Study Scheme

The study was approved by the Ethical Review Committee of the Helsinki University Hospital (HUS 396/13/03/01/12) and was in accordance with the institutional guidelines and the Declaration of Helsinki. A written informed consent was obtained from all patients. Clinical trial was registered with EudraCT (2012-005292-14). Participants were recruited between 1st March 2013 and 29th May 2014. Follow up time of the patients was three days after the dantrolene infusion. Four patients participated the study at the Helsinki University Hospital and two at the Tampere University Hospital, Heart Center. The authors confirm that all ongoing and related trials for this drug are registered.

Patients

The study group consisted of 6 individuals (mean age 50±10 years, range 37–59 years, 5 females), who were molecularly defined heterozygous carriers of different gain-of-function *RyR2*

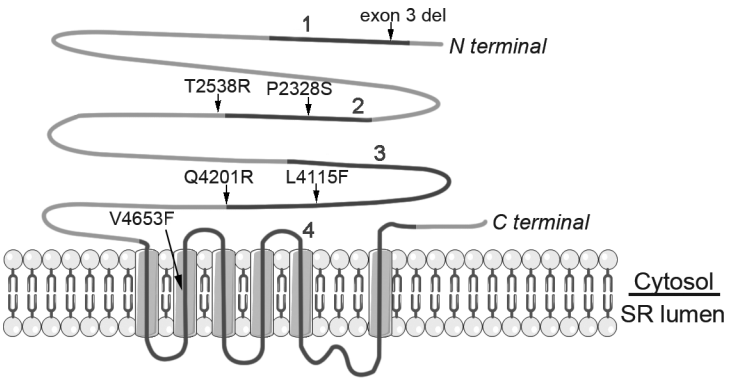

Fig 1. *RyR2* protein, mutations studied in the present study and mutation clusters 1–4. Mutations in this study (arrows) are located in different parts of the *RyR2* protein and mutation clusters. Clusters are represented as black lines numbered from 1 to 4. Cluster 1 comprises of amino acids (AA) 44–466, cluster 2 AA 2246–2534 and cluster 3 AA 3778–4201 and these three clusters are located in the N-terminal and central regions of the protein and form the cytoplasmic domain. Cluster 4 comprises of AA 4497–4959 and forms the transmembrane domain, which is located in the C-terminal region. The figure is modified from [11].

doi:10.1371/journal.pone.0125366.g001

mutations causing CPVT1. CPVT1 patients carried the following mutations: *c.168-301_c.273+722del1128* mutation (later called as *exon 3 deletion)* or point mutations *p.P2328S (c.6982C>T)*, *p.T2538R (c.7613C>G)*, *p.L4115F (c.12343C>T)*, *p.Q4201R (c.12602A>G)* or *p.V4653F (c.13957G>T)*. Mutation nomenclature was based on *RyR2* reference sequence NM_001035.2. The mutations were located in the four mutation hotspot clusters of the *RyR2* gene (Fig 1).[11] Patients and families carrying mutations *P2328S* [3,10,25], *exon 3 deletion* [3,26], *Q4201R* [10,25] and *V4653F* [10,25] have been described in detail earlier.

All mutations were associated with exercise-induced ventricular arrhythmias and syncopal spells. All except *L4115F* were associated with one or more cases of sudden death at young age in the family. An ICD had been implanted in five of them; one has received an adequate shock therapy. Five out of the six patients had a history of syncopal spells upon a frightening situation or physical exercise, and they all used a beta-adrenergic blocking agent (daily dose of 160 mg of propranolol, 7, 5 to 10 mg of bisoprolol or 95 mg of metoprolol) during all study phases. No other medications were in use. The patients were otherwise healthy without hypertension, diabetes, or evidence of other heart disease. None of them had bundle branch block.

In cardiac ultrasonography, left ventricular end diastolic dimension and systolic function were normal in all patients (data not shown). Basic laboratory parameters including hemoglobin, white blood cell count, plasma sodium, potassium, and creatinine concentrations were analyzed prior to administration of the drug and they were all within the normal range in every study patient (data not shown). Two of the patients with ICD showed atrial pacing at rest prior to exercise; all others had sinus rhythm. Electrocardiographic parameters are presented in Table 1.

Clinical Exercise Stress Test

All RyR2 patients underwent the exercise stress test three times. On the first morning a baseline study was carried out. The test was repeated in the afternoon of the first day after intravenous infusion of dantrolene sodium (Dantrium, 1.5 mg per kg of body weight). The third exercise test was performed on the second day to assess the effects after dantrolene sodium washout and to demonstrate the reproducibility of the basic exercise test.

Exercise tests were performed with a bicycle ergometer. The initial load was 30 W, followed by increments of the load by 15 W each minute. In the baseline study, the patient was

Table 1. Electrocardiographic parameters.

	Before dantrolene (n = 6)	After dantrolene (n = 6)	p-value
Heart rate (min-1)	61±5	60±5	NS
P (ms)	109±14	110±14	NS
PQ (ms)	154±31	163±34	NS
QRS (ms)	86±8	87±5	NS
QT (ms)	419±22	407±18	NS
QTc (ms)	418±35	409±35	NS

Comparison of electrocardiographic parameters of all patients before and after the dantrolene infusion. NS indicates no significant.

doi:10.1371/journal.pone.0125366.t001

instructed to target to a submaximal workload in order to be able to repeat the exercise stress test. In the consecutive phases of the study, the workload target was the same as that achieved in the first study. A twelve-lead electrocardiogram (ECG) was recorded continuously at paper speed 25 or 50 mms^{-1} and amplification of 0.1 mV/mm throughout the exercise test. After cessation of exercise, ECG was recorded continuously for the first 8 minutes. Both the maximum workload achieved and the heart rate at which ventricular bigeminy first appeared were recorded whenever applicable. Numbers of PVCs during exercise and at recovery phase as well as the maximum number of consecutive PVCs were counted. Plasma creatinine, sodium, potassium and calcium were measured at rest before the first exercise test. The exercise tests and the iPSC studies were done separately and blinded.

Characterization of iPSC Lines

The iPSC study was approved by the ethical committee of Pirkanmaa Hospital District (R08070) and written informed consent was obtained from all the participants. Patient-specific iPSC lines were established as described earlier.[17] Studied iPSC lines were UTA.05605.CPVT generated from patient with *RyR2 exon 3 deletion*, UTA.05208.CPVT from patient with mutation *P2328S*, UTA.07001.CPVT from patient with mutation *T2538R*, UTA.03701.CPVT from patient with mutation *L4115F*, UTA.05503.CPVT from patient with mutation *Q4201R*, UTA.05404.CPVT from patient with mutation *V4653F* and UTA.04602.WT from a healthy control individual.

All the CPVT-iPSC lines were characterized for their karyotypes, mutations, pluripotency, immunocytochemistry, embryoid body (EB) and teratoma formation. Endogenous and exogenous gene expressions were examined by RT-PCR using 1 μl cDNA and 500 nmol/L of each primer in one PCR reaction. β-actin and GAPDH served as the housekeeping genes. Detailed reaction conditions and PCR primers for iPSC characterization have been described earlier.[27] Endogenous pluripotency markers at the protein level were studied with immunocytochemistry. The iPSCs were fixed with 4% paraformaldehyde (PFA, Sigma-Aldrich, Saint Louis, USA). Primary antibodies anti-SOX2, anti-NANOG and anti-tumor-related antigen (TRA)1-81 (all 1:200, from Santa Cruz Biotechnology, Santa Cruz, CA, USA) and anti-OCT3/4 (1:400, R&D Systems) were used. Cells were mounted with Vectashield (Vector Laboratories, USA) containing DAPI for staining nuclei. To confirm the mutations of the CPVT iPSC lines with sequencing the DNA was isolated using DNA Tissue XS-kit (Macherey-Nagel GmbH & Co., Düren, Germany). The genomic region containing the expected mutation was amplified using PCR. Each PCR product was directly sequenced in both directions using BigDye Terminator v3.1 and ABI 3730xl DNA Analyzer (Applied Biosystems, Carlsbad, CA, USA). In addition to

direct sequencing, *exon 3 deletion* (1128 nucleotides) was also confirmed using PCR and agarose gel electrophoresis. Karyotypes of the cell lines were determined using either standard G-banding chromosome analysis (Medix laboratories, Espoo, Finland) or KaryoLite BoBs assay (Perkin Elmer) based on BACs-on-Beads technology (Molecular and Systems Immunology and Stem Cell Biology, Turku Centre for Biotechnology, University of Turku, Finland). The expression of markers characteristic of ectoderm (*Nestin* or *SOX-1*), endoderm (*AFP* or *SOX-17*), and mesoderm (*VEGF-R2*) development were studied from EBs maintained in EB-medium (KO-DMEM with 20% FBS, Non-Essential Amino Acid (NEAA), L-glutamine and penicillin/streptomycin) for 5 weeks. EB RT-PCR primers can be seen in S1 Table. The teratoma study was approved by ELLA- Animal Experiment Board of Regional State Administrative Agency for Southern Finland (ESAVI/6543/04.10.03/2011). IPSCs were injected into nude mice under the testis capsule and tumor samples collected 8 weeks after injection, followed by fixation with 4% PFA and staining of the sections with hematoxylin and eosin.

Cardiomyocyte Differentiation and Characterization

iPSCs were co-cultured with murine visceral endoderm-like (END-2) cells (Humbrecht Institute, Utrecht, The Netherlands) to differentiate them into spontaneously beating CMs. The beating areas of the cell colonies were mechanically excised and treated with collagenase A (Roche Diagnostics).[28] Single CMs were immunostained with anti-cardiac-troponin-T (1:1500, Abcam, Cambridge, MA, USA), anti-α-actinin (1:1500, Sigma) and anti-connexin-43 (1:1000, Sigma).

Ca^{2+} Imaging

Dissociated spontaneously beating CMs on a coverslip were loaded with 4 μmol/L Fura 2-AM (Life Technologies, Molecular Probes). CMs were continuously perfused with 37°C HEPES based perfusate during measurements and the perfusate consisted of (in mmol/L): 137 NaCl, 5 KCl, 0.44 KH_2PO_4, 20 HEPES, 4.2 $NaHCO_3$, 5 D-glucose, 2 $CaCl_2$, 1.2 $MgCl_2$ and 1 Na-puryvate (pH was adjusted to 7.4 with NaOH). Ca^{2+} measurements were conducted on an inverted IX70 microscope (Olympus Corporation, Hamburg, Germany) and cells were visualized with UApo/340 x20 air objective (Olympus). Images were acquired with an ANDOR iXon 885 CCD camera (Andor Technology, Belfast, Northern Ireland) synchronized with a Polychrome V light source by a real time DSP control unit and TILLvisION or Live Acquisition software (TILL Photonics, Munich, Germany). Fura 2-AM in CMs was excited at 340 nm and 380 nm light and the emission was recorded at 505 nm. For Ca^{2+} analysis, regions of interest were selected for spontaneously beating cells and background noise was subtracted before further data processing. The Ca^{2+} levels are presented as fura ratio units of F340/F380. Ca^{2+} peaks were analyzed with Clampfit version 10.2 (Molecular Devices, USA).

The percentage of abnormal Ca^{2+} transients, such as multiple peaks comprising of two peaks, irregular phases, oscillations, and varying amplitude manifested as low peaks, were calculated from each studied cell line. Beating frequency and diastolic Ca^{2+} levels of CMs were analyzed during spontaneous baseline beating, and during adrenaline perfusion. These parameters were compared between mutated and control cell lines and also between each mutated cell line. Some results of Ca^{2+} cycling of CPVT-*P2328S* and control cell lines have been published before [21] and parts of these results have been included here.

For dantrolene studies, the changes in Ca^{2+} were recorded during spontaneous baseline beating, spontaneous beating during 1 μM adrenaline perfusion and spontaneous beating during 1 μM adrenaline together with 10 μM dantrolene (Sigma) perfusion. If a CM displayed Ca^{2+} transient abnormalities during adrenaline perfusion, it was exposed to dantrolene. Drug

effects of dantrolene were categorized into three groups. In "responder" group dantrolene abolished virtually all the Ca^{2+} handling abnormalities, in "semi-responder" group dantrolene reduced them by more than 50%, in "non-responder" group dantrolene reduced them by less than 50%. Diastolic Ca^{2+} levels and beating frequency were compared between adrenaline and dantrolene responses of responder CMs (*exon 3 del*, *P2328S*, *T2538R*, *L4115F*) and non-responder CMs (*Q4201R*, *V4653F*, controls). For this, adrenaline response values were divided by dantrolene response values, separately for each cell.

Statistical Analysis

Statistical analysis of *in vivo* studies was made with SPSS 21.0 statistical software package (SPSS, Chicago, IL). Data are presented as average + 1 SD. Comparisons between phases were performed by the non-parametric Wilcoxon test. The significance of *in vitro* differences between two groups was evaluated with the unpaired Student's *t*-test. The significance of changes within a group was evaluated with the paired Student's *t*-test. Data are expressed as average ± S.E.M. and n refers to the number of cells. $P<0.05$ was considered statistically significant in both *in vivo* and *in vitro*.

Results

Antiarrhythmic Effects of Dantrolene in Cpvt1 Patients

In the baseline study, patients exercised on an average 8±2 minutes reaching a maximum heart rate of 134±17 min^{-1}. Exercise bicycle testing induced polymorphic PVCs in all patients and non-sustained ventricular tachycardia (NSVT, episodes of 3 to 4 consecutive PVCs) in three of them. The average threshold sinus rate for the appearance of PVCs was 105±9 min^{-1}. The total count of PVCs during the workload was 172±119 (range 43–391).

All six patients tolerated the target dose 1.5 mg/kg of intravenous infusion of dantrolene but reported considerable muscle weakness as a side-effect. Dantrolene did not affect atrioventricular conduction or the QT interval (Table 1). Dantrolene decreased the prevalence of PVCs in four patients, whereas in two patients the number of PVCs remained virtually the same (Fig 2). Dantrolene seemed to reduce arrhythmias in patients with the mutation in the N-terminal or central region of the *RyR2* protein (Figs 1 and 2). Thus, dantrolene abolished 97% of PVCs in the patient with exon 3 deletion (cluster 1), 88% of PVCs in the patient with *P2328S* mutation (cluster 2), 33% of PVSc in the patient with *T2538R* mutation (right after cluster 2) and 77% of PVCs in the patient with *L4115F* mutation (cluster 3). In contrast, dantrolene abolished only 1 to 2% of PVCs in patients carrying mutation closer to (*Q4201R*, end of cluster 3) or within the transmembrane region (*V4653F*, cluster 4).

Fig 3 illustrates an example of the PVCs and NSVT episodes during the baseline study and after dantrolene. Dantrolene increased significantly the threshold at which the arrhythmias appeared from 105±9 to 120±17 min-1. The duration of the exercise phase and the maximal heart rate achieved during the exercise were similar to those in the baseline study. On day 2, after wash-out of dantrolene, the prevalence of PVCs was approaching that in the first baseline test.

Characterization of iPSC Lines Confirms Pluripotent Stem Cell Characteristics

iPSC lines from six CPVT1 patients with above-mentioned *RyR2* mutations were generated. Results of the *P2328S* and control iPSC line characterizations have been published before. [21,27] All studied endogenous pluripotency genes (Nanog, Rex1, Oct 3/4 and Sox2) were

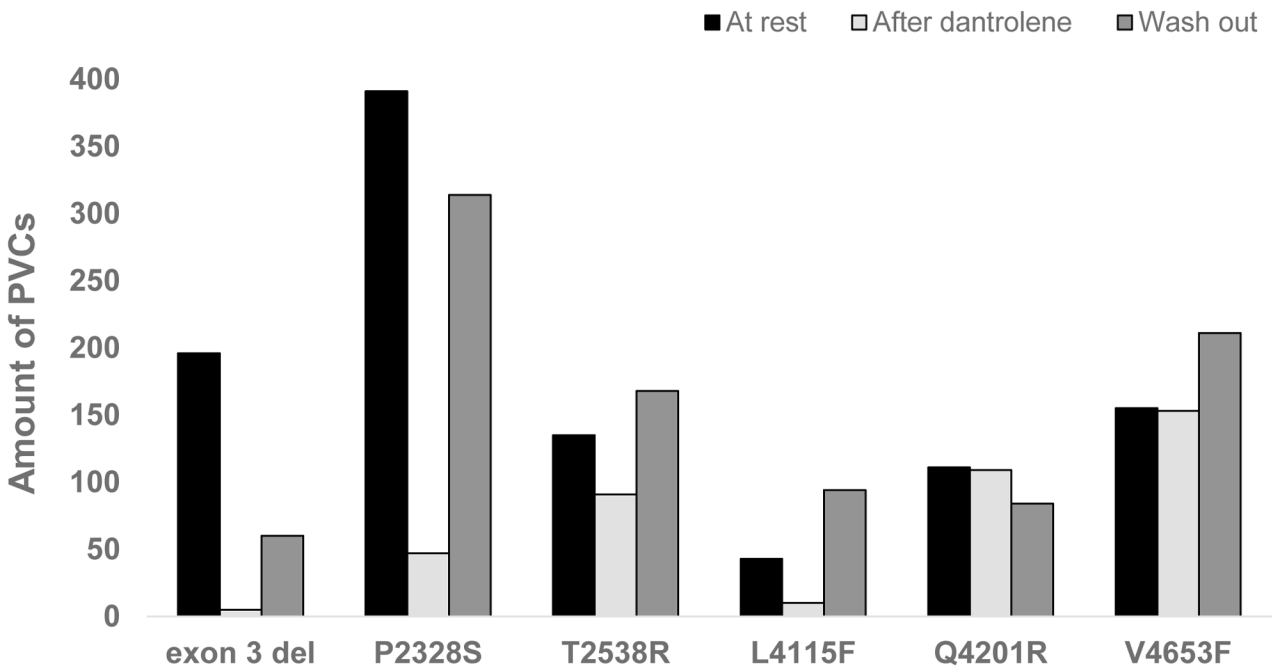

Fig 2. Features of the PVCs. Number of PVCs in exercise stress test before and after administration of intravenous dantrolene and 24 hours after dantrolene wash out.

doi:10.1371/journal.pone.0125366.g002

turned on and the expression of retrovirally encoded reprogramming factors c-Myc, Klf4, Sox2 and Oct 3/4 was silenced (Fig 4A and 4B). CPVT1 iPSC lines expressed endogenous pluripotent markers Nanog, Oct3/4, TRA 1–81 and SOX2 also at the protein level (Fig 4D). Pluripotency was further confirmed by teratoma formation and with *in vitro* embryoid body (EB) formation expressing all three germ layers (Figs 4C and 5G). The presence of the *RyR2* mutations was confirmed from all the CPVT1 iPSC lines with DNA sequence analysis (Fig 4E). All the iPSC lines had a normal karyotype (Fig 4F). In addition to sequencing, the presence of the *exon 3 deletion* was confirmed with PCR (S1 Fig).

iPSC Derived Cms Display Abnormal Ca^{2+} Cycling

iPSCs were differentiated into spontaneously beating CMs (Fig 5A). When compared to CMs derived from the healthy individual, CPVT1 CMs demonstrated marked Ca^{2+} transient abnormalities such as multiple peaks comprising of two peaks, irregular phases, oscillations, and varying amplitude manifested as low peaks (Fig 5B) both in baseline and in response to adrenaline. Although these abnormalities were common with all six mutations examined, some differences between *RyR2* mutations were also observed. Accordingly, Ca^{2+} transient abnormalities were somewhat more common in the cluster 4 mutation than in cluster 1, 2 and 3 mutations (Fig 5C).

Adrenaline increased the beating frequency of each cell line studied (Fig 5D). All *RyR2* mutated CMs had lower beating frequency both at baseline and during adrenaline perfusion than control CMs. Adrenaline produced significantly elevated diastolic Ca^{2+} levels only in *P2328S* CMs, while diastolic Ca^{2+} levels were lower or similar in other mutant CMs compared to control CMs (Fig 5E). *Exon 3 deletion* CMs had both lower beating frequency and diastolic Ca^{2+} level when compared to other mutations (Fig 5 and S2 Table).


A
V1
V2
V3
V4
V5
V6
400ms
B
V1
V2
V3
V4
V5
V6
400ms
C
V1
V2
V3
V4
V5
V6
400ms
D
V1
V2
V3
V4
V5
V6
400ms

Fig 3. ECG examples of a 38-year-old patient carrying the *RyR2 P2328S* mutation. (A) Resting ECG showing sinus rhythm and normal QRS morphology. (B) Exercise ECG at the highest work load of 105 W in the baseline study before dantrolene. PVCs include couplets and polymorphic NSVTs. (C) Disappearance of ventricular arrhythmias after administration of dantrolene (work load 105 W). (D) Exercise test on day two after 20-hours wash-out of dantrolene showing return of PVCs (work load 105 W).

doi:10.1371/journal.pone.0125366.g003

iPSC Derived Cpvt1 Cms Reproduced the Clinical Antiarrhythmic Responses to Dantrolene

Effects of dantrolene were divided into three groups based on their Ca^{2+} responses. In "responder" group dantrolene abolished all the Ca^{2+} handling abnormalities, in "semi-responder" group dantrolene reduced them by more than 50% and in "non-responder" group dantrolene reduced them by less than 50%. iPSC derived CMs were found to markedly reproduce the varying individual clinical responses of dantrolene (Fig 6). In cell lines with the mutation in the N terminal or central region of the *RyR2* protein dantrolene abolished or reduced the majority of Ca^{2+} transient abnormalities (Fig 6). These mutations were within or in close proximity of clusters 1, 2 or 3 (Fig 1). A detailed analysis indicated that in CMs with *exon 3 deletion*, *P2328S*, *T2538R or L4115F*, dantrolene abolished or reduced by more than 50% of Ca^{2+} abnormalities in 65–97% of cells (Fig 6).

In striking contrast, the effect of dantrolene was only minimal in CMs carrying a mutation at the end of cluster 3 (*Q4201R*) or in the transmembrane region (cluster 4, mutation *V4653F*) (Fig 6), in accordance with the *in vivo* dantrolene infusion data. Dantrolene had no effect on the Ca^{2+} transients in control CMs. Dantrolene did not significantly affect the diastolic Ca^{2+} levels of CMs in which Ca^{2+} transient abnormalities were abolished (S2 Fig). Dantrolene increased significantly the diastolic Ca^{2+} levels of control and *Q4201R* CMs where Ca^{2+} transients were unaltered by the drug. There was no correlation between the antiarrhythmic effect of dantrolene and its effect on beating frequency (S2 Fig).

Discussion

We have studied the antiarrhythmic potential of dantrolene in the treatment of CPVT1. To this end, we assessed the efficacy of intravenously administered dantrolene in patients carrying various *RyR2* mutations and compared these effects to *in vitro* studies using iPSC derived CMs generated from the same patients. Our findings demonstrate that intravenous dantrolene, a drug used to treat another ryanodine receptor disorder, malignant hyperthermia, abolished or markedly reduced arrhythmias in a subgroup of CPVT1 patients with specific *RyR2* mutations. By combining evidence from *in vivo* and *in vitro* studies, we propose that the location of the *RyR2* mutation affects the antiarrhythmic effect of dantrolene in CPVT1.

Previously dantrolene has been shown to have beneficial effects on cardiac function in experimental animal models of CPVT1 [13–15,29,30] and in iPSC derived CMs from a CPVT1 patient with an N-terminal *S406L* mutation [20], but no studies in patients have so far been reported. It is also important to take into consideration that even if a drug is found to be beneficial in the patient-derived iPSC-CMs, it cannot be automatically concluded that this will translate into a clinical benefit. Here we show that dantrolene given intravenously has an antiarrhythmic effect also in some but not in all patients with CPVT1. This antiarrhythmic effect was observed only in patients with *RyR2* mutations in the N-terminal or central regions of *RyR2* protein (clusters 1–3), whereas virtually no effect was seen in patients carrying mutations at the end of cluster 3 or in the transmembrane region (cluster 4). Although a dose-dependent effect cannot be excluded, similar observations on mutation-specific drug responses have been obtained in some other genetic disorders including long QT syndrome type 3 [31], cystic fibrosis [32], as well as in certain neoplastic diseases.[33] Recognition of potential mutation-specific

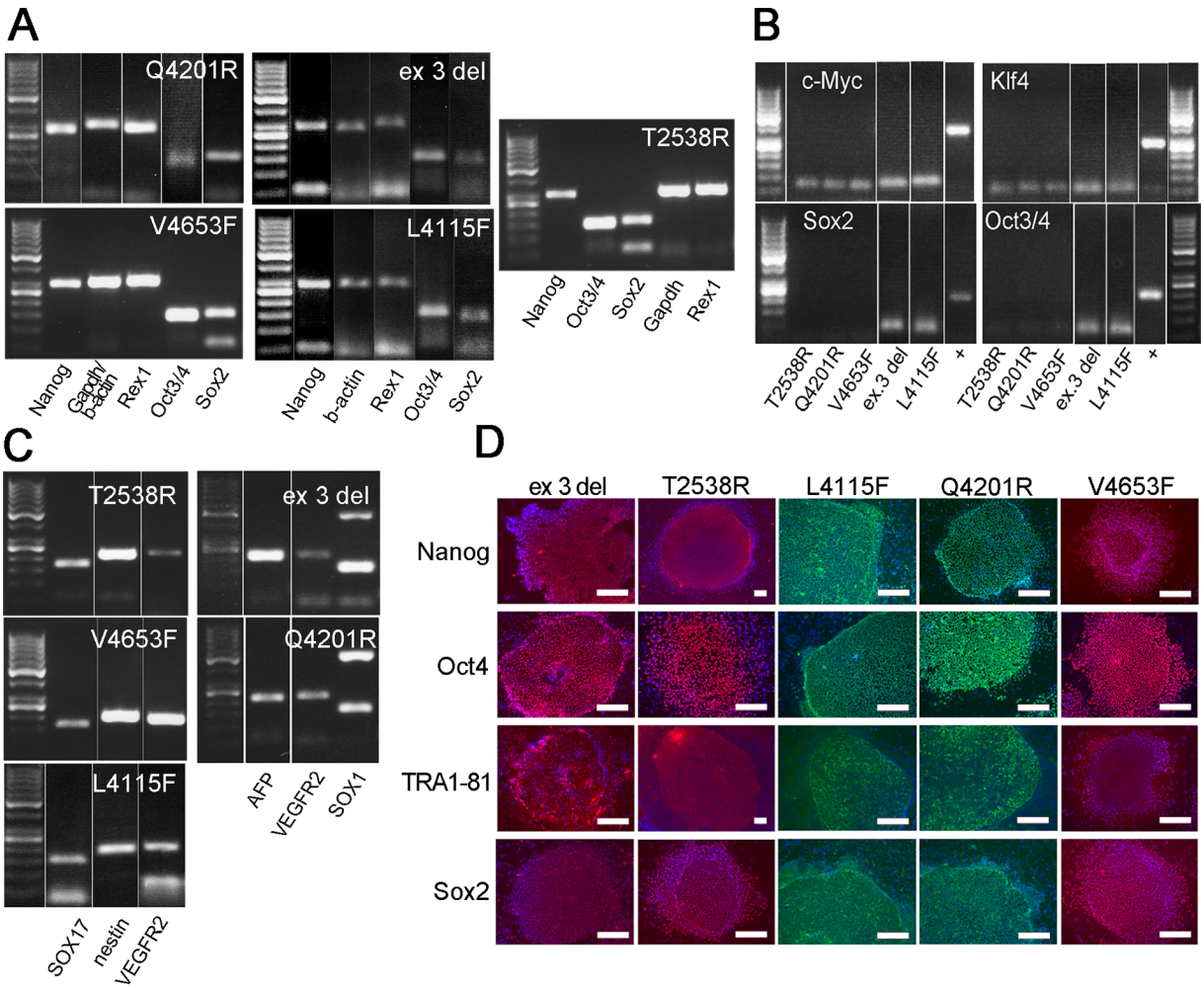
A
Q4201R
ex 3 del
T2538R
V4653F
L4115F
Nanog
Gapdh/ b-actin
Rex1
Oct3/4
Sox2
B
c-Myc
Klf4
Sox2
Oct3/4
T2538R
Q4201R
V4653F
ex.3 del
L4115F
+
C
T2538R
ex 3 del
V4653F
Q4201R
L4115F
AFP
VEGFR2
SOX1
SOX17
nestin
VEGFR2
D
ex 3 del
T2538R
L4115F
Q4201R
V4653F
Nanog
Oct4
TRA1-81
Sox2

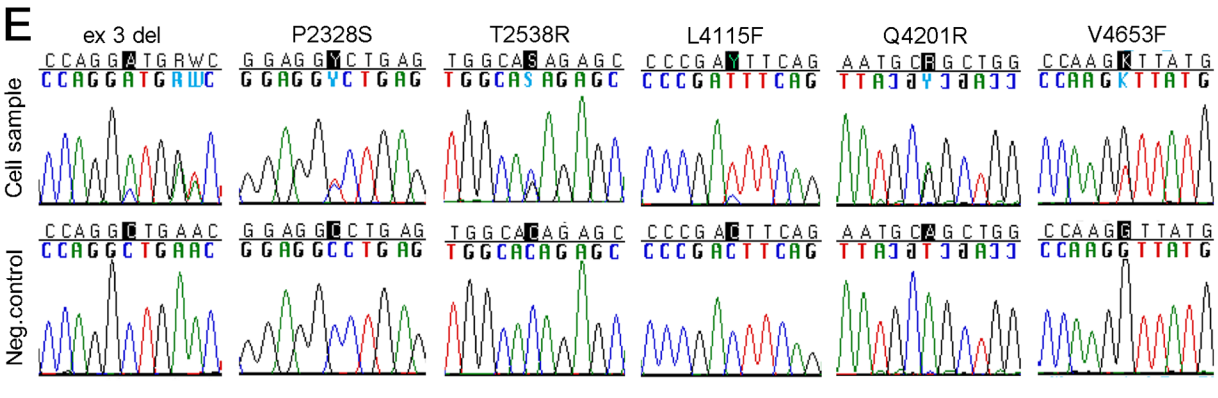
E
ex 3 del
P2328S
T2538R
L4115F
Q4201R
V4653F
Cell sample
Neg.control

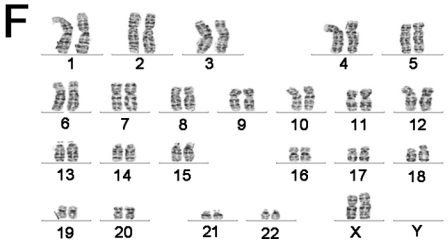
F
1
2
3
4
5
6
7
8
9
10
11
12
13
14
15
16
17
18
19
20
21
22
X
Y

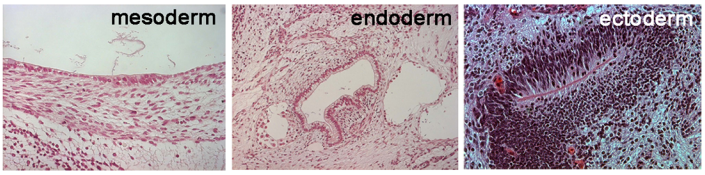
G
mesoderm
endoderm
ectoderm

Fig 4. Characterization of CPVT1 iPSCs. (A) Expression of pluripotency markers shown by RT-PCR, β-actin or GAPDH serving as a housekeeping gene. (B) None of the exogenous genes are expressed in CPVT1 cell lines. (C) EBs express markers from all the three embryonic germ layers. (D) Immunocytochemical stainings and expression of pluripotency markers. Scale bar 200 μm. (E) Sequencing analysis confirmed the *RyR2* mutation in each cell line. (F) All the cell lines had normal karyotype, example picture from *Q4201R* cell line. (G) Teratomas made from a CPVT-iPSC line further confirms pluripotency, example pictures from *L4115F* cell line.

doi:10.1371/journal.pone.0125366.g004

responses will be important for future drug development: one drug may not work for all patients even if the phenotype is the same.

Currently, beta-antiadrenergic medication is the first line antiarrhythmic treatment for all CPVT patients. Flecainide has also shown beneficial effects.[34,35] ICDs are used if severe arrhythmic events occur despite optimal beta-blocking treatment. However, use of ICDs is not without risk since ICD-shocks may further aggravate catecholamine release and initiate an uncontrolled electric storm. Very recent data suggest that left cardiac sympatectomy may be highly effective in patients refractory to medical therapy.[7,36] Although dantrolene as such would not be suitable for long-term treatment of CPVT1 due to its side effects, and although only a subset of patients would benefit from it, our data shows its antiarrhythmic potential. It also suggest that it could be administered by intravenously to CPVT1 patients in emergencies such as incessant ventricular tachycardia.

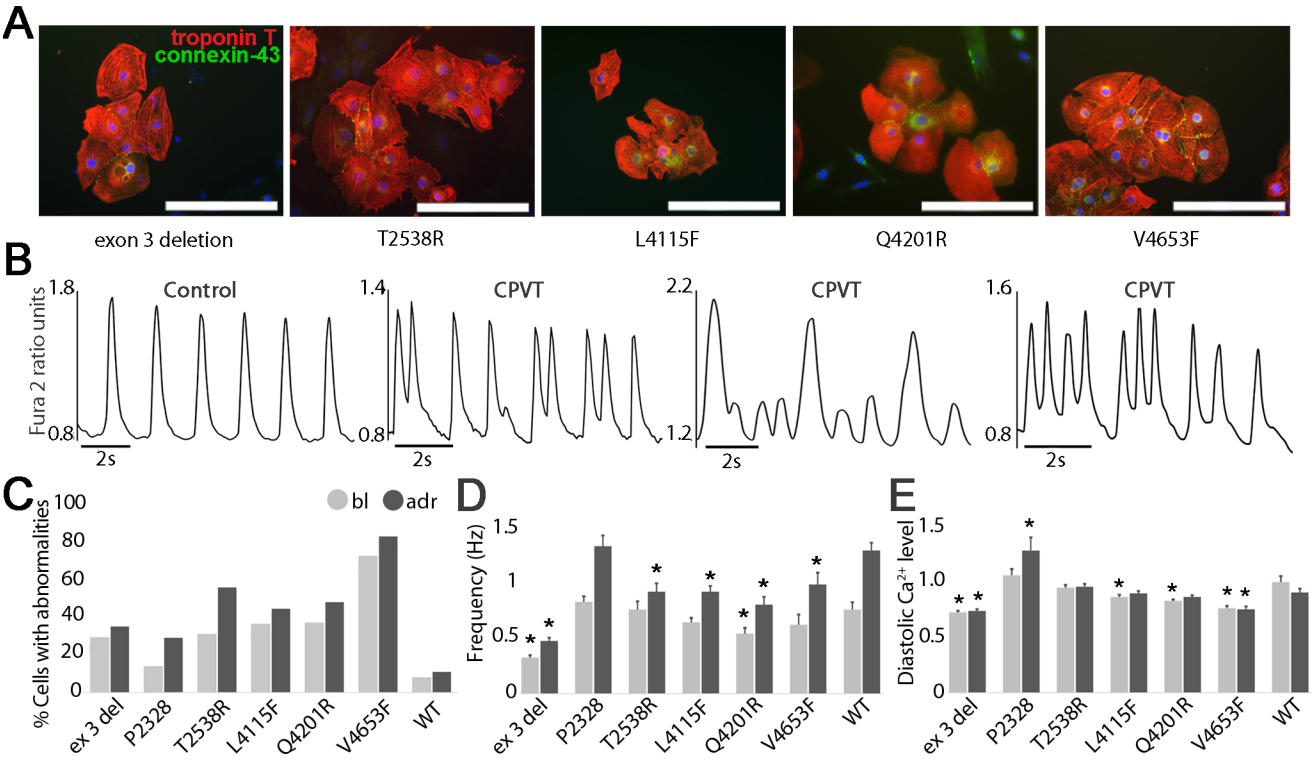

Fig 5. Characterization of CPVT-iPSCs derived CMs. (A) Immunocytochemical stainings of cardiac markers where red represents troponin T, green connexin-43 and blue DAPI-staining for nuclei. Scale bars 200 μm. (B) Representative traces of a control CM showing normal regular Ca^{2+} transients and CPVT1 CMs showing abnormalities like multiple peaks, low peaks, irregular phases and oscillations in Ca^{2+} handling. (C) Quantification of percentage of CPVT1 and control iPSC CMs exhibiting abnormal Ca^{2+} transients at baseline (bl) and during adrenaline perfusion (adr). (D) Frequency and (E) Diastolic level of intracellular Ca^{2+} of all CPVT1 and control CMs. Numbers of cells analyzed in C, D, and E, *exon 3 del* n = 48, *P2328S* n = 72, *T2538R* n = 52, *L4115F* n = 110, *Q4201R* n = 63, *V4653F* n = 29, Controls (WT) n = 28. As an exception, number of WT cells analyzed in D, and E, in bl n = 54 and adr n = 27 and number of *P2328S* cells in bl n = 90 and adr n = 47. Grey bars indicate cells at baseline and black bars during adrenaline perfusion. Error bars, SEM. *P<0.05 CPVT1 versus control, with Student's t-test. Significance's of mutation specific differences, see S2 Table.

doi:10.1371/journal.pone.0125366.g005

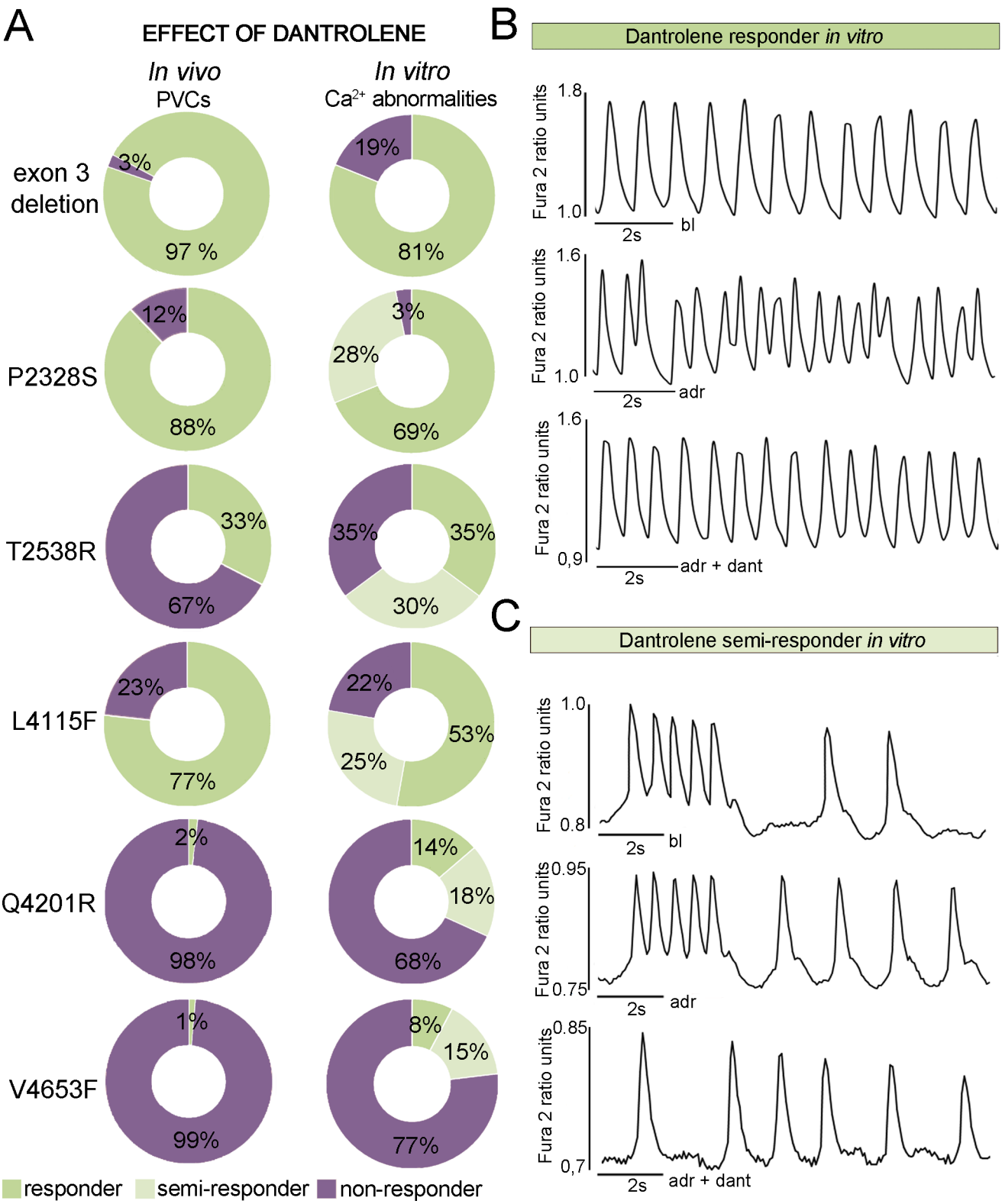

Fig 6. iPSC derived CMs reproduced the clinical responses of dantrolene. (A) *In vivo* and *in vitro* effects of dantrolene correspond within each *RyR2* mutation. *In vitro* drug effects were categorized into three groups (responders, semi-responders and non-responders) depending on how dantrolene affected to the amount of Ca^{2+} abnormalities when compared to adrenaline response. *In vivo* responder group show the percentage of the abolished PVCs when compared to the baseline. Numbers of cells analyzed in *exon 3 del* n = 16, *P2328S* n = 32, *T2538R* n = 17, *L4115F* n = 36, *Q4201R* n = 22, *V4653F* n = 13. (B)

Representative traces of dantrolene responder *in vitro* in an *L4115F* mutated CM. Adrenaline causes Ca^{2+} cycling abnormalities and dantrolene abolishes all the abnormalities. (C) Representative traces of semi-responder *in vitro* in a *P2328S* mutated CM. The cell has abnormal Ca^{2+} cycling at baseline and during adrenaline perfusion and dantrolene reduces the abnormalities by abolishing the oscillation but leaving some low peak Ca^{2+} spiking.

doi:10.1371/journal.pone.0125366.g006

More than 150 mutations in *RyR2* gene have been reported so far and they are clustered in four hotspots.[11] One third of the reported mutations are in clusters 1 and 2 and the rest are equally distributed between clusters 3 and 4. Only 10% of *RyR2* mutations have been found outside these clusters.[11] The location of the *RyR2* mutation appears to be critical for a favorable effect of dantrolene. The binding site for dantrolene is localized in the N-terminus of *RyR2* between amino acid 601 and 620.[13,37] The dantrolene-binding sequence is considered to constitute part of the domain switch region, suggesting that dantrolene is involved in the correction of defective unzipping and allosteric stabilization of interdomain interactions between the N- terminal and central regions of *RyR2*, resulting in inhibition of Ca^{2+} leak [16,30,38] and in fact, this has been demonstrated in previous studies.[13,16,37] Also our data demonstrate that dantrolene abolished arrhythmias in CPVT1 patients with mutations of N terminal or central domain, suggesting that a defective inter-domain interaction within the *RyR2* could be the underlying arrhythmogenic mechanism in the *exon 3 deletion*, *P2328S*, *T2538R* and *L4115F*. However, dantrolene did not suppress *T2538R*-related arrhythmias to the same extent as arrhythmias caused by other central region mutations. It has been speculated that differences in the mode of interdomain interaction in dantrolene binding regions may result in differences in its antiarrhythmic efficacy.[30] Furthermore, other drug-binding regions in the carboxyl-terminal half of the *RyR2* or additional low affinity drug binding sites in the N-terminal area could exist.[13] No previous studies on the effects of dantrolene on *RyR2* mutations in or close to the transmembrane are available; here we show that dantrolene has no or only minimal effect on arrhythmias if mutations are located in these areas. It is interesting that the patient with *Q4201R* mutation did not respond to dantrolene even though this mutation is located in cytosolic portion of *RyR2* and in cluster 3 although in its terminal part. This finding indicates that the location of the mutation in certain mutation cluster does not necessarily determine the antiarrhythmic response, and highlights the utility of the iPSC model for individual functional analysis.

Our data showing similar patient-to-patient variation in dantrolene effects in the clinical setting and corresponding iPSC-CM models suggest that, at least in theory, it may be possible to tailor an individual's medication in cell culture without predisposing the individual to the potentially serious side-effects of a drug. Dantrolene did not affect normally beating CMs. This is consistent with previous reports showing that dantrolene inhibits only abnormal Ca^{2+} release and has no effect on the normal Ca^{2+} transients, suggesting that the native conformation of *RyR2* may restrict binding of the drug and that dantrolene binding to *RyR2* might be dependent on a specific conformational state present only in mutated cells.[13,37] Defective calmodulin binding caused by *RyR2* domain unzipping has also been shown to be restored by dantrolene [29,39] which may as well explain why dantrolene exerts effects on diseased but not healthy hearts.

Besides differences in drug responses, we also saw both similarities and differences in the CPVT1 *in vitro* phenotypes depending on the nature of the mutation. The beating frequency of CPVT1 CMs was lower than that in control CMs. This is in line what has been reported also with CPVT1 patients.[5,40] All the CPVT1 CMs showed similar disturbances in intracellular Ca^{2+} cycling. Ca^{2+} transient abnormalities were somewhat more common in the cluster 4 mutation than in cluster 1, 2 and 3 mutations. *Exon 3 deletion* differed from all the other mutations by having lower diastolic Ca^{2+} levels and beating frequency both at baseline and during

adrenaline perfusion. Exon 3 encodes secondary structure elements that are crucial for folding of the N-terminal domain. It has been proposed that *RyR2* with *exon 3 deletion* has evolved additional means to regulate Ca^{2+} release, by altering the conformation of the domain [41], which may result in the observed differences in Ca^{2+} transients.

There are certain limitations in our study. First, only six CPVT1 patients and their iPSC cell lines were studied; however, we emphasize that despite the very rare nature of this disease we were able to examine in detail six different disease-causing mutations. Second, under the conditions of the study design we were permitted to study only acute effects of intravenously administered dantrolene. Third, although we titrated the dose of dantrolene according to the weights of the patients, serum levels of the drug were not measured and could have varied from patient to patient, resulting in concentration-dependent variation in clinical responses. Fourth, we used only a fixed concentration of dantrolene, selected on the basis of the work by Jung et al. [20], in our iPSC studies. Fifth, immature phenotype of the iPSC-CMs may produce variation in arrhythmias. However, in our previous study [21] the electrophysiology of CPVT1 iPSC-CMs appeared fairly mature. We have also shown here and in our previous study [21] that arrhythmias are substantially more consistent in CPVT1 CMs than in control CMs.

In conclusion, we have shown here the proof of principle that intravenously administered dantrolene suppresses ventricular arrhythmias in the congenital *RyR2* defect and that the location of the *RyR2* mutation may affect the antiarrhythmic effect of this drug. We also demonstrate that iPSC derived patient-specific CMs correctly predict the clinical response to dantrolene in CPVT1 patients with varying *RyR2* mutations. Our data support the notion that iPSC-derived CMs could serve as a platform for drug development and for design of personalized medication.

Supporting Information

S1 Fig. Confirmation of *exon 3 deletion*. *Exon 3 deletion* of 05605. CPVT cell line was also confirmed with PCR and agarose gel electrophoresis.
(TIF)

S2 Fig. Ca^{2+} transient parameters as a response to dantrolene. (A) Diastolic Ca^{2+} level and (B) beating frequency in responder and non-responder CMs. Values during adrenaline perfusion were divided by values during dantrolene perfusion, separately for each cell. Green bars indicate responder CMs and purple bars non-responder CMs. Error bars, SEM. * indicates significant difference between adrenaline versus dantrolene within a group, $^{*}P<0.05$. Numbers of cells analyzed in *exon 3 del* n = 13, *P2328S* n = 29, *T2538R* n = 11, *L4115F* n = 28, *Q4201R* n = 15, *V4653F* n = 10, Control (WT) n = 20.
(TIF)

S1 Protocol. English translated trial study protocol.
(DOCX)

S2 Protocol. Trial study protocol in the original language (Finnish).
(DOC)

S1 Table. Primer sequences for EB RT-PCR.
(DOCX)

S2 Table. Differences between RyR2 mutations in their Ca^{2+} transient properties during baseline and adrenaline perfusion. CL indicates cluster numbers. Upward pointing arrow indicates significantly ($p<0.05$) higher and downward pointing arrow significantly lower diastolic Ca^{2+} level or beating frequency of the first mentioned mutation when compared to the

second mentioned mutation. NS indicates that there was no statistical significance between mutations. As parallel pointing arrows between comparison groups indicate, the average of the beating frequency and diastolic Ca^{2+} level inside one mutation group corresponded and the average of these parameters decrease when moving from *P2328S* towards transmembrane area mutations.
(DOCX)

Acknowledgments

We thank Minna Härkönen, Merja Lehtinen, Henna Venäläinen and Markus Haponen for technical support and Olli Silvennoinen for critical reading of the manuscript.

Author Contributions

Conceived and designed the experiments: KP HS KK KAS. Performed the experiments: KP HS SV AML KAS. Analyzed the data: KP HS JP KAS. Contributed reagents/materials/analysis tools: KAS. Wrote the paper: KP HS SV JP AML KK KAS.

References

1. Coumel P, Fidelle J, Lucet V, Attuel P, Bouvrain Y. Catecholaminergic-induced severe ventricular arrhythmias with adams-stokes syndrome in children: Report of four cases. Br Heart J. 1978; 40: 28–37.
2. Leenhardt A, Lucet V, Denjoy I, Grau F, Ngoc DD, Coumel P. Catecholaminergic polymorphic ventricular tachycardia in children. A 7-year follow-up of 21 patients. Circulation. 1995; 91: 1512–9. PMID: 7867192
3. Swan H, Piippo K, Viitasalo M, Heikkila P, Paavonen T, Kainulainen K, et al. Arrhythmic disorder mapped to chromosome 1q42-q43 causes malignant polymorphic ventricular tachycardia in structurally normal hearts. J Am Coll Cardiol. 1999; 34: 2035–42. PMID: 10588221
4. Leenhardt A, Denjoy I, Guicheney P. Catecholaminergic polymorphic ventricular tachycardia. Circ Arrhythm Electrophysiol. 2012; 5: 1044–1052. doi: 10.1161/CIRCEP.111.962027 PMID: 23022705
5. van der Werf C, Wilde AA. Catecholaminergic polymorphic ventricular tachycardia: From bench to bedside. Heart. 2013; 99: 497–504. doi: 10.1136/heartjnl-2012-302033 PMID: 23390049
6. Priori SG, Wilde AA, Horie M, Cho Y, Behr ER, Berul C, et al. Executive summary: HRS/EHRA/APHRS expert consensus statement on the diagnosis and management of patients with inherited primary arrhythmia syndromes. Heart Rhythm. 2013; 10: e85–108. doi: 10.1016/j.hrthm.2013.07.021 PMID: 23916535
7. Wilde AA, Bhuiyan ZA, Crotti L, Facchini M, De Ferrari GM, Paul T, et al. Left cardiac sympathetic denervation for catecholaminergic polymorphic ventricular tachycardia. N Engl J Med. 2008; 358: 2024–2029. doi: 10.1056/NEJMoa0708006 PMID: 18463378
8. Hayashi M, Denjoy I, Extramiana F, Maltret A, Buisson NR, Lupoglazoff JM, et al. Incidence and risk factors of arrhythmic events in catecholaminergic polymorphic ventricular tachycardia. Circulation. 2009; 119: 2426–2434. doi: 10.1161/CIRCULATIONAHA.108.829267 PMID: 19398665
9. Priori SG, Napolitano C, Tiso N, Memmi M, Vignati G, Bloise R, et al. Mutations in the cardiac ryanodine receptor gene (hRyR2) underlie catecholaminergic polymorphic ventricular tachycardia. Circulation. 2001; 103: 196–200. PMID: 11208676
10. Laitinen PJ, Brown KM, Piippo K, Swan H, Devaney JM, Brahmbhatt B, et al. Mutations of the cardiac ryanodine receptor (RyR2) gene in familial polymorphic ventricular tachycardia. Circulation. 2001; 103: 485–90. PMID: 11157710
11. Priori SG, Chen SR. Inherited dysfunction of sarcoplasmic reticulum Ca2+ handling and arrhythmogenesis. Circ Res. 2011; 108: 871–883. doi: 10.1161/CIRCRESAHA.110.226845 PMID: 21454795
12. Krause T, Gerbershagen MU, Fiege M, Weisshorn R, Wappler F. Dantrolene—a review of its pharmacology, therapeutic use and new developments. Anaesthesia. 2004; 59: 364–373. PMID: 15023108
13. Kobayashi S, Yano M, Suetomi T, Ono M, Tateishi H, Mochizuki M, et al. Dantrolene, a therapeutic agent for malignant hyperthermia, markedly improves the function of failing cardiomyocytes by stabilizing interdomain interactions within the ryanodine receptor. J Am Coll Cardiol. 2009; 53: 1993–2005. doi: 10.1016/j.jacc.2009.01.065 PMID: 19460614

14. Kobayashi S, Yano M, Uchinoumi H, Suetomi T, Susa T, Ono M, et al. Dantrolene, a therapeutic agent for malignant hyperthermia, inhibits catecholaminergic polymorphic ventricular tachycardia in a RyR2 (R2474S/+) knock-in mouse model. Circ J. 2010; 74: 2579–2584. PMID: 20944434

15. Uchinoumi H, Yano M, Suetomi T, Ono M, Xu X, Tateishi H, et al. Catecholaminergic polymorphic ventricular tachycardia is caused by mutation-linked defective conformational regulation of the ryanodine receptor. Circ Res. 2010; 106: 1413–1424. doi: 10.1161/CIRCRESAHA.109.209312 PMID: 20224043

16. Kobayashi S, Bannister ML, Gangopadhyay JP, Hamada T, Parness J, Ikemoto N. Dantrolene stabilizes domain interactions within the ryanodine receptor. J Biol Chem. 2005; 280: 6580–6587. PMID: 15611117

17. Takahashi K, Tanabe K, Ohnuki M, Narita M, Ichisaka T, Tomoda K, et al. Induction of pluripotent stem cells from adult human fibroblasts by defined factors. Cell. 2007; 131: 861–72. PMID: 18035408

18. Novak A, Barad L, Zeevi-Levin N, Shick R, Shtreichman R, Lorber A, et al. Cardiomyocytes generated from CPVT(D307H) patients are arrhythmogenic in response to beta-adrenergic stimulation. J Cell Mol Med. 2011; 3: 468–82. doi: 10.1111/j.1582-4934.2010.01242.x PMID: 21155977

19. Fatima A, Xu G, Shao K, Papadopoulos S, Lehmann M, Arnaiz-Cot JJ, et al. In vitro modeling of ryanodine receptor 2 dysfunction using human induced pluripotent stem cells. Cell Physiol Biochem. 2011; 28: 579–92. doi: 10.1159/000335753 PMID: 22178870

20. Jung CB, Moretti A, Mederos y Schnitzler M, Iop L, Storch U, Bellin M, et al. Dantrolene rescues arrhythmogenic RYR2 defect in a patient-specific stem cell model of catecholaminergic polymorphic ventricular tachycardia. EMBO Mol Med. 2012; 4: 180–191. doi: 10.1002/emmm.201100194 PMID: 22174035

21. Kujala K, Paavola J, Lahti A, Larsson K, Pekkanen-Mattila M, Viitasalo M, et al. Cell model of catecholaminergic polymorphic ventricular tachycardia reveals early and delayed afterdepolarizations. PLoS One. 2012; 7: e44660. doi: 10.1371/journal.pone.0044660 PMID: 22962621

22. Itzhaki I, Maizels L, Huber I, Gepstein A, Arbel G, Caspi O, et al. Modeling of catecholaminergic polymorphic ventricular tachycardia with patient-specific human-induced pluripotent stem cells. J Am Coll Cardiol. 2012; 60: 990–1000. doi: 10.1016/j.jacc.2012.02.066 PMID: 22749309

23. Di Pasquale E, Lodola F, Miragoli M, Denegri M, Avelino-Cruz JE, Buonocore M, et al. CaMKII inhibition rectifies arrhythmic phenotype in a patient-specific model of catecholaminergic polymorphic ventricular tachycardia. Cell Death Dis. 2013; 4: e843. doi: 10.1038/cddis.2013.369 PMID: 24113177

24. Zhang XH, Haviland S, Wei H, Saric T, Fatima A, Hescheler J, et al. Ca2+ signaling in human induced pluripotent stem cell-derived cardiomyocytes (iPS-CM) from normal and catecholaminergic polymorphic ventricular tachycardia (CPVT)-afflicted subjects. Cell Calcium. 2013; 54: 57–70. doi: 10.1016/j.ceca.2013.04.004 PMID: 23684427

25. Lehnart SE, Wehrens XH, Laitinen PJ, Reiken SR, Deng SX, Cheng Z, et al. Sudden death in familial polymorphic ventricular tachycardia associated with calcium release channel (ryanodine receptor) leak. Circulation. 2004; 109: 3208–14. PMID: 15197150

26. Marjamaa A, Laitinen-Forsblom P, Lahtinen AM, Viitasalo M, Toivonen L, Kontula K, et al. Search for cardiac calcium cycling gene mutations in familial ventricular arrhythmias resembling catecholaminergic polymorphic ventricular tachycardia. BMC Med Genet. 2009; 10: 12-2350-10-12.

27. Lahti AL, Kujala VJ, Chapman H, Koivisto AP, Pekkanen-Mattila M, Kerkela E, et al. Model for long QT syndrome type 2 using human iPS cells demonstrates arrhythmogenic characteristics in cell culture. Dis Model Mech. 2012; 5: 220–230. doi: 10.1242/dmm.008409 PMID: 22052944

28. Mummery C, Ward-van Oostwaard D, Doevendans P, Spijker R, van den Brink S, Hassink R, et al. Differentiation of human embryonic stem cells to cardiomyocytes: Role of coculture with visceral endoderm-like cells. Circulation. 2003; 107: 2733–40. PMID: 12742992

29. Xu X, Yano M, Uchinoumi H, Hino A, Suetomi T, Ono M, et al. Defective calmodulin binding to the cardiac ryanodine receptor plays a key role in CPVT-associated channel dysfunction. Biochem Biophys Res Commun. 2010; 394: 660–666. doi: 10.1016/j.bbrc.2010.03.046 PMID: 20226167

30. Suetomi T, Yano M, Uchinoumi H, Fukuda M, Hino A, Ono M, et al. Mutation-linked defective interdomain interactions within ryanodine receptor cause aberrant ca(2)(+)release leading to catecholaminergic polymorphic ventricular tachycardia. Circulation. 2011; 124: 682–694. doi: 10.1161/CIRCULATIONAHA.111.023259 PMID: 21768539

31. Ruan Y, Liu N, Bloise R, Napolitano C, Priori SG. Gating properties of SCN5A mutations and the response to mexiletine in long-QT syndrome type 3 patients. Circulation. 2007; 116: 1137–1144. PMID: 17698727

32. O'Reilly R, Elphick HE. Development, clinical utility, and place of ivacaftor in the treatment of cystic fibrosis. Drug Des Devel Ther. 2013; 7: 929–937. doi: 10.2147/DDDT.S30345 PMID: 24039402

33. Willyard C. Companies compete over mutation-specific melanoma drugs. Nat Med. 2011; 17: 268–268a. doi: 10.1038/nm0311-268a PMID: 21383725

34. Watanabe H, Chopra N, Laver D, Hwang HS, Davies SS, Roach DE, et al. Flecainide prevents catecholaminergic polymorphic ventricular tachycardia in mice and humans. Nat Med. 2009; 15: 380–383. doi: 10.1038/nm.1942 PMID: 19330009

35. Khoury A, Marai I, Suleiman M, Blich M, Lorber A, Gepstein L, et al. Flecainide therapy suppresses exercise-induced ventricular arrhythmias in patients with CASQ2-associated catecholaminergic polymorphic ventricular tachycardia. Heart Rhythm. 2013; 10: 1671–1675. doi: 10.1016/j.hrthm.2013.08.011 PMID: 23954267

36. Cusi V, De Ferrari G, Bos M, Moir C, Shkolnikova M, Abrams D, et al. Left cardiac sympathetic denervation for catecholaminergic polymorphic ventricular tachycardia (CPVT). Heart Rhythm. 2014; 11 (May Suppl): S176 (abstract).

37. Paul-Pletzer K, Yamamoto T, Ikemoto N, Jimenez LS, Morimoto H, Williams PG, et al. Probing a putative dantrolene-binding site on the cardiac ryanodine receptor. Biochem J. 2005; 387: 905–909. PMID: 15656791

38. Wang R, Zhong X, Meng X, Koop A, Tian X, Jones PP, et al. Localization of the dantrolene-binding sequence near the FK506-binding protein-binding site in the three-dimensional structure of the ryanodine receptor. J Biol Chem. 2011; 286: 12202–12212. doi: 10.1074/jbc.M110.194316 PMID: 21262961

39. Ono M, Yano M, Hino A, Suetomi T, Xu X, Susa T, et al. Dissociation of calmodulin from cardiac ryanodine receptor causes aberrant ca(2+) release in heart failure. Cardiovasc Res. 2010; 87: 609–617. doi: 10.1093/cvr/cvq108 PMID: 20388639

40. Postma AV, Denjoy I, Kamblock J, Alders M, Lupoglazoff JM, Vaksmann G, et al. Catecholaminergic polymorphic ventricular tachycardia: RYR2 mutations, bradycardia, and follow up of the patients. J Med Genet. 2005; 42: 863–870. PMID: 16272262

41. Lobo PA, Kimlicka L, Tung CC, Van Petegem F. The deletion of exon 3 in the cardiac ryanodine receptor is rescued by beta strand switching. Structure. 2011; 19: 790–798. doi: 10.1016/j.str.2011.03.016 PMID: 21645850

PLOS ONE

CORRECTION

Correction: Antiarrhythmic Effects of Dantrolene in Patients with Catecholaminergic Polymorphic Ventricular Tachycardia and Replication of the Responses Using iPSC Models

Kirsi Penttinen, Heikki Swan, Sari Vanninen, Jere Paavola, Annukka M. Lahtinen, Kimmo Kontula, Katriina Aalto-Setälä

There are errors in Fig 2, "Features of the PVCs," and its caption. Please see the corrected Fig 2 and its caption here.

Citation: Penttinen K, Swan H, Vanninen S, Paavola J, Lahtinen AM, Kontula K, et al. (2015) Correction: Antiarrhythmic Effects of Dantrolene in Patients with Catecholaminergic Polymorphic Ventricular Tachycardia and Replication of the Responses Using iPSC Models. PLoS ONE 10(7): e0134746. doi:10.1371/journal.pone.0134746

Published: July 31, 2015

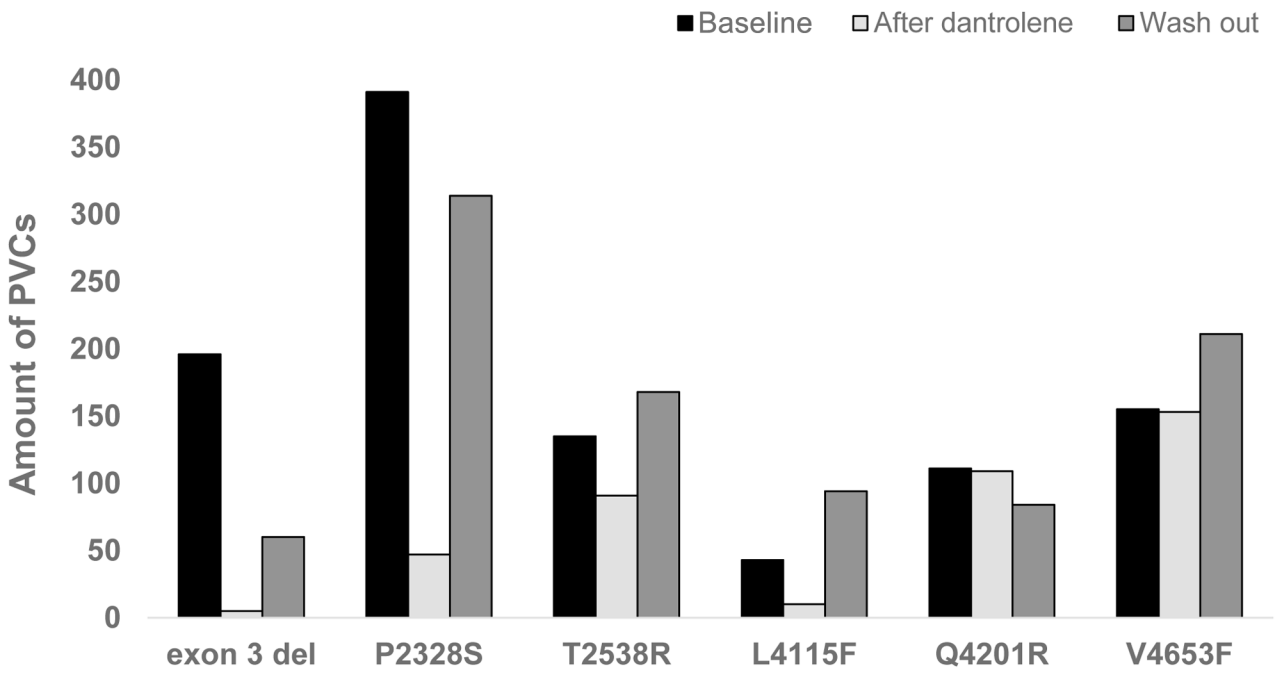

Fig 2. Features of the PVCs. Number of PVCs in exercise stress test before (baseline) and after administration of intravenous dantrolene and 24 hours after dantrolene wash out.

doi:10.1371/journal.pone.0134746.g001

Reference

1. Penttinen K, Swan H, Vanninen S, Paavola J, Lahtinen AM, Kontula K, et al. (2015) Antiarrhythmic Effects of Dantrolene in Patients with Catecholaminergic Polymorphic Ventricular Tachycardia and Replication of the Responses Using iPSC Models. PLoS ONE 10(5): e0125366. doi: 10.1371/journal.pone.0125366 PMID: 25955245

SUPPORTING INFORMATION
STUDY III

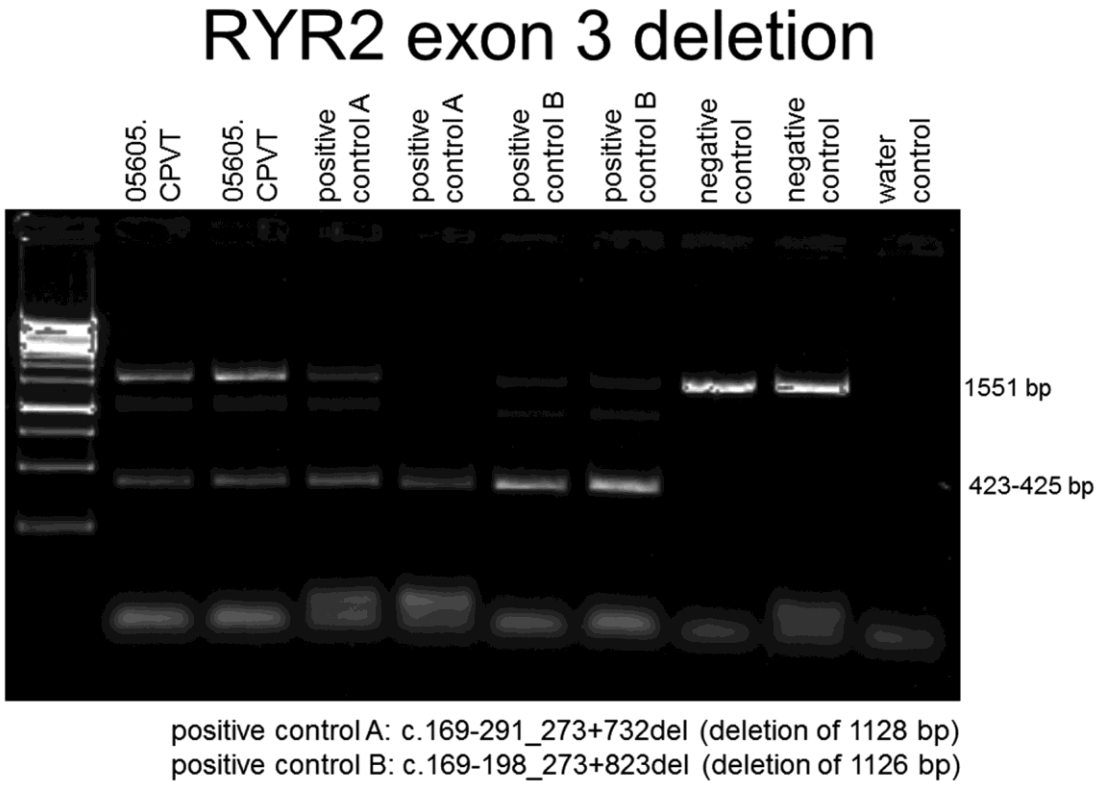

S1 Fig. Confirmation of *exon 3 deletion*. *Exon 3 deletion* of 05605.CPVT cell line was also confirmed with PCR and agarose gel electrophoresis.

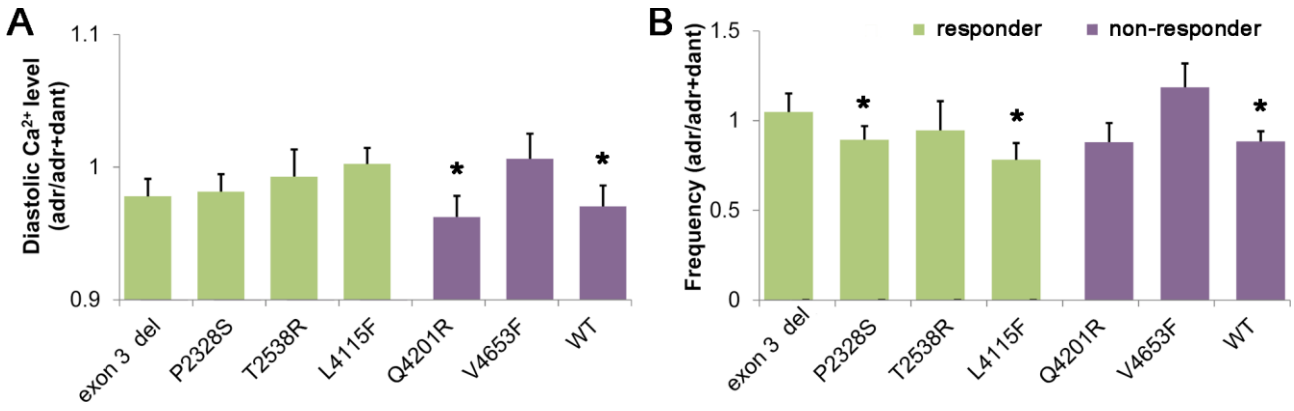

S2 Fig. Ca^{2+} transient parameters as a response to dantrolene. (A) Diastolic Ca^{2+} level and (B) beating frequency in responder and non-responder CMs. Values during adrenaline perfusion were divided by values during dantrolene perfusion, separately for each cell. Green bars indicate responder CMs and purple bars non-responder CMs. Error bars, SEM. * indicates significant difference between adrenaline versus dantrolene within a group, *P<0.05. Numbers of cells analyzed in *exon 3 del* n= 13, *P2328S* n=29, *T2538R* n=11, *L4115F* n=28, *Q4201R* n=15, *V4653F* n=10, Control (WT) n=20.

S1 Protocol. English translated trial study protocol.

Study protocol

Study title: Dantrolene in CPVT

The purpose of the study is to study whether

1. dantrolene has an effect on ventricular arrhythmias induced during stress exercise test in patient carrying different mutations for CPVT
2. dantrolene has an effect on baseline beating rate, conduction or QTc in patient carrying different mutations for CPVT

The following parameters are monitored:

- sinus rhythm at baseline
- the amount of ventricular extrasystole at baseline during 5 minutes
- beating rate, where ventricular extrasystole start to appear during stress exercise test
- The amount of ventricular extrasystole /min during each ramp
- The longest ventricular tachycardia event during each ramp
- QTc interval is measured during baseline, during exercise test and during recovery
- the duration of the exercise test is measured (minutes)
- the beating rate (sinus rhythm) is measured at the end of each ramp
- the maximal beating rate is monitored (sinus rhythm)

Patients to be recruited

For this study 5-6 CPVT patients with a sequenced RyR2 mutation are recruited. Patients to be included have already earlier donated a skin biopsy for iPS cell studies. All the patients are on beta-blocker treatment, usually propranolol 80-160 mg/day or bisoprolol 5-10 mg/day. Other than CPVT, the patients are healthy. All the patients have already earlier participated studies about CPVT and for this study they are contacted either by phone or by a letter, where they will be informed about the study and the potential risks. All the patients will receive written information about the study as well as the informed consent form. The consent form will be signed during the first visit for the study. All participants will be on their regular medication during the entire study. This study does not affect the medication of the participants after

the study. The participants do not benefit from this study at least in the near future, but the study aims at producing new data for future medication.

All the participants are Finnish speaking and they are all over 18 years of age, no pregnant nor lactating individuals are recruited. All the participants have performed earlier stress exercise tests and no problems or complications have been experienced with the previous tests. The following laboratory tests will be analyzed during the the first day before the first exercise test as well as on the morning of the second day: PVK, K, Na, fs-Ca, Krea. During dantrolene test, all the participants have an intra-venous (iv) infusion and thus a route for additional medication if needed during the tests in this proposal. The participants are covered by the insurance of the hospitals.

Exclusion criteria

- Calcium blocker treatment
- Pregnancy
- Any musculoskeletal problem affecting their performance
- Systolic blood pressure over 160 or diastolic over 95 mmHg
- Previously diagnosed coronary artery disease, congenital heart problem, or a pacemaker implanted for bradycardia
- ECG: PQ>200 ms, QRS>120 ms, RV5 or SV1>29 mm, delta-wave

Study protocol

1. day

All the participants take their beta-blocker medication normally in the morning before coming to the hospital. An iv-catheter is placed and saline is infused slowly during exercise test. The participants are in continuous ECG monitoring during all exercise test and during dantrolene infusion as well as 24 hours after the infusion. Blood pressure is monitored regularly with a cuff in the upper arm.

During the first exercise test, participants cycle 30 W + 15W/one minute ramps until about 80% of the maximum beating rate for the age. Due to the beta-blocker medication, it is possible that the desired heart is not reached.

The participants rest for at least 2 hours before the second exercise test. Before that dantrolene is infused 1.5 mg/kg. Dantrolene concentrate (20 mg) is diluted into 60 ml and infused in 5 minutes and thus the whole infusion time is about

30 minutes. The heart rate in continuously monitored for the next 24 hours as well as blood pressure is regularly analyzed.

2. day

The third exercise test is performed (about 18 hours after the second one).

S2 Protocol. Trial study protocol in the original language (Finnish).

14.01.2013

DANTROLEENI KATEKOLIAMIINIHERKÄSSÄ KAMMIOTAKYKARDIASSA

Tutkimus dantroleenin vaikutuksista perinnöllistä monimuotoista kammiotiheälyöntisyyttä sairastavien potilaiden rytmihäiriöiden ilmaantuvuuteen sekä sydämen sähköiseen repolarisaatioon

Koejärjestelyllä pyritään saamaan vastaus seuraaviin kysymyksiin:

- estääkö tai vähentääkö suonensisäisesti annettu kerta-annos dantroleenia kammioperäisten lisälyöntien ilmaantumista submaksimaalisessa rasituksessa perinnöllistä monimuotoista kammiotiheälyöntisyyttä sairastavilla verrattuna ennen lääkkeen antoa vallinneeseen tilaan (beetasalpaajalääkityksen käytössä ollessa)
- vaikuttaako dantroleeni leposykkeeseen, johtumiseen tai QTc-aikaan perinnöllistä monimuotoista kammiotiheälyöntisyyttä sairastavilla

Tutkimuksessa mitataan seuraavia tekijöitä:

- sinustaajuus levossa
- kammiolisälyöntien määrä levossa 5 minuutin aikana
-syketaso, jossa kammiolisälyönnit ilmaantuvat ensi kertaa rasituksen aikana
-kammiolisälyöntien määrä/minuutti kunkin rasitusportaan aikana
-pisimmän perättäisten kammiokompleksien sarjan pituus kunkin rasitusportaan (á 1 min) aikana
-sydämen sähköisen palautumisen muutoksia mitataan lepo-EKG:sta sekä rasituksen ja sitä seuraavan palautumisen aikana rekisteröidystä EKG:sta QT -ajan pituutta seuraamalla.
- rasituksen kesto minuuteissa
- sinustaajuus kunkin kuormaportaan päättyessä
- saavutettu maksimaalinen sinustaajuus

Tutkittavat potilaat

Pilottiluonteiseen tutkimukseen otetaan mukaan 5-6 genotyypiltään tunnettua RYR2 -potilasta, joilla on kliinisesti todettu RYR2 -mutaatiosta johtuva perinnöllinen monimuotoinen kammiotiheälyöntisyys. Ensisijaisesti tutkimukseen kutsutaan potilaita, joista on jo iPS-soluviljelmät *in vitro*-tutkimuksia varten. Tutkimukseen otettavilla on jo käytössään beetasalpaajalääkitys, tavallisesti propranololia 80-160 mg/vrk tai bisoprololia 5-10 mg/vrk ja he ovat perinnöllistä monimuotoista kammiotiheälyöntisyyttä lukuunottamatta muuten terveitä. Tutkittavia, jotka ovat olleet jo tutkimusryhmän muissa tutkimuksissa aiemmin mukana, pyydetään tutkimukseen puhelimitse, jolloin heille selostetaan tutkimuksen kulku ja mahdolliset riskit suullisesti ja heidän alustavan suostumuksensa jälkeen heille toimitetaan kirjallinen informaatio tutkimuksesta postitse. Tutkittavat allekirjoittavat suostumuslomakkeensa tutkimukseen saapuessaan. Tutkittavien hoito jatkuu tutkimuksen ajan ja sen jälkeen ennallaan. Tutkimus ei vaikuta tutkittavien potilaiden hoitoon välittömästi mutta saattaa mahdollistaa täydentävän hoidon käyttöönoton olemassa olevan lisäksi lisätutkimusten jälkeen tutkittaville tai heidän perheenjäsenilleen.

Tutkittavat ovat kaikki suomenkielisiä. Tutkimus ei kohdistu vajaakykyisiin, alaikäisiin, ras-kaana oleviin eikä imettäviin naisiin, eikä vankeihin. Tutkittavissa ei ole muita myöskään muita hen-kilöryhmiä, joiden vapaaehtoisuus voidaan kyseenalaistaa. Tutkittaville on tehty rasituskokeita toistu-vasti aiemmin eikä niiden suorittamiseen ole liittynyt ongelmia tai komplikaatioita. Rasituskokeen yh-teydessä on tavanomaisen komplikaatioiden hoitovalmiuden lisäksi myös nopea mahdollisuus suonen-sisäiseen nesteen- ja lääkkeenantoon tutkimuksen alussa asetettavan laskimokanyylin vuoksi. Tutkit-tavien vakuutusturva sisältyy sairaalalle projektipotilaista maksettaviin käynti- ja toimenpidemaksuihin.

Poissulkukriteereinä on

- kalsiumkanavasalpaaja- tai metoklopramidilääkitys
- raskaus
- liikuntaa rajoittava tuki- ja liikuntaelimistön sairaus
- tarve kuljettaa moottoriajoneuvoa lääkkeen antoa seuraavan vuorokauden aikana
- verenpaine levossa yli 160 (S) tai yli 95 (D)
- aiemmin todettu sepelvaltimotauti, läppävika, synnynnäinen sydänvika, tahdistinhoito
- EKG: PQ>200 ms, QRS>120 ms, RV5 tai SV1>29 mm, delta-aalto

TUTKIMUKSEN KULKU

1. päivä

Tutkittavat ottavat tutkimukseen tullessaan ja tutkimuksen aikana beetasalpaajalääkityksensä tavanomaiseen tapaan. Tutkittavalle asetetaan laskimokanyyli, jonka kautta infusoidaan hitaasti fysiologista keittosuolaa kunkin rasituskokeen aikana. Potilailla on lääkkeiden annon, rasituskokeiden ja niiden jälkeisen palautumisvaiheen ajan jatkuva EKG -seuranta sekä olkavarsimansetilla suoritettava verenpaineseuranta.

Suoritetaan ensimmäinen rasituskoe polkupyöräergometrilla, jossa potilas polkee 30 W + 15 W/1 min portain syketasolle, joka on n. 80 % iänmukaisesta maksimista. Koska potilailla on jo käytössään beetasalpaajalääkitys, saattaa saavutettava syketaso jäädä kuitenkin tätä matalammaksi.
Vähintään 2 tunnin lepotauon jälkeen suoritetaan toinen rasituskoe, jota ennen infusoidaan dantroleenia 1.5 mg/kg. Kukin 20 mg:n infuusiokonsentraattipakkaus laimennetaan 60 ml:n nestemäärään, joka infusoidaan n. 5 minuutissa, jolloin painon mukainen kokonaislääkeannoksen infuusion kesto on n. 30 minuuttia. Tutkittavia seurataan sairaalassa sydämen rytmiä monitoroiden seuraavaan aamuun asti.

3. päivä

Suoritetaan edellä kerrotulla tavalla kolmas rasituskoe (n. 18 tuntia edellisestä).

Tutkimuskeskukset

Tutkimus suoritetaan HYKSin Kardiologian klinikassa Sydäntutkimusosastolla tai Kolmiosairaalan vuodeosastolla (3-4 potilasta) sekä TAYSissä (2 potilasta).

POTILAIDEN JA VERROKKIHENKILÖIDEN SUOSTUMUS

Potilaille ja verrokkihenkilöille kerrotaan tutkimuksen tarkoitus, sen kulku ja mahdolliset haitat suullisesti ja tiedotteella, joka on tämän tutkimussuunnitelman liitteenä. Tutkimuksiin osallistuville ei makseta palkkiota.

TIEDOTE TUTKIMUKSESTA

DANTROLEENI KATEKOLIAMIINIHERKÄSSÄ KAMMIOTAKYKARDIASSA

Sinua pyydetään mukaan tutkimukseen, jonka tarkoituksena on selvittää, vähentääkö sydänlihassolujen kalsiumkanaviin vaikuttava dantroleenilääke rasituksessa ilmeneviä rytmihäiriöitä rytmihäiriösairaudessasi. Olemme arvioineet, että soveltuisit mukaan tutkimukseen, koska sairastat perinnöllistä katekoliamiiniherkkää kammiotakykardiaa (CPVT). Tämä tiedote kuvaa tutkimusta ja osuuttasi siinä.

Osallistumisen vapaaehtoisuus

Osallistuminen tähän tutkimukseen on täysin vapaaehtoista. Voit kieltäytyä osallistumasta tutkimukseen tai keskeyttää osallistumisesi syytä ilmoittamatta milloin tahansa. Sinun ei tarvitse osallistua tähän tutkimukseen saadaksesi hoitoa. Lääkärisi kertoo Sinulle sairautesi hoitovaihtoehdoista. Tutkijalääkäri voi joutua keskeyttämään osallistumisesi. Jos näin tapahtuu, kanssasi keskustellaan lopettamiseen liittyvistä jatkotoimenpiteistä.

Lue rauhassa tämä tiedote. Jos Sinulla on kysyttävää, voi olla yhteydessä tutkijalääkäriin tai tutkimushoitajana. Jos päätät sallistua tutkimukseen, pyydämme Sinua allekirjoittamaan liitteenä olevan suostumuslomakkeen.

Tutkimuksen toteuttaja

Tämän tutkimuksen toteuttavat HYKSin Meilahden sairaalassa dos. Heikki Swan ja TAYSin Sydänkeskuksessa dos Katriina Aalto-Setälä. Tutkimuksen rekisterinpitäjä on dos Heikki Swan tutkimusryhmineen, joka vastaa tutkimuksen yhteydessä tapahtuvan henkilötietojen käsittelyn lainmukaisuudesta.

Tutkimuksen tausta ja tarkoitus

Perinnöllinen polymorfinen kammiotakykardia on harvinainen, pahanlaatuinen rytmihäiriösairaus. Kyseessä on sydämen sähköisen toiminnan häiriö. Rakenteellista sydänvikaa ei ole todettavissa ja levossa tutkittu EKG:kin (sydänfilmi) on tautia kantavilla normaali. Potilaiden rytmihäiriöt ilmenevät tyypillisesti aina syketason noustua tietyn yksilöllisen kynnyksen yläpuolelle. Taudin toteamisessa keskeinen menetelmä onkin rasituskoe, jossa alun normaalin rytmin kiihtyessä rasituksen myötä alkaa ilmaantua kammiolisälyöntisyyttä yhä enenevässä määrin. Rytmihäiriöalttius johtuu sydänlihassolujen sisäisestä kalsiumaineenvaihdunnan häiriöstä.

Oireyhtymää sairastavien potilaiden hoidossa käytetään tavallisesti beetasalpaajalääkitystä, josta on parhaat kokemukset rytmihäiriöiden estossa. Beetasalpaajat ovat lääkkeitä, joita käytetään myös mm. sepelvaltimotautia ja verenpainetautia sairastavien hoidossa. Beetasalpaajat eivät yleensä poista rytmihäiriöiden ilmaantumista rasituksessa mutta kokemukset viittaavat siihen, että alttius pahemmanlaatuisiin rytmihäiriöihin, joiden seurauksena verenkierto saattaisi romahtaa, pienenee. Beetasalpaajalääkityksen aikana on harvoin esiintynyt tajunnanmenetyskohtauksia. Eräät beetasalpaajalääkkeet ovat vasta-aiheisia mm. astmaa sairastavilla. Vain harvoin beetasalpaajalääkitystä ei voida käyttää sen sivuvaikutusten vuoksi.

Tarkoituksenamme on selvittää, vähentääkö sydänlihassolujen kalsiumkanaviin vaikuttava dantroleenilääke rasituksessa ilmeneviä rytmihäiriöitä rytmihäiriösairaudessasi. Mikäli rytmihäiriöiden ilmaantuminen tutkimuslääkkeen antamisen jälkeen olisi vähäisempää kuin beetasalpaajalääkityksen käytössä ollessa, voitaisiin kyseistä lääkettä edelleen tutkimalla mahdollisesti löytää lisälääke niille perinnöllistä monimuotoista kammiotiheälyöntisyyttä sairastaville potilaille, joille beetasalpaajalääkitys ei yksinään ole joko riittävä tai jotka eivät sitä sivuvaikutusten vuoksi voi käyttää.

Tutkimukseen pyydetään mukaan henkilöitä, jotka ovat täysi-ikäisiä ja joilla on RYR2-geenin mutaatiosta johtuva perinnöllinen katekoliamiiniherkkä kammiotiheälyöntisyys ja sen hoidoksi käytössään

beetasalpaajalääkitys mutta ei muita rytmihäiriölääkkeitä eikä muita merkittäviä sydän- ja verisuonisairauksia. Tutkimukseen osallistuu noin 5-6 tutkittavaa.

Tutkimusmenetelmät ja tutkimuksen toimenpiteet

Tutkimukseen osallistuminen kestää runsaan vuorokauden, jonka ajan olet sairaalassa. Ensimmäisenä tutkimuspäivänä otetaan verinäyte ja asetetaan laskimoon muovikanyyli (”tippa”) tutkimuslääkkeiden antoa varten. Ensimmäisenä päivänä suoritat rasituskokeen kahdesti. Ennen toista rasituskoetta, annetaan laskimoon dantroleenilääkettä. Kolmas rasitus-koe tehdään seuraavana päivänä, minkä jälkeen voit kotiutua. Lääkkeen vaikutusta verenpai-neeseen ja sykkeeseen seurataan tutkimuksen aikana EKG:n ja verenpainemittausten avulla.

Käyttämistäsi lääkkeistä tutkimuksen alkaessa sinun tulee ilmoittaa tutkijoille. Tutkimuksen aikana mahdollisesti potilaan tai koehenkilön tarvitsemien muiden lääkkeiden sekä tupakan tai alkoholin käyttöön on pyydettävä tutkijoiden lupa.Tutkimuksen aikana kaikkien hedelmällisessä iässä olevien naisten on käytettävä luotettavaa ehkäisyä. Tutkijalääkäri keskustelee tarvittaessa kanssasi käyttämästäsi ehkäisymenetelmästä. Raskaana olevat, imettävät tai raskautta suunnittelevat naiset eivät voi osallistua tähän tutkimukseen.

Tutkimuksen mahdolliset hyödyt

Dantroleenilääkkeen tutkiminen ei vaikuta välittömästi hoitoosi mutta tutkimus voi auttaa uuden lääkehoidon löytymisessä rytmihäiriöiden ehkäisemiseksi. Tutkittavasta sairaudesta voidaan myös saada hyödyllistä lisätietoa. Saat tietoa terveydentilastasi tutkimuksen aikana tehtävistä lääkärintarkastuksista ja laboratoriokokeista.

Tutkimuksesta mahdollisesti aiheutuvat haitat ja epämukavuudet

Tutkimuksessa tarvittavan laskimokanyylin asettaminen on tavallinen toimenpide sydänpotilaiden tutkimuksessa ja hoidossa mutta joskus toimenpiteeseen saattaa liittyä paikallista kipua tai verenpurkauman muodostumista ihonalaiskudokseen. Lääkkeen sivuvaikutuksena saattaa esiintyä lyhytaikaista lihasvoiman heikentymistä tai paikallista laskimoärsytystä lääkkeenantokohdassa. Rasituskokeeseen liittyvä rytmihäiriöriski on samankaltainen kuin muussakin samalla tavalla kuormittavassa liikunnassa. Mahdollisiin rytmihäiriöongelmiin ja verenpaineen laskuun on varauduttu kuten rasituskoetta suoritettaessa yleensäkin varaudutaan.Tutkijalääkäri voi kertoa Sinulle muista mahdollisista haitoista.

Tutkimuslääkkeen käyttöön saattaa liittyä ennalta tuntemattomia riskejä. Jos tutkimuksen aikana saadaan turvallisuutesi kannalta oleellista uutta tietoa tutkimusvalmisteesta, tutkijalääkäri ottaa Sinuun välittömästi yhteyttä ja keskustelee kanssasi siitä, haluatko edelleen jatkaa tutkimuksessa.

Tietojen luottamuksellisuus ja tietosuoja

Tutkimuksessa henkilöllisyytesi sekä muut tunnistettavat tiedot ovat ainoastaan tutkimuksen henkilökunnan tiedossa, ja he kaikki ovat salassapitovelvollisia. Tutkimukseen liittyvistä tutkimustuloksista, selvityksistä tai julkaisuista ei yksittäisiä tutkittavia voi tunnistaa.

Tutkimusrekisteristä on laadittu henkilötietolain 10 §:n mukainen rekisteriseloste, jonka saat halutessasi nähtäväksi.

Terveydentilaasi koskevia ja tutkimuksen kannalta tarpeellisia tietoja voidaan luvallasi kerätä myös muista terveydenhuollon toimintayksiköistä. Tutkijalääkäri voi tällöin hankkia tarvitsemansa tiedot henkilötunnuksesi avulla. Sinulla on oikeus tarkastaa omat henkilötietosi ja tarvittaessa pyytää niihin korjauksia.

Suomessa lääkevalvontaviranomaisella (Lääkealan turvallisuus- ja kehittämiskeskus Fimea) on oikeus varmistaa, että tutkimustiedot on hankittu ja tutkimus toteutettu asianmukaisella tavalla. Kaikissa tapauksissa tietojasi käsitellään luottamuksellisesti.

Jos osallistumisesi tutkimukseen jostain syystä keskeytyy, keskeyttämiseen mennessä kerättyjä tietoja käytetään osana tutkimusaineistoa ja lääkkeen turvallisuusarviointia.

Tutkimuksen kustannukset ja taloudelliset selvitykset

Tutkimus on Sinulle maksuton. Tutkimuskäynneistä aiheutuvat mahdolliset matkakustannukset korvataan todellisten kustannusten mukaan tositteiden perusteella.

Tutkimus rahoitetaan sairaalan tutkimusmäärärahoista ja Suomen Sydäntutkimussäätiön apurahalla.

Tutkittavien vakuutusturva

Jos tutkimuslääkkeestä tai tutkimuksen takia tehdystä toimenpiteestä aiheutuu Sinulle henkilövahinko, voit hakea korvausta potilasvakuutuksesta. Se korvaa potilasvahinkolain mukaisesti terveyden ja sairaanhoidon yhteydessä aiheutuneita henkilövahinkoja laissa tarkemmin säädellyin edellytyksin. Potilasvakuutuskeskus huolehtii potilasvahinkojen korvauskäsittelystä.

Tutkimuksen päättyminen

Hoitosi jatkuu nykyisellään tutkimuksen jälkeen. Tarvittaessa tutkijalääkäri keskustelee kanssasi hoidostasi tutkimuksen päättymisen jälkeen.

Lisätietoja

Jos Sinulla on kysyttävää tutkimuksesta, voit olla yhteydessä tutkijalääkäriin tai muuhun tutkimuksen henkilökuntaan. Heidän kanssaan voit keskustella kaikista tutkimuksen aikana mahdollisesti ilmenneistä haittavaikutuksista, epäilyttävistä oireista ja muista mieltäsi askarruttavista asioista.

Tutkimukseen liittyvissä asioissa yhdyshenkilönä on Meilahden sairaalassa dos. Heikki Swan, HYKS Sydäntutkimusosasto, Haartmanink. 4, 00290 Helsinki, puhelin 050-4286591 tai 09-4711, Tampereen Yliopistosairaalassa dos. Katriina Aalto-Setälä, TAYS Sydänkeskus, Biokatu 6, 33520 Tampere, puhelin03 - 311 66088 tai 040-5829567.

SUOSTUMUS LÄÄKETUTKIMUKSEEN

Minua on pyydetty osallistumaan dantroleeni-lääkkeellä suoritettavaan rytmihäiriöiden hoitotutkimukseen.

Olen saanut, lukenut ja ymmärtänyt tutkimuksesta kertovan tiedotteen 23.11.2012. Tiedotteesta olen saanut riittävän selvityksen tutkimuksesta (dantroleeni katekoliamiiniherkässä kammiotakykardiassa) ja sen yhteydessä suoritettavasta tietojen keräämisestä, käsittelystä ja luovuttamisesta. Tiedotteen sisältö on kerrottu minulle myös suullisesti ja olen saanut riittävän vastauksen kaikkiin tutkimusta koskeviin kysymyksiini. Tiedot antoi _____ , ___/___/ 20__ . Minulla on ollut riittävästi aikaa harkita osallistumistani tutkimukseen.

Minulle kerrotaan, mistä minua koskevia tietoja hankitaan. Annan luvan itseäni koskevien, tutkimuksen kannalta tarpeellisten tietojen keräämiseen perinnöllisten rytmihäiriösairauksien tutkimusrekisteriin. Tietoja voidaan lääketutkimuksen sitä edellyttäessä pyytää niistä terveydenhoitopaikoista, joissa on potilastietojani. Tätä tarkoitusta varten lääkäri saa kirjata henkilötunnukseni sekä käyttää sitä tietojen saamiseksi.

Kaikki minusta tutkimuksen aikana kerättävät tiedot käsitellään luottamuksellisina.

Lääkevalvonnasta ja –turvallisuudesta vastaavan viranomaisen, Suomessa Lääkealan turvallisuus- ja kehittämiskeskus Fimean edustajilla on oikeus varmistaa tutkimustietojen totuudenmukaisuus ja tutkimuksen asianmukainen suorittaminen. Tämä tapahtuu vertaamalla tutkimustietoja alkuperäisiin sairaskertomuksiini ja terveydentilaani koskeviin tietoihin. edellä mainitut tahot ovat velvollisia pitämään tiedot salassa.

Tässä tutkimuksessa kerättäviä tietoja voidaan käsitellä muualla kuin tiedot keränneen tutkijalääkärin tiloissa ja laitteissa. Tällöin tiedot ovat koodatussa muodossaan.

Tässä lääketutkimuksessa kerättävä tieto voi olla hyödyksi myös selvitettäessä dantroleeni-lääkkeen uutta käyttötarkoitusta, josta tämän suostumuksen antamisen hetkellä ei ole tietoa. Hyväksyn, että minusta kerättäviä tietoja voidaan viranomaisen luvalla käyttää tällaiseen tarkoitukseen.

Ymmärrän, että osallistumiseni tähän tutkimukseen on täysin vapaaehtoista. Minulla on oikeus milloin tahansa tutkimuksen aikana ja syytä ilmoittamatta keskeyttää tutkimukseen osallistuminen. Tutkimuksesta kieltäytyminen tai sen keskeyttäminen ei vaikuta jatkohoitooni. Olen tietoinen siitä, että minusta keskeyttämiseen mennessä kerättyjä tietoja käytetään osana tutkimusaineistoa ja lääkkeen turvallisuusarviointia.

Allekirjoituksellani vahvistan osallistumiseni tähän tutkimukseen ja suostun vapaaehtoisesti tutkimushenkilöksi.

_____ _____

Allekirjoitus Päiväys

_____ _____

Nimen selvennys Syntymäaika

_____

Osoite

Suostumus vastaanotettu

_____ _____

Tutkijalääkärin allekirjoitus Päiväys

_____

Nimen selvennys

Alkuperäinen allekirjoitettu tutkimushenkilön suostumus sekä kopio tutkimushenkilötiedotteesta jäävät tutkijalääkärin arkistoon. Tutkimushenkilötiedote ja kopio allekirjoitetusta suostumuksesta annetaan tutkimushenkilölle.

Kirjallisuus

Swan H, Laitinen PJ. Familial polymorphic ventricular tachycardia - intracellular calcium channel disorder. Cardiac Electrophysiol Rev 2002;6:81-7.

Laitinen P, Brown KM, Piippo K, et al. Mutations of the cardiac ryanodine receptor (RyR2) gene in familial polymorphic ventricular tachycardia. Circulation 2001;103:485-90.

Priori SG, Napolitano C, Tiso N, et al. Mutations in the cardiac ryanodine receptor gene (hRyR2) underlie catecholaminergic polymorphic ventricular tachycardia. Circulation 2001;103:196-201.

Lahat H, Pras E, Olender T, et al. A missense mutation in highly conserved region of CASQ2 is associated with autosomal recessive catecholamine-induced polymorphic ventricular tachycardia in Bedouin families from Israel. Am J Hum Genet 2001;69:1378-84.

Wappler F. Malignant hyperthermia. Eur J Anaesthesiol 2001;18:632-52.

Paavola J, Viitasalo M, Laitinen-Forsblom PJ, Pasternack M, Swan H, Tikkanen I, Toivonen L, Kontula K, Laine M. Mutant ryanodine receptors in catecholaminergic polymorphic ventricular tachycardia generate delayed afterdepolarizations due to increased propensity to Ca2+ waves. Eur Heart J. 2007 May;28(9):1135-42.

Liu N, Rizzi N, Boveri L, Priori SG. Ryanodine receptor and calsequestrin in arrhythmogenesis: what we have learnt from genetic diseases and transgenic mice. J Mol Cell Cardiol. 2009;46:149–159.

Suetomi T, Yano M, Uchinoumi H, Fukuda M, Hino A, Ono M, Xu X, Tateishi H, Okuda S, Doi M, Kobayashi S, Ikeda Y, Yamamoto T, Ikemoto N, Matsuzaki M. Mutation-linked defective interdomain interactions within ryanodine receptor cause aberrant Ca^{2+}release leading to catecholaminergic polymorphic ventricular tachycardia. Circulation. 2011 Aug 9;124(6):682-94.

Jung CB, Moretti A, Mederos y Schnitzler M, Iop L, Storch U, Bellin M, Dorn T, Ruppenthal S, Pfeiffer S, Goedel A, Dirschinger RJ, Seyfarth M, Lam JT, Sinnecker D, Gudermann T, Lipp P, Laugwitz KL. Dantrolene rescues arrhythmogenic RYR2 defect in a patient-specific stem cell model of catecholaminergic polymorphic ventricular tachycardia. EMBO Mol Med. 2012 Mar;4(3):180-91.

Parness J, Palnitkar SS. Identification of dantrolene binding sites in porcine skeletal muscle sarcoplasmic reticulum. J Biol Chem 1995;270:18465-72.

Kentsch M, Roewer N, Kunze K-P, Kuck K-H. Intravenous dantrolene does not exhibit calcium channel blocking effects on the caddiac conduction system in humans. Anesthesiology 1991;75:583-7.

Kim JY, Chun S, Bang MS, Shin HI, Lee SU. Safety of low-dose oral dantrolene sodium on hepatic function. Arch Phys Med Rehabil. 2011 Sep;92:1359-63.

Flewellen EH, Nelson TE, Jones WP, Arens JF, Wagner DL. Dantrolene dose response in awake man: implications for management of malignant hyperthermia. Anesthesiology 1983; 59: 275-80.

Brandom BW, Larach MG, Chen MSA, Young MC. Complications associated with the administration of dantrolene 1987 to 2006: a report from the North American malignant hyperthermia registry of the malignant hyperthermia association of the United States. Anesth Analg 2011; 112: 1115-1123.

S1 Table. Primer sequences for EB RT-PCR.

Gene	Forward Primer	Reverse Primer
Endodermal		
AFP	AGAACCTGTCACAAGCTGTG	GACAGCAAGCTGAGGATGTC
SOX-17	CGCACGGAATTTGAACAGTA	CACACGTCAGGATAGTTGCAG
Ectodermal		
Nestin	CAGCTGGCGCACCTCAAGATG	AGGGAAGTTGGGCTCAGGACTGG
SOX-1	AAAGTCAAAACGAGGCGAGA	AAGTGCTTGGACCTGCCTTA
Mesodermal		
VEGF-R2	GGAGTTATGGTGGGTATGGGTC	AGTGGTGACAAAGGAGTAGCCA

S2 Table. Differences between RyR2 mutations in their Ca^{2+} transient properties during baseline and adrenaline perfusion. CL indicates cluster numbers. Upward pointing arrow indicates significantly ($p<0.05$) higher and downward pointing arrow significantly lower diastolic Ca^{2+} level or beating frequency of the first mentioned mutation when compared to the second mentioned mutation. NS indicates that there was no statistical significance between mutations. As parallel pointing arrows between comparison groups indicate, the average of the beating frequency and diastolic Ca^{2+} level inside one mutation group corresponded and the average of these parameters decrease when moving from P2328S towards transmembrane area mutations.

			BASELINE		ADRENALINE	
	CLUSTERS	**MUTATIONS**	**Diastolic Ca^{2+} level**	**Beating frequency**	**Diastolic Ca^{2+} level**	**Beating frequency**
Exon 3 deletion versus point mutations	CL 1 vs. CL 2	exon 3 del vs. P2328S	↓	↓	↓	↓
	CL 1 vs. CL2-3	exon 3 del vs. T2538R	↓	↓	↓	↓
	CL 1 vs. CL 3	exon 3 del vs. L4115F	↓	↓	↓	↓
	CL 1 vs. CL3	exon 3 del vs. Q4201R	↓	↓	↓	↓
	CL 1 vs. CL 4	exon 3 del vs. V4653F	NS	↓	NS	↓
Comparison of point mutations exceeding towards transmembrane area	CL 2 vs. CL 2-3	P2328S vs. T2538R	NS	NS	↑	↑
	CL 2 vs. CL 3	P2328S vs. L4115F	↑	↑	↑	↑
	CL 2 vs. CL 3	P2328S vs. Q4201R	↑	↑	↑	↑
	CL 2 vs. CL 4	P2328S vs. V4653F	↑	↑	↑	↑
	CL 2-3 vs. CL 3	T2538R vs. L4115F	↑	NS	↑	NS
	CL 2-3 vs. CL 3	T2538R vs. Q4201R	↑	↑	↑	NS
	CL 2-3 vs. CL 4	T2538R vs. V4653F	↑	NS	↑	NS
	CL 3 vs. CL 3	L4115F vs. Q4201R	NS	NS	NS	NS
	CL 3 vs. CL 4	L4115F vs. V4653F	↑	NS	↑	NS
	CL 3 vs. CL 4	Q4201R vs. V4653F	↑	NS	↑	NS

Study IV

Penttinen K, Siirtola H, Ávalos-Salguero J, Vainio T, Juhola M, Aalto-Setälä K

Novel Analysis Software for Detecting and Classifying Ca^{2+} Transient Abnormalities in Stem Cell-Derived Cardiomyocytes

PLoS One. 2015 Aug 26;10(8):e0135806

PLOS | ONE

RESEARCH ARTICLE

Novel Analysis Software for Detecting and Classifying Ca^{2+} Transient Abnormalities in Stem Cell-Derived Cardiomyocytes

Kirsi Penttinen[1,2]*, Harri Siirtola[3], Jorge Àvalos-Salguero[3], Tiina Vainio[3], Martti Juhola[4], Katriina Aalto-Setälä[1,2,5]

1 BioMediTech, University of Tampere, Tampere, Finland, **2** School of Medicine, University of Tampere, Tampere, Finland, **3** Tampere Unit for Computer-Human Interaction, University of Tampere, Tampere, Finland, **4** Research Center for Information and Systems, University of Tampere, Tampere, Finland, **5** Heart Center, Tampere University Hospital, Tampere, Finland

* kirsi.penttinen@uta.fi

OPEN ACCESS

Citation: Penttinen K, Siirtola H, Àvalos-Salguero J, Vainio T, Juhola M, Aalto-Setälä K (2015) Novel Analysis Software for Detecting and Classifying Ca^{2+} Transient Abnormalities in Stem Cell-Derived Cardiomyocytes. PLoS ONE 10(8): e0135806. doi:10.1371/journal.pone.0135806

Editor: Derek Laver, University of Newcastle, AUSTRALIA

Received: March 11, 2015

Accepted: July 27, 2015

Published: August 26, 2015

Data Availability Statement: The AnomalyExplorer conforms to the Open Source Definition and has been designed to facilitate the abnormality analysis of Ca2+ recordings obtained from CMs. Website for downloading the program: (https://github.com/siirtola/AnomalyExplorer). More information about the software can be found from S1 Supporting Information. All other relevant data are within the paper and its Supporting Information files.

Funding: This work was supported by TEKES (http://www.tekes.fi/), Biocenter Finland (http://www.biocenter.fi/), the Finnish Cultural Foundation (https://

Abstract

Comprehensive functioning of Ca^{2+} cycling is crucial for excitation–contraction coupling of cardiomyocytes (CMs). Abnormal Ca^{2+} cycling is linked to arrhythmogenesis, which is associated with cardiac disorders and heart failure. Accordingly, we have generated spontaneously beating CMs from induced pluripotent stem cells (iPSC) derived from patients with catecholaminergic polymorphic ventricular tachycardia (CPVT), which is an inherited and severe cardiac disease. Ca^{2+} cycling studies have revealed substantial abnormalities in these CMs. Ca^{2+} transient analysis performed manually lacks accepted analysis criteria, and has both low throughput and high variability. To overcome these issues, we have developed a software tool, *AnomalyExplorer* based on interactive visualization, to assist in the classification of Ca^{2+} transient patterns detected in CMs. Here, we demonstrate the usability and capability of the software, and we also compare the analysis efficiency to manual analysis. We show that *AnomalyExplorer* is suitable for detecting normal and abnormal Ca^{2+} transients; furthermore, this method provides more defined and consistent information regarding the Ca^{2+} abnormality patterns and cell line specific differences when compared to manual analysis. This tool will facilitate and speed up the analysis of CM Ca^{2+} transients, making it both more accurate and user-independent. *AnomalyExplorer* can be exploited in Ca^{2+} cycling analysis to study basic disease pathology and the effects of different drugs.

Introduction

Calcium (Ca^{2+}) cycling plays an essential role in the excitation-contraction coupling of cardiomyocytes (CMs) and is therefore vital for cardiac functionality. However, cardiac diseases and different drugs can cause changes and variability in Ca^{2+} cycling that can affect the function and phenotype of CMs. Characterizing these disturbances and abnormalities is vital to improving the studies of the disease pathology and disease prevention and treatment. Intracellular

www.skr.fi/en), the Finnish Cardiovascular Foundation (http://www.sydantutkimussaatio.fi/welcome-to-the-finnish-foundation-for-cardiovascular-research/?lang = en), Pirkanmaa Hospital District (EVO) funding (http://www.tays.fi/default.aspx?contentid=2488), the Council of Tampere Region (http://www.pirkanmaa.fi/en/home/council-tampere-region), the European Regional Development Fund (http://europa.eu/legislation_summaries/agriculture/general_framework/g24234_en.htm), Ida Montin Foundation (http://www.idamontininsaatio.fi/pages/suomi/etusivu.php), the Aarne Koskelo Foundation (http://www.aarnekoskelonsaatio.fi/) and the Orion-Farmos Research Foundation (http://www.orion.fi/tutkimus/orionin-tutkimussaatio/). The funders had no role in study design, data collection and analysis, decision to publish, or preparation of the manuscript.

Competing Interests: A patent application "FI20145358—Calcium cycling analysis" related to calcium cycling analysis has been filed by Kirsi Penttinen and Katriina Aalto-Setälä. This patent does not alter the authors' adherence to PLOS ONE policies on sharing data and materials. The authors have no competing interests.

Ca^{2+} cycling of CMs is analyzed *in vitro* with Ca^{2+} sensitive dyes that change their fluorescence properties when binding to Ca^{2+} ions.

Induced pluripotent stem cell (iPSC) technology, in which pluripotent stem cells are generated by reprogramming differentiated cells back into the pluripotent state, provides a method for studying the pathophysiology of various disorders in human cells.[1] iPSCs can be differentiated into the desired cell type and retain the original genotype. New insights into the Ca^{2+} cycling of different cardiac diseases have been achieved since the invention of iPSC technology. The functionality of CMs and their drug responses could be studied more thoroughly with investigation of Ca^{2+} transients. Disease modeling with iPSCs has been successfully exploited to study cardiac diseases such as catecholaminergic polymorphic ventricular tachycardia (CPVT) [2–9], dilated cardiomyopathy [10], hypertrophic cardiomyopathy [11,12] and Timothy syndrome [13]. In these studies, Ca^{2+} cycling analyses have revealed substantial defects and abnormalities in CMs that reflect the cardiac phenotype observed in patients. However, analyzing these Ca^{2+} transient abnormalities, which consist of cycling patterns that vary in shape and frequency, is difficult, and their quantification is very challenging. To the best of our knowledge, Ca^{2+} cycling abnormality patterns have thus far only been subjectively analyzed based on visual information, which is labor-intensive, slow and often user-dependent. Manual data analysis performed with visual recognition is also a bottleneck for high-throughput screening and can occasionally be unreliable because of the poor quality of the Ca^{2+} transients. Having general criteria for Ca^{2+} cycling abnormality analysis could simplify the comparison between different studies and facilitate the analysis of Ca^{2+} cycling parameters. In addition, an automated Ca^{2+} cycling classification software would be beneficial for the future analysis of Ca^{2+} cycling of CMs on a large scale to screen for adverse cardiac effects of new potential compounds.

The aim of the study was to develop and test a Ca^{2+} cycling abnormality analysis software based on interactive visualization with a direct manipulation user interface (UI). The software, *AnomalyExplorer*, can user-independently assist in the classification of the Ca^{2+} transient patterns detected in CMs by using criteria that are similar to those used in manual analyses that are performed with visual recognition. We demonstrate the usability and capability of the software using iPSC-derived CMs that were generated from patients with cardiac ryanodine receptor (RyR2) gene mutations causing CPVT. Opening of RyR2 Ca^{2+} channels underlies intracellular Ca^{2+} release from the sarcoplasmic reticulum in CMs. CPVT is an exercise-induced arrhythmogenic cardiac disease with intracellular Ca^{2+} cycling defects [14]; therefore, CPVT-specific CMs [5,9] are suitable for evaluating this program. The usability of the *AnomalyExplorer* is demonstrated with the data generated by two different Ca^{2+} imaging recording software programs with different sampling frequencies. The analysis of data using *AnomalyExplorer* is compared with the manual analysis results to establish the reliability of the analysis software. This software tool will improve the accuracy, reliability and throughput rate for Ca^{2+} cycling data analysis.

Materials and Methods

Generation of patient-specific iPSCs and cardiac differentiation

The study was approved by the ethical committee of Pirkanmaa Hospital District (R08070). Patient-specific iPSC lines were established as described earlier and written informed consent was obtained from all the participants.[1] The studied RyR2 mutated CPVT cell lines were UTA.05605.CPVT, generated from a patient with exon 3 deletion (c.168–301_c.273+722del1128 mutation); UTA.05208.CPVT, generated from a patient with a p.P2328S (c.6982C>T) mutation; UTA.07001.CPVT, from a patient with a p.T2538R (c.7613C>G) mutation; UTA.03701.CPVT, from a patient with a p.L4115F (c.12343C>T) mutation;

UTA.05503.CPVT, from a patient with a p.Q4201R (c.12602A>G) mutation; and UTA.05404.CPVT, from a patient with a p.V4653F (c.13957G>T) mutation. UTA.04602.WT cell line was generated from a healthy control. Mutation nomenclature was based on RyR2 reference sequence NM_001035.2. The results of the characterization of iPSC lines have been previously described.[5,9] For illustration of the RyR2 protein and locations of the mutations, see [9].

Differentiation into CMs was performed by co-culturing iPSCs with murine visceral endoderm-like (END-2) cells (Humbrecht Institute, Utrecht, The Netherlands) as previously described.[15] For Ca^{2+} cycling measurements, CMs were dissociated by mechanically excising the beating areas of the cell colonies and treating them with collagenase A (Roche Diagnostics) [15].

Ca^{2+} imaging recordings and data analysis

Ca^{2+} imaging was conducted in spontaneously beating Fura-2 AM (Life Technologies, Molecular Probes) loaded, dissociated CMs that were perfused with extracellular solution as previously described.[5] Ca^{2+} measurements were performed on an inverted IX70 microscope (Olympus Corporation, Hamburg, Germany) and CMs were visualized with a UApo/340 x20 air objective (Olympus). Images were recorded with an ANDOR iXon 885 CCD camera (Andor Technology, Belfast, Northern Ireland) that was synchronized with a Polychrome V light source by a real-time DSP control unit and TillVision (TILL Photonics, Munich, Germany) or Live Acquisition software (FEI, OR, USA). TillVision and LiveAcquisition are further referred as Recording Software 1 and 2, respectively. Fura-2 AM in CMs was excited at 340 nm and 380 nm light and the emission was recorded at 505 nm. For Ca^{2+} analysis, regions of interest were selected for spontaneously beating cells and background noise was subtracted before further data processing. The Ca^{2+} transients were acquired as the ratio of the emissions at 340/380 nm wavelengths and presented as Fura-2 ratio units of F340/F380. Throughout the remainder of this manuscript, the Ca^{2+} recording of a single cell is called the Ca^{2+} signal.

The data were generated with two separate softwares (Recording Software 1 and 2) with different sampling frequencies that affected the noise level of the recordings. Therefore, the Ca^{2+} signals were divided into two groups and analyzed separately depending on the recording software. The Ca^{2+} signals were manually analyzed with visual recognition by identifying the signals as normal or abnormal and categorizing the abnormalities into six subgroups according to their abnormality patterns. In manual analysis, a criterion for the double peak group was a Ca^{2+} peak with paired peaks that did not reach the baseline. Oscillation was detected if Ca^{2+} fluctuated for three or more peaks without reaching the baseline. For the low peaks group, the presence of a small amplitude Ca^{2+} peak of at least 10% of the preceding Ca^{2+} peak amplitude was required. In the middle Ca^{2+} peaks, 30 to 80% amplitude of the preceding Ca^{2+} peak amplitude was required. Plateau abnormality was detected if the rise or decay time of the Ca^{2+} peak was prolonged, and an irregular beating rhythm was required for the irregular phase group. Here, the Ca^{2+} peak represents a Ca^{2+} transient consisting of Ca^{2+} rise and decay. For comparison studies, the Ca^{2+} data was analyzed with *AnomalyExplorer*, in which suitable user-defined percentage limits for each abnormality subgroup were selected for both recording software data groups.

Software tool description

AnomalyExplorer is an interactive software tool that can assist in the visual classification of Ca^{2+} signals. It is based on the information visualization approach with the following two major components: representation of data and interaction with the data. The representation component of *AnomalyExplorer* is based on the detail+overview design pattern, and an

overview and detailed view of an information space are displayed simultaneously. Generally, the overview provides a high-level view of the information space, and the detailed view shows the current focus of interest in full detail.

The detailed view in *AnomalyExplorer* is a conventional 2D plot of the signal value over time. The plot is similar to what a human observer would use to detect anomalies in the shape of a signal. The idea in *AnomalyExplorer* is to express the human observer's criteria for abnormality as rules that can be programmed into *AnomalyExplorer*. The tool then highlights the detected anomalies in a plot, which allows the user to adjust the sensitivity of anomaly detection by user-defined parameters for signal noise and six different abnormality subgroups.

The most important qualitative aspect in *AnomalyExplorer* is to define whether the signal is normal or not, and to further analyze the quality and distribution of detected anomalies. Thus, the overview in *AnomalyExplorer* was designed to be a stacked bar chart of detected anomalies where a bar represents the number of anomalies in a signal, and stacking shows how the anomalies are distributed. Only the abnormal signals are present in the bar chart because the signals deemed normal are not of interest. Information in such a bar chart can be acquired rapidly, and the conventional representation allows for further insight-generating interactions.

User interface (UI). Fig 1 shows the UI of *AnomalyExplorer* and illustrates the workflow. The current UI design has the following elements: a file chooser to open the signals that will undergo analysis, the stacked bar chart of observed anomalies (overview), dynamic controllers for the anomaly detection sensitivity, and the currently open set of detailed signal views. After these main components there is a section showing how the currently open signals are classified as normal and abnormal (as two text lists, not shown in the Fig 1), and a text view summarizes the anomalies found in the current set.

The designed workflow with *AnomalyExplorer* starts by choosing the signal files that will undergo analysis. The open file dialog allows for the selection of a single file, multiple files, or all of the files in the current directory. *AnomalyExplorer* then updates the overview to show the anomalies with the current default settings. Subsequently, the user may open one or more signals in the detailed view for closer inspection by clicking on a file name of the signal above the detailed view (Fig 1D) or if the signal includes anomalies, also by clicking a bar in the overview (Fig 1B). User can also adjust the dynamic controllers for the anomaly detection, observe the changes in both the overview and detailed view, and sort the overview according to any of the abnormality subgroup. The manipulation of dynamic controllers is immediately reflected in both the overview and detailed view and allow for a rapid what-if exploration of anomaly thresholds. When the satisfactory user-defined parameters for anomaly detection of a certain data set are found, the *AnomalyExplorer* tool can be used as a rapid user-independent classifier. The preset values of dynamic controllers serve only as a starting point to seek the best parameter set for the current data set. Once the parameter values that correspond the analyst's view of the anomalies are found, the presets can easily be made default to facilitate easy classification of multiple files without changing the parameters.

Anomaly detection. *AnomalyExplorer* is designed to detect the anomalies in the same fashion as a human observer. The automated analysis software is based on the concepts of sections and regression lines, which act as points of reference for the rules defining the anomaly subgroups. A section is a part of a signal which ascends or descends monotonously; it thus marks and separates the Ca^{2+} rise and decay, which together comprise a Ca^{2+} transient. Sections allow for a small amount of noise in the signal. The noise threshold determines how much the signal may exhibit direction changes without considering it to be a change in monotonous movement. The regression lines are needed as a reference for the anomaly rules because the amplitude of a Ca^{2+} signal may fade over time from the Ca^{2+} indicator photobleaching. The software uses the following three regression lines (Fig 1): one that approximates the

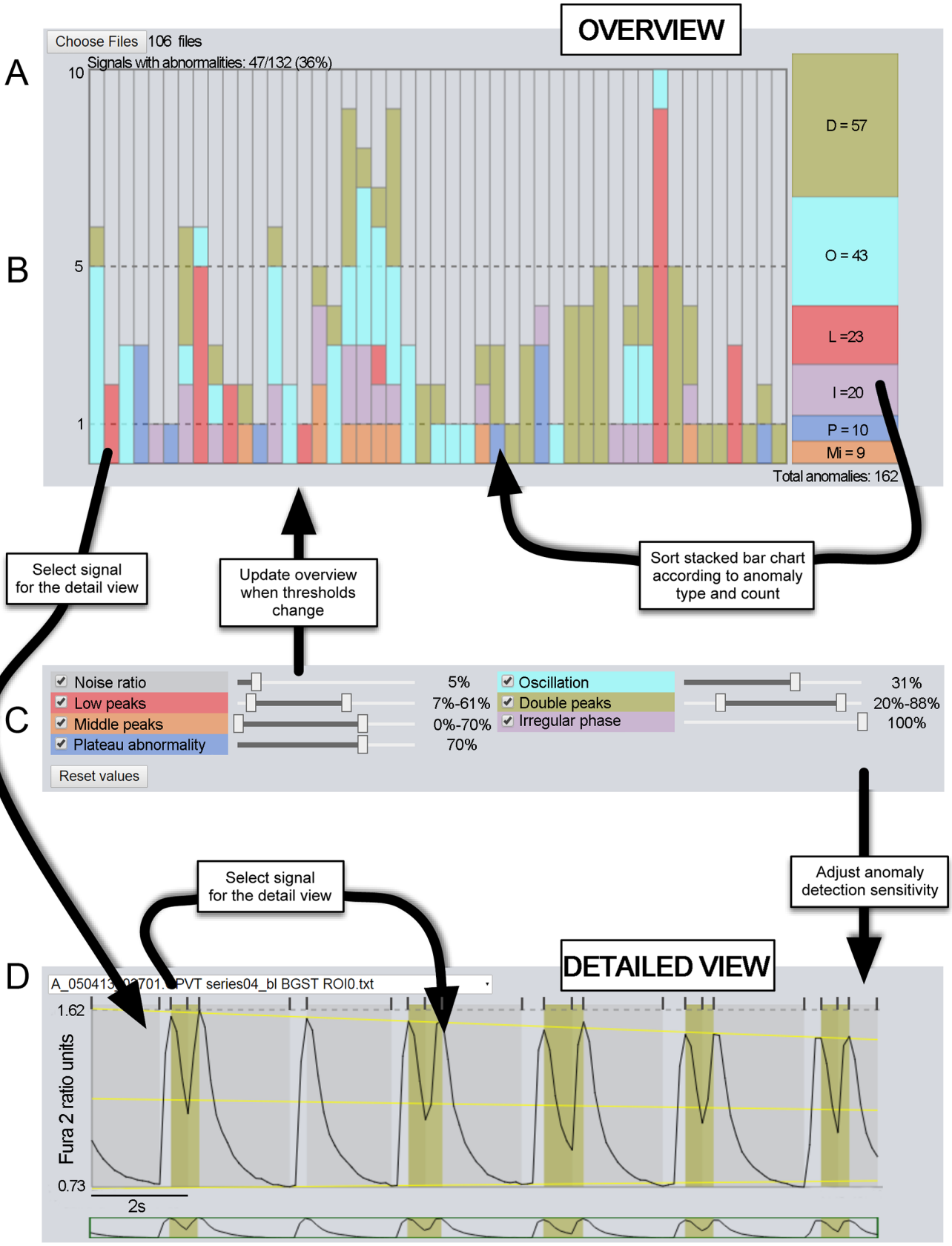
OVERVIEW
A
B
Choose Files
106 files
Signals with abnormalities: 47/132 (36%)
10
5
1
D = 57
O = 43
L =23
I =20
P = 10
Mi = 9
Total anomalies: 162
Select signal for the detail view
Update overview when thresholds change
Sort stacked bar chart according to anomaly type and count
C
Noise ratio
Low peaks
Middle peaks
Plateau abnormality
5%
7%-61%
0%-70%
70%
Oscillation
Double peaks
Irregular phase
31%
20%-88%
100%
Reset values
Adjust anomaly detection sensitivity
Select signal for the detail view
D
DETAILED VIEW
1.62
Fura 2 ratio units
0.73
2s

Fig 1. *AnomalyExplorer* program. A) Overview of the software. B) Each bar presents a single Ca^{2+} signal of a single cell and shows the distribution of abnormality patterns in the recording. The total number of anomalies in all of the files can be observed on the right. C) Dynamic controllers for the anomaly detection. D) The detailed view of one Ca^{2+} signal plot showing color-coded anomalies detected with the help of three yellow regression lines (top, bottom and middle) and the sections subsequently rising and decaying separated with small grey vertical lines above the signal showing how the Ca^{2+} transients ascend (light bars) and descend (dark bars).

doi:10.1371/journal.pone.0135806.g001

signal's local maximum (in a transient, top), another for signal's local minimum (bottom), and a third one that is averaged from these two, which approximates the local middle of the signal (middle). The computation of the simple linear regression lines is based on the local maximum and minimum data values in each section, and it is meant to approximate how a human observer would place them. In addition to the regression height, the section heights are also used in the computations. The section height is simply the data range in the section (i.e., the local maximum data value minus the local minimum data value), and the regression height is the distance between the top and bottom regression lines in the current section. With these reference values the anomaly subgroups can be defined. In addition, the anomaly definitions refer to predefined and user-defined parameters. The predefined ones are implementation-dependent constants and the user-defined are values that can be manipulated via the UI to correspond to Ca^{2+} measurement settings such as the frame-rate of the recordings.

The current implementation of *AnomalyExplorer* detects the following six abnormality subgroups: low, middle, oscillating and double peak anomalies as well as irregular phase and plateau abnormality (Fig 2).[16] Each of these anomaly subgroups are described in more detail below. User-defined parameters can be manipulated by using the dynamic controllers in the UI.

An ascending signal section is flagged to have a *low peak* (Fig 2) if the following conditions are met: 1) the transient minimum value is within 15% of the local regression height from the local bottom regression line, 2) the transient maximum value is between user-defined percentage limits of the local regression height, and 3) the previous and the following transient do not contain double peak anomalies. Once the ascending section is classified as a low peak, the following descending section is also flagged as a low peak if its minimum value is within ±10% of the current section's minimum, i.e., the peak is fairly symmetrical.

The *middle peak anomaly* (Fig 2) is flagged if the following conditions are met: 1) the section height is within the user-defined percentage limits of the local regression height, 2) the transient maximum value is within 60% of the local middle regression line, 3) the transient minimum value is within 40% of the local middle regression line, 4) the section height is less than 75% of the height of the surrounding sections, and 5) there is no low peak anomaly in the previous or this section.

When determining the *oscillation* (Fig 2) of the Ca^{2+} signal the software compares the section and transient heights and lengths, and the consecutive transients that are dwarfed below the user-defined percentage limit are flagged as oscillating. The oscillating transients are not analyzed for any further anomalies. Oscillations can also be generated by a double peak anomaly, which is discussed below.

A *double peak anomaly* (Fig 2) is flagged if the transient does not descend sufficiently low before ascending to the next peak, such that only the descending sections are considered. The double peak anomaly is flagged if the following conditions are met: 1) the section maximum value is within 40% of the section height of the local top regression line, 2) the height of the section is within user-defined percentage limit of the local regression height, 3) the upper percentage limit determines how deep the double peak can be (where 100% is the local bottom regression line and 50% is the local middle regression line), and 4) the height of the section is

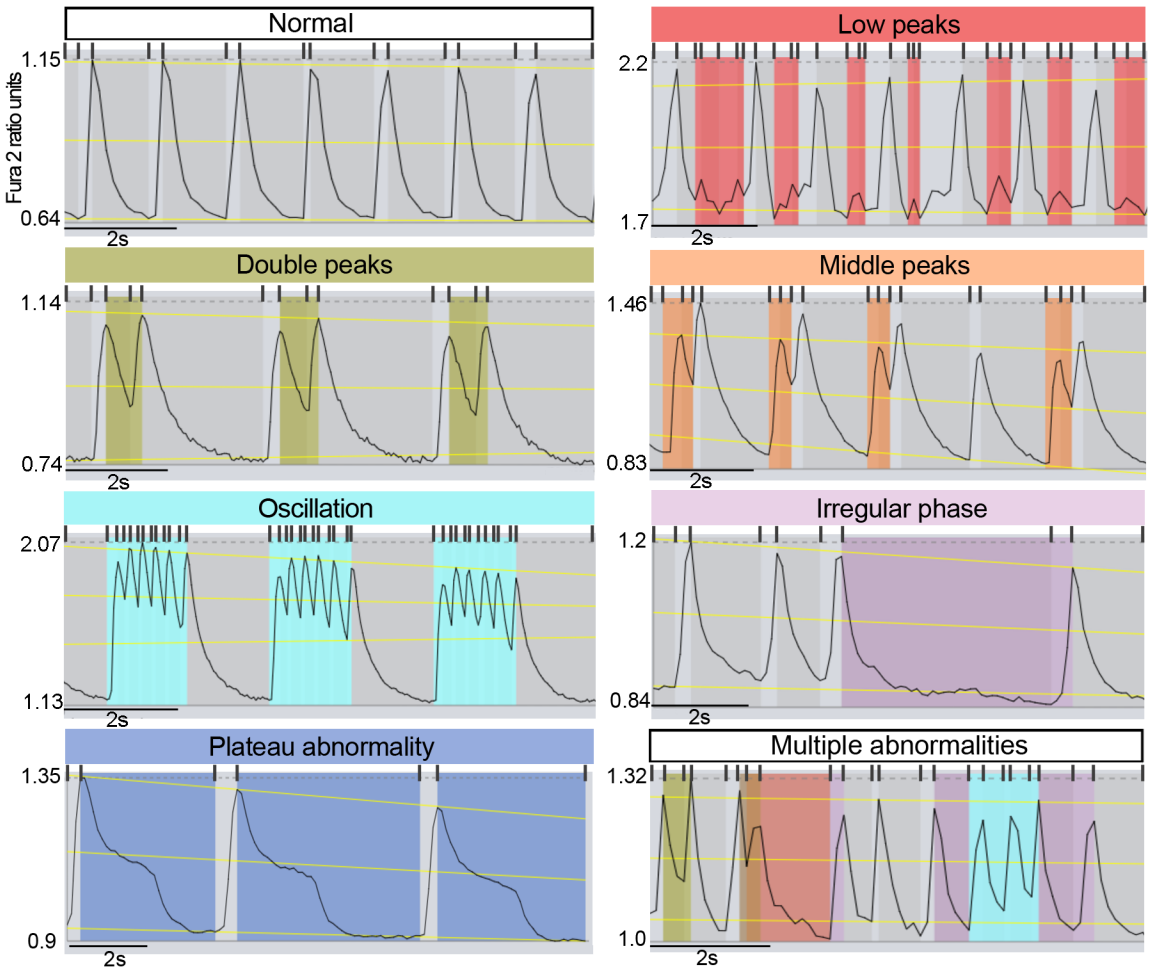

Fig 2. Detected Ca^{2+} signal abnormality patterns from *AnomalyExplorer* analysis. Examples of the color-coded abnormality subgroups that *AnomalyExplorer* detects as well as normal Ca^{2+} signals as follows: low peaks, double peaks, middle peaks, oscillation, irregular phase, plateau abnormality, and a signal with multiple different abnormalities. Abnormalities are detected with the help of three yellow regression lines and subsequently rising and decaying sections separated with small grey vertical lines above the signal showing how the Ca^{2+} transient ascends and descends monotonously. The same abnormality patterns were detected in a manual analysis made with visual recognition.

doi:10.1371/journal.pone.0135806.g002

within ±25% of the height of the following section. There can only be two consecutive peaks in a double peak anomaly and sequences of more than two peaks are flagged as oscillations.

Irregular phase (Fig 2) is flagged if the distance of peaks differs by a user-defined percentage (for example, 90%) from the median of the peak distances. Only those peaks that do not exhibit any anomalies are considered, except the peaks that exhibit double peaks anomaly which are treated as a single peak that has the mean of the positions of double peaks as its reference value. Treating a double peak as a single peak prevents the overlap of irregularity and double peak anomaly.

Plateau abnormality (Fig 2) is flagged if the transient changes its rate of ascent or descent more than a user-defined percentage (for example 75%) within a section. Its recognition is also affected by the setting of the noise ratio, i.e., how much of the signal noise is tolerated.

Availability of Software. The *AnomalyExplorer* conforms to the Open Source Definition and has been designed to facilitate the abnormality analysis of Ca^{2+} recordings obtained from CMs. Website for downloading the program: https://github.com/siirtola/AnomalyExplorer. More information about the software can be found from S1 Supporting Information.

Results

Ca^{2+} transient abnormality patterns of CMs derived from iPSC lines with RyR2 mutations causing CPVT varied remarkably as a function of time. We investigated the reliability and efficiency of the *AnomalyExplorer* in detecting the normal and abnormal Ca^{2+} transients and categorized the abnormal signals into pattern specific subgroups, and compared these results to the manual analysis.

The data were generated with two different Ca^{2+} transient recording software programs. As a result, the signals were recorded with various sampling frequencies, which ranged from 9 to 10 Hz on Recording Software 1 and from 23 to 26 Hz on Recording Software 2. This affected the noise level of the recordings, and it was thus necessary to find the optimal *AnomalyExplorer* user-defined anomaly detection parameters for both recording software groups. In total, 132 Ca^{2+} signals were recorded with Recording Software 1 and 212 Ca^{2+} signals with Recording Software 2, and the lengths of recordings varied from approximately 11 to 23 s.

Each Ca^{2+} signal was manually analyzed with visual recognition and compared with the results obtained from *AnomalyExplorer*. On both manual and *AnomalyExplorer* analysis, the Ca^{2+} signals were categorized as abnormal if at least one abnormality pattern was visualized in the signal and as normal if no abnormalities were found in the recordings. Abnormal signals were further categorized into different subgroups based on the following types of Ca^{2+} abnormalities observed visually: double peaks, oscillating peaks, low amplitude peaks, plateau abnormalities with prolonged Ca^{2+} rise or decay time or irregular phase in the beating rhythm (Fig 2). Then, the total numbers of subgroup specific abnormalities were quantified from the Ca^{2+} signals. One signal could belong to more than one abnormality subgroup and could include several abnormalities.

At first, in *AnomalyExplorer* analysis, optimal analysis parameters were found for both recording software programs. For signals generated with Recording Software 1 the user-defined percentage limits for analysis were the following: noise 5%, low peaks 7–61%, middle peaks 0–70%, plateau abnormality 70%, oscillation 31%, double peaks 20–88%, and irregular phase 100%. For signals generated with Recording Software 2, the user-defined percentage limits were the following: noise 8%, low peaks 10–61%, middle peaks 0–70%, plateau abnormality 70%, oscillation 31%, double peaks 20–88%, and irregular phase 100%. When comparing the detection of normal and abnormal Ca^{2+} signals between the manual analysis and *AnomalyExplorer* (S1 Fig), there was only 2% inconsistency between the manual and *AnomalyExplorer* analysis for Recording Software 1 signals. This inconsistency was specified as false abnormal, which indicated that they were manually categorized as normal but that the *AnomalyExplorer* categorized them as abnormal. For Recording Software 2 signals, there was 9% inconsistency with manual analysis; 4% were false abnormal and 5% were false normal, which indicated that they were manually categorized as abnormal but that the software categorized them as normal.

The majority of the spontaneously beating control WT and CPVT CMs were categorized as normal in both the manual analysis (66% and 58% of Recording Software 1 and 2 signals, respectively) and the *AnomalyExplorer* analysis (64% and 57% of Recording Software 1 and 2 signals, respectively), without any observed abnormalities. Overall, 17% of the control WT CMs (n = 23) were categorized as abnormal with *AnomalyExplorer* analysis and 13% with manual analysis. Table 1 summarizes the overall percentage of detected abnormal signals with both recording software programs as well as the consistency of the manual and *AnomalyExplorer* analysis of different Ca^{2+} transient abnormality subgroups. To visualize the same results, see S2 Fig. Many signals that were categorized as abnormal presented with various Ca^{2+} transient abnormalities, which can be observed from the detailed analysis results in the *AnomalyExplorer* overview in Fig 3.

Table 1. Comparison of detected Ca^{2+} transient abnormalities and different abnormality subgroups analyzed manually and with *AnomalyExplorer* software. Each analyzed signal represents a recording from a single cell. The percentages show the amount of each subgroup specific abnormality when compared to the amount of all the abnormalities in all the signals. One signal could belong to more than one abnormality subgroup and could include several abnormalities. Last row of the table shows the overall percentage of the abnormal signals from all the analyzed signals. The signal was analyzed as abnormal if there were one or more Ca^{2+} transient abnormalities in the whole signal.

	Recording Software 1		Recording Software 2	
	Manual analysis, abnormalities (n = 171)	AnomalyExplorer analysis, abnormalities (n = 157)	Manual analysis, abnormalities (n = 301)	AnomalyExplorer, analysis abnormalities (n = 284)
Double peaks	29%	30%	33%	34%
Low peaks	20%	15%	15%	6%
Middle peaks	5%	6%	9%	9%
Oscillations	26%	30%	26%	28%
Plateau abn.	6%	6%	7%	15%
Irregular phase	14%	13%	13%	8%
Signals categorized as abnormal	34% (n = 132)	36% (n = 132)	43% (n = 212)	42% (n = 212)

doi:10.1371/journal.pone.0135806.t001

When comparing the manual and *AnomalyExplorer* analysis of different RyR2 mutated CPVT cell lines, analyses revealed that there were mutation-specific differences in the Ca^{2+} transient abnormalities with both analysis methods (Fig 4). Double peaks were common abnormality types in all RyR2 mutated CPVT cell lines with some small differences between mutations. In *AnomalyExplorer* analysis double peaks were seen in 31 to 37% of the signals with mutations located with N-terminal or central cytosolic region of the *RyR2* protein (exon 3 deletion, P2328S, T2538R, L4115F) and in 21 to 26% of the signals with mutations in or near the transmembrane domain (Q4201R and V4653F). Oscillation was also common abnormality type in all of the mutated cell lines in *AnomalyExplorer* analysis, particularly in V4653F and T2538R mutated CMs (47% and 52%, respectively). Low peaks were rather common in P2328S and Q4201R mutated CMs (16% and 23%, respectively), and plateau abnormalities in Q4201R and exon 3 deletion mutated CMs (25% to 38%, respectively) in *AnomalyExplorer* analysis. Middle peaks and irregular phases were least common abnormality types in all mutated CPVT CMs. When comparing the consistency of the manual and *AnomalyExplorer*, it was shown that in P2328S and L4115F mutated CMs the analyses were comparable. Over 5% difference between analyses was seen in low peak abnormalities (with exon 3 deletion, T2538R and V4653F mutated CMs) with difference of 7–15%, irregular phase abnormalities (with exon 3 deletion, T2538R and V4653F mutated CMs) with difference of 6–10%, plateau abnormalities (with exon 3 deletion and Q4201R CMs) with difference of 10–18% and double peak abnormalities (with T2538R and Q4201R CMs) with difference of 8–14%.

Discussion

Ca^{2+} cycling is fundamental for the electrical signaling and mechanical contraction of the heart. It is controlled via ion currents, channels, and exchangers. Comprehensive functioning of Ca^{2+} cycling is essential for the excitation–contraction coupling of CMs.[17] Ca^{2+} cycling abnormalities may cause arrhythmic features such as delayed after depolarizations (DADs), where depolarizing oscillations in the membrane potential follow an action potential after completion of repolarization [18], or early afterdepolarizations (EADs) which occur during repolarization.[19–21] Dysfunction in Ca^{2+} cycling may also produce Ca^{2+} alternans, a beat-to-beat alternation in the amplitude of the intracellular Ca^{2+} transient.[22] Previous studies have shown that disease-specific iPSC-derived CMs with Ca^{2+} cycling abnormalities manifest

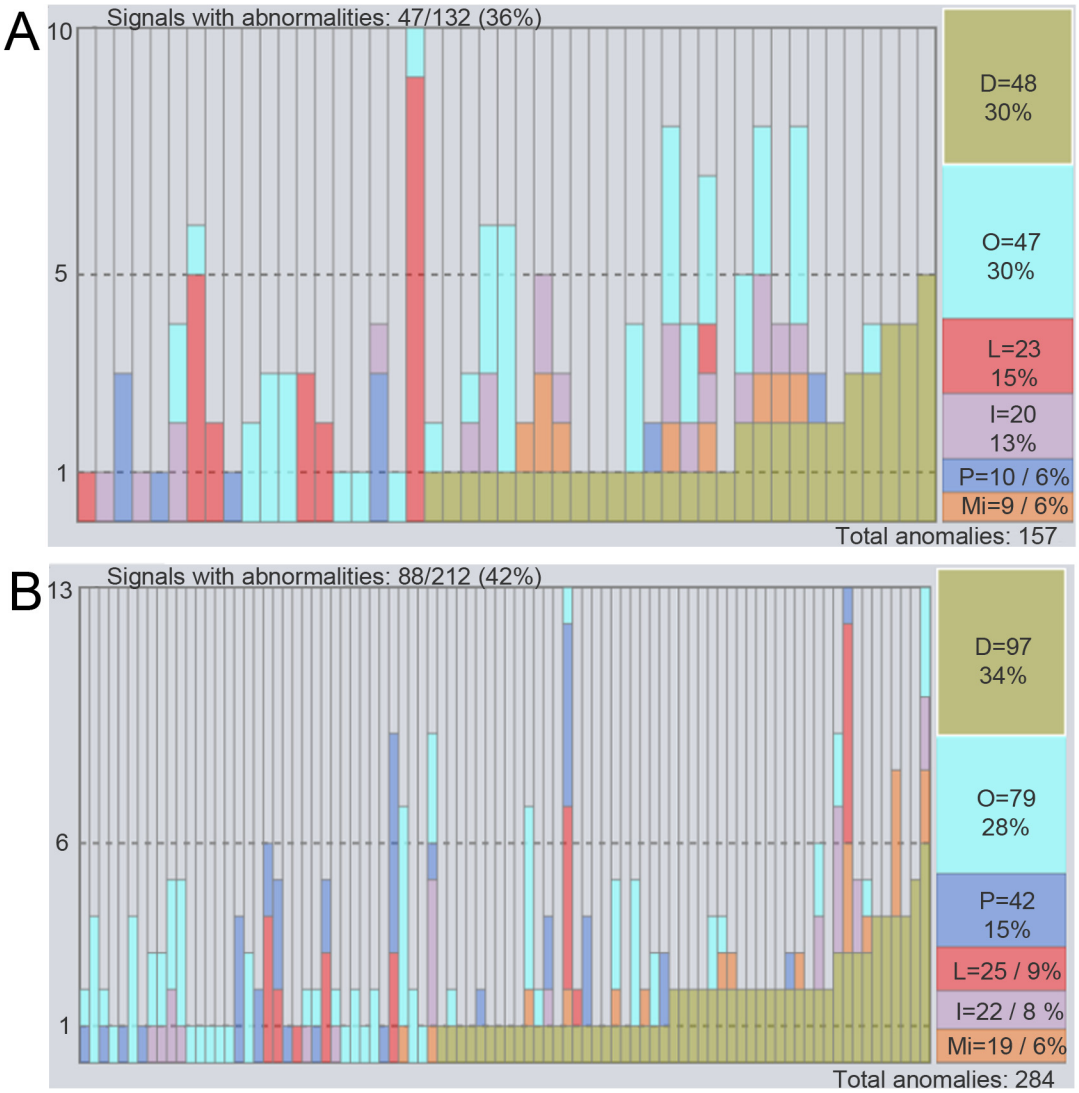

Fig 3. Detailed results in the *AnomalyExplorer* overview. View of the *AnomalyExplorer* analyzed Ca^{2+} signals summarizing the results recorded with A) Recording Software 1 and B) Recording Software 2. It shows the detailed number of subgroup specific abnormalities in each Ca^{2+} signal in one bar and the total number and percentages of all abnormality subgroups. Each bar represents a single cell (signal) and only signals presenting with abnormalities are shown. Altogether, 132 Ca^{2+} signals were recorded with Recording Software 1, 47 which (36%) presented abnormalities. The corresponding number from 212 Ca^{2+} signals recorded with Recording Software 2 was 88 (42%).

doi:10.1371/journal.pone.0135806.g003

arrhythmic features such as DADs or EADs in their action potential [2–6,11,13]. Additionally, simultaneous AP and Ca^{2+} recordings of long QT-specific CMs have revealed that Ca^{2+} cycling is involved in prolonging the AP duration and in the formation of EADs as demonstrated by comparable changes in the APs and Ca^{2+} transients.[23] Therefore, disease phenotype-specific changes in electrophysiology can be mirrored by changes in Ca^{2+} cycling, thereby highlighting the importance of the analysis of these transients and abnormalities.

After the invention of iPSC technology, disease modeling with patient-specific CMs has been constantly increasing and has revealed Ca^{2+} transient abnormalities in many CM disease phenotypes. Consistent rules for the analysis of Ca^{2+} transient abnormalities are currently lacking; thus, the results obtained from different studies cannot be compared. Thus far, the detection of Ca^{2+} cycling abnormalities has been based on how the researchers categorize data based

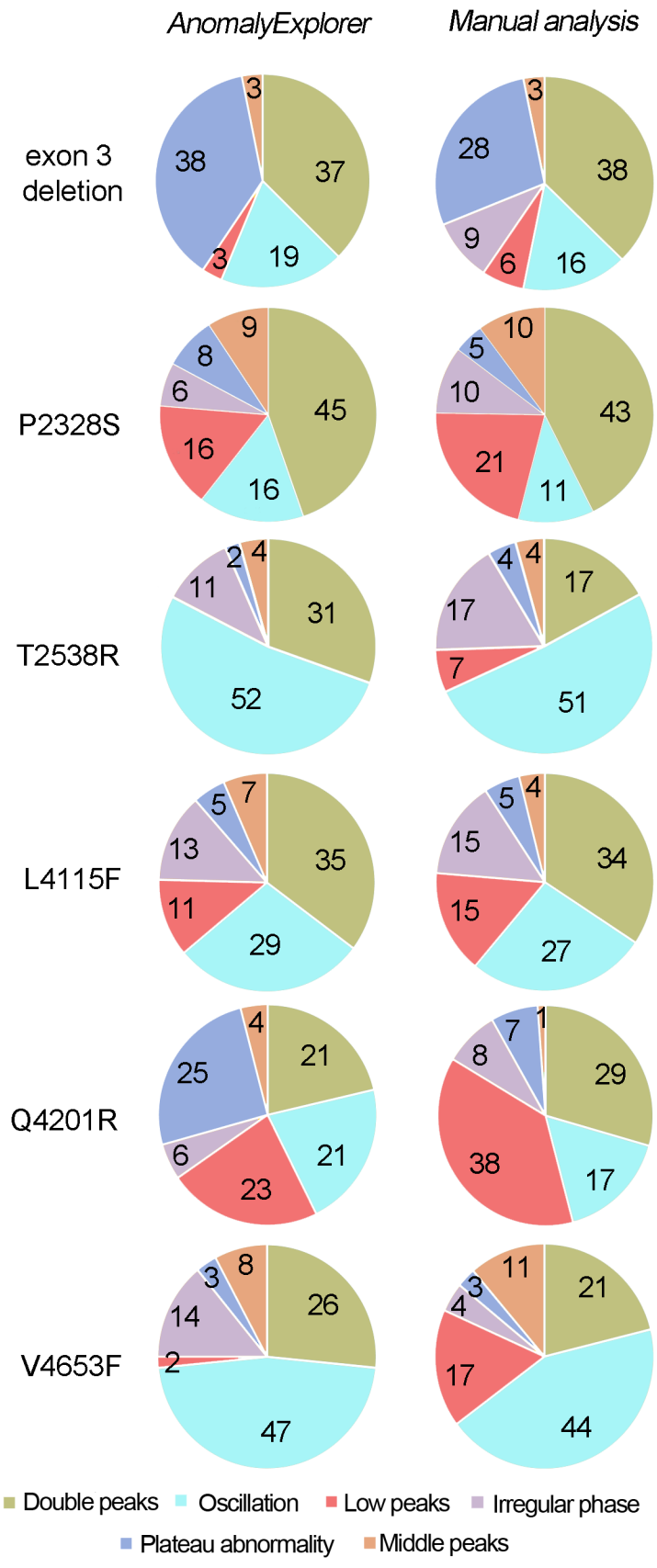
AnomalyExplorer
Manual analysis
exon 3 deletion
38
37
3
19
3
28
38
3
9
6
16
P2328S
6
8
9
45
16
16
5
10
10
43
21
11
T2538R
11
2
4
31
52
4
4
17
17
7
51
L4115F
13
5
7
35
11
29
15
5
4
34
15
27
Q4201R
25
4
21
6
21
23
8
7
1
29
38
17
V4653F
14
3
8
26
2
47
4
3
11
21
17
44
Double peaks
Oscillation
Low peaks
Irregular phase
Plateau abnormality
Middle peaks

Fig 4. Comparison of *AnomalyExplorer* and manual Ca^{2+} signal analysis of the different RyR2 mutated CPVT cell lines. Pie charts indicate the percentage of the Ca^{2+} cycling abnormalities and show mutation specific differences in the abnormalities with both analysis methods. One Ca^{2+} signal can belong to several subgroups and consist of many abnormalities. The numbers of the signals analyzed from different RyR2 mutation specific CMs are the following: exon 3 del n = 46, P2328S n = 32, T2538R n = 51, L4115F n = 106, Q4291R n = 57 and V4653F n = 29.

doi:10.1371/journal.pone.0135806.g004

on the individual's reasoning, experience and observations. Previously in our study and in other studies, earlier classification methods have involved categorizing a Ca^{2+} signal as abnormal if at least one abnormality is detected without indicating the absolute amount or duration of Ca^{2+} abnormalities in each signal.[3–6,11,12] In some cases, abnormalities have been divided into subgroups that do not necessarily consider that one signal can express different abnormal patterns and can thus belong to several subgroups.[4–6] A common problem has also been that the naming and/or illustration of the abnormalities differ between studies and they have been categorized, for example as after-contractions or triggered contractions [3], as significant Ca^{2+} transient irregularities, such as multiple events [11], or as significant irregularities in Ca^{2+} transients, including at least an irregular rhythm and multiple peaks.[12] Additionally, no specific analysis criteria have been reported because the nature of the analysis has been visual inspection. Therefore, it is unclear whether all of the patterns have been calculated as abnormalities and how these abnormalities have been considered in the numerical analysis of the data. Additionally, with the traditional method of presenting signal abnormalities, it is not possible to identify disease-specific Ca^{2+} abnormality patterns when comparing the already published reports.

The human visual system is an ingenious pattern recognizer, and our cognitive activity is largely based on this capability.[24] Detecting patterns is easy for a human, and the brain does it effortlessly on the subconscious level. For example, the activity of analyzing and classifying signals is trivial to those who know what to look for. However, regardless of the ability to categorize patterns manually, it is highly subjective. Two people might make different classifications, and the same person might classify signals differently at different times. Therefore, there is a huge demand for specific criteria for different subgroups of Ca^{2+} abnormalities with specific analysis software that could automatically classify and calculate the abnormal signals according to preset specifications. For these reasons, *AnomalyExplorer*, an interactive software tool that can assist in the visual classification of Ca^{2+} signals was developed to help researchers working with Ca^{2+} data of CMs. *AnomalyExplorer* is based on interactive visualization with a direct manipulation UI, in which the analysis and classification approach of the researcher has been transferred into a software tool to improve the accuracy, reliability and throughput rate for Ca^{2+} cycling analysis. The user can set the user-defined anomaly detection parameters for each subgroup and the background noise level of the recordings. This direct manipulation of the UI allows for the use of *AnomalyExplorer* with different measurement settings wherein the recording software, sampling frequency or environment of the measurement setup can vary and optimal settings can be found for each occasion. Once the optimal user-defined anomaly detection parameters have been identified for recordings made with specific measurement settings, there is no need to manipulate the UI.

The purpose of information visualization is to use perception to amplify cognition. The idea of *AnomalyExplorer* was to generate task-specific visual representations of data with which the user can interact, thereby amplifying users' cognition. The means to amplify users' cognition are numerous, and here the most relevant ones were enhancing the pattern recognition, facilitating the comparisons, and supporting the short-term memory by using external representations. [25] The interaction component of the software allowed the user to have a dialog with

the data, and this exploration uncovered insights.[26] The representation component of *AnomalyExplorer* was based on the detail+overview design pattern, and an overview and detailed view of an information space are displayed simultaneously.[27] Overview has been defined to imply a qualitative awareness of one aspect of some data, preferably acquired rapidly and pre-attentively without cognitive effort. [28] The most important qualitative aspect in *AnomalyExplorer* was to define whether the signal is normal or not, and to further analyze the quality and distribution of detected anomalies. Therefore overview in *AnomalyExplorer* was designed to be a stacked bar chart of detected anomalies where a bar represents the number of anomalies in a signal, and stacking shows how the anomalies are distributed. The first question in the design of an interactive visualization tool is if often whether we need to support a workflow from the overview to detailed view or vice versa. Shneiderman [29] advocated for the former approach in designing visualization tools by stating "overview first, zoom and filter, then details-on-demand". In *AnomalyExplorer*, the free movement between the overview and detailed views must be supported to reduce the cognitive load. In addition, the views need to be tightly coupled. In the detailed view, the appropriate parameters for anomaly detection are sought, and it must be continuously monitored how this affects the overall outcome, until suitable parameters for data analysis are found. In the overview, the inspection may reveal signals that seem to be outliers or that are otherwise suspicious, and the details on the demand need to be seen.

It can be roughly estimated that manual analysis of one Ca^{2+} signal takes from 10 to 120 seconds, and the overall manual analysis time in this study was approximately 90 minutes and 140 minutes with Recording Software 1 and 2 signals, respectively. With *AnomalyExplorer*, the analysis of the Ca^{2+} signals is much faster, and was approximately only 10 seconds in this study with both Recording Software 1 and 2 signals, because the analysis results are immediately shown after loading the signals into the software regardless of the number of signals. Therefore, with *AnomalyExplorer*, the saved time compared with manual analysis increases with the number of analyzed signals. Other benefits of *AnomalyExplorer* include the fact that the classifications are repeatable and user-independent and that the accuracy and repeatability of the analysis can be enhanced. The definition of signal abnormalities in terms of visual properties, is more flexible than numerical or analytical specification. However, it needs to be highlighted that this type of abnormality analysis does not exclude the need for the numerical analysis of different Ca^{2+} cycling parameters, such as the amplitude, frequency and peak duration. AnomalyExplorer is anyhow a good tool for screening through the Ca^{2+} recordings for more extensive analysis and it can facilitate the numerical analysis by determining the abnormality analysis criteria that can be exploited when defining how abnormalities should be considered in numerical analysis, such as when calculating the duration of double or oscillating peaks. To further analyze the mechanism behind different Ca^{2+} cycling abnormalities, combined electrophysiology and other functional methods together with Ca^{2+} imaging measurements are needed.

When Ca^{2+} signals are analyzed with *AnomalyExplorer*, the results are more comparable between different studies than they are with manual analysis because the user-defined anomaly detection parameters are specifically determined. Once the optimal user-defined parameters have been identified for specific measurement settings, there is no need for manipulating these parameters. With *AnomalyExplorer* exploiting the interactive visualization, it is easy to catch all of the abnormalities in a sample and obtain a more accurate and complete classification. In this study, we have shown that optimal analysis parameters can be found for data recorded with two different recording software programs and that the detection of normal and abnormal signals as well as the abnormality patterns with *AnomalyExplorer* is quite consistent with the manual analysis. Some variation in the manual and *AnomalyExplorer* analysis was observed in the categorization of abnormalities. When classifying the signals as normal or abnormal,

inconsistency of the analysis could be seen in 2% and 9% of signals with Recording Software 1 and 2, respectively, which was quite reasonable. When categorizing the abnormalities into subgroups and calculating the number of different subgroup specific abnormalities, the abnormalities were detected with 0 to 5% difference between the manual and *AnomalyExplorer* analyses. The exception was in the amount plateau and low peak abnormalities in Recording Software 2 signals with 8 and 10% differences between manual and *AnomalyExplorer* analysis. When comparing manual and *AnomalyExplorer* analyses of different RyR2 mutated CPVT cell lines it was shown that detection of oscillation and middle peaks were equivalent with 0 to 5% differences in addition to double peak detection, which was quite similar between analyses with 0 to 5% differences in 4 out of 6 mutations. Detection of low peaks, irregular phases and plateau abnormalities differed the most between analyses. Overall, the inconsistency between manual and *AnomalyExplorer* analysis may be due to differences between human and software analyses because the accuracy of the manual analysis varies since it is performed only by visual recognition without clear abnormality detection rules. Higher percentages of low peak abnormalities were detected in manual analysis than in *AnomalyExplorer* analysis. This could be explained with background noise of the Ca^{2+} recordings, which is challenging to recognize visually in the manual analysis. Also irregularity of the beating rhythm as well as the prolonged rise and decay time (plateau abnormalities) of Ca^{2+} transients are challenging to detect visually in manual analysis since criteria for these abnormality types is difficult to define. With *AnomalyExplorer* the noise and abnormality detection rules are clearly defined and therefore the anomaly detection is more compatible between signals. Inconsistency between manual and *AnomalyExplorer* analysis can also be seen due to problems in the Ca^{2+} recording setup, such as with photobleaching of the Ca^{2+} indicator or its toxicity together with UV light to CMs, which can interfere with the loading of the cells and cause the transients and thus the whole signal to have extra noise. This can also affect the validity of *AnomalyExplorer* analysis and may be stated as one limitation of this study.

When comparing the analysis of different CPVT cell lines generated from patients carrying different RyR2 mutations the percentage of different abnormality subgroups varied between cell lines. Overall, double peaks and oscillations were most common and middle peaks and irregular phases least common abnormality types in all CPVT mutations. Other than that, no specific trend between abnormality subgroup percentages and different mutations could be seen and it could be concluded that there were mutation-specific differences in the Ca^{2+} transient abnormalities like we have previously shown with these cell lines [9].This finding showed the future usefulness of *AnomalyExplorer* for detecting cell line- and mutation-specific variability in the Ca^{2+} transient abnormalities. These types of differences reflect the mutation specific pathology of the disease and reveal that the location of the mutation can affect the disease phenotype. This result is in accordance with our previous study [9], where we showed that the Ca^{2+} abnormalities of these different CPVT cell lines are more common in some mutations than in others and that these Ca^{2+} cycling abnormalities can be rescued or reduced with a specific drug as in actual patients. In the future, *AnomalyExplorer* can speed up and improve the accuracy of the analysis of this type of drug study, where the effect of a specific type of drug on the amount Ca^{2+} cycling abnormalities is quantified. Further Ca^{2+} cycling studies combined with electrophysiological studies, are needed to assess how different Ca^{2+} cycling abnormalities reflect the mechanism of the disease or drug effect because these are not yet known. Presumably, at least some Ca^{2+} cycling abnormalities reflect the arrhythmogenic features such as DADs and EADs. Because electrophysiological studies are time-consuming and challenging and because only a restricted number of cells can be measured, these methods are not often combined and more optimization is needed.

AnomalyExplorer was designed for the data analysis of <50 Hz sampling frequency data with recording duration of tens of seconds, and it performs flawlessly under these requirements. *AnomalyExplorer* is able to analyze data with higher sampling frequencies, at least to 100 Hz, but it could be improved to suit for analysis of even higher frequency data in the future. With functional recordings it is problematic to set a certain recording duration limit that is sufficient to define the overall behavior of a cell and there is always uncertainty how well the recording reflects the overall behavior of the cell. In our study the recording duration was implemented for our specific use case with varying recording durations of 11 to 23 seconds. The analysis software does not have a limit for the recording length, but it can be estimated that responsiveness and user experience will suffer with several minute recordings. Short duration signals may not represent the long-term behavior of the cell correctly and for the future Ca^{2+} cycling analysis, the use of longer recordings with standard duration could be more beneficial, if it would be suitable for the study design. Ín these analyses, the duration of each abnormal Ca^{2+} transient could be compared to the duration of the whole signal to see the percentage of the abnormal Ca^{2+} transients in the recording. To improve the analysis of long-term behavior of the cells, long recordings could be also broken up into a series of segments and analyzed separately before averaging. Sampling frequency and recording duration of this study can be stated as a limitation of this study and the current prototype, as it was designed and implemented for a specific use case and for the specific digitization systems. Nevertheless, recording durations of tens of seconds and sampling frequencies of <50 Hz have been utilized successfully before, when studying Ca^{2+} cycling of iPSC derived disease specific CMs [2,5,9,23].

As the use of iPSC-derived CMs for disease modeling and drug screening continues to increase, there is a significant demand for faster and more consistent analysis methods. *AnomalyExplorer* is suitable for analyzing high number of Ca^{2+} signals, which can be a bottleneck for high-throughput Ca^{2+} imaging analysis and screenings in manual data analysis. This tool will facilitate and speed up the analysis of CM Ca^{2+} transients; furthermore it should be more accurate and user-independent. At present, we are not aware of any similar software that is suitable for single Ca^{2+} signal analysis that is recorded with any type of recording software. In the future, iPSC-derived CMs can be exploited for screening of potential new chemical compounds and this software and analysis method can be exploited for evaluating different drug responses and in Ca^{2+} cycling analysis to study basic disease pathology. This method will also be beneficial when analyzing Ca^{2+} cycling of CMs on a large scale for screening the adverse cardiac effects of new potential compounds.

Conclusions

In this study, the *AnomalyExplorer* tool was developed to assist in analyzing and classifying Ca^{2+} signal abnormalities of disease specific human iPSC-derived CMs. Ca^{2+} cycling has a central role in CM contraction-relaxation, and it also is essential in the electrical signaling of CMs. As a result, detailed characterization of the abnormal Ca^{2+} transients present in different cardiac diseases would allow for a more detailed evaluation of the physiological function of the diseased CMs. Because Ca^{2+} transient abnormalities are difficult to specify and analyze by computational methods, in the *AnomalyExplorer* tool the abnormalities are recognized by the visual features alone, using interactive visualization with a similar approach as in traditional manual analysis. It is based on the multiple coordinated views paradigm and a direct manipulation UI. Using *AnomalyExplorer* the classifications are repeatable and user-independent. The software is also capable of screening large datasets faster than manual analysis. By utilizing fast kinetic fluorescence imaging of intracellular Ca^{2+} levels, together with *AnomalyExplorer*, the

Ca^{2+} transient abnormalities of spontaneously contracting CMs can be detected and classified, which provides more information regarding the Ca^{2+} cycling phenotype in these cells.

Supporting Information

S1 Fig. Consistency of the manual analysis and *AnomalyExplorer* analysis. Totally 132 Ca^{2+} signals recorded with Recording Software 1 (A) and 212 Ca^{2+} signals recorded with Recording Software 2 (B) were analyzed.
(TIF)

S2 Fig. Comparison of manual and *AnomalyExplorer* Ca^{2+} signal analysis of the data generated with Recording Software 1 and 2. A) Pie charts indicate the percentage of normal (white) and abnormal (black) Ca^{2+} signals in manual and *AnomalyExplorer* analyzed signals. B) Color-coded pie charts indicate the percentage of the different abnormalities in both manually and *AnomalyExplorer* analyzed signals. One Ca^{2+} signal can belong to several subgroups and consist of many abnormalities. In Recording Software 1 signals, totally 171 and 157 abnormalities were found in manual and *AnomalyExplorer* analysis, respectively. In Recording Software 2 signals, totally 301 and 284 abnormalities were found in manual and *AnomalyExplorer* analysis, respectively.
(TIF)

S1 Supporting Information. Availability of software including link to the software licensed under MIT, documentation for running and installing the software, and a test dataset for running the software.
(DOCX)

Acknowledgments

We thank Henna Venäläinen and Markus Haponen for the technical support.

Author Contributions

Conceived and designed the experiments: KP HS MJ KAS. Performed the experiments: KP HS JAS TV. Analyzed the data: KP. Contributed reagents/materials/analysis tools: MJ KAS. Wrote the paper: KP HS MJ KAS.

References

1. Takahashi K, Tanabe K, Ohnuki M, Narita M, Ichisaka T, Tomoda K, et al. Induction of pluripotent stem cells from adult human fibroblasts by defined factors. 2007; 131: 861–72. PMID: 18035408
2. Fatima A, Xu G, Shao K, Papadopoulos S, Lehmann M, Arnaiz-Cot JJ, et al. In vitro Modeling of Ryanodine Receptor 2 Dysfunction Using Human Induced Pluripotent Stem Cells. 2011; 28: 579–92. doi: 10.1159/000335753 PMID: 22178870
3. Novak A, Barad L, Zeevi-Levin N, Shick R, Shtreichman R, Lorber A, et al. Cardiomyocytes generated from CPVT(D307H) patients are arrhythmogenic in response to beta-adrenergic stimulation. 2011; 3: 468–82.
4. Jung CB, Moretti A, Mederos y Schnitzler M, Iop L, Storch U, Bellin M, et al. Dantrolene rescues arrhythmogenic RYR2 defect in a patient-specific stem cell model of catecholaminergic polymorphic ventricular tachycardia. EMBO Mol Med. 2012; 4: 180–191. doi: 10.1002/emmm.201100194 PMID: 22174035
5. Kujala K, Paavola J, Lahti A, Larsson K, Pekkanen-Mattila M, Viitasalo M, et al. Cell model of catecholaminergic polymorphic ventricular tachycardia reveals early and delayed afterdepolarizations. PLoS One. 2012; 7: e44660. doi: 10.1371/journal.pone.0044660 PMID: 22962621
6. Itzhaki I, Maizels L, Huber I, Gepstein A, Arbel G, Caspi O, et al. Modeling of catecholaminergic polymorphic ventricular tachycardia with patient-specific human-induced pluripotent stem cells. J Am Coll Cardiol. 2012; 60: 990–1000. doi: 10.1016/j.jacc.2012.02.066 PMID: 22749309

7. Zhang XH, Haviland S, Wei H, Saric T, Fatima A, Hescheler J, et al. Ca2+ signaling in human induced pluripotent stem cell-derived cardiomyocytes (iPS-CM) from normal and catecholaminergic polymorphic ventricular tachycardia (CPVT)-afflicted subjects. Cell Calcium. 2013; 54: 57–70. doi: 10.1016/j.ceca.2013.04.004 PMID: 23684427
8. Di Pasquale E, Lodola F, Miragoli M, Denegri M, Avelino-Cruz JE, Buonocore M, et al. CaMKII inhibition rectifies arrhythmic phenotype in a patient-specific model of catecholaminergic polymorphic ventricular tachycardia. Cell Death Dis. 2013; 4: e843. doi: 10.1038/cddis.2013.369 PMID: 24113177
9. Penttinen K, Swan H, Vanninen S, Paavola J, Lahtinen AM, Kontula K, et al. Antiarrhythmic Effects of Dantrolene in Patients with Catecholaminergic Polymorphic Ventricular Tachycardia and Replication of the Responses using iPSC Models. PLoS One. 2015; 10: e0125366. doi: 10.1371/journal.pone.0125366 PMID: 25955245
10. Sun N, Yazawa M, Liu J, Han L, Sanchez-Freire V, Abilez OJ, et al. Patient-specific induced pluripotent stem cells as a model for familial dilated cardiomyopathy. Sci Transl Med. 2012; 4: 130ra47. doi: 10.1126/scitranslmed.3003552 PMID: 22517884
11. Lan F, Lee AS, Liang P, Sanchez-Freire V, Nguyen PK, Wang L, et al. Abnormal calcium handling properties underlie familial hypertrophic cardiomyopathy pathology in patient-specific induced pluripotent stem cells. Cell Stem Cell. 2013; 12: 101–113. doi: 10.1016/j.stem.2012.10.010 PMID: 23290139
12. Han L, Li Y, Tchao J, Kaplan AD, Lin B, Li Y, et al. Study familial hypertrophic cardiomyopathy using patient-specific induced pluripotent stem cells. Cardiovasc Res. 2014.
13. Yazawa M, Hsueh B, Jia X, Pasca AM, Bernstein JA, Hallmayer J, et al. Using induced pluripotent stem cells to investigate cardiac phenotypes in Timothy syndrome. 2011; 471: 230–4. doi: 10.1038/nature09855 PMID: 21307850
14. Cerrone M, Napolitano C, Priori SG. Catecholaminergic polymorphic ventricular tachycardia: A paradigm to understand mechanisms of arrhythmias associated to impaired Ca(2+) regulation. 2009; 6: 1652–9. doi: 10.1016/j.hrthm.2009.06.033 PMID: 19879546
15. Mummery C, Ward-van Oostwaard D, Doevendans P, Spijker R, van den Brink S, Hassink R, et al. Differentiation of human embryonic stem cells to cardiomyocytes: role of coculture with visceral endoderm-like cells. 2003; 107: 2733–40. PMID: 12742992
16. Siirtola H, Àvalos-Salguero J, Penttinen K, Aalto-Setälä K, Juhola M. Interactive biosignal analysis and classification. 2014: 327–332.
17. Bers DM. Calcium cycling and signaling in cardiac myocytes. Annu Rev Physiol. 2008; 70: 23–49. PMID: 17988210
18. Schlotthauer K, Bers DM. Sarcoplasmic reticulum Ca(2+) release causes myocyte depolarization. Underlying mechanism and threshold for triggered action potentials. 2000; 87: 774–80. PMID: 11055981
19. January CT, Moscucci A. Cellular mechanisms of early afterdepolarizations. 1992; 644: 23–32. PMID: 1562117
20. Volders PG, Vos MA, Szabo B, Sipido KR, de Groot SH, Gorgels AP, et al. Progress in the understanding of cardiac early afterdepolarizations and torsades de pointes: time to revise current concepts. 2000; 46: 376–92. PMID: 10912449
21. Xie LH, Weiss JN. Arrhythmogenic consequences of intracellular calcium waves. 2009; 297: H997–H1002. doi: 10.1152/ajpheart.00390.2009 PMID: 19561309
22. Lehnart SE, Terrenoire C, Reiken S, Wehrens XH, Song LS, Tillman EJ, et al. Stabilization of cardiac ryanodine receptor prevents intracellular calcium leak and arrhythmias. Proc Natl Acad Sci U S A. 2006; 103: 7906–7910. PMID: 16672364
23. Spencer CI, Baba S, Nakamura K, Hua EA, Sears MA, Fu CC, et al. Calcium Transients Closely Reflect Prolonged Action Potentials in iPSC Models of Inherited Cardiac Arrhythmia. Stem Cell Reports. 2014; 3: 269–281. doi: 10.1016/j.stemcr.2014.06.003 PMID: 25254341
24. Ware C. Information visualization: perception for design. 2nd ed. San Francisco CA: Morgan Kaufmann; 2004.
25. Card SK. Readings in information visualization: using vision to think. San Francisco, Calif.; Great Britain: Morgan Kaufmann Publishers; 1999.
26. Yi J, Kang ah Y, Stasko J, Jacko J. Towards a deeper understanding of the role of interaction in information visualization. 2007; 13: 1224–1231.
27. Cockburn A, Karson A, Bederson B. A review of overview+detail, zooming, and focus+context interfaces. 2008; 41: 2.
28. Spence R. Information visualization: design for interaction. 3rd ed: Springer International Publishing; 2014.
29. Shneiderman B. The eyes have it: A task by data type taxonomy for information visualizations. 1996: VL:336–343.

SUPPORTING INFORMATION

STUDY IV

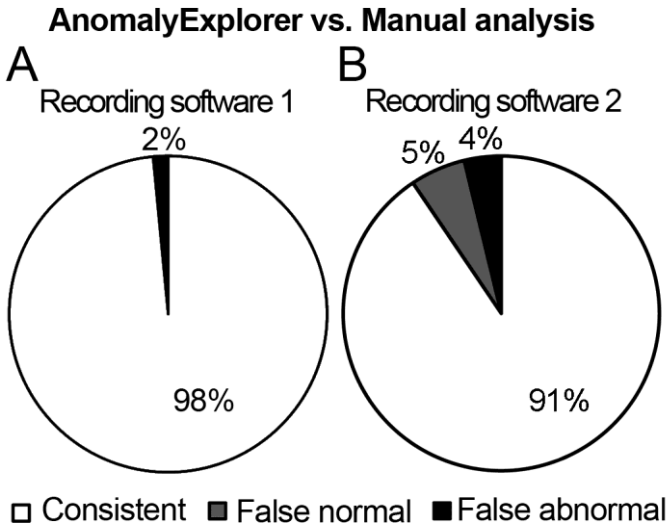

S1 Fig. Consistency of the manual analysis and *AnomalyExplorer* analysis. Totally 132 Ca^{2+} signals recorded with Recording Software 1 (A) and 212 Ca^{2+} signals recorded with Recording Software 2 (B) were analyzed.

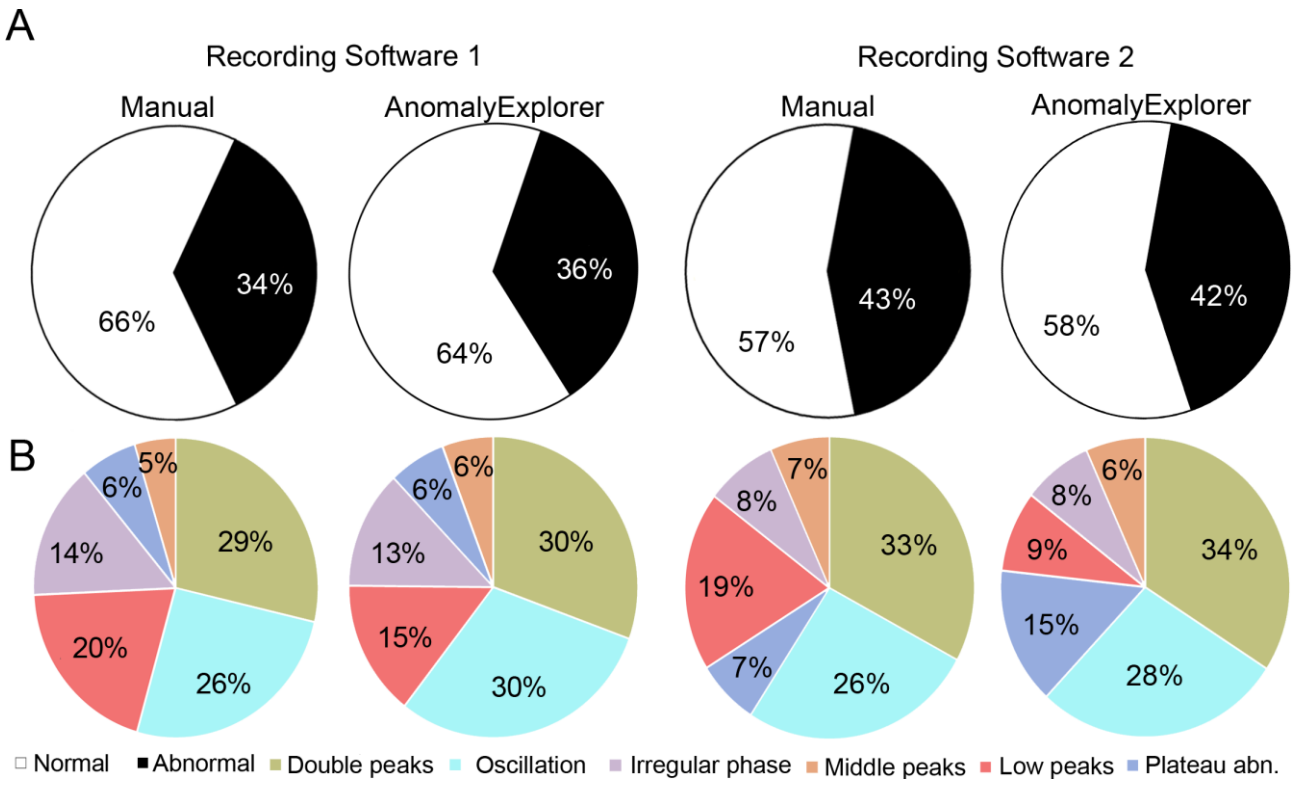

S2 Fig. Comparison of manual and *AnomalyExplorer* Ca^{2+} signal analysis of the data generated with Recording Software 1 and 2. A) Pie charts indicate the percentage of normal (white) and abnormal (black) Ca^{2+} signals in manual and *AnomalyExplorer* analyzed signals. B) Color-coded pie charts indicate the percentage of the different abnormalities in both manually and *AnomalyExplorer* analyzed signals. One Ca^{2+} signal can belong to several subgroups and consist of many abnormalities. In Recording Software 1 signals, totally 171 and 157 abnormalities were found in manual and *AnomalyExplorer* analysis, respectively. In Recording Software 2 signals, totally 301 and 284 abnormalities were found in manual and *AnomalyExplorer* analysis, respectively.

AnomalyExplorer software

The AnomalyExplorer (AE) is a HTML5-based analysis tool for calcium cycling. It is based on the earlier Java implementation (Siirtola et al. 2014).

AE is a one-page web application implemented mainly in JavaScript. It should run on any modern web browser, but it has been specifically tested with Google Chrome and Safari. Software conforms the Open Source Definition.

The Latest Version

AE can be found on the AnomalyExplorer project page under
https://github.com/siirtola/AnomalyExplorer

Documentation

Currently, the only documentation is the accepted PLOS-One article. The distribution contains test dataset files demonstrating the anomaly types that can be detected with AE. The most up-to-date documentation can be found at https://github.com/siirtola/AnomalyExplorer

Installation

AE does not require any installation beyond copying the test dataset files and the folder structure into a new location. AE does not require a web server as it can be run from a local copy.

Running of the software

Files include test dataset, which can be uploaded to AE from “Choose files” function. Suitable control parameter settings for this test dataset are set as default but can be as well controlled by user. Immediately after the files to be analyzed are uploaded to the software, results with the default parameter settings are shown.

Licensing

AE is distributed under MIT license.

Contacts

- For questions related to biomedical aspects of AE,

please contact Kirsi Penttinen, kirsi.penttinen@uta.fi

- For questions related to technological aspects of AE,

please contact Harri Siirtola, harri.siirtola@uta.fi

References

Siirtola, H., Àvalos-Salguero, J., Penttinen, K., Aalto-Setälä, K., and Juhola, M. (2014). Interactive biosignal analysis and classification. In Information Visualisation (iV2014), 18th International Conference, pages 327–332. (PDF available upon request.)

Tampereen teknillinen yliopisto
PL 527
33101 Tampere

Tampere University of Technology
P.O.B. 527
FI-33101 Tampere, Finland

ISBN 978-952-15-3722-6
ISSN 1459-2045